The Physical Chemistry of pMDI Formulations Derived from Hydrofluoroalkane Propellants

A Study of the Physical Behaviour of Poorly Soluble

Active Pharmaceutical Ingredients; Bespoke Analytical

Method Development Leading to Novel Formulation

Approaches for Product Development.

Richard Telford

Submitted for the degree of Doctor of Philosophy

Department of Chemical and Forensic Science

University of Bradford

2013

Abstract

Active Pharmaceutical Ingredients (APIs) are frequently prepared for delivery to the lung for local topical treatment of diseases such as Chronic Obstructive Pulmonary Disease (COPD) and asthma, or for systemic delivery. One of the most commonly used devices for this purpose is the pressurised metered dose inhaler (pMDI) whereby drugs are formulated in a volatile propellant held under pressure. The compound is aerosolised to a respirably sized dose on actuation, subsequently breathed in by the user.

The use of hydrofluoroalkanes (HFAs) in pMDIs since the Montreal Protocol initiated a move away from chlorofluorocarbon (CFC) based devices has resulted in better performing products, with increased lung deposition and a concomitant reduction in oropharyngeal deposition. The physical properties of HFA propellants are however poorly understood and their capacity for solubilising inhaled pharmaceutical products (IPPs) and excipients used historically in CFCs differ significantly. There is therefore a drive to establish methodologies to study these systems *in-situ* and post actuation to adequately direct formulation strategies for the production of stable and efficacious suspension and solution based products.

Characterisation methods have been applied to pMDI dosage systems to gain insight into solubility in HFAs and to determine forms of solid deposits after actuation. A novel quantitative nuclear magnetic resonance method to investigate the physical chemistry of IPPs in these preparations has formed the centrepiece to these studies, accessing solubility data *in-situ* and at pressure for the first time in HFA propellants. Variable temperature NMR has provided thermodynamic data through van't Hoff approaches. The methods have been developed and validated using budesonide to provide limits of determination as low as 1 µg/mL and extended to 11 IPPs chosen to represent currently prescribed inhaled corticosteroids (ICS), β_2-adrenoagonists and antimuscarinic bronchodilators, and have highlighted solubility variations between the classes of compounds with lipophilic ICSs showing the highest, and hydrophilic β_2-agonist / antimuscarinics showing the lowest solubilities from the compounds under study.

To determine solid forms on deposition, a series of methods are also described using modified impaction methods in combination with analytical approaches including spectroscopy (µ-Raman), *X*-ray diffraction, SEM, chromatography and thermal analysis. Their application has ascertained (i) physical form / morphology data on commercial pMDI formulations of the ICS beclomethasone dipropionate (QVAR® / Sanasthmax®, Chiesi) and (ii) distribution assessment *in-vitro* of ICS / β_2-agonist compounds from combination pMDIs confirming co-deposition (Seretide® / Symbicort®, GlaxoSmithKline / AstraZeneca).

In combination, these methods provide a platform for development of new formulations based on HFA propellants. The methods have been applied to a number of 'real' systems incorporating derivatised cyclodextrins and the co-solvent ethanol, and provide a basis for a comprehensive study of solubilisation of the ICS budesonide in HFA134a using two approaches: mixed solvents and complexation. These new systems provide a novel approach to deliver to the lung, with reduced aerodynamic particle size distribution (APSD) potentially accessing areas suitable for delivery to peripheral areas of the lung (ICS) or to promote systemic delivery.

Keywords: pMDI, HFA, Analytical Method Development, Inhalation, Formulation, Complexation.

i

List of Publications

M. Saunders, P. G. Rogueda, R. Telford, I. J. Scowen, *Respir. Drug Delivery*, 2009, **2**: p. 369-372.

C. I. Granger, M. Saunders, F. Buttini, R. Telford, L. L. Merolla, G. P. Martin, S. A. Jones, B. Forbes, *Mol. Pharmaceutics*, 2012, **9**(3): p. 563-569.

Acknowledgements

I wish to express my sincere gratitude to my supervisors Professor Ian Scowen and Dr Tasnim Munshi for their continued support and enthusiasm throughout this project. Particularly Ian, for his seemingly endless ideas, his willingness to advise and, above all, offer friendship at the difficult points in the process.

To my other colleagues in the department, particularly Mr Andrew Healey and Mr Dennis Farwell for their help and support.

To the people I continue to collaborate with, specifically Dr Mark Saunders and Dr Philippe Rogueda for sharing their ideas and making our on going research so interesting.

Finally to Hannah, my family and my friends for their unquestioning support throughout.

For Hannah.

Contents

List of Abbreviations and Symbols

% CV	% Coefficient of Variation
°C	Degrees Centigrade
®	Registered Trademark
^{13}C NMR	Carbon 13 NMR
^{1}H NMR	Proton NMR
Å	Angstrom
ACI	Anderson Cascade Impactor
ADI	Aqueous Droplet Inhaler
API	Active Pharmaceutical Ingredient
APSD	Aerodynamic Particle Size Distribution
B_0	Applied Magnetic Field
BDP	Beclomethasone dipropionate
BP	British Pharmacopoeia
CD	Cyclodextrin
CD_3CN	Deuterated Acetonitrile
$CDCl_3$	Deuterated Chloroform
CFC	Chlorofluorocarbon
CITDAS	Copley Inhaler Testing Data Analysis Software
cm^{-1}	Wavenumber
COPD	Chronic Obstructive Pulmonary Disease
COSY	Correlation Spectroscopy
Cp	Heat Capacity
D_2O	Deuterated Water
dB	Decibel

DCLS	Direct Classical Least Squares
DLS	Dynamic Light Scattering
DPI	Dry Powder Inhaler
DSC	Differential Scanning Calorimetry
DSC-Raman	Raman Detected Differential Scanning Calorimeter
ERETIC	Electronic Reference to Access *In-vivo* Concentration
EtOH	Ethanol
FPD	Fine Particle Dose
FPF	Fine Particle Fraction
FTIR	Fourier Transform Infra-red
GC	Gas Chromatography
GHz	Gigahertz
GSD	Geometric Standard Deviation
GSK	GlaxoSmithKline
h	Hour
HFA	Hydrofluoroalkane
HFA134a	1,1,1,2-tetrafluoroethane
HFA227	1,1,1,2,3,3,3-heptafluoropropane
HPFP	2H,3H-decafluoropentane
HPLC	High Performance (Pressure) Liquid Chromatography
HSQC	Heteronuclear Single Quantum Coherence Spectroscopy
Hz	Hertz
ICS	Inhaled Corticosteroid
IPP	Inhaled Pharmaceutical Product
J	Joule

K	Degrees Kelvin
k	kilo
KBr	Potassium Bromide
KCL	King's College London
kV	Killovolt
L	Litre
LD	Laser Diffraction
ln	Natural Logarithm
LABA	Long Acting β-agonist
LAMA	Long Acting Muscarinic Agonist
LOD	Limit of Determination
LogP	Log Partition Coefficient
Logχ	Log Mole Fraction Solubility
LOQ	Limit of Quantification
MeCN	Acetonitrile
MeOD	Deuterated Methanol
MeOH	Methanol
mg	Millgram
MHz	Megahertz
min	Minute
mL	Milliliter
mm	Millimeter
mM	millimolar
MMAD	Mass Median Aerodynamic Diameter
MMI	Marple Miller Impactor

MOC	Micro Orifice Collector
Mol	Mole
MSLI	Multi-Stage Liquid Impinger
mW	Milliwatt
N_A	Numerical Aperture
NGI	Next Generation Impactor
nm	Nanometer
NMR	Nuclear Magnetic Resonance
PCA	Photo-calorimeter Accessory
PCA	Principal Component Analysis
PDA	Photodiode Array Detector
PFG	Pulsed Field Gradients
Ph. Eur	European Pharmacopoeia
pL	picolitre
pMDI	Pressurised Metered Dose Inhaler
ppm	part per million
PSD	Particle Size Distribution
PSD	Particle Size Distribution
PTFE	Polytetrafluoroethylene
PXRD	Powder *X*-Ray Diffraction
QNP	Quattro Nucleus Probe
R	Ideal Gas Constant
r^2	Correlation Coefficient
Rf	Response Factor
RGB	Red Green Blue

RIAS	Raman in a Suitcase
σ	Population standard deviation
S:N	Signal to noise ratio
SABA	Short Acting β Agonist
SAMA	Short Acting Muscarinic Agonist
SEM	Scanning Electron Microscopy
TGA	Thermo Gravimetric Analysis
TGA-MS	Thermo Gravimetric Analysis Mass Spectrometry
T_m	Melting Temperature
TRIMEB	Heptakis (2,3,6-tri-O-methyl)-β-cyclodextin
TSI	Twin Stage Impinger
UCL	University College London
uLABA	Ultra Long Acting β Agonist
UoB	University of Bradford
USP	US Pharmacopoeia
UV	Ultraviolet
v/v	Volume / Volume
VT-NMR	Variable Temperature Nuclear Magnetic Resonance
VWD	Variable Wavelength Detector
w/v	Weight / Volume
w/w	Weight / Weight
WiRE	Renishaw Windows Raman Environment Software
X_{10}	PSD Corresponding to 10% Cumulative Distribution
X_{50}	Median PSD
X_{90}	PSD Corresponding to 90% Cumulative Distribution

γ_e	Gyromagnetic Ratio
δ	Chemical Shift
ΔG	Gibb's Free Energy
ΔH	Change in Partial Molar Enthalpy
ΔS	Change in Partial Molar Entropy

List of Figures

Figure 3.1.5 – ^{1}H-^{1}H COSY NMR spectrum of budesonide in CDCl$_3$ shown with X and Y projections taken from high resolution ^{1}H spectrum (Figure 3.1.2).

Figure 3.1.6 – ^{1}H-^{13}H HSQC NMR spectrum of budesonide in CDCl$_3$ shown with X and Y projections taken from high resolution ^{1}H and ^{13}C spectra.

Figure 3.1.2.1 – A typical coaxial NMR tube set up shown in isolation (upper) and assembled (lower) with addition of a deuterated solvent and standard material added to the inner capillary.

Figure 3.1.2.2 – ^{1}H NMR spectrum of a saturated suspension of budesonide in HPFP acquired using a co-axial tube set-up containing a reference solution of CHCl$_3$ in CD$_3$CN.

Figure 3.1.2.3 – ^{1}H NMR spectrum of a saturated suspension of budesonide in HPFP using presaturation solvent suppression methodology to suppress the HPFP signal.

Figure 3.1.2.4 – Plot of peak area values of budesonide A-ring resonances *vs.* irradiation power of solvent suppression applied.

Figure 3.1.2.5 – ^{1}H NMR spectrum of a saturated suspension of budesonide in HPFP using presaturation solvent suppression methodology at 55 dB to suppress the HPFP signal.

Figure 3.1.2.6 – Spectra of saturated budesonide in HPFP obtained with (lower) and without (upper) solvent suppression (55 dB) both using 2048 scans.

Figure 4.1.2.1 – Van't Hoff plot of mean solubility (n=3, ± σ) *vs.* temperature for the compound beclomethasone dipropionate in HPFP, HFA134a and HFA227 over the temperature range 278 to 298 K.

Figure 4.2.1.1.1 – Mean budesonide solubility (n=3, ± σ) as a function of ethanol co-solvent concentration (% v/v) in HPFP.

Figure 4.2.1.1.2 – Van't Hoff plot of solubility (n=3, ± σ) *vs.* temperature for budesonide in HPFP co-solvated with 10 % v/v ethanol over the temperature range 278 to 303 K.

Figure 4.2.1.2.1 – Mean budesonide solubility (n=3, ± σ) as a function of ethanol co-solvent concentration (% v/v) in HFA134a.

Figure 4.2.2.2 – Van't Hoff plot of mean solubility (n=3, ± σ) *vs.* temperature for the compounds budesonide, TRIMEB, and the mix (budesonide / TRIMEB) in HPFP over the temperature range 278 to 308 K.

Figure 4.2.2.3 – ^{1}H NMR spectra of budesonide (a) and budesonide / TRIMEB complex (b) in HPFP expanded in the high field region showing budesonide A-ring chemical shift and multiplicity changes.

Figure 4.2.2.4 – ^{1}H NMR spectra of TRIMEB (blue) and budesonide / TRIMEB complex (red) in HPFP expanded in the region showing CD chemical shift changes.

Figure 4.2.2.5 – ^{1}H NMR spectra of budesonide (a) and budesonide / TRIMEB complex (b) in HFA134a expanded in the high field region showing budesonide A-ring chemical shift and multiplicity changes.

Figure 5.2.2.3.4 – White light image and Raman map of Seretide® Evohaler 250 (ACI plate 4) processed using DCLS component matching for fluticasone (green) and salmeterol (red).

Figure 5.2.2.3.5 – White light image and Raman map of Symbicort® 80/4.5 (ACI plate 4) processed using DCLS component matching for formoterol (green) and budesonide (red).

Figure 5.2.2.3.6 – White light image and Raman map of Symbicort® 160/4.5 (ACI plate 4) processed using DCLS component matching for formoterol (green) and budesonide (red).

Figure 5.2.3.1.1 – Diffraction patterns obtained for blank Mylar (grey) and reference preparation (black) shown with reference pattern positions for the simulated PXRD pattern for BDP anhydrate (WOYPAB).

Figure 5.2.3.1.2 – PXRD patterns over a 250 minute period (grey) of the emitted dose of QVAR® 100 pMDI device (160 actuations) collected in the modified second stage of the Copley TSI apparatus shown with reference BDP (black) and simulated pattern positions for BDP hydrate [blue (BCLMSN)].

Figure 5.2.3.1.4 – PXRD patterns over a 430 minute period (grey) of the emitted dose of Synasthmax® 100 pMDI device (160 actuations) collected in the modified second stage of the Copley TSI apparatus shown with reference BDP (black) and simulated pattern positions for BDP hydrate [blue (BCLMSN)].

Figure 6.1.1 – Representative laser diffraction PSD and X_{90}, X_{50} and X_{10} values for the micronised budesonide used in the preparation of the pMDI devices.

Figure 6.1.2 – SEM photomicrographs at x2 k (a), x5 k (b), x10 k (c) and x 15 k (d) of the micronised budesonide used in the preparation of the pMDI devices showing the micronised particulates of less than 5 µm dimensions and therefore suitable for formulation as suspended solids in HFA for pMDI delivery.

Figure 6.3.1.1 – Aerodynamic particle parameters for budesonide formulations prepared with (i) HFA134a (ii) HFA134a/EtOH (iii) HFA134a+TRIMEB and (iv) HFA134a/EtOH+TRIMEB.

Figure 6.3.2.1 – SEM photomicrographs of material deposited (ACI plate 4) from (a) budesonide in HFA134a shown, (b) budesonide in HFA134a / ethanol (10% v/v), (c) budesonide / TRIMEB in HFA134a and (d) budesonide / TRIMEB in HFA134a / ethanol (10% v/v) at magnifications between x5 and x20 k (specified in the data bar).

Fig 6.3.2.2 - SEM photomicrographs of material deposited (ACI plate 7) from (a) budesonide / TRIMEB in HFA134a and (b) budesonide / TRIMEB in HFA134a / ethanol (10% v/v) at magnifications between x4 and x10 k (specified in the data bar).

Figure 6.3.3.1 – Representative Raman spectra in the region 1800 and 500 cm^{-1} for six budesonide particles deposited on ACI stage 4 from (i) budesonide in HFA134a (blue) and (ii) budesonide in HFA134a / ethanol (10 % v/v) (purple) formulation compared to pure budesonide (red).

Figure 6.3.3.2 – Representative Raman spectra in the region 1800 and 800 cm^{-1} for five spheroid particles deposited on ACI stage 6 from budesonide / TRIMEB in HFA134a / 10% v/v formulation compared to (i) pure budesonide (red) and (ii) TRIMEB (blue) spectra.

Figure 6.3.3.3– Representative Raman spectra in the region 1800 and 1500 cm^{-1} for five spheroid particles deposited on ACI stage 6 from budesonide / TRIMEB in HFA134a / 10% v/v formulation compared to (i) pure budesonide (red) and (ii) TRIMEB (blue) spectra.

Figure 6.3.3.4 – Representative Raman spectra in the region 1800 to 800 cm^{-1} acquired on ACI stage 6 from pure HFA134a formulation showing instances of pure (i) budesonide (red); (ii) pure TRIMEB (blue) and; (iii) host / guest complex (black).

Figure 6.4.3.1 – Schematic illustration of the facilitation of Ostwald ripening processes by the inclusion of solubilising agents TRIMEB / ethanol (represented by an ellipse) in the pMDI preparations of budesonide.

List of Tables

1   Introduction

1.1   Aim

The overall aim of this study is to develop analytical methods to profile the physical chemistry of inhaled pharmaceutical products (IPPs) formulated in hydrofluoroalkane (HFA) propellants. Through development of novel analytical approaches, important product performance parameters such as solubility, solution speciation, and physical form (solid state and particulate forms post-deposition) will be obtained for the first time for these systems. Such insight will form the basis for development of formulation strategies for IPPs in HFA media and allow new approaches for more effective solubilisation and controlled deposition to be applied in concept formulations of IPPs.

The objectives for study, describing key stages towards the overall aim, were developed in the context of study and are described in Section 1.3.

1.2   Context for Study

1.2.1   Diseases of the Lung and Associated Responses

Active Pharmaceutical Ingredients (APIs) are commonly prepared as formulations for introduction directly into the lungs of humans. The physiology of the lung with its large surface area, moist mucosal membrane and excellent blood supply can be used as an organ for fast and efficient systemic delivery,[1,2,3,4] with advantages including the non-invasive nature of the route, increased speed of uptake *via* the thin epithelium[5] and reduced metabolism compared to delivery *via* oral routes.[4] Recent research is

showing particular interest in the delivery of peptides and proteins in this manner, as it avoids the necessity for injection (providing cost and patient adherence benefits) and metabolism in the gastro-intestinal tract (though there are metabolic enzymes present in the lungs).[4] A recent example is the treatment of diabetes mellitus by the administration of adenosine deaminase or insulin *via* the lung.[6,7]

The most widespread group of therapeutics delivered to the lung are however locally acting topical medications used in the direct treatment of lung diseases.[8] A recent review by Ritchie *et al.* identifies 81 marketed respiratory drugs at the time of writing (2009), of which 29 are administered to the lungs directly for topical treatment of respiratory diseases.[9] The low concentrations needed for significant therapeutic effect can aid in the minimisation of systemic concentrations (hence side effects) and the onset of action is rapid. They are used in the treatment of diseases such as cystic fibrosis, pulmonary arterial hypertension and infectious pulmonary diseases, but are used most extensively in the treatment of chronic obstructive pulmonary disease (COPD) and asthma and are the mainstay treatments for these indications.[10] These two diseases are considered to be causes of substantial worldwide social and economic burden through morbidity and mortality.[11] Asthma treatments have progressed enormously over recent years and its management with traditional and newer drugs in various dosage forms has led to greater control of symptoms.[12] Conversely, COPD currently has less effective treatment regimes, and there have been fewer advances in development of successful drug therapies. Worldwide, it is the only cause of mortality that is continuing to increase in prevalence.[13]

The two diseases are frequently categorised together as they are both chronic inflammatory disorders causing bronchoconstriction, and until recently their distinction has been broadly in the reversibility (or lack) of the airflow obstruction caused by the disease: asthma being considered reversible and COPD not so.[14] More recently however, the pathophysiology of the diseases has become better understood, and statements including these characteristics have been developed to define the diseases:

The Global Initiative for Asthma (GINA) states that Asthma is classed as a chronic inflammatory disorder of the airways in which many cells and cellular elements play a role. The chronic inflammation is associated with airway hyperresponsiveness that leads to recurrent episodes of wheezing, breathlessness, chest tightness and coughing and is usually associated with widespread airflow obstruction within the lung that is often reversible either spontaneously or with treatment.[14] The inflammation is persistent in asthma affecting all airways including the upper-respiratory tract and the nose, though the effects are most pronounced in the medium sized bronchi.[15] The symptoms occur in episodes, with the presence of inflammatory cells having been detected including mast cells, eosinophils, T-lymphocytes and dendritic cells,[15] though a recently published review by Barnes[16] concludes that greater than 100 mediators are involved in the complex inflammation processes.

The Global Initiative for Chronic Obstructive Lung Disease (GOLD) states that COPD is characterised by persistent airflow limitation associated with an enhanced and abnormal chronic inflammatory response in the airways and the lung to noxious particles or gases. It is usually progressive though is

classed as a preventable and treatable disease.[11,17] COPD is also characterised by systemic inflammation thought to be a cascade effect from the inflammation in the lung mediating circulatory inflammation cells and cytokines including neutrophils, T-lymphocytes and eosinophils.[18] The diagnosis of and differentiation between the two diseases is difficult. Asthma usually has its onset early in adolescence, however does have instances of adult onset.[15] COPD is typically diagnosed in patients in their fifties and sixties[14] and is primarily a disease of smokers in first world countries, though exacerbations are frequently observed in developing countries caused by pollution and working environment.

The treatment of asthma and COPD is wide ranging, and includes avoidance of allergens, cessation of smoking and exposure to other toxic entities in addition to pharmacological approaches. Studies have included administration of theophylline,[19,20] broad-spectrum antibiotics,[21] mediator antagonists,[22,23] influenza vaccines,[24-26] oligonucleotides,[27] dietary antioxidants[28,29] and immunomodulators such as methotrexate[30,31] and newer biological TNF inhibitor treatments (adalimumab and etanercept).[32,33] By far the most prevalent form of pharmacological control however is in the use of inhaled corticosteroids as anti-inflammatory agents, β_2 adrenoceptor agonist compounds (bronchodilators) and antimuscarinic (anticholinergic) bronchodilators prescribed in isolation or in combination.[14] A brief review of each in the context of the formulation of these materials into usable products is given in Sections 1.2.1.1 to 1.2.1.4.

1.2.1.1   Inhaled Corticosteroids (ICS)

ICS compounds act in asthmatic patients to suppress the inflammation in the airways and their use is widespread and successful.[34] They are recommended as the first line therapy for all patients with persistent asthma and they are shown to be effective in controlling symptoms in patients of all ages and severity.[15] Their use in COPD treatments is, however, more controversial, and recent findings suggest they have no effect on the pulmonary inflammation associated with this condition.[14] Their action is in diffusion across cell membranes, binding to glucocorticoid receptors in the cytoplasm and inhibiting the recruitment of inflammatory cells in the airways, including eosinophils, T-lymphocytes and mast cells. They have a rapid effect on the suppression of mucosal inflammation.[35] Steroid compounds have been and continue to be given systemically in some asthma treatment regimes particularly in hospital emergency department early treatments,[36] but the inhaled approach is the mainstay of routine management.[14] Commonly used ICSs include beclomethasone dipropionate (BDP), budesonide, fluticasone propionate, mometasone furoate, hydrocortisone and flunisolide, delivered to the lung *via* pressurised metered dose inhalers (pMDI), dry powder inhalers (DPI), nebulisers and nasal sprays.[37] The compounds have relatively high molecular mass[9] and tend to be lipophilic in nature, with low aqueous solubility.[38,39] They are broadly speaking formulated as suspensions[40,41] or solutions for certain products such as BDP[42] and flunisolide[43] in modern propellant and aqueous based devices for dosing to the lung, as well as in solid form in DPIs.

1.2.1.2 β₂ Adrenoceptor Agonist Compounds (β₂ Agonists)

β_2 agonists act in the airways of patients with asthma and COPD by binding

to the β_2-adrenoreceptors present in a number of airway cells, with their

major site of action thought to be in the smooth muscle surrounding the

bronchi and bronchioles.[44] Their action is in the signalling cascade triggering

a number of events contributing to the relaxation of the muscle post-binding

activity;[14] this is primarily in the stimulation of the enzyme adenylate cyclase

causing the increased production of cyclic adenosine monophosphate

(cAMP), leading to relaxation of the smooth muscle and bronchodilation. The

development of isoprenaline in the 1960s was the first to be studied

extensively,[45] though acting on β_1 and β_2 adrenoreceptors it had little β_2

selectivity.[14] The development of short acting β_2 agonists (SABA) such as

salbutamol and terbutaline gave marked improvements in reducing

associated side effects and more recently long acting β_2 agonists (LABA)

such as salmeterol xinafoate, formoterol fumarate and bambuterol have

become commonly used treatments. There is an intense drive for

pharmaceutical companies to develop new LABAs with increased duration[46]

and hence reduction in dosing frequency leading to increased patient

adherence.[47] Indacterol is a compound marketed by Novartis, recently

approved for use in COPD control and termed an ultra long acting β_2 agonist

(uLABA) due to its once daily dosing requirement. The compounds exhibit

different physico-chemical characteristics and these are thought to have a

significant effect on their pharmacodynamics in the body.[48] A review by

Anderson *et al.*[48] proposes that the difference in polarity (logP) of

salbutamol, formoterol and salmeterol (SABA, LABA and LABA respectively) is one of the key reasons they have different durations of action.

1.2.1.3 Antimuscarinic (Anticholinergic) Bronchodilators

Antimuscarinic bronchodilators are used in the control of the resting tone of the bronchial smooth muscle, which in cases of COPD is increased and is a cause of bronchoconstriction. The inhaled compounds block the cholinergic receptors (hence the synonym anticholinergic).[44] These agents are administered through the inhaled route avoiding systemic side effects associated with other anti-muscarinic receptors found in many other areas of the body. They are available in short and long acting forms *i.e.* short acting muscarinic antagonists (SAMA) and long acting muscarinic antagonists (LAMA). Currently available preparations of inhaled muscarinic antagonists are ipratropium bromide (SAMA) and tiotropium bromide (LAMA).[14] LAMAs are approved and used in the treatment of COPD but not currently asthma. They are considered less useful in asthma patients than LABAs,[14] though studies by Magnussen *et al.*[49] have shown benefits of tiotropium in patients with concomitant COPD / asthma and Fardon *et al.*[50] have noted improvements in patients administered with tiotropium and an ICS (fluticasone) in combination. Recently developed LAMAs include glycopyrrolate in its racemic and pure (R,R)- form (Novartis)[51] and aclidinium bromide (Menarini).[52,53] The quaternary ammonium substructure common to all LAMAs delivered *via* inhalation serves to promote hydrophilicity and limit systemic adsorption, hence side effects.[54]

1.2.1.4 Combination Products

Management of asthma and COPD is a complex process, with different approaches being used by clinicians that are dependent on many variables, not least the presence of asthma or COPD or both concomitantly. Management has moved from the treatment of bronchoconstriction using SABA / LABA, to ICS, and more recently has used a combination of the two to act on bronchoconstriction and inflammation together.[55] Recent studies have shown that the administration of an inhaled ICS in combination with a LABA is more effective than increasing the dose of the ICS alone.[55,56] Further studies by researchers including Papi *et al.*[57] and Britton *et al.*[58] have concluded that the delivery of the ICS and LABA together have a synergism, increasing the therapeutic effect seen in doses administered sequentially from separate devices. These combination products are available in the form of Advair® / Seretide® (fluticasone propionate and salmeterol xinafoate) and Symbicort® (budesonide / formoterol fumarate) inhalers (GlaxoSmithKline and AstraZeneca respectively). It is now understood that there are important molecular interactions between these two classes of drugs in that LABAs may affect glucocorticoid receptors enhancing the anti-inflammatory effect of the ICS, and the ICS enhance the β_2 agonist effect, reversing the uncoupling of β_2 receptors occurring in response to inflammatory mediators.[14]

1.2.2 Delivery to the Lung

Successful delivery of drugs to the lung in an efficacious, accurate and precise manner is heavily dependent on the API, the formulation and the

delivery system.[59] The system is required to aerosolise the API in the correct particle size distribution to reach the desired region of the lung,[60] and it must do so in a precise manner so as to provide an accurate dose time after time.[61] It is broadly accepted that the aerodynamic particle size must be < 5 μm to achieve successful deposition in the airways of the lung, with particles > 5 μm tending to be deposited in the oropharynx and swallowed. Particles of between 1 and 5 μm will deposit in the large and conducting airways whilst those < 1 μm are likely to reach the peripheral airways / alveoli or be exhaled.[62,63] It is however important to consider the mode of action for the therapeutic agent in question and where the optimum deposition may be for that particular medication. As discussed (Sections 1.1.1 to 1.1.3) there are three principal types of therapeutic agent for the treatment of asthma and COPD (i) ICS (ii) β_2 agonists and (iii) antimuscarinic bronchodilators. It is known that airway smooth muscle predominates in the trachea and small airways and the β_2 receptors are primarily located in the small airways and alveoli.[64,65] Airway inflammation is however present throughout the respiratory tract, though the peripheral airways demonstrate these effects the most.[66] It follows that different particle sizes and hence deposition regions may be required for different treatments, with ICS treatments potentially requiring particles in the range 1 to 5 μm to reach the peripheral airways and upper regions, whilst β_2-agonists and antimuscarinic bronchodilators would be required in the upper range to allow deposition in regions of both smooth muscle and β_2 receptors.[64,67] The depositions discussed occur through three principal mechanisms (i) inertial impaction (ii) sedimentation and (iii) Brownian motion / diffusion,[62] though further work by Gonda[68] suggests that

9

two further processes, interception and electrostatic precipitation, occur particularly when the aerosolised particles are very small (< 1 μm). Inertial impaction occurs at bifurcations of the bronchial tree, particularly in the large central airways, when particles with high inertia are unable to follow the airstream and impact on the airway wall. Sedimentation is a product of a particle's mass and residence time allowing smaller particles to sediment during breath holding / slow breathing, highlighting the importance of defined device instruction and patient adherence. Both impaction and sedimentation predominate in aerosol therapies between 1 and 10 μm.[62] Diffusion is only thought to occur for particles < 1 μm and is often overlooked for inhaled therapies, though this may be of consequence for more modern devices with mass median aerodynamic diameters (MMAD) approaching the lower size in the range.[69]

Three principal types of medical device exist for the purpose of aerosolising APIs and introducing them to the lung (i) nebuliser systems (ii) dry powder inhaler (DPI) devices and (iii) pressurised metered dose inhaler (pMDI) devices. Nebuliser systems transfer solutions or suspensions of therapeutic agent into breathable aerosols that are subsequently breathed in to the lung, usually under normal tidal breathing. DPI devices act by transferring dry particles of API (and excipient) to the lung by a breath actuated mechanism and pMDI devices create an aerosol of medication using a volatile propellant subsequently breathed in to the airway after activation of the device. Each has their advantages and disadvantages, and an overview of each device is given in Sections 1.2.2.1 to 1.2.2.3.

1.2.2.1 Nebulisation Devices

These devices are summarised as those that transfer solutions or suspensions of a medication into a breathable aerosol ready for introduction to the lung during tidal breathing. Nebulisation devices have been used in the delivery of drugs to the lungs for many years, with the first hand powered systems being developed in the mid-19th century, later becoming electrical devices in the 1930s.[70,71] Much research and development has been performed since these initial devices leading to an efficacious means of drug delivery in modern incarnations of the apparatus. Figure 1.2.2.1.1 shows a schematic representation of a typical nebulisation device (pneumatic type) whereby a compressed gas source is fed into a reservoir of the formulated API producing a breathable aerosol fed to the patient *via* a mouthpiece.
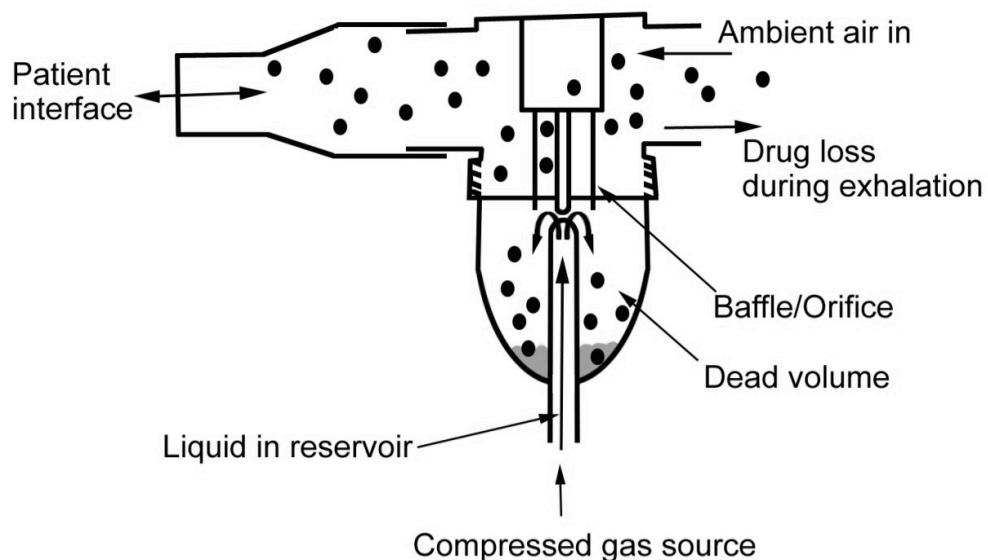
Figure 1.2.2.1.1 – Schematic representation of a typical pneumatic type nebuliser device.[61]

Two principal types of nebulisers are utilised in modern medical practice with the aforementioned pneumatic devices being the first (and most common) and ultrasonic devices the second. Compressed gas nebulisers introduce a compressed gas through a nozzle causing negative pressure drawing liquid up the tube and incorporating it into the gas stream. This is then sheared into the gas stream and broken into droplets by surface tension forces.[72] Ultrasonic nebulisers generate high frequency waves from electrical energy that are passed to the surface of the formulated solution to create an aerosol. Aerosol delivery is then typically by fan or using the patient's inspiratory flow. The design of both types of device and the incorporated formulation is primarily focussed on the production of droplets in the respirable range of 1 to 5 µm to ensure delivery to the lower airways and maximise efficacy. Although this type of introductory system is being used less in light of the increased use of pMDI and DPI devices, it remains extremely important in the administration of medications in selected patient groups; specifically those who are too ill or too young to use pMDI / DPI devices. In addition to this, nebulisers do offer several other advantages over other devices, namely large dose administration over extended time periods and the removal of patient coordination requirements that are so essential with pMDI and DPIs.[70] They are however far less portable, have a significantly longer set up and administration time and have a higher cost associated to the hardware. They may also require the availability of compressed gases (air / oxygen) for their operation, all of which tends to restrict their use to patients treated in hospital or *via* home-based protocols.

A related device is the aqueous droplet inhaler (ADI), also referred to as solution metering or soft mist inhalers. These are relatively new portable devices designed to overcome some of the problems associated with DPI and pMDI devices, namely the coordination difficulties for users and the low lung deposition values sometimes achieved. They are similar in design to pMDIs but lack the volatile propellant. They dose a precisely measured liquid (most commonly water or ethanol based) to generate an aerosol in a mechanical (or electromechanical) manner, or *via* fine nozzle systems through which the formulation is forced. They offer a high respirable fraction when compared to DPI and pMDI devices,[73,74,75] though their commonly used aqueous formulation base has led to questioning of their microbial safety and stability in the case of multi-dose devices where material is stored in a reservoir.[69,74] Examples of the ADI in current use that rely on (i) soft mists formed by converging jet technology and (ii) electrostatic energy to produce a fine mist are Boeringer Ingelheim's Respimat® and Battelle's Mystic® devices respectively.[77]

1.2.2.2 Dry Powder Inhalers (DPI) Devices

DPI devices typically comprise API and a carrier particle, most commonly a sugar such as lactose, stored in a capsule or a proprietary blister type arrangement (incorporated into the device) punctured or released prior to actuation. These breath-actuated devices have been in existence in various forms since the first patented example in the 1860s, however major developments in the familiar multi-dose portable devices has been prevalent since the early 1960s.[61]

These devices require a strong inhalation from the patient *via* the mouthpiece to administer the dose to the lung post actuation of the device *i.e.* a short and powerful intake of breath. It is here where the most significant disadvantage to the DPI device lies, as patients suffering from diseases affecting the lungs can find this process too strenuous to successfully inhale an efficacious dose. Other disadvantages include high deposition in the throat and the upper airways such as tracheal regions of the lung and the necessity to keep the device and its contents dry; moisture and increased exposure to atmospheric humidity can cause powder clumping and reduced fine particle mass on actuation. Modern DPI devices exist in three major forms (i) capsule devices whereby individual capsules are loaded and punctured prior to each actuation (ii) multiple unit dose inhalers using an integral blister pack that punctures / peels individual blisters prior to actuation and (iii) reservoir devices using a reservoir of formulated API from which each dose is taken at actuation.[70,78,79] Many major pharmaceutical companies have their own proprietary technologies covering these three types of devices for example the Aerolizer® (Merck), the Accuhaler® (GSK) and the Turbuhaler® (AstraZeneca) respectively. A schematic of a reservoir type device is shown (Figure 1.2.2.2.1).
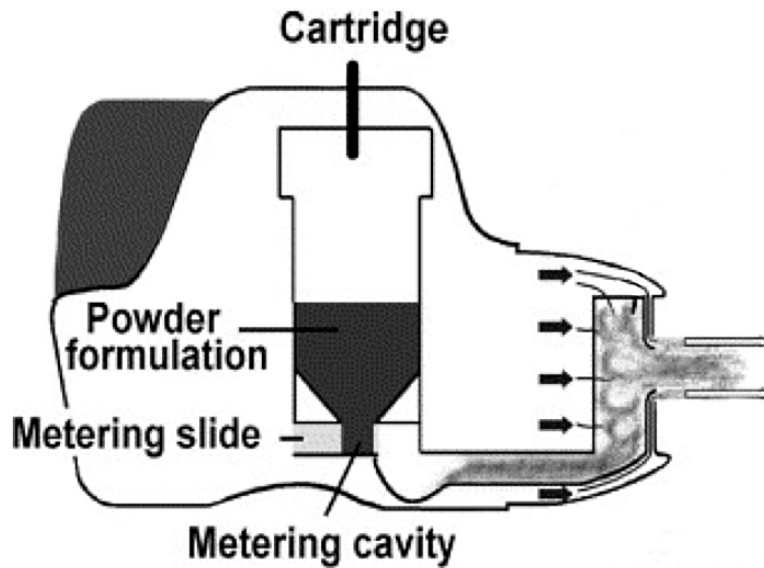
Figure 1.2.2.2.1 - Schematic representation of a reservoir type DPI device.[80]

1.2.2.3 Pressurised Metered Dose Inhaler (pMDI) Devices

pMDI devices are a more recent approach to the delivery of drugs to the lung, and as such have only been in development since the 1950s when the first device of this type was developed at Riker Laboratories (3M) using cold fill technologies and new metering valves first applied in the Medihaler-iso (isoprenaline) and Medihaler-epi (adrenalin) devices launched in 1956.[79,81] The devices consist of a suspension / solution of API in a volatile liquid propellant contained within a pressurised canister, often with the addition of one or more surfactants to the formulation chosen to aid in stability or to manipulate performance. Metering valves are used to form a controlled dose of formulated API in a fine atomised spray over *ca.* 100 to 200 milliseconds on actuation of the device, which is subsequently inhaled by the user. Figure 1.2.2.3.1 shows a schematic representation of a typical pMDI device.
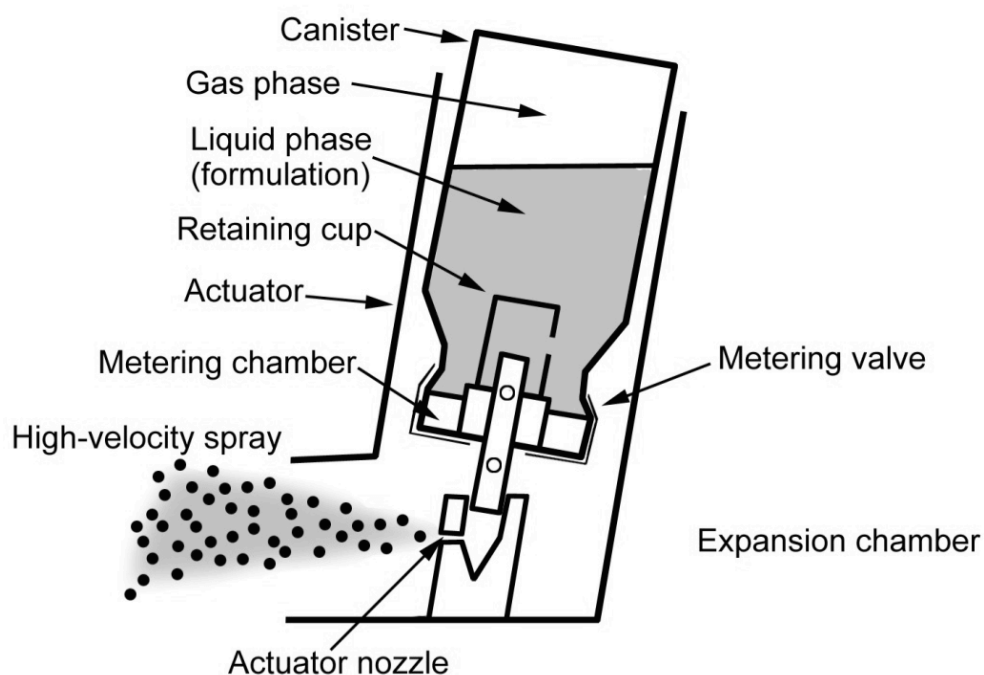
Figure 1.2.2.3.1 – Schematic representation of a typical pMDI device.[61]

pMDI devices are considered advantageous due to (i) their small size and portability providing benefits over nebulisation systems (ii) the cost of production being relatively low and (iii) their containment of multiple doses. They also offer the user a breathable aerosol, do not require a significant inspiratory flow as with DPI devices (beneficial for users with reduced lung efficiency) and are not as susceptible to humidity and moisture exposure.[82] They are considered disadvantageous in some respects however leading to high deposition in the mouth and throat owing to their relatively large droplet production and high particle velocity at the mouthpiece,[4] though newer devices have improved this significantly as discussed in Section 1.2.3. Patient coordination also remains a problem, requiring inhalation and activation of the device to be timed accurately by the user.

1.2.3 pMDI Formulations; Chlorofluorocarbons (CFC) and Hydrofluoroalkanes (HFA)

Historically, the use of chlorofluorocarbons (CFCs) in these devices was commonplace; however since the phasing out of these propellants under the Montreal Protocol (Substances that Deplete the Ozone Layer)[83] in 1987 alternatives have been sought in the form of hydrofluoroalkanes (HFAs).[1,2,3,61] The drive to reformulate using HFAs has been slower than anticipated, and has not been simply a switching from CFCs to HFAs as was initially predicted.[84] The two most common propellants used in the formulation of pMDIs in modern pharmaceutics are 1,1,1,2-tetrafluoroethane and 1,1,1,2,3,3,3-heptafluoropropane, HFAs 134a and 227 respectively. The transition to these propellants is well underway, and should be essentially complete in developed countries at the time of writing.[84] The change has involved replacement of the materials used in the valves and canister linings of pMDI devices, and it has been found that excipients used in CFC preparations are not necessarily applicable in HFAs.[85] The final reformulated products have not only led to more environmentally acceptable products, but also more efficient ones, generally producing aerosols with smaller particle sizes aiding with deposition in the deep lung and reducing oroparyngeal deposition, hence more efficacious medications at equivalent doses compared to CFC formulations with reduced systemic side effects.[61] Figure 1.2.3.1 shows a representation of the deposition profiles of the SABA salbutamol from CFC and HFA pMDI formulations taken using lung scintigraphy, clearly highlighting the reduced oropharyngeal deposition and concomitant increase in deposition in the lung.[86]
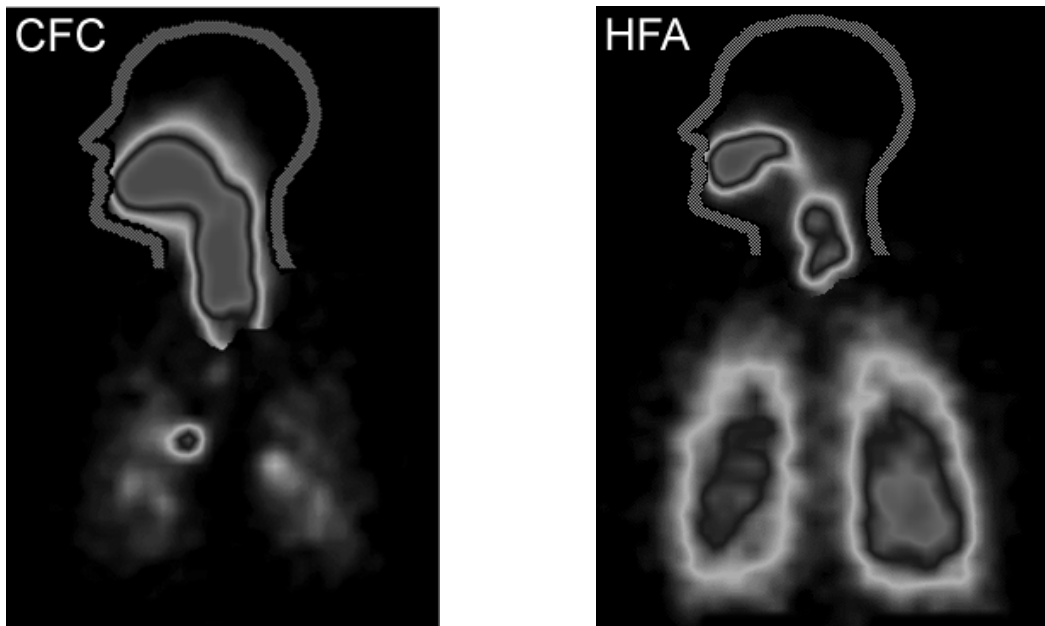
Figure 1.2.3.1 – Representative deposition profiles showing the increased lung / decreased oropharyngeal deposition in HFA *vs*. historic CFC based formulations.[86]

Many studies have been performed to verify these characteristics and delivery improvements have been observed using both *in-vitro* and *in-vivo* measurements. *In-vitro* studies by Leach *et al*.[69] noted a reduction in oropharyngeal deposition from between 90-94% to 29-30% for a CFC preparation of the ICS beclomethasone dipropionate (BDP) *vs.* the preparation in HFA134a, with a corresponding increase in lung deposition of 55-60% *vs.* 4-7% for the CFC. Similar results were published by Cheng *et al*.[86] and Chuffart *et al*.[87] in their studies of the SABA compound salbutamol. Chuffart reported an increase from 33-55% for respirable particles from an HFA based formulation *vs.* those from CFC (multi-stage liquid impingement) and Cheng an increase from 16-24% from CFC to HFA based formulations, with corresponding decrease in deposition in the oropharynx from 78-56%. Pharmacokinetic / pharmacodynamic (PKPD)

studies of salmeterol and the ICS flunisolide by Kempsford *et al.*[88] and Nolting *et al.*[89] respectively have demonstrated lower systemic uptake of the drugs delivered from HFA *vs.* CFC based formulations, with lower maximum concentration (C_{max}) values observed in each case. In slight contrast, work by Goldberg *et al.*[90] showed the SABA and LABA compounds fenoterol and formoterol to have little effect on the symptoms of asthmatics (Forced Expiration Volume, FEV) when administered from formulations using HFA and CFC in direct comparison. Busse *et al.*[91] however demonstrated a significant benefit in *in-vivo* trialling of the ICS BDP at equivalent doses in HFA *vs.* CFC, and concluded that 2.6 times the dose in CFC would be required to achieve the same improvement in FEV. A similar study using HFA and CFC prepared BDP by Micheletto *et al.*[42] used bronchial response to metacholine to model clinical efficacy and concluded a significantly reduced therapeutic dose in HFA was needed for clinical asthma management.

It appears to be generally accepted that the HFA formulations bring about reduced oropharyngeal deposition *vs.* CFC and a concomitant increase in the respirable dose.[69,86,87,88,89] What is less clear is the effect this has on real patients *in-vivo* with studies showing little difference in the FEV for treatments with β-agonist compounds,[90,92] though a marked difference when using ICS compounds is observed.[42,91] Consideration of these findings seems consistent with the therapeutic effect of the different classes of compounds. These are discussed in more detail (Section 1.1.5), however in summary the reduced particle size of HFA based formulations is likely to have more benefit for ICS compounds, leading to deposition in the peripheral airways where the most significant inflammation occurs.[66] Antimuscarinic bronchodilators and

β_2 agonists targeting the smooth muscle and β_2 receptors present in the trachea, small airways and alveoli may have less benefit from the reduced aerodynamic particle size brought about by the reformulation in HFAs.

1.2.4   Critical Characteristics of HFA pMDIs

The reformulation of inhaled products in HFA based preparations has brought about the general increase in aerodynamic performance *in-vitro* and *in-vivo* as summarised in Section 1.1.3.1. These improvements have been largely attributed to lower initial spray velocity, rate of initial droplet evaporation, and the formation of initial droplet sizes, and how they differ in HFA *vs.* CFC preparations.[86] In this sense, the behaviour and subsequent performance of the pMDI preparations of IPPs is strongly dependent on the propellant characteristics particularly in terms of (i) their volatility / vapour pressure in combination with the device and (ii) their solubilising capacity for the drug(s), and potentially excipients, in question.[93] The use of HFA134a and HFA227 post the adoption of the Montreal Protocol are essentially fixed as these are the only two propellants to date to have undergone toxicology testing and gained approval. It is interesting to note that no low volatility propellants are approved for modification of vapour pressure as with the historic CFC based systems where trichlorofluoromethane and dichlorotetrafluoroethane (CFC-11 and -114) could be used to reduce the vapour pressure of dichlorodifluoromethane (CFC-12) as required. The physical properties of the new HFA preparations are then less easy to control, with the addition of excipients such as glycerol or polyethylene glycol the only means by which to control volatility. The use of these excipients may also be limited by solubility.[84,94,95]

The solubility of the drug in HFA based media is of paramount importance in the design and behaviour of pMDI devices. A solute dissolves in a solvent until the solution is saturated; this saturation is an equilibrium, with the dissolved solute in equilibrium with the undissolved solute.[96] This equilibrium solubility will be defined for a given solute in a given solvent at a given set of conditions (temperature / pressure) and will define the type of formulation that can be prepared for a pMDI. The solubility levels of the IPPs used tends to be very low (of the order of low µg/mL) meaning suspension based formulations are common, though strategies are often employed to increase the solubility using excipients and / or co-solvents such as ethanol[97,98] discussed later in this section. Other work has been performed modifying the IPP to produce salts to improve solubility[99,100] and a study by Seville *et al.*[101] has investigated the possibility of delivery of salbutamol as a prodrug with complete miscibility in HFA134a (compared to very low solubility in its normal form) that is metabolised in lung homogenates by esterase to liberate salbutamol *in-vivo*.

Formulations of pMDIs are then often classified as two distinct types (i) suspensions and (ii) solution preparations and they exhibit markedly different properties.

Suspension formulations are most commonly prepared using material micronised to particulates of respirable size (between 1 and 5 µm) before addition to the HFA.[93] These suspensions are commonplace, as IPPs tend to have low solubility in HFA propellants and fit well with this strategy. They do however suffer from stability issues including (i) creaming, whereby particles of IPP being less dense than the HFA propellant form a cream like

layer which floats on the propellant[102] (ii) sedimentation, where particles more dense than the propellant sink and (iii) flocculation, where differences in hydrophillicity / hydrophobicity between the propellant and the IPP may lead to flocculation or deposition on the canister walls.[103,104] All of these factors can lead to problems with emitted dose variability.[105] Correct patient use of these devices with prescriptive shaking and orientation is essential for reproducible dosing.[106,107] Excipients have been used to control these problems, with historic CFC preparations using oleic acid, sorbitan trioleate and soya lechtin to promote suspension stability, though the solubility of these excipients in HFAs is too low to make their transfer a useful option.[108] This has led a drive to investigate HFA compatible excipients, with oligolactic acids (OLAs) used as suspension stabilisers, and acylamide acids / mono-functionalised M-PEGS showing promise for further evaluation as solubility enhancers. Stefely *et al.*[85] show a small but significant improvement in the solubility of amine containing entities using this approach in HFA134a / ethanol systems.

Partial solubility of the IPP can also lead to stability problems in the form of the Ostwald ripening phenomenon. Ostwald observed in the early part of the 20th century that a saturated solution of a compound containing small and large crystals is supersaturated with respect to the large and undersaturated with respect to the small particles.[109] Solubility is increased for smaller particles through surface to volume ratio effects (Gibbs-Thompson Effect), hence over time the smaller crystals dissolve and the larger crystals grow *i.e.* Ostwald ripening.[110,111,112] This can have significant effects on the concentration, and most importantly, the crystal size of API in solution over

time, which can clearly have a detrimental effect on aerosolisation characteristics.[113,114]

Solution formulations are those which completely solubilise the IPP in the HFA based propellant. These have benefits in terms of homogeneity and reproducibility of delivered dose. Physical stability can also be improved with the avoidance of Ostwald ripening, sedimentation, flocculation and creaming effects described earlier for suspension approaches, though if they are near their limit of solubility at the formulated concentration, precipitation can occur as moisture slowly ingresses the system.[108] Increased chemical instability has also been noted.[115] For solution approaches to be feasible, the drug must have sufficient solubility in the propellant to allow delivery of a therapeutically appropriate dose in a small number of actuations.[116] As the solubility of the IPPs tends to be very low,[108] this is often a difficult situation to reach. Certain historic CFC preparations were prepared as solutions with the addition of excipients as flavours or anti-oxidants.[93] Strategies to achieve a solution pMDI often require the addition of further excipients / co-solvents to increase the solubilising capacity of the propellant. Mixed HFA / ethanol systems form the basis of several studies[108,117,118] and recent commercial products have been approved such as QVAR® / Sanasthmax®, (Chiesi) using HFA134a / ethanol / glycerol to produce a solution pMDI of BDP, and Aerospan® solubilising flunisolide in HFA134a / ethanol (Acton). Other strategies for producing solutions include the addition of further excipients in the formulation. Evans *et al*.[21] studied the formation of micelles in CFC based systems using lecithin and approaches using soya phosphatidylcholine in CFC blends has been investigated by Labiris *et al*.[59]

Studies in HFAs are less widely reported however, though work has been described recently by Stefely *et al.*[85] using acylamide acids and mono-functionalised M-PEGS to increase solubility of albuterol in HFA134a and HFA134a / ethanol mixtures, noting significant solubility increases of up to 30 x (1.5 % w/w). Williams *et al.*[119] have reported the use of cyclodextrins in HFA134a based suspension formulations of aspirin and their effect on the stability of the systems. Similarly Steckel *et al.*[120] have investigated the use of derivatised cyclodextrin in the stabilisation of the ICS compound budesonide in HFA134a / ethanol / polyethylene glycol (PEG) mixtures. Their work uses CDs to stabilise budesonide suspensions produced from solutions of the drug *in-situ* in a pMDI and shows promise in delivering higher fine particle fraction (FPFs) and lower mass median aerodynamic diameters (MMAD). They do not however assess the solubility changes imparted by the inclusion of CD in the system and this may have a significant effect on the potential for promoting the Ostwald ripening effect through marginal increases in solubility.

There are stability and homogeneity advantages inherent in the complete solubilisation of IPPs in pMDI formulations. As summarised, strategies using co-solvents and other excipients show promise in this area, and systematic study of relevant IPPs using such strategies is warranted. Work presented later in this thesis aims to investigate the physical chemistry occurring in the addition of ethanol co-solvents and cyclodextrins as solubility enhancers in HFA propellants.

In addition to the stability and dose variability issues discussed, a further key difference in suspension and solution based pMDI formulations are the solids

delivered from the device on actuation. Suspension pMDIs limit the emitted droplet size with the size of the particles suspended. The particles emitted are in general different in size from the primary particles used in the formulation.[68] Their size is dependent on the size of the droplet formed on actuation, the number and size of the particles this contains, and the presence of non-volatile excipients if present. These variables were summarised in a recent study by Stein *et al.*[121] seeking to develop new prediction models for aerodynamic particle size distribution (APSD) of suspension pMDI formulations. Solution pMDIs produce particles *in-situ* on actuation of the device. Once atomised, the droplets undergo rapid evaporation of the propellant and particles are formed. Their size depends on the droplets formed initially as they are homogenous solutions of solubilised IPP (large droplets forming larger particles, small forming smaller particles), a parameter that is controllable using the actuator design (valve size), vapour pressure of the propellant and non-volatile excipients.[116,121] As the process is rapid it tends to lead to the formation of smaller, spherical particles.[121]

1.3   Strategy for Study and Key Objectives

As highlighted, the characteristics of IPPs in HFA propellants are of paramount importance in understanding the behaviour and performance of these systems. Much research has been performed on the aerodynamic performance of the devices, including the assessment of product improvements post phasing out of CFCs and adoption of HFA propellants as summarised in Section 1.2.3. However, with a few notable exceptions the physical chemistry of these pMDI formulations is poorly understood. The studies presented in this thesis aim to develop novel approaches using

modern analytical techniques to access information on the properties of the formulations both *in-situ* and post actuation of the device. These approaches are in two distinct areas (i) analytical methodologies based around the *in-situ* characterisation of IPPs in solution *i.e.* the solubility and physical chemistry of the IPP in the formulation and (ii) solid state studies on the materials post actuation of the pMDI device for the study of physical form, morphology and distribution.

1.3.1 Solution Studies

As summarised, the solubility of drug in the propellant system is an essential parameter to ascertain formulation strategies (solution *vs*. suspension). Methods to assess solubility in volatile propellants with and without excipients / co-solvents is complicated by their gaseous nature at ambient conditions, and analysis by conventional means is very challenging. Approaches using filtration and off-line analysis using chromatographic techniques have been studied by Traini *et al.,*[100] Dalby *et al.,*[122] Williams III *et al.*[123] and Myrdal *et al.*[124] Although elegant, these approaches are time-consuming in the preparation and equilibration of pMDI canisters, use relatively large amounts of expensive drug in doing so, and can suffer large cumulative errors in the processing steps involved. The approaches investigated and presented in these studies focus on quantitative nuclear magnetic resonance (qNMR) as a method of analysing the above systems and aim to highlight for the first time the advantages provided by analysis *in-situ*. Primarily, the analysis of systems *in-situ* at pressure using qNMR allows the determination of solubility in true dynamic equilibrium *i.e.* with partitioning between solution and solid phase without the removal of solids from the system. The filtration based

26

methods summarised[100,122,123,124] do not allow for this. Secondly, the ease with which NMR can be operated at variable temperatures (VT-NMR) allows experiments to be performed to access the thermodynamics of the systems under study through data manipulated using van't Hoff approaches. Thirdly, structural data inherent in the NMR spectra recorded provide further insight into the systems under study, not previously available and lost when using off-line methods.
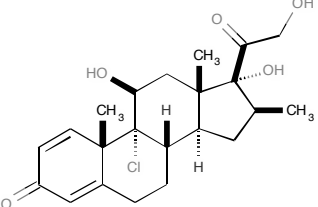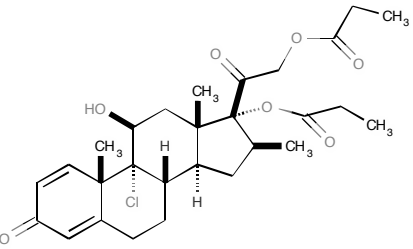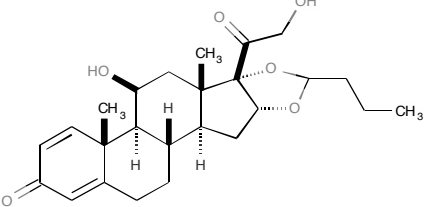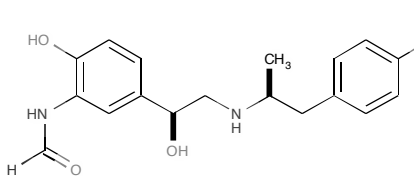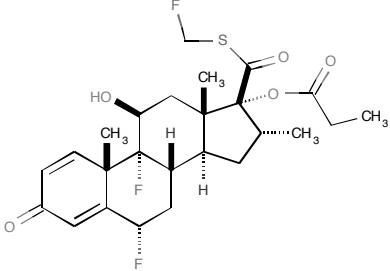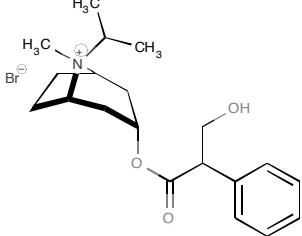
Additional benefits to the NMR approach include (i) ease of sample preparation using very small quantities of drug; saturated suspensions can be transferred to conventional NMR tubes for liquid based samples (studies in model propellants), with cold transfer and pressurisation allowing preparation *in-situ* of the volatile propellants HFA134a and HFA227 and (ii) residual solids in prepared solutions will not affect the measurement being performed.* Only material dissolved in solution will give rise to a signal in the NMR experiment, therefore removing any need for pre-filtration steps as with other techniques and (iii) preparation and equilibration of the samples is considerably less labour intensive than pressurised filtration based methods, and automation of NMR acquisitions can lead to significant time-savings. *Residual solids in the NMR solution should not affect the quantitative response of the approach, however it is appreciated that the solid content of the sample preparation may lead to line broadening effects and a resultant loss in resolution / sensitivity from distortion of the local magnetic field.[125]
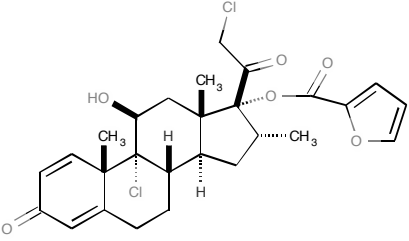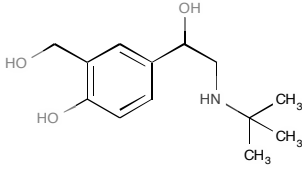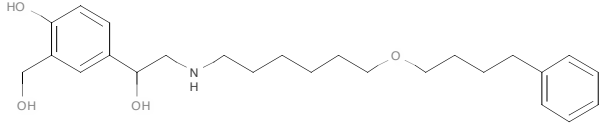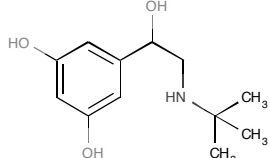
It is the objective of these studies to develop and validate a robust and efficient qNMR methodology capable of determining solubility of IPPs in the volatile HFA propellants used in current pMDI formulations. The method will

be used to ascertain solubility of IPP compounds chosen to represent a broad range of currently available ICS, β_2-agonist and antimuscarinic brochodilator compounds in model propellant HPFP and HFAs 134a and 227. An overview of these compounds and their chemical structures is provided in Table 1.3.1.1.

Table 1.3.1.1 – Summary of the classification and structures of the ICS, β_2-agonist and antimuscarinic bronchodilator compounds under study.

Compound	Classification	Compound Structure
Beclomethasone	ICS	
Beclomethasone dipropionate	ICS	
Budesonide	ICS	
Formoterol	LABA	
Fluticasone propionate	ICS	
Ipratropium bromide	SAMA	

Mometasone furoate	ICS	
Salbutamol	SABA	
Salmeterol	LABA	
Terbutaline	SABA	

The methods will be used to investigate the solubility enhancements achievable and the potential for solution based pMDI formulation using excipients such as ethanol as a co-solvent and derivatised cyclodextrins added to form host / guest complexes. The inherent structural data in the NMR measurements potentially aids in characterisation of the complexes. A further objective is to undertake VT-NMR studies on the systems to further our understanding of the physical chemistry involved in the dissolution processes of compounds in these solvents with and without the excipients chosen to enhance solubility.

Methods will be developed using HPFP (2H,3H-decafluoropentane) as a model propellant based on the work carried out by Rogueda,[126] who concluded the properties were comparable to those of HFAs 134a and 227. This helps in the early method development phases of the studies as the

compound is liquid at room temperature and is therefore considerably easier to work with. By its comparability to HFAs 134a and 227 used in current pMDI formulations[126] it also provides meaningful data in terms of actual solubility, and the values will be used in conjunction with these in many cases. Some common physico-chemical properties of HPFP, HFA134a and HFA227 are shown in Table 1.3.1.2.[126]

Table 1.3.1.2 – Common physico-chemical properties of HFA134a, HFA227 and HPFP.[126]

Property (293 K)	HFA134a	HFA227	HPFP
Molecular Mass (g/mol)	102.0	170.0	252.1
Melting Point (K)	172.0	142.0	193.0
Boiling Point (K)	246.7	256.5	326.6
Vapour Pressure (bar)	5.72	3.90	0.25
Density of liquid (kg/L)	1.226	1.408	1.598
Refractive Index of liquid (n_D)	1.19	1.22	1.26
Dielectric constant of liquid	9.8	4.1	15.1

The potential for disadvantages of the NMR based approaches will also be considered. As NMR is an inherently insensitive technique when compared to methodologies such as HPLC with high sensitivity detection such as UV, fluorescence and mass spectrometry used in previously published methods to assess solubility[100,122,123,124] careful consideration will be required to ensure suitable sensitivities can be achieved. Modern NMR spectrometers have however developed considerably in recent years and have the sensitivity improvements brought about by increased field strength, modern electronics and probe designs. Pulsed field gradient shimming protocols and stabilised lock referencing have also served to reduce peak broadening and maximise peak heights, thus increasing signal to noise (S:N). Forms of referencing to allow the data to be used in a quantitative manner will be

considered. Several possibilities exist here and investigations into their applicability will be included in these studies (i) calibration using the external standard approach[127] and (ii) incorporation of a physical reference material into the analytical solution at a known concentration – a type of internal standardisation. This approach may be acceptable if it can be guaranteed that the inclusion of the reference does not inherently affect the property being measured. This problem can be overcome if the reference can be physically isolated from the analytical solution by use of glassware such as co-axial inserts (iii) ERETIC (**E**lectronic **RE**ference **T**o access *In-vivo* **C**oncentrations) methods have been utilised in recent studies to introduce an electronic reference appearing as a peak in the NMR spectrum that can be used quantitatively, for example those by Remaud *et al.*[128] and Akoka *et al.*[129]

1.3.2 Solid State Studies

The solid state of the expelled API from the actuated pMDI device is important to consider. As highlighted earlier in this section, topical treatment of inflammation in the indications of asthma and COPD require the administration of ICS, β_2-agonist and / or antimuscarinic bronchodilators to specific regions of the lung and their efficacy is heavily dependent on the physico-chemical properties of the material. For materials poorly soluble in the primarily aqueous based airway lining fluids the crystal form (including hydrates / solvates) or amorphous nature of the materials can have profound effects on the efficacy of the delivered dose. This process can dictate pulmonary targeting with an optimum dissolution profile existing for locally acting compounds, or a differing form for those targeted for systemic

delivery.[123] The control of these characteristics is heavily dependent on the design and formulation properties of the device. As previously discussed, products formulated as suspensions in HFA media are likely to deliver different solid forms on actuation to those formulated as solutions using co-solvent systems and / or other excipients; actuation and formation of solids during the rapid evaporation of volatile propellant systems favours the formation of amorphous materials. Further, many of the available prescribed medications in the form of pMDI devices are formulated to incorporate combination therapies. As summarised in Section 1.2.1.4, ICS compounds are frequently formulated with LABAs, for example Symbicort® pMDI devices containing budesonide and formoterol fumarate (GSK) and Seretide® containing fluticasone propionate and salmeterol xinafoate (AstraZeneca). Clinical trials have shown that addition to formulations is more beneficial in controlling symptoms of COPD than increasing the dose of the steroid alone and there are data to suggest that delivery *via* combination devices is more beneficial than delivering separately.[57,130,131] These characteristics have the potential for investigation using modern analytical techniques combined with novel deposition approaches using standard and modified impaction / impingement apparatus.

The objectives of the solid state studies presented herein are to develop and utilise standard and modified impactors / impingers to deposit materials from commercially available and novel pMDIs produced in-house. Study of the deposited materials will be undertaken using Powder *X*-ray Diffraction (PXRD), Scanning Electron Microscopy (SEM), and spectroscopic analysis (Fourier Transform Infrared [FTIR] and Raman). These techniques, used in

combination with the deposition methods developed, aim to provide a powerful means by which to assess distribution, form and morphology of the systems under study and enable conclusions to be drawn on their potential behaviour *in-vivo.*

A combination of the developed methods will be used to assess commercially available combination pMDIs (Seretide® and Symbicort®) and prototype pMDI formulations generated in-house for the study of ethanol (co-solvent) and a derivatised cyclodextin inclusion on HFA134a prepared budesonide.

2. Experimental

2.1 Materials

The source and batch numbers of materials used in these studies are summarised in Table 2.1.1.

Table 2.1.1 – Source and batch information for materials used in these studies.

Name	Source	Batch Code
HPFP	Apollo Scientific	Q15C-95
HFA134a	Solvay	A0150N0047
HFA227	Solvay	A0150A0111
Budesonide	Sigma Aldrich	017K1779
Beclomethasone dipropionate	Jai Radhe	BMD-N-004-09
Beclomethasone base	Jai Radhe	BMD-N-006-09
Fluticasone propionate	Jai Radhe	408901-FP
Salbutamol base	Jai Radhe	SB/101/09-10
Salbutamol sulphate	Jai Radhe	SS/103/09-10
Formoterol fumarate dihydrate	Sigma Aldrich	019K4705
Mometasone fuorate	Jai Radhe	APL/72/C-09
Terbutaline sulphate	Jai Radhe	TBS/105/07/08

Ipratropium bromide	Jai Radhe	IPI/0109001
Isonicotinamide	Sigma Aldrich	1404358
Benzoic Acid	Sigma Aldrich	MKF4260V
Seretide®	GlaxoSmithKline	2000035C00
Symbicort®	AstraZeneca	.0185R

All chromatography solvents were of HPLC grade (Fisher Scientific) unless otherwise stated.

2.2　Analytical Method Development for *In-Situ* Measurement of IPPs in HFAs

2.2.1　NMR Spectral Assignment (HPFP and Budesonide)

A solution of budesonide was prepared for NMR analysis by dissolving *ca.* 15 mg in deuterated chloroform ($CDCl_3$). The solution was filtered to remove residual solids into a standard field matched 5 mm NMR tube. The sample was locked and shimmed using pulsed field gradients (PFGs) before obtaining standard ^1H, ^1H-^1H COSY and ^1H-^{13}C HSQC NMR spectra using the JEOL ECA 600 MHz spectrometer. A solution of HPFP was prepared in $CDCl_3$ by taking *ca.* 15 mg into the solvent and transferring to a 5 mm NMR tube. Acquisition of a standard ^1H spectrum was obtained in the same manner.

2.2.2　Purity of HPFP

HPFP was characterised by injection of a liquid sample into the heated inlet of an Agilent 6890 gas chromatograph (GC) equipped with flame ionisation detection (FID) according to the method summarised (Table 2.2.2.1).

Table 2.2.2.1 – Summary of gas chromatography conditions used to ascertain purity of HPFP sample.

Column

Supplier:	Agilent
Material:	Fused silica
Length:	30 m
Internal diameter:	0.25 mm

Phase:	HP5 MS

Film thickness:	0.250 µm

Carrier Gas

Type and grade:	Hydrogen, Grade A

Flow:	50 mL/min

Injection

Mode of injection:	Manual, split (10:1)

Temperature:	300°C

Injector liner:	4 mm ID straight glass liner fitted with glass wool plug

Load:	1 µL

Detector

Type:	FID

Temperature:	325°C

Gases:	H_2:	30 mL/min
	Air:	350 mL/min
	Make-up:	30 mL/min (Nitrogen)

Initial temp (°C):   40°C (10 min), 20°C/min to 100°C (2 min),

20°C/min to 280°C (10 min)

Area % calculations were carried out on the resulting peak integration values obtained from the chromatogram, showing the purity to be > 99.9 % by peak area.

2.2.3   Co-axial NMR

Standard co-axial NMR tubes (Wilmad Labglass, NJ, USA) consisted of a field matched NMR tube of suitable dimensions for insertion within the standard 5 mm NMR tube, incorporating a small capillary tube within the sampling volume of the NMR probe allowing addition of a physically isolated reference solution. The tube setup was utilised throughout the experimentation with the reference volume filled with deuterated acetonitrile (CD$_3$CN). The outer volume of the co-axial setup was filled with 530.0 µL of a saturated suspension of budesonide in HPFP. The solution was prepared by adding excess budesonide to HPFP and allowing equilibration for > 24 hours. The transferred suspension was added unfiltered to the tube.

2.2.4   Method Optimisation

A co-axial tube setup prepared with a saturated suspension of budesonide in the analytical (outer) capacity and a reference solution of CHCl$_3$ in CD$_3$CN in the reference (inner) capacity was inserted into the JEOL 600 MHz NMR spectrometer. The sample was locked and shimmed using PFGs (CD$_3$CN)

and a standard ^{1}H NMR spectrum acquired. A repeat ^{1}H experiment was performed using a solvent suppressed parameter set summarised below:

Suppression Type: Presaturation

Chemical Shift: 4.36 ppm

Attenuation: 25 dB

The acquisition of solvent suppressed data was repeated with attenuation levels increased from 25 to 55 dB with 5 dB step size. Peak area values were obtained for the 3 budesonide resonances between 5 and 7 ppm chemical shift values (A-ring protons) by peak integration. Plots of the peak area values *vs.* attenuation level were produced.

A co-axial tube setup was prepared and analysed for a standard ^{1}H NMR spectrum in an identical manner to that used in the solvent suppression investigation with an attenuation value of 55 dB. Solvent suppressed spectra were obtained using sequentially longer acquisition times (scan number) of 16 minutes (256 scans), 134 minutes (2048 scans) and 935 minutes (14,336 scans). Signal to noise (S:N) ratios were calculated for budesonide resonance at 6.5 ppm chemical shift values for each of the experiments performed.

2.2.5   Quantitative Method Development

A co-axial tube setup was prepared and analysed to acquire a standard ^{1}H NMR spectrum in an identical manner to that used in the solvent suppression investigation with an attenuation value of 55 dB and 2048 scans. HPLC validation of the methodology was performed by preparation of a saturated

solution of budesonide in HPFP (excess budesonide was added to HPFP and equilibrated at room temperature for > 24 hours). The saturated suspension was filtered through 0.45 µm syringe filters before diluting further (x2) in HPFP to dissolve any solids that may have passed through the filtration step. A further dilution was made in HPLC mobile phase to create the analytical solution. Reference solutions were created in duplicate at 21.0 and 16.5 µg/mL in HPLC mobile phase. Injections of the reference and sample solutions were made on a Waters 2695 Separations Module HPLC system with 2487 variable wavelength detector (VWD) using conditions summarised in Table 2.2.5.1.

Table 2.2.5.1 – Summary of HPLC conditions used to analyse filtered saturated suspensions of budesonide.

Column: Phenomenex C_{18} – 250 mm x 2.1 mm (5 µm)

Mobile Phase: A – Water

                 B – MeCN

                 Isocratic 40% A : 60% B (0.2 mL/min)

Temperature: 40°C

Injection: 5 µL

Detection: UV at 240 nm

Peak area values from integration of the budesonide peaks were used to calculate the concentration of budesonide in the prepared saturated solution using the external standard approach as follows:

Response factor, Rf = budesonide concentration (μg/mL) / peak area = 1.336 x 10^{-3}

Sample concentration (μg/mL) = sample peak area x Rf = 21.7 μg/mL

Dilution factor = 4, therefore budesonide solubility = **86.8 μg/mL (± 0.32)**

A series of reference solutions of budesonide in HPFP at known concentrations were prepared for analysis and validation of the quantitation provided by the NMR method developed. A dilution series was generated by creation of a solution of budesonide (0.634 mg) in HPFP (10 mL) and sonicating to ensure complete dissolution. Serial dilutions were performed in HPFP to generate a reference series as outlined in Table 2.2.5.2.

Table 2.2.5.2 – Serial Dilutions to generate a reference series of budesonide in HPFP.

Solution	Solution volume (mL)	Total dilution volume (mL)	Resultant Concentration (μg/mL)
A	-	-	63.4
B	0.8 mL A	1	50.7
C	0.8 mL B	1	40.6
D	0.8 mL C	1	32.5
E	0.8 mL D	1	26.0

Each solution was transferred to the sample capacity of separate quantitative co-axial NMR tube arrangements and analysed using the 2048 scans and 55 dB attenuation level solvent suppression method previously established on the JEOL 600 MHz spectrometer. The values obtained were used to calculate a quantitative value of budesonide concentration, which was directly compared to the known values allowing the calculation of a

calibration factor for the experimental arrangement used as shown below for the 63.4 µg/mL solution as a worked example:

Peak area for $CHCl_3$ (271.3 µg/mL) = 24.87

Mean budesonide peak area = 18.24

$$\frac{CHCl_3 \text{ conc. x budesonide area } (^1H)}{CHCl_3 \text{ area } (^1H)} = 199.0$$

True budesonide concentration = 63.4 µg/mL

Calibration factor = 63.4 / 199.0 = **0.318**

Calculation of solute solubility using the co-axial arrangement (and calibration factor) was carried out as follows:

Peak area for $CHCl_3$ (297.1 µg/mL) = 35.27

Mean budesonide peak area = 32.69

$$\frac{CHCl_3 \text{ conc. x budesonide area } (^1H)}{CHCl_3 \text{ area } (^1H)} = 275.4$$

Applying calibration factor (0.316) = 275.4 x 0.316 = **87.0 µg/mL**

2.2.6   Reverse Co-axial NMR

In order that pressurised systems could be analysed by the developed methods, it was necessary to devise a J Young style NMR set up whilst still allowing insertion of a co-axial type insert. Wilmad Labglass, NJ USA, produced bespoke tube arrangements whereby a J Young top fitting was

added to a coaxial insert. A simple reversing of the standard mode of operation of these tubes now allowed a pressurised inner capacity for addition of analytical solution, with the reference capacity sitting in the outer volume at ambient pressure. In order to maximise the sensitivity of this arrangement, tubes were manufactured with a larger than standard inner volume. Inserts with an inner capacity of 190 µL and 410 µL were manufactured. Both tube types were tested within standard 5 mm NMR tubes, though it was apparent that the reduced volume of reference solution in the reference capacity of the larger tube setup imparted operational problems with sample locking and precision of quantitation.

A repeat of the validation exercise carried out for the original co-axial set up was carried out by creating a series of reference solutions of budesonide in HPFP at known concentrations. A dilution series was generated by creation of a solution of budesonide (0.605 mg) in HPFP (10 mL) and sonicating to ensure complete dissolution. Serial dilutions were performed in HPFP to generate a reference series as outlined in Table 2.2.6.1.

Table 2.2.6.1 – Serial Dilutions to generate a reference series of budesonide in HPFP.

Solution	Solution volume (mL)	Total dilution volume (mL)	Resultant Concentration (µg/mL)
A	-	-	60.5
B	0.8 mL A	1	48.4
C	0.8 mL B	1	38.7
D	0.8 mL C	1	31.0

Each solution was transferred to the sample capacity of separate quantitative reversed co-axial NMR tube arrangements, with the addition of 300 µL of

reference solution prepared accurately to contain *ca.* 10 µg/mL $CHCl_3$ in CD_3CN to the outer reference capacity. The samples were analysed using the 2048 scans and 55 dB attenuation solvent suppression method previously established on the JEOL ECA 600 MHz spectrometer.

2.2.7   ERETIC NMR

A sample of $CHCl_3$ in CD_3CN was created at 13 mg/mL and transferred to a standard 5 mm NMR tube. The sample was loaded in the JEOL 600 MHz NMR spectrometer before locking and shimming using PFGs. The ERETIC method was run using an ERETIC phase of 0 (zero) and offset of 10.0 ppm chemical shift (8 scan experiment). Processing of the resultant spectrum established a phase value of – 58, hence the experiment was repeated on the locked / shimmed sample (without removal of the lock or ejection of the tube) with a phase of +58 to provide a correctly phased ERETIC signal. The experiment was repeated with an offset of -1.0 ppm chemical shift. Integration of the ERETIC peak and the reference ($CHCl_3$) peaks obtains the numerical data necessary for the calibration of the system. A sample of an unknown can subsequently be run on the system under identical conditions after loading, locking and shimming using PFGs. It is important to remember not to retune the probe at this point as the ERETIC signal will once more become out of phase. Integration of the resonances of interest for the unknown sample can now be assessed *vs.* the calibrated ERETIC peak and used to calculate the concentration of the unknown in the system. A freshly prepared solution of in CD_3CN was created at 84 µg/mL and transferred to a standard 5 mm NMR tube. The sample was loaded in the JEOL 600 MHz NMR spectrometer before locking and shimming using PFGs. An ERETIC

procedure, modified to incorporate a pre-saturation of the HPFP signal (4.368 ppm) and incorporate the ERETIC signal at 9.0 ppm chemical shift was carried out as previously with initial assessment of the phasing of the ERETIC signal, followed by re-run of the same sample using the negative of the phasing applied. A total of 1064 scans were acquired in anticipation of the low level signals of the saturated budesonide suspension. The procedure was repeated immediately on a solution of saturated budesonide in HPFP (> 24 hours) without alteration of the spectrometer parameters. Calibration of the system was carried out using the peak area integral values of the $CHCl_3$ peak and the ERETIC signal. This calibration was applied to the unknown budesonide suspension for calculation of solubility.

Calculation of the solubility of budesonide in HPFP using this experimental approach is shown:

Calibration

Peak area for $CHCl_3$ (84.0 µg/mL) = 5.87

Peak area for ERETIC signal = 4.98

$$\text{ERETIC conc} = \frac{CHCl_3 \text{ conc. x ERETIC area}}{CHCl_3 \text{ area}} = 71.27$$

Determination

Mean budesonide peak area = 0.71

$$\text{Budesonide conc.} = \frac{\text{ERETIC conc. x budesonide area}}{\text{ERETIC area}} = 75.5$$

Budesonide conc. = **75.5 µg/mL**

2.2.8   Temperature Calibration of NMR Probe

A sample of MeOH in MeOD was created at *ca.* 15 mg/mL and transferred to a standard 5 mm NMR tube. The sample was loaded in the JEOL 600 MHz NMR spectrometer before locking and shimming using PFGs. The FTS Systems TC84 Variable Temperature Module temperature control system was set to 310 K and allowed to equilibrate the sample for 10 minutes, before acquiring a standard ^{1}H NMR spectrum. The temperature was reduced by 5 K and equilibrated for 10 minutes before repeating acquisition of the ^{1}H NMR acquisition. The process was repeated with sequentially lower temperature set points down to a registered value of 253 K. Chemical shift differences between the CH_3 and the OH resonances were utilised to calculate the true temperature of the sample at registered values on the temperature control apparatus.

2.2.9   Quantitation of Budesonide in HPFP (278, 283 and 298 K)

Samples of saturated budesonide were created in HPFP by addition of excess budesonide to HPFP solution in pressurise-able co-axial inners from the reverse co-axial tube arrangement. Three separate solutions were prepared in order to allow triplicate measurements to be performed. The suspensions were allowed to equilibrate at 298 K in a temperature controlled water bath for > 24 hours before preparing and analysing. The co-axial inners were added to a standard 5 mm NMR tube as previously described, pre-filled with 300 µL of reference solution (a solution of *ca.* 10 µg/mL $CHCl_3$ in CD_3CN prepared accurately). The samples were removed from the water bath and immediately transferred to the JEOL 600 MHz NMR spectrometer pre-

equilibrated to 298 K and allowed 15 minutes to re-equilibrate tube solutions to 298 K. The tubes were locked and shimmed using PFGs and analysed using the 2048 scans and 55 dB attenuation solvent suppression method previously established.

The process was repeated in exactly the same manner for the same three saturated suspensions of budesonide in HPFP at 278 and 283 K, with > 24 hours equilibration time allowed for each temperature change. Fresh reference solution was prepared before each experiment was acquired. Solvent suppression parameters were modified slightly to accommodate the chemical shift movement of the solvent response brought about by the temperature difference of the acquisition.

2.2.10 Cold Transfer of HFA134a and HFA227 and Associated Method Modification

A specifically designed cold transfer system has been assembled for use in handling liquefied gases and their transfer to pressurisable NMR tubes. The system was used to charge pressure vessels with liquefied gases, namely HFA134a and HFA227, through a cold transfer system refrigerated with solid CO_2. The pressurised liquid was subsequently transferred to the J Young style co-axial inserts through a series of valves allowing saturated suspensions of APIs in the pressurised solvents to be generated *in-situ*. A photograph of the set-up is shown as Figure 2.2.10.1.
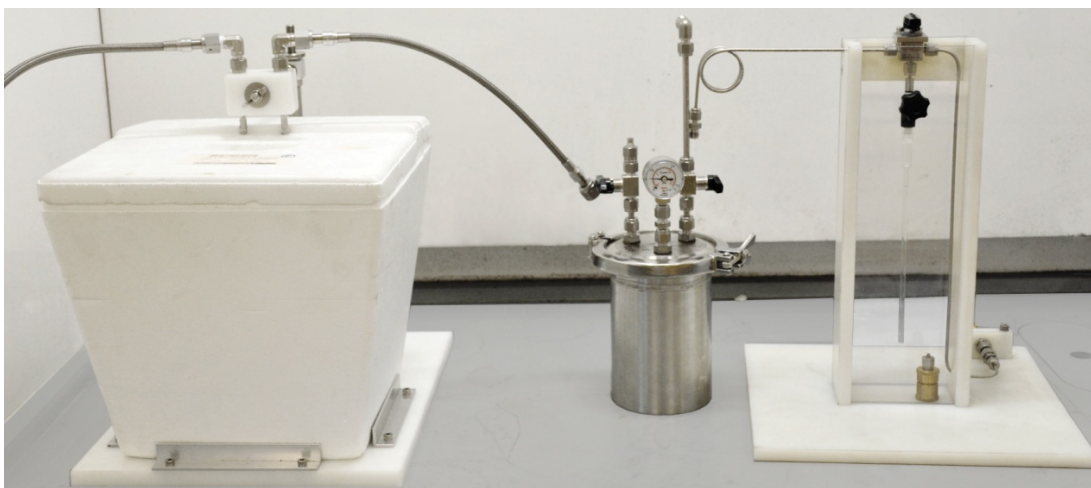
Figure 2.2.10.1 – Cold transfer system designed and assembled to allow the filling of pressurisable NMR tubes with liquefied gases HFA134a and HFA227.

Samples of HPFP, HFA134a and HFA227 were prepared using the reverse co-axial arrangement set up to include reference solution in the outer capacity as used in the quantitatively prepared solubility solutions. Each was loaded separately to the JEOL 600 MHz spectrometer. For each of the solvent systems, ^{1}H NMR data was acquired after equilibration in the probe at 298, 283 and 273 K for 15 minutes. The chemical shift values for the centre of the main resonance for each of the fluorinated solvents was recorded at each temperature. This chemical shift value was written to individual method parameter files allowing a separate solvent suppression method to be established for each of the three solvent systems at each temperature (9 separate methods in total).

2.2.11   NMR Assignment of Inhaled Compounds

For each of the API samples under study, a solution was created in $CDCl_3$, CD_3CN, MeOD or D_2O dependent on their respective solubility. The solutions were filtered to remove any residual solids into standard 5 mm NMR tubes. The samples were locked and shimmed using the automated sequence before obtaining standard ^{1}H NMR spectra using the Bruker 400 MHz spectrometer equipped with 5 mm QNP probe. Limited spectral assignment was completed for each of the APIs examined to establish resonances that could be utilised in the quantitation of solubility in the fluorinated solvent systems.

2.3 **Physical Chemistry of Inhaled Pharmaceutical Products in HFAs**

2.3.1 **Solubility Measurements at Ambient (298K) and Reduced Temperature (283 & 278K)**

Saturated suspensions of each of the APIs were created separately *in-situ* in HPFP, HFA134a and HFA227 and left to equilibrate at 298 K by placing the co-axial tube in a temperature controlled water bath for a minimum of 24 hours. The co-axial inners were added to standard 5 mm NMR tubes as previously described, pre-filled with 300 µL of reference solution (a solution of *ca*. 10 µg/mL $CHCl_3$ in CD_3CN prepared accurately and freshly before each analysis). The samples were immediately transferred to the JEOL 600 MHz NMR spectrometer pre-equilibrated to 298 K and allowed 15 minutes to re-equilibrate tube solutions to 298 K within the probe. The tubes were locked and shimmed using PFGs and analysed using the 2048 scans and 55 dB attenuation solvent suppression methods previously established for each of the solvents. Each sample preparation and acquisition was carried out in triplicate.

The results for each of the APIs in each of the three solvents were reviewed and quantitatively worked up if there was sufficient analyte signal to allow reliable results to be determined (S:N > 3:1). In the event that reliable resonances were found and quantitation was possible, a result was recorded for each of the replicate measurements and the solutions we re-equilibrated at 283 K for a minimum of 24 hours, before repeating the analytical procedure. A final re-equilibration and repeat of procedure was carried out at

278 K under the same conditions if a positive result was obtained at 283 K. Should there be no identifiable analyte resonances, or should the S:N values be insufficient for the experimentation carried out at 298 K, no further experimentation was carried out.

2.3.2   Solubility of Materials Using HPLC

HPLC approaches were utilised in order to provide quantitative information on the samples in HPFP that were below the LOD values obtained using the final NMR methodology. For each API in question, a 6 point calibration series was created in 50:50 MeCN : Water over the range 100 to 0.1 µg/mL. A full scan UV spectrum was acquired to determine the optimum detection wavelength for each compound allowing optimisation of sensitivity and selectivity.

Samples were equilibrated as saturated suspensions of each API separately in HPFP at 298 K for > 24 hours. Any residual solids were removed from the suspension by gravity filtration though paper filters (Whatman Ashless No.1). A portion of the filtered solution was evaporated to dryness at 40°C and reconstituted in mobile phase solution to pre-concentrate the analyte. The samples were analysed using a Waters 2695 Separation Module with 2487 VWD according to a standard isocratic method (Table 2.3.2.1)

Table 2.3.2.1 – Summary of HPLC conditions used in the analysis of IPPs in HPFP.

Column: Phenomenex C_{18} – 250 mm x 2.1 mm (5 µm)

Mobile Phase: 60% MeCN : 40% water

Flow:	200 µL/min

Temperature:	40°C

Detection:	UV (λ API specific)

Providing these reverse phase conditions were appropriate for the analyte, linearity and LOD were calculated from the calibration series generated, with quantitation provided by triplicate determinations *vs.* the calibration series using the external standard approach.

In some cases (salbutamol base, salbutamol sulphate and terbutaline) poor peak shapes were observed under the conditions applied. Mobile phase was modified and the analysis repeated under the conditions outlined in Table 2.3.2.2.

Table 2.3.2.2 – Summary of HPLC conditions used in the analysis of salbutamol base, salbutamol sulphate and terbutaline in HPFP.

Column:	Phenomenex C$_{18}$ – 250 mm x 2.1 mm (5 µm)

Mobile Phase:	60% MeCN : 40% 10 mM ammonium formate, pH 3.8

Flow:	200 µL/min

Temperature:	40°C

Detection:	UV (λ API specific)

2.3.3 Van't Hoff Solubility Plots

The values obtained for solubility in the three propellant systems under study allow the evaluation of thermodynamic properties by plotting of data in the format of the van't Hoff equation. Full details are given (Section 4.2.1.3); in summary, plots of lnχ (mole fraction) *vs.* 1/T (K^{-1}) allow the derivation of thermodynamic properties (ΔH, ΔG and ΔS) from the slope of the curves produced.

2.4 Strategies for Solubility Enhancement in HFAs

2.4.1 Co-Solvent Model

To allow the determination of budesonide solubility in a series of ethanol doped HPFP / HFA134a solutions, a further stage in the previously developed sample preparation protocol was incorporated. The HPFP / ethanol solution production was straight forward, with the addition of relevant volumes of ethanol incorporated into the co-axial inner of the tube set up. However, ethanol introduction in volatile HFA134a required a modification to the approach as the HFA134a volatility necessitates transfer under pressure. A summary of both procedures is given.

HPFP / EtOH - Saturated suspensions of budesonide were created separately *in-situ* in HPFP doped with 2.5, 5, 10, 15 and 20% ethanol levels (v/v). The HPFP was added initially to the solid in the co-axial NMR tube inner, and ethanol added to bring to volume – both additions were made accurately using gas tight syringes to ensure the final ratio of solvent was as accurate as practicable. A summary of the volumes is shown (Table 2.4.1.1).

Table 2.4.1.1 – volumes of HPFP and EtOH used to prepare saturated suspensions of budesonide at 2.5, 5, 10, 15 and 20% EtOH in HPFP.

Concentration (% v/v)	Volume HPFP (μL)	Volume EtOH (μL)
2.5	185	5
5	181	9
10	171	19
15	162	28
20	152	38

HFA134a / EtOH - The HFA134a systems were prepared in a modified way. The same volumes were required to produce systems with ethanol concentrations of the same values, however incorporation was made difficult due to the volatility and transfer procedures required to charge the HFA134a (See section 2.3.10 for a summary of cold transfer procedure). Initial attempts at adding the HFA134a after addition of budesonide and ethanol appeared problematic as the ethanol had a tendency to be 'pushed' out of the tube on charging of the HFA134a. The modified procedure, allowing a more accurate volume control to be employed, required the charging of budesonide initially to the co-axial insert, followed by HFA134a to the desired volume. The system was then sealed with the J Young cap, and frozen by immersion in liquid nitrogen. Once solidified, the J Young cap was removed without loss of any volatile propellant, and ethanol added accurately to the desired volume using gas tight syringe as previously. The sample was capped, and allowed to warm (and melt) resulting in a suspension of budesonide in HFA134a / EtOH at the desired solvent concentration.

Both HPFP / EtOH and HFA134a / EtOH preparations were left to equilibrate at 298 K by placing the co-axial tube in a temperature controlled water bath for a minimum of 24 hours. The co-axial inners were added to standard 5 mm

NMR tubes as previously described, pre-filled with 300 µL of reference solution (a solution of *ca.* 10 µg/mL $CHCl_3$ in CD_3CN prepared accurately and freshly before each analysis). The samples were immediately transferred to the JEOL 600 MHz NMR spectrometer pre-equilibrated to 298 K and allowed 15 minutes to re-equilibrate tube solutions to 298 K within the probe. The tubes were locked and shimmed using PFGs and analysed using a modified ^1H NMR method allowing suppression of HPFP / HFA134a solvent signal and CH_3 / CH_2 resonances of EtOH in concert (Section 3.1.12).

2.4.2   Solubility Measurements of IPPs in Ethanol / HPFP

Solutions of all 11 IPPs under study have been prepared as saturated suspensions in HPFP / EtOH and analysed to determine the solubility change from standard HPFP solutions. The saturated suspensions were produced in exactly the same manner as described in Section 2.5.1 to a final solvent concentration of 10% (v/v) EtOH in HPFP. The solutions were left to equilibrate at 298 K by placing the co-axial tube in a temperature controlled water bath for a minimum of 24 hours. The co-axial inners were added to standard 5 mm NMR tubes as previously described, pre-filled with 300 µL of reference solution (a solution of *ca.* 10 µg/mL $CHCl_3$ in CD_3CN prepared accurately and freshly before each analysis). The samples were immediately transferred to the JEOL 600 MHz NMR spectrometer pre-equilibrated to 298 K and allowed 15 minutes to re-equilibrate tube solutions to 298 K within the probe. The tubes were locked and shimmed using PFGs and analysed using a modified ^1H NMR method allowing suppression of HPFP / HFA134a solvent signal and CH_3 / CH_2 resonances of EtOH in concert (Section 3.1.12).

2.4.3   Solubility Measurements in Cyclodextrin / HFAs

For each of the cyclodextrin (CD) samples, a solution was created in D_2O. The solutions were filtered to remove any residual solids into standard 5 mm NMR tubes. The samples were locked and shimmed using the automated sequence before obtaining standard ^{1}H NMR spectra using the Bruker 400 MHz spectrometer equipped with 5 mm QNP probe. Limited spectral assignment was completed for the two CDs examined to establish potential resonances that could be utilised in the quantitation of solubility in the fluorinated solvent systems.

Solutions of budesonide and heptakis-(2,3,6)-trimethyl-β-cyclodextrin (TRIMEB) were produced as saturated suspensions in the same manner as used for the pure APIs in this study (Section 2.4.1.1). A 50:50 w/w mix of the host and complex molecules was prepared remotely before transferring to a co-axial inner and adding HPFP, HFA134a and HFA227 separately to form a saturated suspension. The samples were left to equilibrate at 298 K by placing the co-axial tube in a temperature controlled water bath for a minimum of 24 hours. The co-axial inners were added to standard 5 mm NMR tubes as previously described, pre-filled with 300 µL of reference solution (a solution of *ca*. 10 mg/mL $CHCl_3$ in CD_3CN prepared accurately and freshly before each analysis). The samples were immediately transferred to the JEOL 600 MHz NMR spectrometer pre-equilibrated to 298 K and allowed 15 minutes to re-equilibrate tube solutions to 298 K within the probe. The tubes were locked and shimmed using PFGs and analysed using the 2048 scan* and 55 dB attenuation solvent suppression methods previously

established for each of the solvents. Each sample preparation and acquisition was carried out in triplicate.

*Where appropriate, the analysis time (scan number) was reduced as sufficient signal to noise was obtained in greatly reduced times owing to the increased solubility levels observed in the sample preparations incorporating CD.

2.4.4 Generation of Host / Guest Complexes (Budesonide / TRIMEB)

Further experimentation was carried out on the complexed budesonide / TRIMEB samples. A set of screening samples was created in the model propellant HPFP doped with EtOH at 10% (v/v) in order to isolate solid samples of the materials post evaporation of the solvent. Solutions were created at mole ratios of 0.5:1, 1:1 and 2:1 as summarised in Table 2.4.4.1 and dissolved fully under sonication before allowing a slow evaporation of the solvent (*via* a single pierced hole in the cap of a standard 5 mm NMR tube) to produce solid samples that were harvested for further investigation.

Table 2.4.4.1 – Sample preparation for the production of budesonide / TRIMEB samples at 0.5:1, 1:1 and 2:1 mole ratios.

Mole Ratio	Budesonide (mg)	TRIMEB (mg)
0.5:1	2.43	15.91
1:1	4.85	15.90
2:1	9.70	15.90

2.4.5 Evaluation of Host / Guest Complexes

2.4.5.1 FTIR

Samples of each of the isolated solids were prepared as KBr discs for analysis by FTIR. A sample (*ca.* 5 mg) was taken to an agate mortar and pestle, pre-dried in an oven at 80°C, and ground to a fine powder with KBr (*ca.* 350 mg) also pre-dried in the same manner. The resultant mixture was pressed to a 12 mm KBr disc under 10 tonne pressure using a SpecAc hydraulic press and die set, before removing and analysing using the Digilab UMA 400 FTIR in transmission mode. Spectra were acquired using 64 scans and 2 cm^{-1} spectral resolution post acquisition of a background spectrum under the same conditions for automated subtraction using the Digilab software.

2.4.5.2 Raman

Samples of each of the isolated solids were mounted for acquisition of Raman spectra on aluminium microscope slides and brought to focus using the x100 objective lens (0.90 N$_A$) of the Renishaw InVia Raman microscope (calibrated daily prior to use wrt wavenumber shift using the internal silicon reference; manual adjustment to 520.0 cm^{-1}). Spectra were acquired for each of the samples produced using 10 second exposure and 10 averaged accumulations. Scans were recorded over the range 100 to 3200 cm^{-1} using 785 nm high powered diode laser to excite the samples at 100% power (*ca.* 1 mW at sample).

2.5 Solid State Characterisation of IPPs Post Deposition

2.5.1 Raman Acquisition of Reference Compounds

Raman spectra were acquired on the reference materials (APIs and excipients) by placing a small amount of the solid material onto an aluminium slide and bringing to focus under the 100 x objective (0.90 N_A) of the Renishaw InVia Raman microscope (calibrated daily prior to use wrt wavenumber shift using internal silicon reference; manual adjustment to 520.0 cm^{-1}). Reference spectra were acquired using 785 nm high powered diode laser for excitation, with parameters chosen to obtain good quality spectra in a reasonable time-scale (10 second exposure, 5 averaged accumulations, *ca.* 1 mW applied laser power at sample).

2.5.2 Deposition using Anderson Cascade Impactor

A Copley Scientific Anderson Cascade Impaction (ACI) system was utilised to deposit material from the pMDI devices onto plates for subsequent analysis by remote techniques; primarily Raman and SEM. The ACI system was operated without pre-separation device, with the throat attachment directly applied to the upper chamber of the apparatus. Glass microscope cover slips and subsequently aluminium plates were placed on top of the ACI plate to collect deposited material and allow for subsequent removal and remote analysis. A flow rate of 28.3 L/min was applied for 8.3 seconds giving a total inspired volume of 4.0 L using a Copley high flow pump and calibrated Copley TPK flow controller. The flow was measured by means of an external Copley DFM2000 flow meter attached to the mouthpiece of the throat. The method was operated in accordance to the European Pharmacopoeia 7.1,

Section 2.9.18; Preparations for Inhalations: Aerodynamic Assessment of Fine Particles.[132] 11 'dummy' actuations were carried out with the pMDI device (directly to air) before the device was attached to the ACI system and the 12th actuation carried out for collection. The apparatus was dismantled and the cover slips / aluminium plates removed for remote analysis.

2.5.3 Raman Analysis of Deposited Materials

The ACI plates of interest were brought to focus under the x50 objective (0.75 N_A) of the Renishaw InVia Raman microscope (calibrated daily prior to use wrt wavenumber shift using internal silicon reference; manual adjustment to 520.0 cm^{-1}). Point analysis was performed on selected deposited regions of the plates using the optimised conditions developed for the reference materials. Point spectra were acquired for Seretide® and Symbicort® depositions. Acquisitions were repeated using the x100 (0.90 N_A) objective to assess spatial resolution improvements.

Hyper-spectral arrays were collected using 785 nm hi-powered laser for excitation over an area of *ca.* 15 x 15 µm. Data were acquired over a reduced spectral range to expedite the procedure, with scans centred at 1550 and 1450 cm^{-1} for Seretide® and Symbicort® depositions respectively. Final 'mapping' procedures were developed for each of the formulations and are summarised in Table 2.5.3.1.

Table 2.5.3.1 – Raman acquisition parameters for Seretide® and Symicort® deposited materials.

	Seretide®	Symicort®
Excitation wavelength, nm	785	785
Applied power, *ca.* mW at sample	1	1
Number of averaged accumulations	2	2
Exposure time, s	2	2
Acquisition centre, cm^{-1}	1550	1450

The hyper-spectral arrays acquired on each of the preparations of Seretide® and Symbicort® were carried out using the Renishaw demonstration apparatus Renishaw UK (Wotton-under-Edge, Gloucestershire) equipped with the StreamLine™ Raman Imaging system, allowing acquisition of maps over considerably larger areas in vastly reduced times. The deposited samples were focused with x100 objective (0.90 N_A) and regions of *ca.* 100 x 100 μm were acquired for each sample separately, with 0.7 μm step-size (*ca.* 20,500 spectra for each map). The other spectral parameters were kept constant. Each data set was processed to remove cosmic rays (nearest neighbour method), noise filtered and processed using DCLS component analysis using the previously acquired reference spectra.

2.5.4 Deposition Using Twin Stage Impinger

The twin stage impinger apparatus (Copley Scientific) was utilised to deposit materials of respirable fraction of the actuated pMDI device into the second stage of the glassware. A flow rate of 60.0 L/min was applied for 4.0 seconds giving a total inspired volume of 4.0 L using a Copley high flow pump and calibrated Copley TPK flow controller. The flow was measured by means of an external Copley flow meter attached to the mouthpiece of the throat. The method was operated in accordance to the European Pharmacopoeia 7.1,

Section 2.9.18; Preparations for Inhalations: Aerodynamic Assessment of Fine Particles.[132] The second stage of the impinger was modified to allow collection of the deposited material directly to apparatus ready to transfer for remote analysis. Two approaches were utilised; i) deposition directly to an aluminium sample pan for removal and remote analysis by DSC and ii) deposition directly onto an upturned aluminium sample pan covered with mylar film cut to a small disc of the same diameter using a cork borer. The mylar disc containing the deposited material was removed and placed on a PXRD silicone wafer sample holder, of the type used for acquisition of PXRD patterns on small amounts of material. The disc was then covered in another larger disc of mylar, and sealed down using adhesive plastic. This set up allowed sealing of the system and minimisation of moisture ingress during the analysis. A schematic of the collection mechanism and PXRD set up is shown (Figure 2.5.4.1).
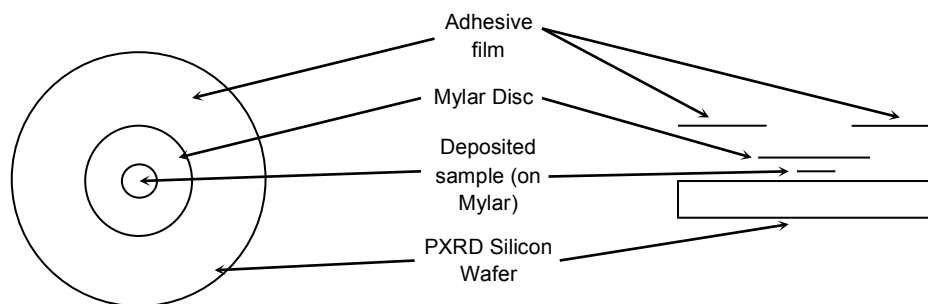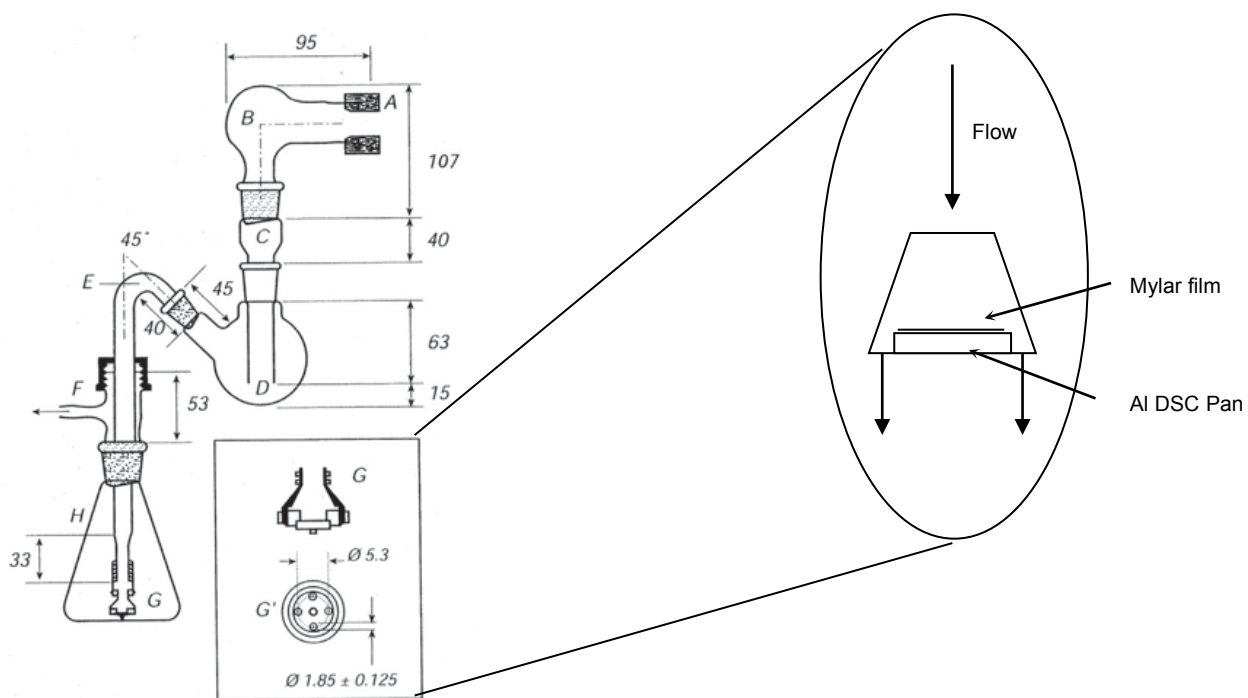
Figure 2.5.4.1 – Schematic representation of the standard TSI[132] and the modified stage 2 collection system. Also shown is the sample preparation approach for remote PXRD analysis.

2.5.5 Powder *X*-Ray Diffraction Analysis of QVAR® and Synasthmax® pMDI Devices

Deposition using the modified TSI set up was performed using 160 actuations (over 10 – 12 minutes) of a QVAR® 100 pMDI device from 3M Ltd, UK, and the Synasthmax® pMDI device, Chiesi, Italy. The collected material was analysed remotely using the Bruker D8 powder *X*-Ray diffractometer under the following operating parameters; [λ(Cu-Ka) = 1.5418 Å, voltage 40 kV, filament emission 40 mA] with 1 mm divergence slit, 1 mm receiving slit and 0.2 mm scatter slit. Samples were scanned under ambient conditions from 3-40° (2θ) using a 0.01° step width and a 1 s count time. The acquisitions were repeated in a cyclical fashion (9 repeats) with a 30 minute delay in-between each. A system blank was analysed in the same manner *i.e.* blank mylar sheet prepared analysed in the same way without the depositions of QVAR® product.

2.5.6 Thermal Analysis of QVAR® and Synasthmax® pMDI Devices

TGA and DSC data were recorded at King's College London (KCL) on the material deposited on the aluminium foil substrate placed to receive material entering stage 2 of the TSI apparatus. QVAR® and Synasthmax® pMDI devices were actuated 80 and 50 times respectively in to the TSI, operated at 60 L/min for 4.0 seconds giving a total inspired volume of 4.0 L over a period of *ca.* 6 minutes. The resultant foil was subsequently removed, weighed accurately and placed directly inside a hermetically sealed aluminium DSC pan with a 1 mm pinhole cap. DSC was performed between ambient and

350°C with a heating rate of 10°C/min under nitrogen purge gas. TGA was performed in open aluminium pans between ambient and 200°C with a heating rate of 10°C/min (TA Instruments TA2920 and TGA2050 respectively).

2.6 Product Studies

2.6.1 Generation of pMDI Formulations

A series of pMDI products were prepared for evaluation post actuation / deposition using Copley impaction systems. The preparation of solid samples was carried out at the University of Bradford as summarised in Table 2.6.1.1. Budesonide used in the preparations was first milled using the FPS Labomill laboratory scale Jet mill with an injection pressure of 7 barg and grinding pressure of 5 barg. Budesonide (500 mg) was added manually to the feed hopper of the mill, and micronized material was recovered from the collection vessel post processing. A relatively low yield was achieved (196 mg, 39.2 %) using this small-scale approach, though adequate material for formulation was harvested. Formulation of these systems into pMDI preparations was kindly arranged by collaborators at the University of Bath (Professor Robert Price, Dr. Jag Shur and Ms. Charlotte McDonnell) using a 3M laboratory scale pMDI production apparatus.

Table 2.6.1.1 – Samples prepared for formulation in pMDI propellants.

Budesonide (mg)	TRIMEB (mg)	Mole Ratio	Propellant System	Fill Volume (mL)
32	-	-	HFA134a	10.0
32	108	1 : 1	HFA134a	10.0
33	-	-	HFA134a w. 10% EtOH	10.0
32	110	1 : 1	HFA134a w. 10% EtOH	10.0

The solid samples were added to aluminium pMDI canisters and 1.0 mL ethanol added. The crimp cap and metering valve were applied and sealed to the canister, before filling 9.0 mL of HFA134a to the canister using the 3M laboratory rig. HFA134a (10.0 mL) was added to formulations in pure HFA. The canisters were stored inverted for 14 days to ensure the elastomer seal was swollen and the canisters were adequately sealed.

2.6.2   Solution and Solid State Analysis

The canisters were used (actuated) with a 3M device, freshly sourced from a QVAR® 100 product. A Copley Scientific Anderson Cascade Impaction (ACI) system was utilised to deposit material from the pMDI devices onto aluminium plates for subsequent analysis by remote techniques (HPLC, SEM, Raman). The ACI system was operated without pre-separation device, with the throat attachment directly applied to the upper chamber of the apparatus. A flow rate of 28.3 L/min was applied for 8.3 seconds giving a total inspired volume of 4.0 L using a Copley high flow pump and calibrated Copley TPK flow controller. The flow was measured by means of an external Copley DFM2000 flow meter attached to the mouthpiece of the throat. Vigorous shaking of the canister followed by 11 'dummy' actuations were performed with the pMDI device (directly to air) before the device was attached to the ACI system and the 12th actuation carried out for collection. The apparatus was dismantled and the plates removed for remote analysis. A repeat of the procedure was performed with 5 actuations for collection and dissolution for HPLC analysis (APSD determination). Deposition using the modified TSI set up as summarised in section 2.6.4 was not possible with these samples due to the requirement for multiple (> 100) actuations for the

desired sensitivity; only a single 200 actuation canister was available for each preparation and many of these acquisitions had been performed for the NMR, SEM, Raman and HPLC investigations.

2.6.2.1   SEM and PSD

SEM was performed on the feed and micronized material used in the preparation of the pMDI canisters to confirm visually the particle morphology and size of the material ensuring its appropriateness for formulation. Particle size distribution (PSD) was also performed on the micronized material prior to incorporation in the pMDI systems using the Sympatec laser diffraction PSD analyser with HELOS attachment (R1 lens, 4 barg pressure). Each of the samples generated using the ACI method of deposition was added to the chamber of the FEI Quanta 400 SEM and evacuated. Images ranging from x40 to x15 k magnification were captured at a minimum of 3 sites for each sample using 20 kV energy under high vacuum conditions. Working distance and spot size were optimised for each image captured.

2.6.2.2   Raman

Raman spectra were acquired on the reference materials (budesonide and TRIMEB) by placing a small amount of the solid material onto an aluminium slide and bringing to focus under the 100 x objective (0.90 N_A) of the Renishaw InVia Raman microscope (calibrated daily prior to use wrt wavenumber shift using internal silicon reference; manual adjustment to 520.0 cm^{-1}). Reference spectra were acquired at 785 nm laser excitation, with parameters chosen to obtain good quality spectra in a reasonable time-

scale (10 second exposure, 3 averaged accumulations, *ca.* 1 mW applied

laser power at sample).

The ACI plates of interest were brought to focus under the 100 x objective

(0.90 N_A) of the Raman microscope. Point analysis was performed on

selected deposited regions of the plates using the optimised conditions

developed for the reference materials (10 second exposure, 3 averaged

accumulations, *ca.* 1 mW applied laser power at sample). Analysis was

performed at a minimum of 8 sample sites on plates 4, 5, 6 and 7 of the ACI.

2.6.2.3 HPLC and APSD

Five actuations of the pMDI device were performed immediately after one another under the conditions specified (Section 2.6.2). The material was collected into HPLC mobile phase for each stage of the ACI including the throat (5 mL total volume). Injections were made on a Waters 2695 Separation Module equipped with 2487 VWD detector installed with the method summarised in Table 2.6.2.3.1, and concentrations at each stage calculated by peak area using the external standard method *vs.* a calibration curve constructed from peak areas of reference solutions between 500 and 5 µg/mL.

Table 2.6.2.3.1 – HPLC conditions used to analyse ACI collected budesonide.

Column:	Phenomenex C_{18} – 250 mm x 2.1 mm (5 µm)
Mobile Phase:	A – Water
	B – MeCN
	Isocratic 40% A : 60% B (0.2 mL/min)
Temperature:	40°C
Injection:	50 µL
Detection:	UV at 240 nm

MMAD and GSD were estimated using the method outlined in Ph.Eur[132] using Copley CITDAS software to construct log normal plots of the cumulative fraction of active substance *vs.* cut-off diameter. FPF was

70

calculated as a total of the material < 5 μm *i.e.* stages 2 to 7 inclusive of the ACI.

2.6.2.4   NMR

A sample of each formulation was transferred from the pMDI canister directly to separate co-axial NMR inners by repeat actuation of the device positioned on top of the J Young cap. The tube was cooled throughout the process by submersion in liquid N_2 held in a dewar to solidify the transferred material and hold until the transfer was complete (*ca.* 5 actuations) to the desired level within the tube. The preparations were allowed to warm to ambient temperature and equilibrated at 298 K by immersion in a temperature controlled water bath for a minimum of 24 hours. The co-axial inners were added to standard 5 mm NMR tubes as previously described, pre-filled with 300 μL of reference solution (a solution of *ca.* 10 μg/mL $CHCl_3$ in CD_3CN prepared accurately and freshly before each analysis). The samples were immediately transferred to the JEOL 600 MHz NMR spectrometer pre-equilibrated to 298 K and allowed 15 minutes to re-equilibrate tube solutions to 298 K within the probe. The tubes were locked and shimmed using PFGs and analysed using the appropriate solvent suppression methods previously established for each of the solvents (HFA134a or HFA134a / ethanol). Each sample preparation and acquisition was carried out in triplicate.

3 Analytical Method Development for *In-Situ* Measurement of HFAs

The following chapter describes the development work performed to establish an NMR based methodology for *in-situ* determination of solubility in HFA based propellants. The rationale has been made in Section 1.2.1. Method development was undertaken with the commonly used IPP budesonide, an ICS used in the treatment of asthma, and the model propellant HPFP. This chapter covers the key steps in method development (i) NMR spectral assignment (ii) development of co-axial tube configurations and (iii) developments to maximise sensitivity and minimise data acquisition time to determine the sparingly soluble analytes. Extension of the method to the quantitation of solutes in volatile propellants that are gaseous under standard temperature and pressure (HFA134a and HFA227) are also described. Validation by secondary techniques (chromatographic) and calibration of variable temperature systems are summarised, allowing the acquisition of data at sub-ambient and elevated temperatures.

3.1　　　　NMR Method Development

3.1.1　　　　Spectral Assignment (HPFP and Budesonide)

NMR spectra were obtained for HPFP and budesonide prepared in CDCl$_3$.
The ^{1}H spectrum of HPFP shows there is a complex multiplet arising from the
2H and 3H protons in the molecule, split into a complex pattern by the
coupling with fluorines present in the structure (Figure 3.1.1.1). Work by
Foris[134] observes the ^{1}H NMR spectrum of HPFP to show severely
overlapped CHF patterns. In these studies, a similar pattern was observed
for HPFP in CDCl$_3$ and comparable coupling constants were extracted from a
first-order analysis of the peak (Table 3.1.1.1).

Figure 3.1.1.1 – ^{1}H NMR spectrum of HPFP in CDCl$_3$.
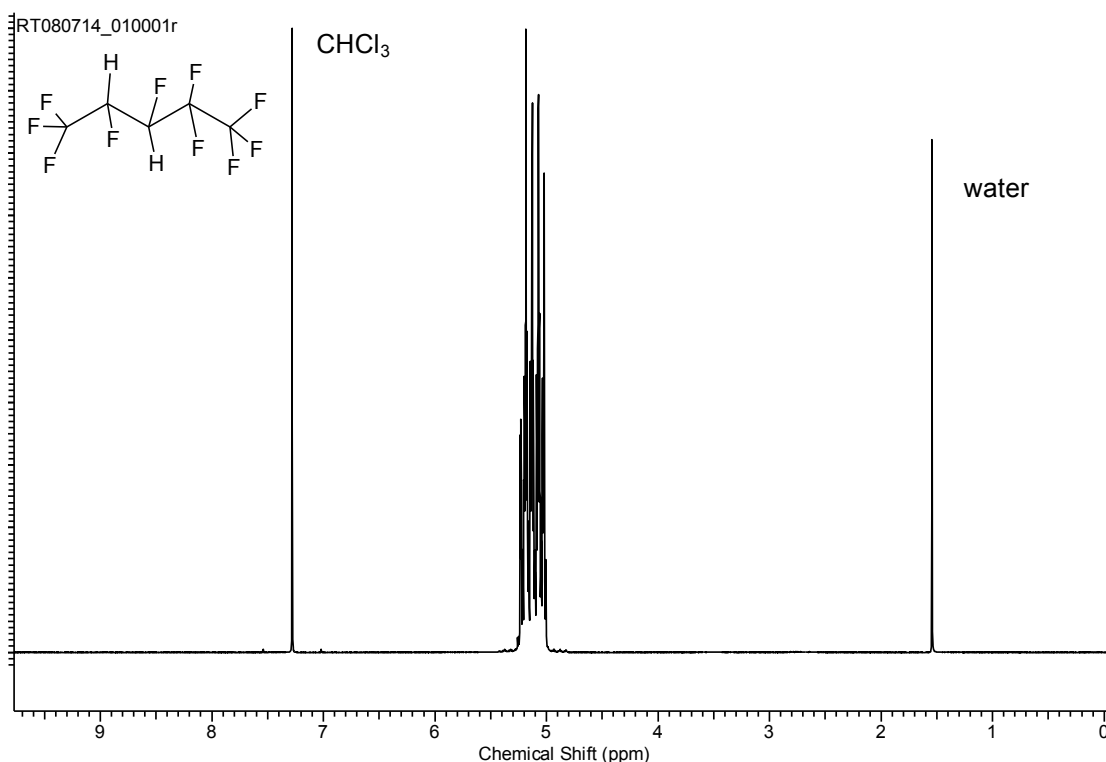
Table 3.1.1.1 - Coupling Constant Data for ^{1}H NMR HPFP.

Chemical Shift (ppm)	Spin-Spin Coupling
5.1	$^2J(H,F) = 46.1$ Hz, $^3J(CHCF) = 19.0$ Hz, $^3J(CHCF_3) = 6.3$ Hz, $^3J(CHCH_a) = 5.2$ Hz, $^3J(CHCH_b) = 2.9$ Hz; H_a at 5.08 ppm, $^2J(CH_aF) = 46.8$ Hz, $^3J(CH_aCF) = 23.5$ Hz, $^2J(CH_aH_b) = 11.5$ Hz, $^3J(CH_aHF) = 5.2$ Hz, $^4J(CH_aCCF_3) \approx 0.7$ Hz, H_b at 5.12 ppm $^2J(CH_bF) = 46.0$ Hz, $^3J(CH_bCF) = 24.7$ Hz, $^2J(CH_bCH_a) = 11.5$ Hz, $^3J(CH_bCH) = 2.8$ Hz, $^4J(CH_b\text{-}CCF_3) \approx 0.9$ Hz

Figures 3.1.1.2 to 3.1.1.4 show standard ^{1}H spectra of budesonide (full scale and spectral expansion in the low and high field regions). The spectrum is consistent with that described by Yang[135] and Thalen[136] and is assigned accordingly (Table 3.1.1.2). Correlation experiments including a ^{1}H-^{1}H COSY and ^{1}H-^{13}C HSQC (Figures 3.1.1.5 and 3.1.1.6), were included to show consistency with the couplings observed in the published spectra[135,136] and were used to aid in confirmation of these assignments.
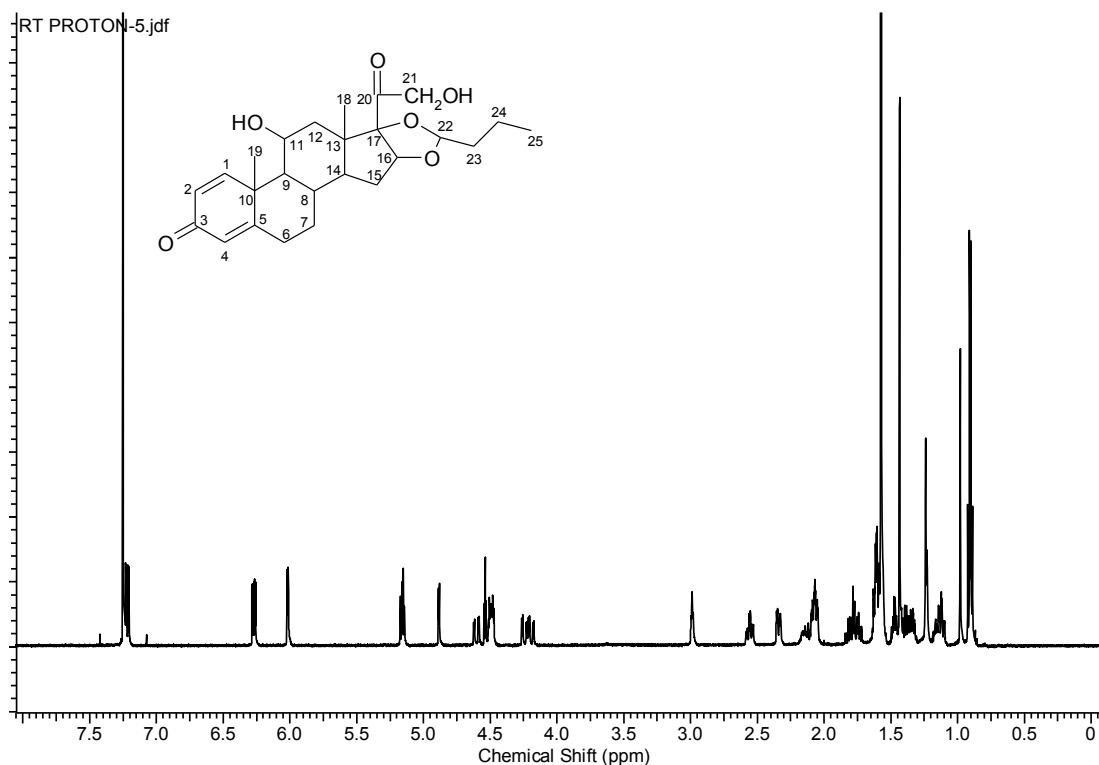
Figure 3.1.1.2 – ^{1}H NMR spectrum of budesonide in CDCl$_3$.
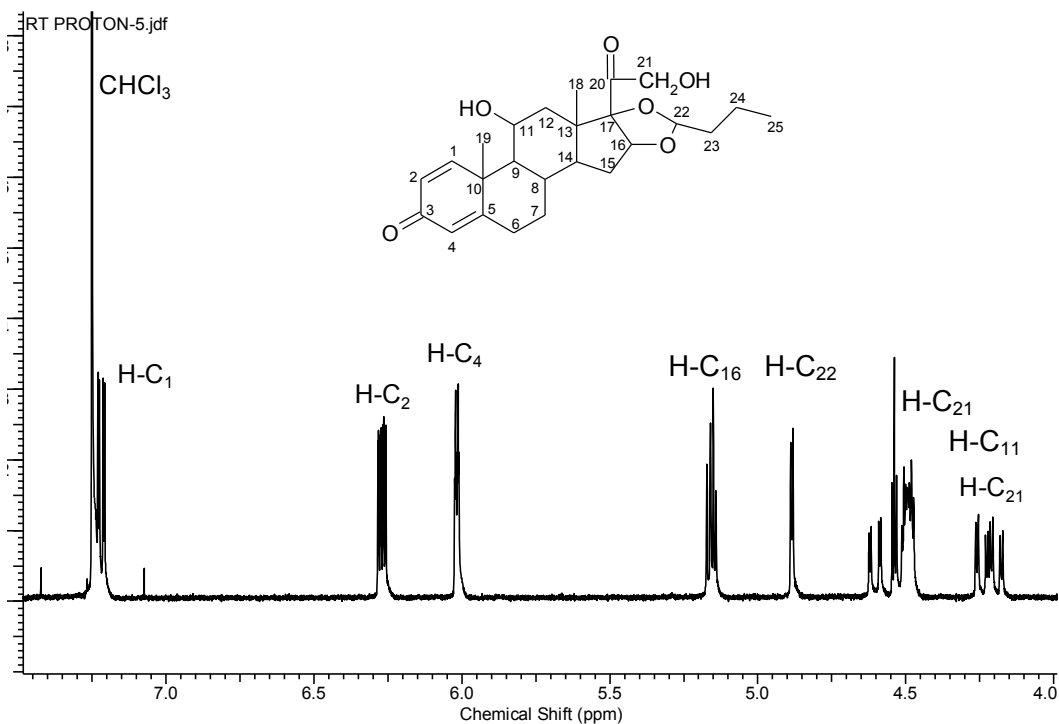
Figure 3.1.1.3 – ^{1}H NMR spectrum of budesonide in CDCl$_3$ (spectral expansion in the low field region).
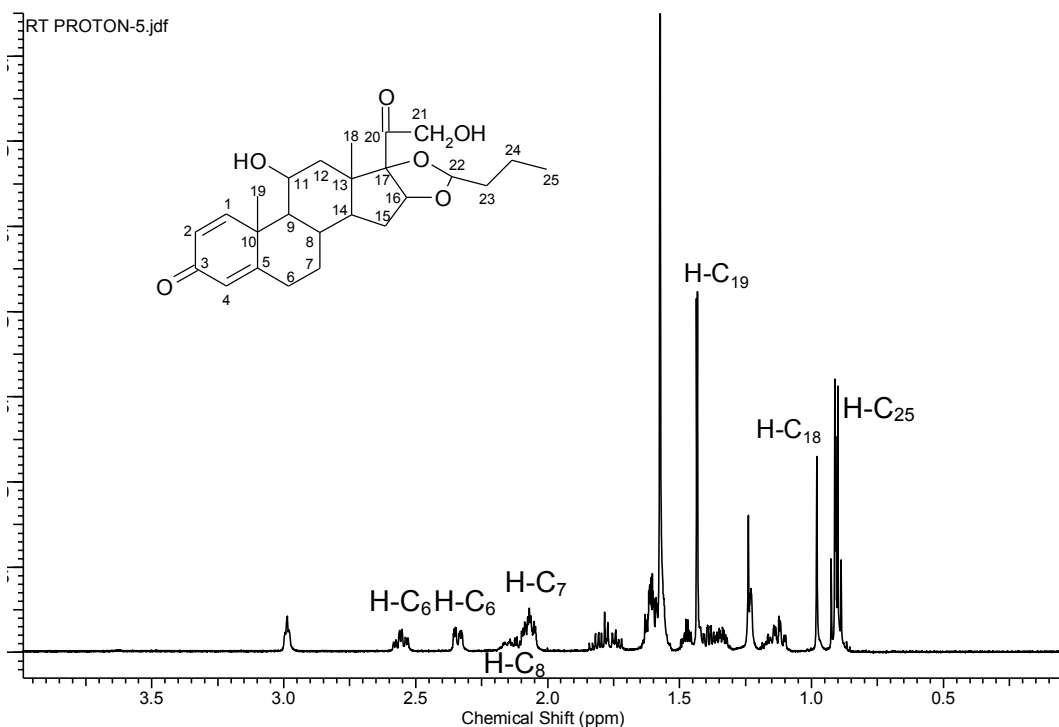
Figure 3.1.1.4 – ^{1}H NMR spectrum of budesonide in CDCl$_3$ (spectral expansion in the high field region).
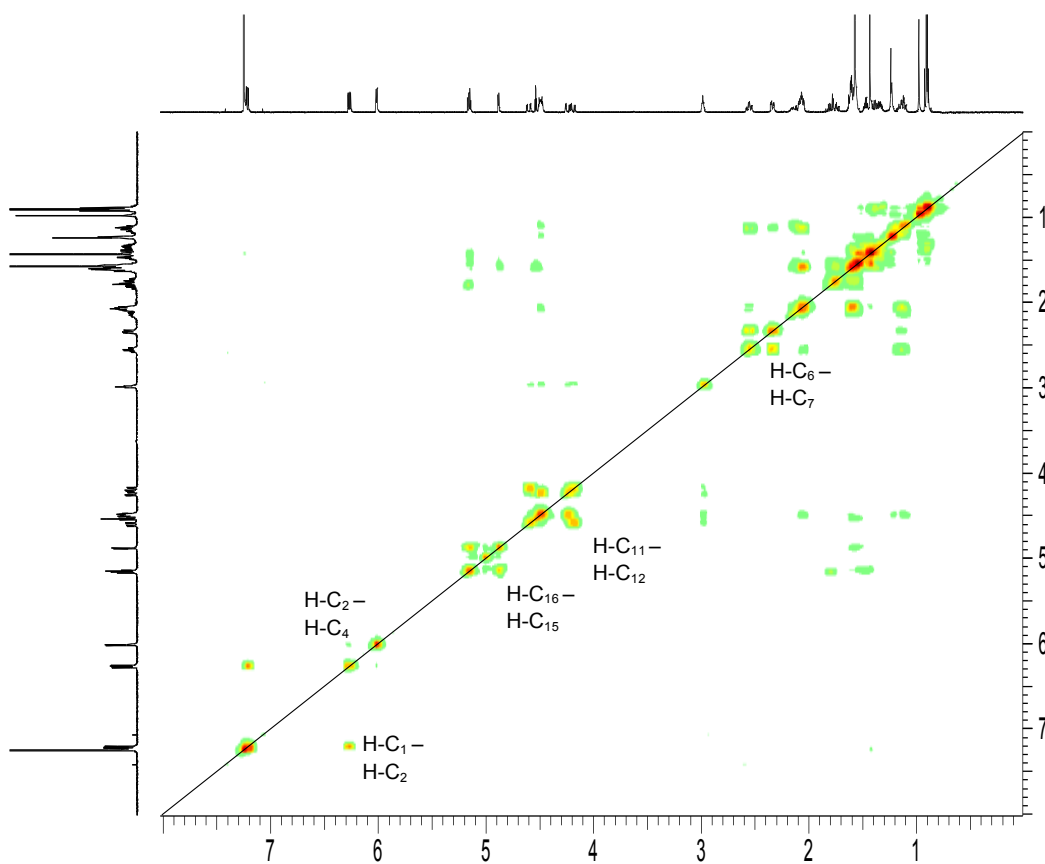
Figure 3.1.1.5 – ^{1}H-^{1}H COSY NMR spectrum of budesonide in CDCl$_3$ shown

with X and Y projections taken from high resolution ^{1}H spectrum (Figure

3.1.1.2).
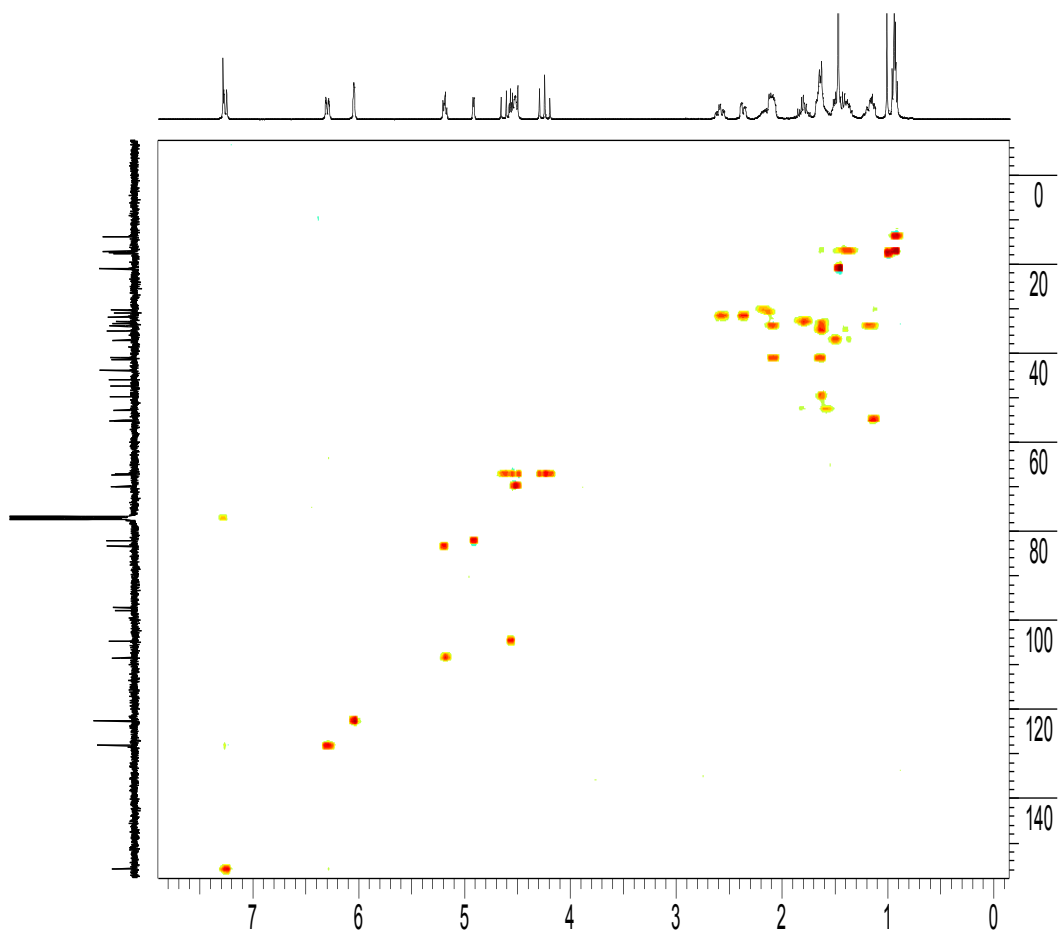
Figure 3.1.1.6 – ^{1}H-^{13}C HSQC NMR spectrum of budesonide in CDCl$_3$ shown with X and Y projections taken from high resolution ^{1}H and ^{13}C spectra.

Table 3.1.1.2 – NMR chemical shift assignments for budesonide in CDCl$_3$.[135,136]

C$_x$-H	Chemical shift (ppm)	Spin-Spin Coupling Data
1	7.22	(dd, J=10.1, 2.9 Hz)
2	6.27	(ddd, J=10.1, 4.8, 1.8 Hz)
4	6.02	(dt)
6	2.36	(dd, J=4.0, 13.1 Hz)
7	1.16	(ddd, J=4.0, 12.0, 12.0 Hz)
8	2.18	(dq, J=4.0, 11.0, 12.0 Hz)
9	1.12	(dd, J=3.0, 4.5 Hz)
11	4.49	(m)
16	5.16	(dd J=5.0, 2.5 Hz)
18	0.98	(s)
19	1.43	(s)
21	4.50	(R) (dd, J=20.2, 4.8 Hz), 4.25 (R) (dd, J=20.2, 4.8 Hz)
	4.60	(S) (dd, J=20.2, 4.8 Hz), 4.20 (S) (dd, J=20.2, 4.8 Hz)
22	4.55	(R) (t, J=4.2 Hz)
	5.15	(S) (t, J=4.6 Hz)
25	0.91	(t, J=7.3 Hz)

Chemical shifts given relative to residual chloroform at 7.26 ppm. Multiplicity indicated with the abbreviations: s (singlet), d (doublet), t (triplet), q (quartet), dd (doublet of doublets), dt (doublet of triplets), m (multiplet).

3.1.2 Co-axial NMR

Most modern NMR spectroscopy is carried out in deuterated solvents allowing observation of the analyte resonances in the presence of the solvent in excess. For the experimentation reported here no deuterated analogues of the solvent were commercially available, presenting two practical problems for ^{1}H NMR (i) absence of deuterium lock signal and (ii) dynamic range issues arising from intense proton signals from the solvent.

To compensate for field drift, modern NMR spectrometers have a dedicated deuterium (^{2}H) observe channel known as the lock. This allows for field drift over the period of time taken to acquire the spectrum, and minimises peak broadening effects associated with a drifting field (hence maximising peak height and resolution / sensitivity).[125]

However, as outlined in (i), for experimentation to take place in non-deuterated solvent systems, the spectrometer needs to be operated 'unlocked' or allow for incorporation of a deuterium signal into the tube set up used.

Inclusion of a deuterated reference material into the prepared analyte solution would allow the locking procedure to take place in the conventional way. However, the inclusion of these solvents would inherently alter the solvent system used and invalidate any solubility measurements determined. A NMR tube setup commonly used to address this is the co-axial NMR tube set up (Figure 3.1.2.1). The apparatus allows the insertion of a smaller NMR tube (coaxial insert) within the standard tube allowing addition of a deuterated reference solution into the analytical solution separated by a glass capillary; the advantage being that the system can be locked in the conventional way by the spectrometer and, importantly, it allows the addition of an NMR active reference material for calibration and quantitation purposes.
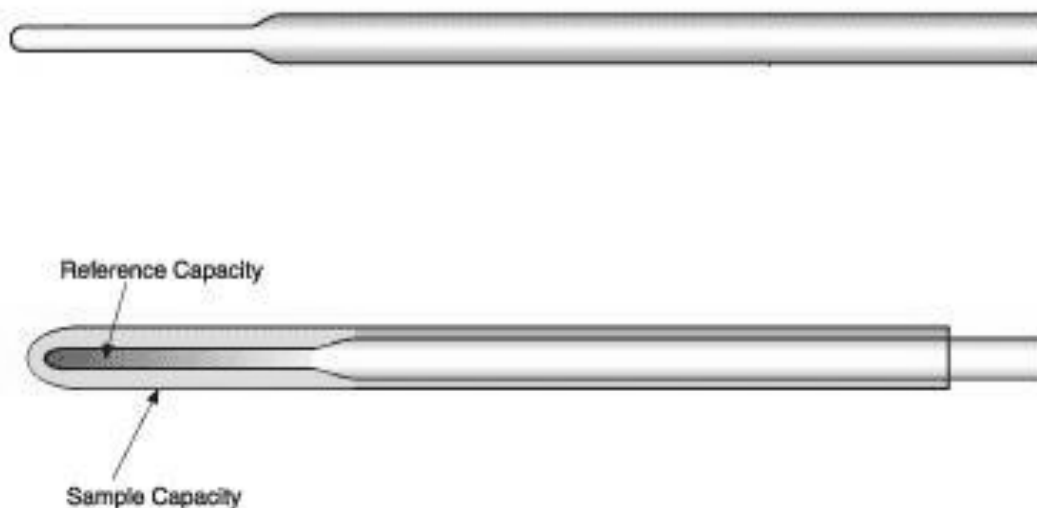
Figure 3.1.2.1 – A typical coaxial NMR tube set up shown in isolation (upper) and assembled (lower) with addition of a deuterated solvent and standard material added to the inner capillary.[137]

The tube set up was prepared as summarised (Section 2.2.3) with a saturated suspension of budesonide in HPFP in the sample capacity and CD_3CN in the reference capacity. The resulting NMR spectrum (Figure 3.1.2.2) shows evidence of the A-ring resonances of budesonide, however the spectrum is dominated by the HPFP proton resonances as expected. As a result, the budesonide resonances are too low in intensity to be used in a quantitative workup of the data; signal to noise (S:N) is estimated at *ca.* 2:1 by ratio of peak height to the difference of maximum and minimum signals in a region of background well removed from any signals.
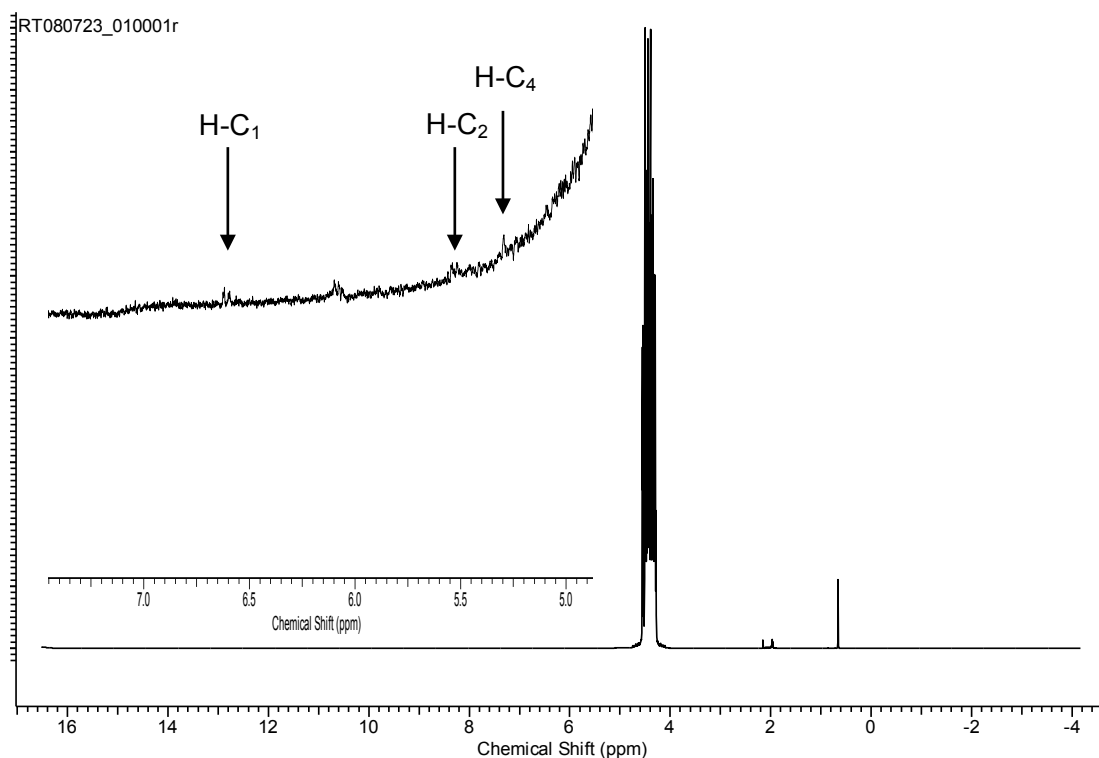
Figure 3.1.2.2 – ^{1}H NMR spectrum of a saturated suspension of budesonide in HPFP acquired using a co-axial tube set-up containing a reference solution of $CHCl_3$ in CD_3CN.

As highlighted (ii), it is most likely that dynamic range issues are the cause of the low intensity analyte signals in the presence of the intense HPFP resonances, and careful consideration of solvent suppression methodologies offers an ideal means to overcome this.

Solvent suppression allows the reduction in intensity of the large signals present from any protonated solvent present in large excess. The techniques have been in use for many years, particularly for the suppression of the water resonance when analysing aqueous solutions.[138] This aids in matching of the dynamic range of the instrument allowing the enhancement of the small resonances of interest without the presence of the large solvent peak. Without suppression of the solvent proton signals, the receiver gain of the

spectrometer cannot be adjusted sufficiently to permit reliable detection of small resonances without causing an overflow in the analogue to digital converter. Analogue to digital converters in modern NMR spectrometers are commonly 16-bit which represent values in the range ±32767, hence the ratio between the largest and smallest detectable value, 32767 : 1 gives the dynamic range of the instrument. In reality, this means that if the largest signal in the spectrum is set to fill the digitiser, the smallest detectable signal has a value of 1.[125] Thus, any signal below 1 will not trigger the digitiser and will not be recorded. In this study, if the receiver gain was set to fill the digitiser with the HPFP signal, the small signals obtained for the analyte resonances are unlikely to be recorded.

Several methods of solvent suppression including zero excitation, methodologies based on pulsed field gradients (PFGs) and presaturation (selective saturation) methods are utilised in modern NMR spectroscopy.[125] Zero excitation, as the name suggests, involves pulse sequences designed to avoid excitation of the solvent signals in the first instance, hence avoiding observation of the solvent resonance. PFG methods are similar in that they avoid producing observed solvent resonances by destruction of the net solvent magnetisation, thus ensuring that nothing of this remains observable immediately prior to acquisition. Pre-saturation methods involve the application of continuous, weak radio frequency irradiation at the solvent frequency prior to excitation and acquisition, rendering the solvent spins saturated and therefore unobservable. They are by far the most commonly applied and the easiest / most robust to control for the routine user of NMR.[125,139] They are simple to add to pre-existing standard NMR

experiments and leave (non-exchangeable) resonances away from the pre-saturated signal unaffected, hence their use in the development of methods in these studies.

A presaturation method was established and used to suppress the signal from the HPFP protons. The saturation was centered at 4.36 ppm chemical shift, and an attenuation (power) of 25 dB was applied. The acquired spectrum of the saturated budesonide in the coaxial tube set up is shown (Figure 3.1.2.3).
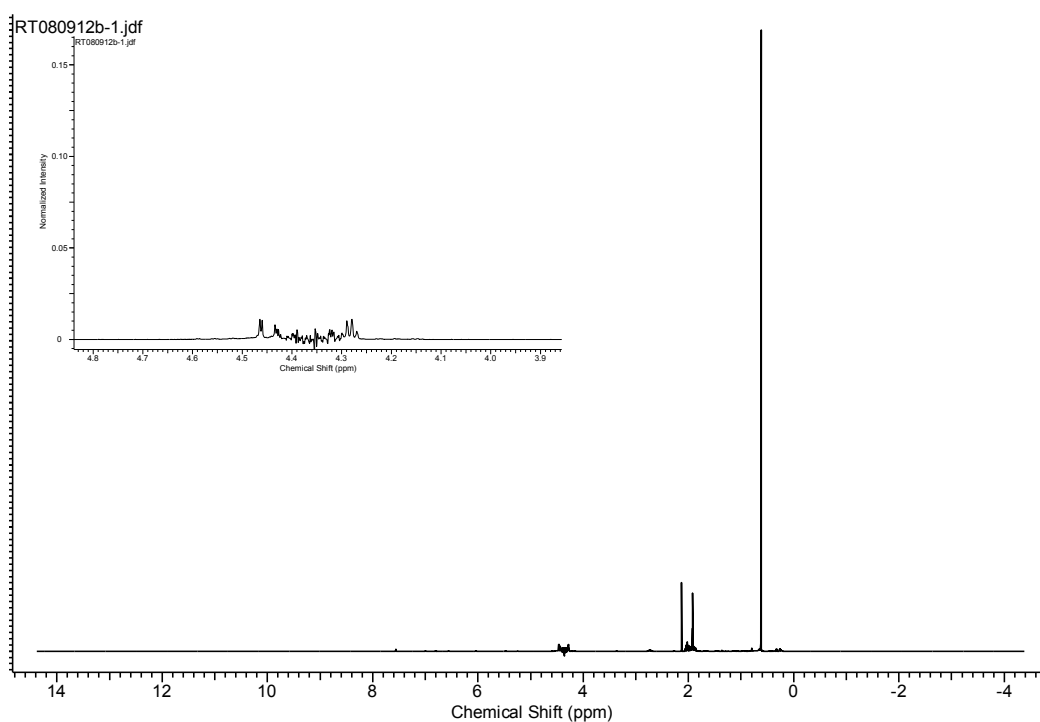
Figure 3.1.2.3 – ^{1}H NMR spectrum of a saturated suspension of budesonide in HPFP using presaturation solvent suppression methodology to suppress the HPFP signal.

Clearly, the large multiplet has been significantly reduced in intensity. In order to optimise the presaturation power and avoid suppression of the adjacent budesonide signals, the peak areas of the three A-ring signals were

monitored over a succession of different experiments carried out with sequentially reduced attenuation (increasing dB signal applied by the spectrometer). The higher field signals are being affected by the suppression up to values of 50 dB, though the resonance at 6.5 ppm chemical shift appears unaffected above *ca.* 35 dB (Figure 3.1.2.4). Subsequent experimentation utilises solvent suppression parameters based on this investigation at 55 dB attenuation and 4.36 ppm chemical shift. A representative ^{1}H NMR spectrum of a saturated suspension of budesonide in HPFP using these optimised conditions is shown (Figure 3.1.2.5).
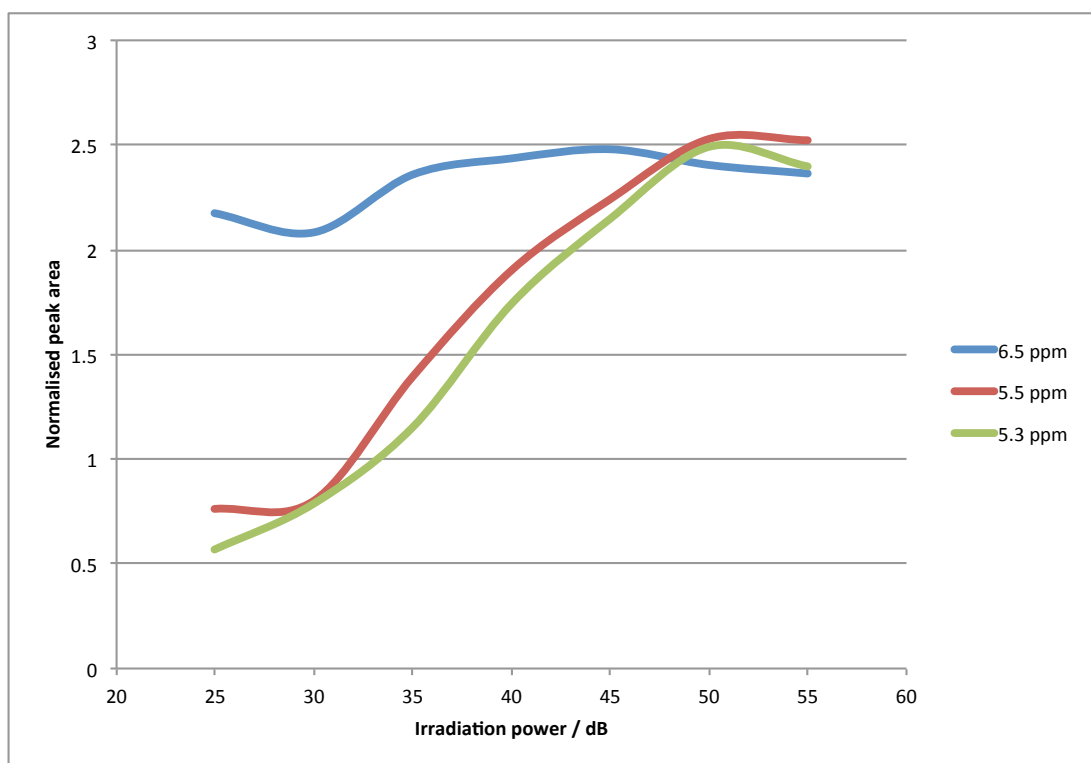
Figure 3.1.2.4 – Plot of peak area values of budesonide A-ring resonances *vs.* irradiation power of solvent suppression applied.
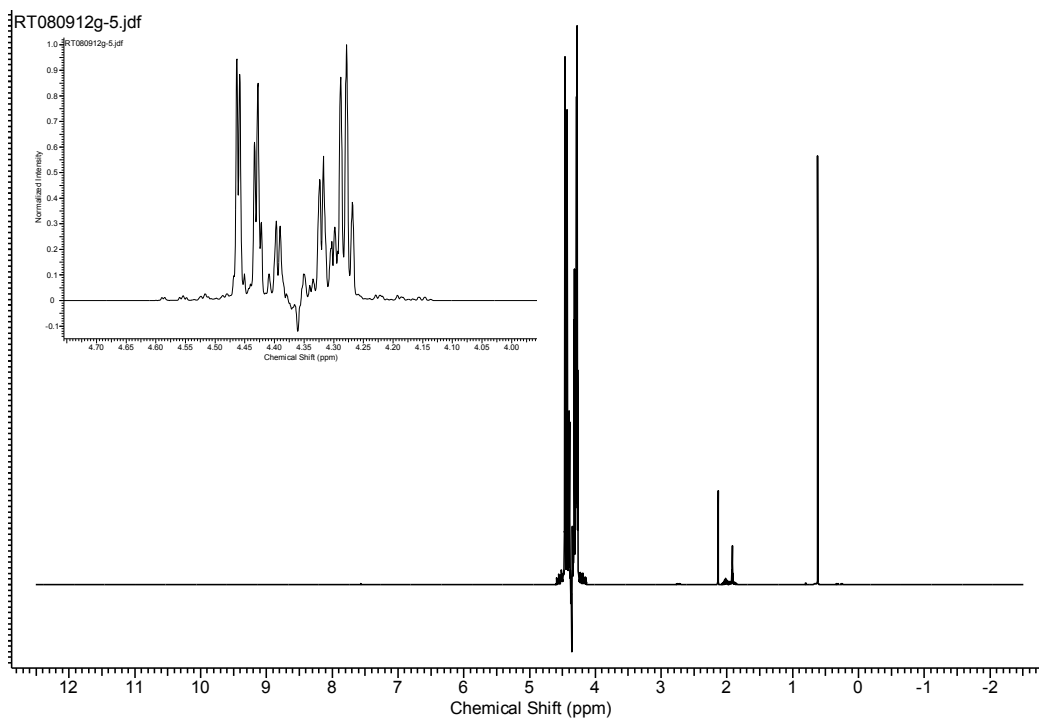
Figure 3.1.2.5 - ^{1}H NMR spectrum of a saturated suspension of budesonide in HPFP using presaturation solvent suppression methodology at 55 dB to suppress the HPFP signal.

Under comparable conditions, introduction of solvent suppression leads to a significant improvement in S:N ratios; for the 2048 scan experiment, the S:N of the H-C_1 resonance was 9:1 and 24:1 respectively (Figure 3.1.2.6). With such improvement, quantitative measurements of the IPPs are now feasible *in situ*.
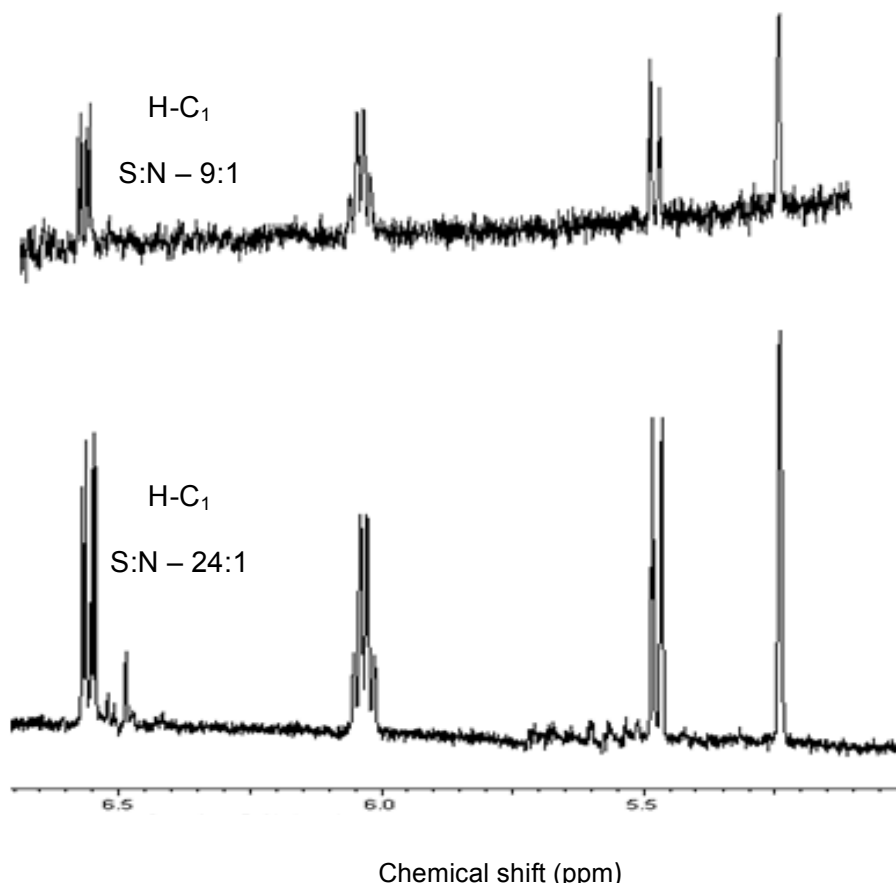
Figure 3.1.2.6 – Spectra of saturated budesonide in HPFP obtained with (lower) and without (upper) solvent suppression (55 dB) both using 2048 scans.

3.1.3 Method Optimisation (Maximising Signal to Noise)

For the signal intensities to be increased sufficiently for reliable use in quantitative methods of analysis, further development of the methodology was required. Sensitivity in NMR experiments can be increased in a number of ways. S:N in NMR is conventionally given by Equation 3.1.3.1,[125] where N is the number of spins being observed, γ_e is the gyromagnetic ratio of the spin being excited, γ_d is the gyromagnetic ratio of the spin being detected, B_0 is the applied magnetic field and t is the acquisition time.

86

$$S:N \propto N\gamma_e\sqrt{\gamma_d^2 B_0^3}t \qquad\qquad \textbf{Equation 3.1.3.1}$$

This offers two primary routes to improve S:N (i) increasing the acquisition times, t (*i.e.* the number of scans acquired) and (ii) increasing the field strength, B_0, applied. In addition it is also possible to increase S:N ratios by using alternative probe technologies (*e.g.* cryoprobe, high sensitivity proton observe probes – a brief review of these are included in further work Section 7.4).

It is clear that an increase in field strength, B_0, has a positive effect on the sensitivity of the experiment (following a $\sqrt[3]{}$ relationship). It is therefore sensible to utilise the largest field available for experiments where sensitivity becomes problematic or needs to be maximised. All the quantitative experimentation carried out here has been executed on a 600 MHz magnet, which is the largest field instrument located at the University of Bradford (UoB) in order to maximise this effect.

Increasing the acquisition times of the experiments carried out in the NMR spectrometer is a simple process. Signal averaging, *i.e.* the repeated acquisition and summation of the FID recorded leads to an overall increase in signal to noise. The signal adds coherently as the subsequent scans are added, whereas the noise tends to cancel as it can be positive or negative and adds according to $\sqrt{NS}$. Hence, over an extended number of scans the signal to noise improves according to the relationship $\sqrt{NS}$. If we consider the sensitivity increases available through acquisition times, a doubling of acquisition time (*i.e.* doubling scan number) will yield a S:N increase of 1.4, quadrupling the acquisition time yields a S:N increase of 2 etc. However, for

a practical method, acquisition times cannot be increased indefinitely; methods that can be practically applied to a number of samples in a time and cost effective manner are the goal of this activity.

The absolute effect of acquisition times on the budesonide system in question was investigated formally by increasing the scan number of the experiment sequentially and obtaining S:N measurements on the three A-ring resonances. Experiments were performed with 256, 2048 and 14336 scans respectively yielding increasing S:N values conforming to the $\sqrt{NS}$ relationship stated in Equation 3.1.3.1. The resultant S:N values calculated from the budesonide A-ring resonance at 6.5 ppm chemical shift are shown (Figure 3.1.3.1), confirming the $\sqrt{NS}$ relationship for this system.
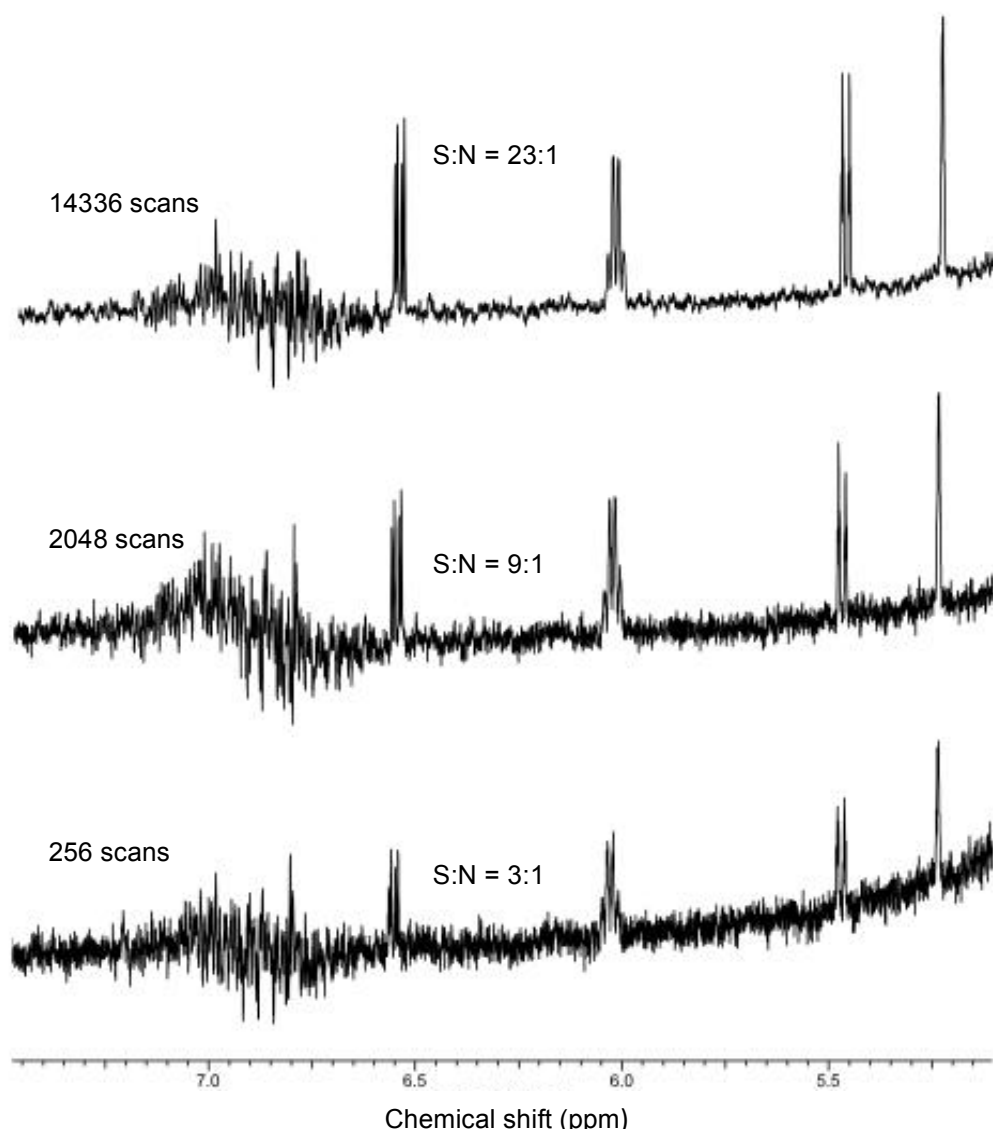
Figure 3.1.3.1 – Experiments showing $\sqrt{NS}$ relationship between sensitivity (S:N) and scan number (acquisition time).

For these studies, where optimal S/N and resolution were required, efforts were made to enhance experimentation through applying gradient shimming procedures (Section 2.3.1) rather than simply optimising z^1 and z^2 shims to maximise the deuterium lock signal in a conventional shimming approach. Additionally, NMR tubes matched to the appropriate field strength were used. These factors minimised peak broadening maximising peak height and hence the sensitivity of the experiment.

With the method operated under the developed conditions, LOQ values are estimated at *ca.* 15 µg/mL using the A-ring resonances of the budesonide molecule, with LOD values of *ca.* 8 µg/mL. These values are estimated using S:N ratios with a minimum of 10:1 and 3:1 respectively.[127] The LOQ / LOD levels are however strongly dependent on the type of resonance being monitored for quantitative purposes. For example, a single proton exhibiting no spin-spin coupling will produce a peak three times less intense than that of a methyl proton with no coupling. Further, any spin-spin coupling that is apparent will have a similar effect; a single proton with coupling producing a triplet will have a reduced signal intensity compared to that of a single proton with no coupling (singlet) as the same peak area is now split between three peaks of 1:2:1 intensity ratio *i.e.* half the overall peak height. The same is true of any resonance with increasing coupling (multiplicity) decreasing the sensitivity accordingly.

3.1.4 Quantitative Method Development

With the S:N improvements described in Section 3.1.3, a method capable of determining budesonide concentration in HPFP was developed in principle. The methodology was utilised to analyse a saturated suspension of budesonide at 298 K. Well defined signals observed for the A-ring protons of the budesonide molecule show S:N values ≥ 20:1 (Figure 3.1.4.1).
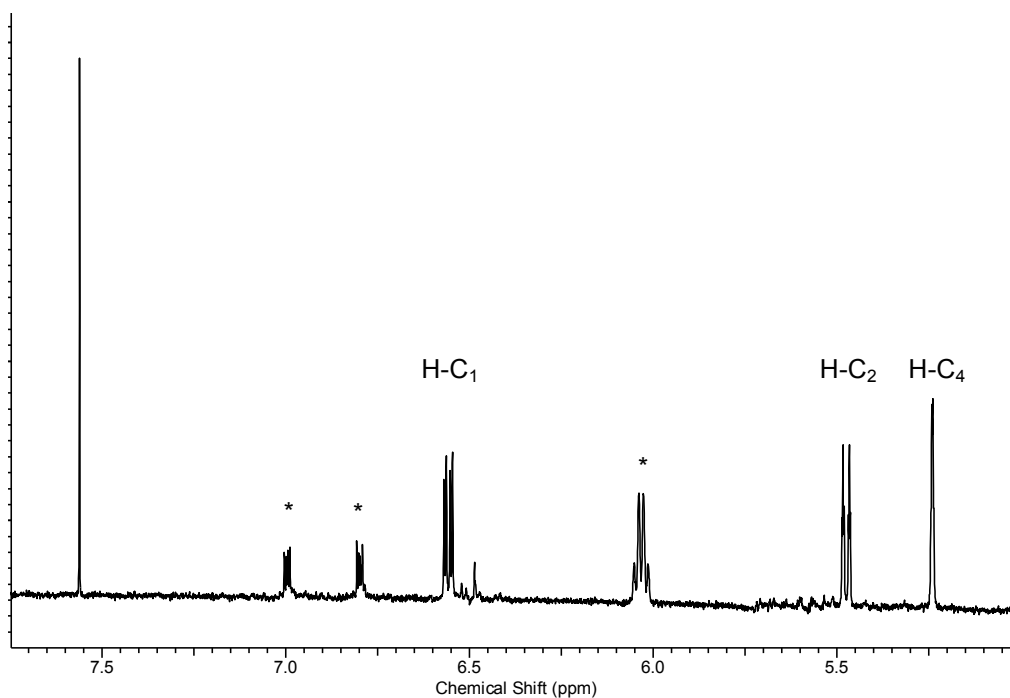
Figure 3.1.4.1 – ^{1}H NMR spectrum of a saturated suspension of budesonide in HPFP acquired using the optimised methodology.

Three additional resonances are apparent in the system (marked * in Figure 3.1.4.1). These also appear in the blank spectrum and clearly arise from impurities in HPFP / CD$_3$CN. The precise nature of these has not been determined but signal integration indicates the concentration is less than 100 µg/mL. Their resolution from the A-ring resonances of budesonide ensures they do not interfere with the peak integration used in quantitative data processing.

Solutions of known budesonide concentration in HPFP were created to allow the system to be 'calibrated' for the determination of true quantitative values of saturated suspensions *i.e.* solubility. The calibration of the system was necessary to take account of the co-axial tube arrangement, given that different volumes of reference and sample solutions are presented to the instrument, and are in effect in different positions relative to the probe coils. It is sensible therefore to generate a calibration factor to take account of these fixed conditions and use in subsequent experiments obtained using the same experimental setup.

Analysis of five separately prepared solutions of budesonide at known concentrations was performed using the developed acquisition parameters. Peak area values were obtained for the three A-ring resonances of budesonide and the singlet $CHCl_3$ proton from the reference solution. The values obtained were used to calculate a quantitative value of budesonide concentration, which was directly compared to the known values allowing the calculation of a factor that could be used in subsequent experiments to determine unknown solubility values (Section 2.2.5). The peak areas obtained and the calculated factor are shown (Table 3.1.4.1), with an example calculation. The mean factor for the system was calculated to be 0.316 ± 0.002, with a % coefficient of variation (% CV) value of 0.7 %. The results agree well over the concentration range investigated.

Table 3.1.4.1 – Peak area values for the A-ring protons of budesonide and CHCl$_3$ proton, with calculation of a system constant suitable for use in the calculation of unknown solubility values.

Budesonide concentration (µg/mL)	Peak Area				Mean	Normalised area (BUD/CHCl$_3$)	Raw result (µg/mL BUD)	Factor (Conc. BUD / Raw result)
	CHCl$_3$ IS*	6.55 ppm	5.5 ppm	5.25 ppm				
63.4	24.87	18.32	18.21	18.21	18.24	0.73	199.04	0.318
50.7	23.96	14.17	14.32	14.37	14.28	0.59	161.76	0.314
40.5	22.77	10.92	10.88	10.71	10.83	0.47	129.11	0.314
32.4	23.27	8.72	8.84	8.70	8.75	0.37	102.05	0.318
25.9	8.83	2.69	2.74	2.63	2.68	0.30	82.54	0.315
							Mean	0.316
							s	0.002
							% CV	0.659

* CHCl$_3$ = 271.3 µg/mL

Use of the factor for calculation of the solubility of budesonide in HPFP from experimentation carried out on saturated suspensions of the system is summarised (Section 2.2.5). The value obtained for the solubility of budesonide in HPFP was 87.0 µg/mL.

Accuracy of the methods was checked using saturated suspensions of budesonide in HPFP at ambient pressures, as determined by HPLC. The suspensions were prepared, equilibrated and filtered to remove residual solids. A two-fold dilution in HPFP was performed to ensure dissolution of any residual solids prior to the final (accurate) dilution step in HPLC mobile phase. Injections of the solutions were made onto the HPLC system according to the method specified (Section 2.2.5) alongside injections of reference standards of budesonide created at known concentrations in mobile phase. Peak area values for the budesonide peak eluting at retention time of *ca.* 6.5 minutes were obtained by integration and used to calculate

the amount of budesonide dissolved in the HPFP solution. Representative chromatograms for the reference material and the solutions in HPFP are shown as Figures 3.1.4.2 and 3.1.4.3.
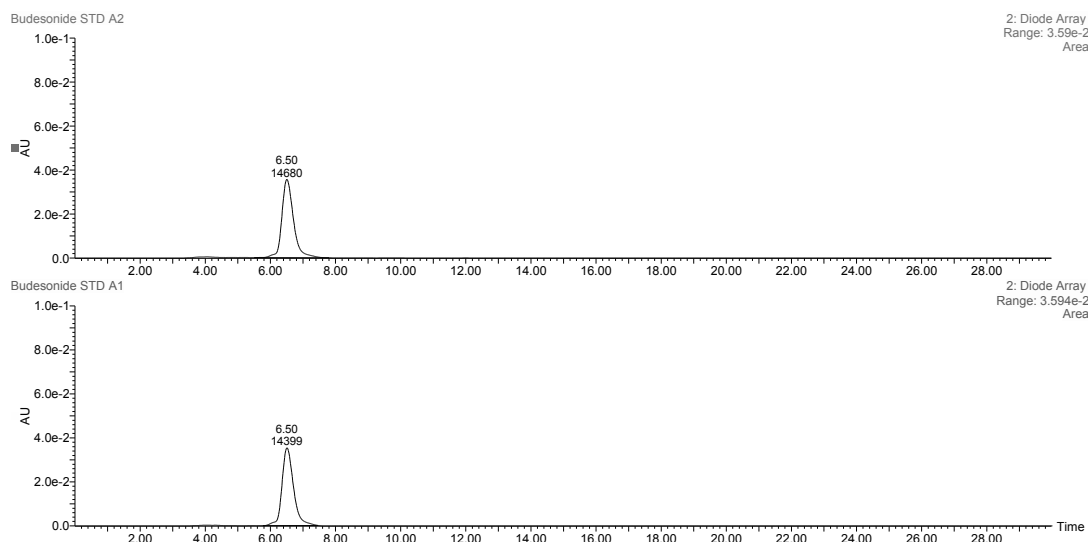
Figure 3.1.4.2 - Representative HPLC chromatograms showing replicate injections of budesonide reference standard.
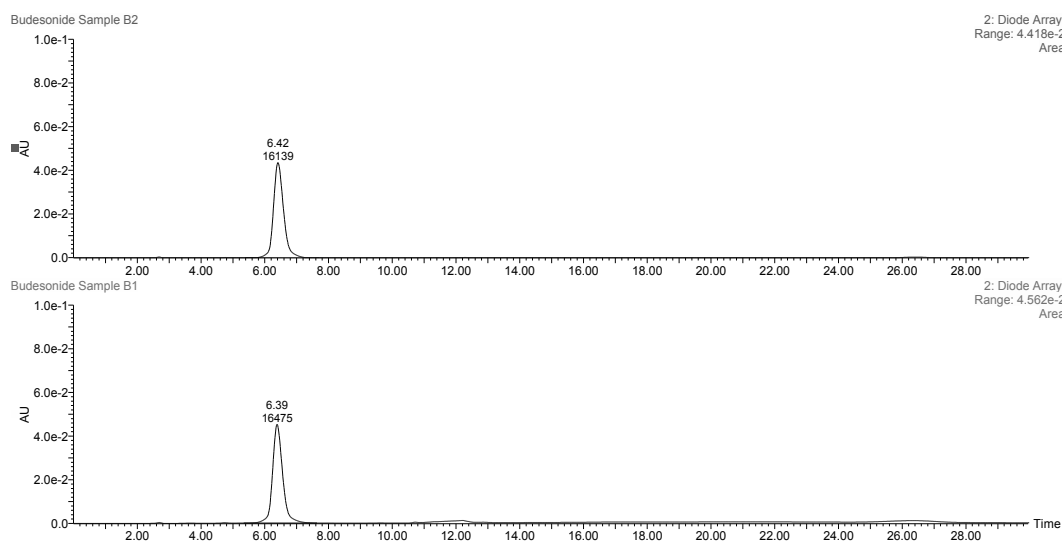
Figure 3.1.4.3 - Representative HPLC chromatograms showing replicate injections of HPFP prepared budesonide.

Quantitative solubility levels from the filtered saturated suspensions of budesonide in HPFP were calculated using a response factor based on the duplicate reference standards prepared as outlined (Section 2.2.5). A value of 86.8 μg/mL (± 0.32) was obtained, comparing favourably with those obtained from the NMR approach.

3.1.5 Reverse Co-axial NMR

A novel NMR approach for the determination of solubility in the model propellant HPFP has been developed. For the *in-situ* investigation of solubility at pressure of volatile propellants such as HFAs 134a and 227 used in commercial pMDI formulations, a novel approach to the experimental tube arrangements used was required. A standard NMR tube would not allow volatile propellants to be held at pressure in their liquid state, and transfer to the tubes would be problematic.

NMR tubes exist for the study of samples at elevated and reduced pressures and are commercially available from several suppliers; their use being well documented for the monitoring, for example, of pressurised reactions *in-situ* as in studies by Jonas *et al.* and Foley.[140,141] A PTFE screw fitting at the head of the tube commonly known as a J Young assembly allows for the increasing or reducing of pressure of the tube and its contents thus allowing, for example, volatile liquids to be held in this state by maintenance of a vapour pressure.

An image of a typical pressurisable NMR tube is shown (Figure 3.1.5.1).

Figure 3.1.5.1 – A typical pressurisable NMR tube assembly with PTFE screw fitting allowing reduction / increasing of pressure to the tube inner.[137]

These NMR tube types work well for the analysis of volatile solvents allowing maintenance of vapour pressure, however incorporation of the coaxial insert through the screw head of the tube assembly would prove impossible, thus not allowing the locking and referencing procedures already discussed to be carried out. There appears to be no simple way of incorporating a reference material into such a tube setup whilst still retaining the physical barrier between the two solutions.

In order to address the highlighted problems, a novel design of NMR tube was proposed; the co-axial arrangement previously operated was reversed, placing the sample solution into the inner capacity and the reference solution in the outer capacity. The co-axial insert could be equipped with a pressurisation mechanism sitting within and above that of the reference capacity that would remain at atmospheric pressure. A schematic representation (Figure 3.1.5.2) shows the proprietary tube assembly.
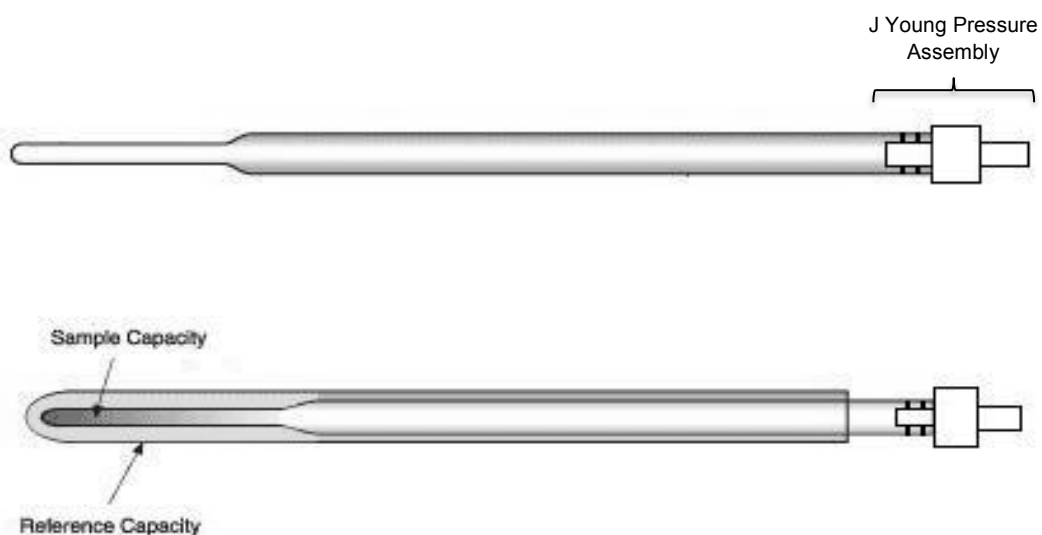
Figure 3.1.5.2 – The novel reversed co-axial tube arrangement allowing pressurisation of the inner volume (sample capacity) with an outer volume (reference capacity) remaining at atmospheric pressure.[137]

Specialist manufacture of such a tube assembly was commissioned and was carried out by Wilmad labglass, NJ, USA. Two primary designs were manufactured, with stems chosen to fit within a standard 5 mm NMR tube incorporating a J Young pressure assembly. The sensitivity of the method would reduce compared to that of the previously utilised tube setup as the diameter of the sample capacity, hence the sample volume, would be reduced. The stems of the two were therefore chosen to maximise the sample capacity of the designs; if the standard co-axial insert had been used for the basis of the tube manufacture, a sample capacity of only 60 µL would have resulted. The submitted designs featured the stems from tubes designed as stem coaxial inserts for 8 and 10 mm NMR tubes, with capacities of 190 and 410 µL respectively.

Testing of the two stem inserts manufactured demonstrated that the larger of the two inserts left only a very small reference capacity on the outside of the

stem insert when inserted into a standard 5 mm NMR tube. From a practical

operational point of view, this led issues in maintaining a reproducible lock

signal in the spectrometer. The smaller of the two tube setups did not suffer

from this problem and reproducible addition of accurate volumes of reference

solution resulted in precise and easy manipulation. Several of these tubes

were manufactured to allow routine operation of the developed method; one

of the tubes is shown (Figure 3.1.5.3).

Figure 3.1.5.3 – Pressurisable stem co-axial insert for use with a standard 5

mm NMR tube.

The reversal of the sample and reference capacities and the different

volumes in each presented to the instrument was anticipated to lead to a

different calibration factor applied when utilising the system to quantitatively

determine solute solubility. A repeat of the exercise carried out on the

standard co-axial set up was performed to calculate a new factor for the new

arrangement. A series of reference solutions of budesonide in HPFP at

known concentrations were prepared as summarised (Section 2.3.6) and

prepared for analysis in the revised tube arrangement, with 190 µL in the

sample capacity and 300 µL in the reference capacity. Table 3.1.5.1 shows a

summary of the peak areas obtained and the calculated factor. The mean

factor for the system was calculated to be 8.008 ± 0.08, with a % coefficient

of variation (% CV) value of 1.0 %. The results agree well over the

concentration range investigated and this factor has been used in calculations using this method.

It should be noted that reference solution of $CHCl_3$ in CD_3CN was reduced in concentration for this experimentation as i) the increased volume of the reference and ii) its position in the probe relative to the receiver coils leads to peak areas considerably greater than those of the analyte signals. It is desirable to have the peak area of the reference standard closely match the peak areas of the analyte, in a similar approach to internal standardisation.

Table 3.1.5.1 – Summary of the peak areas obtained and the calculated system factor.

Budesonide concentration (µg/mL)	Peak Area				Mean	Normalised area (BUD/CHCl₃)	Raw result (µg/mL BUD)	Factor (Conc. BUD / Raw result)
	CHCl₃ IS	6.55 ppm	5.5 ppm	5.25 ppm				
60.50	440	12.46	12.16	12.54	12.39	0.028	7.609	7.951
48.40	510	11.43	11.28	11.13	11.28	0.022	5.978	8.096
38.72	460	8.53	8.17	8.24	8.31	0.018	4.885	7.926
30.98	410	5.82	5.85	5.82	5.83	0.014	3.844	8.059
							Mean	8.008
							S	0.082
							% CV	1.028

* $CHCl_3$ = 270.8 µg/mL

3.1.6   ERETIC NMR

A second referencing approach (summarised in Section 1.3.2) has been investigated as part of these studies. **E**lectronic **RE**ference **T**o access *In-vivo* **C**oncentrations or ERETIC NMR methods offer the ability to perform quantitative NMR measurements without the need to incorporate a reference standard in the system analysed. Its use in quantitative NMR is limited, though work by Remaud *et al.*[128] and VanLockeren *et al.*[142] highlights the usefulness of the technique. The work reported to this point in these studies has involved the physical incorporation of a standard reference compound ($CHCl_3$) into the experimental setup to allow quantitative calculations to be performed on the resultant data. ERETIC methods aim to avoid this by using the electronics of a free channel of the NMR spectrometer to incorporate a signal of known magnitude and position electronically into the spectrum; this can be subsequently used for quantitative purposes in much the same way as a signal from a reference compound can using peak integrations. All modern spectrometers can generate shaped Rf pulses; an ERETIC pulse uses an exponential decay shape to incorporate a peak of Lorentzian shape which is detected simultaneously to the sample FID during acquisition. The rate of decay of the FID dictates the linewidth of the incorporated signal. The technique offers several advantages over the more conventional approaches to quantitative NMR including (i) once established, the method is easier and faster in its operation *i.e.* little or no standard preparation (ii) the method could be run in standard pressurisable NMR tubes for the volatile propellants studied here (as the ERETIC signal removes the need to incorporate a reference compound) and (iii) the ERETIC signal can be chosen to have

variable magnitude and to fall anywhere in the spectrum, away from interferences generated by the analytical resonances of interest or other contaminating signals in the spectra.[129,142,143,144]

The potential for using ERETIC in this study was assessed. A pulse programme allowing the incorporation of ERETIC signals was generously provided by Dr. Peter Meadows, JEOL UK Ltd. The writing of these pulse sequences is considered outside the scope of this project, and JEOL kindly agreed to provide a pre-written sequence allowing the trial of its usefulness here. Assessment of a simple solution of $CHCl_3$ in CD_3CN (13.0 mg/mL) was performed in a standard 5mm NMR tube to calibrate the ERETIC pulse. The procedure is described in detail (Section 2.3.7) and is required to incorporate a correctly phased signal. Experiments were carried out with a 10.0 ppm chemical shift selected for the ERETIC signal away from interfering resonances and was repeated with a -1.0 ppm shift. Correctly phased ERETIC spectra of $CHCl_3$ in CD_3CN (13 mg/mL) with offsets of 10.0 and -1.0 ppm chemical shift are shown (Figures 3.1.6.1 and 3.1.6.2).
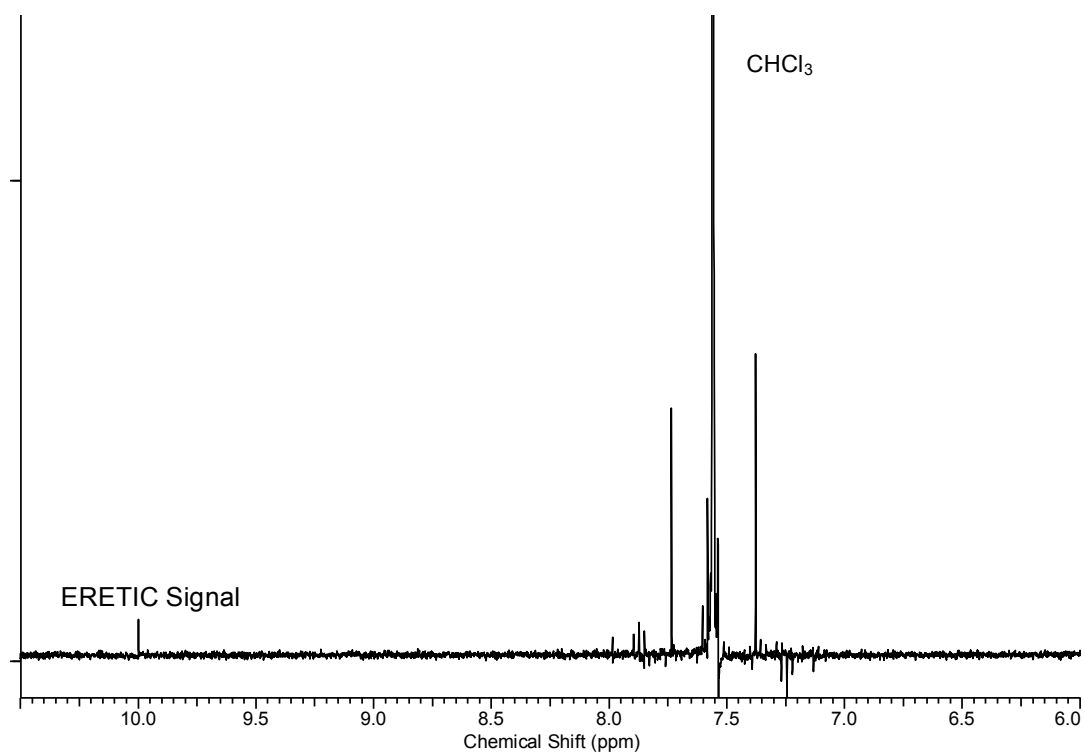
Figure 3.1.6.1 – ^{1}H NMR spectrum of $CHCl_3$ in CD_3CN (13 mg/mL) acquired using correctly phased ERETIC experiment chosen to place the signal at 10.0 ppm chemical shift.
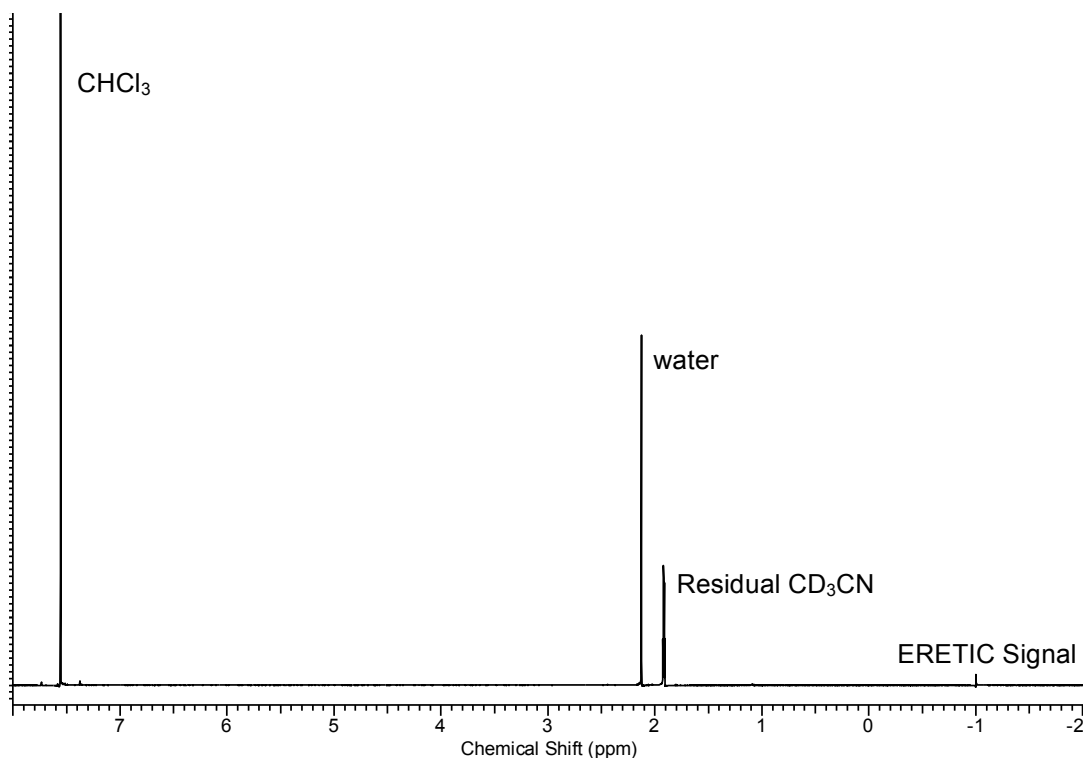
Figure 3.1.6.2 – ^{1}H NMR spectrum of $CHCl_3$ in CD_3CN (13 mg/mL) acquired using correctly phased ERETIC experiment chosen to place the signal at -1.0 ppm chemical shift.

The signal intensity incorporated using the ERETIC method is very low when compared to that of the $CHCl_3$ signal at this concentration. This difference in magnitude will differ according to the final concentration of $CHCl_3$ chosen to calibrate the system, however as stated it is also possible to control the magnitude of the ERETIC signal simply by choosing the power input (a 6 dB increase should bring about a doubling of the signal observed).[125] An overlay of 3 experiments performed using sequentially increasing power of the ERETIC signal is shown (Figure 3.1.6.3), giving full control over the magnitude of the signal detected.
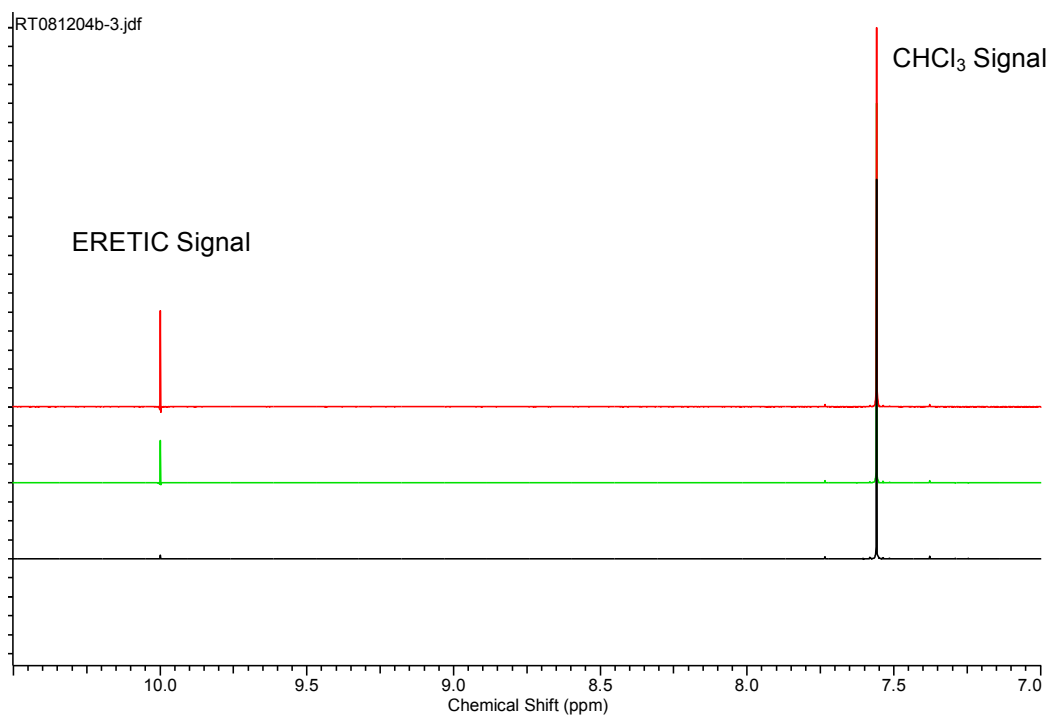
Figure 3.1.6.3 – Overlaid ^{1}H NMR spectra showing the effect of increasing power of the ERETIC signal incorporated into the experiment (black=1 dB, green=10 dB and red=20dB) showing the magnitude of the signal increasing with applied power.

The final method modification applied to the system was incorporation of a pre-saturation solvent suppression protocol to address the dynamic range issues already discussed at length (Section 3.1.4). An ERETIC methodology was created (Dr. Peter Meadows, JEOL UK Ltd) to allow the incorporation of the ERETIC signal in concert with pre-saturation suppression programming. This approach was utilised to assess a saturated sample of budesonide in HPFP for direct comparison to that carried out previously with the externally standardised co-axial methods. The ^{1}H spectrum obtained from the ERETIC calibration experiment using $CHCl_3$ in CD_3CN (84 µg/mL) is shown (Figure 3.1.6.4). Also shown is the ^{1}H spectrum of a saturated suspension of

budesonide in HPFP with the incorporation of an ERETIC signal at 9.0 ppm

chemical shift, expanded in the low field region (Figure 3.1.6.5).

RT090119c-4.jdf
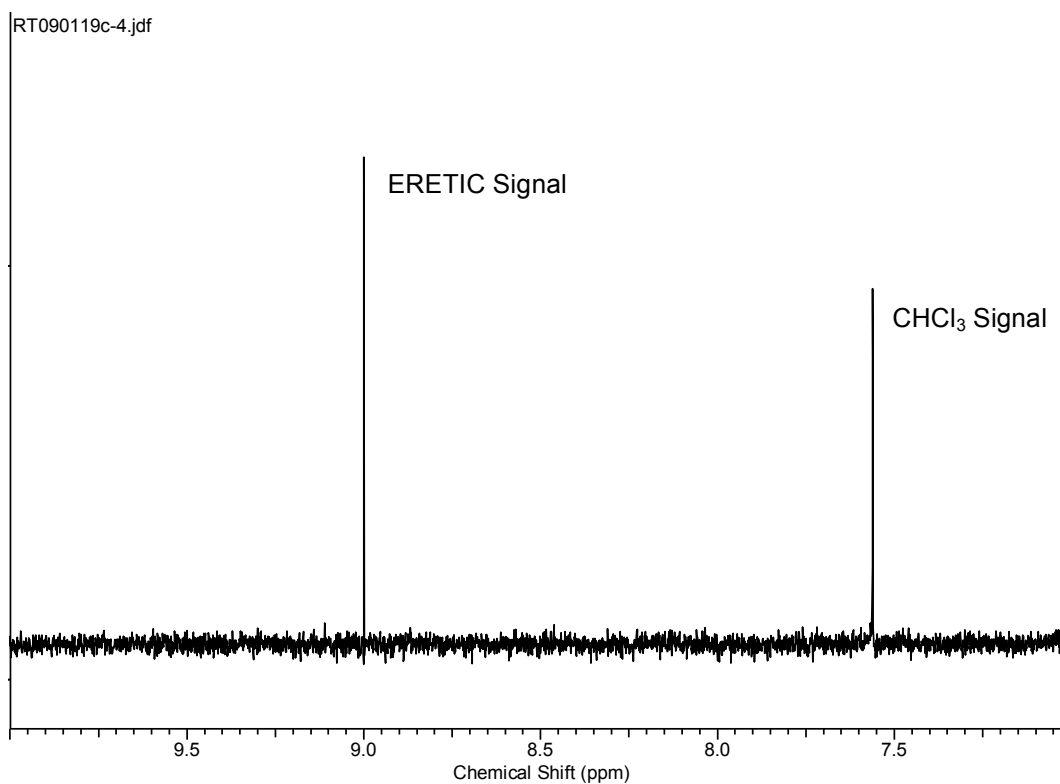
Figure 3.1.6.4 – ^{1}H NMR spectrum of CHCl$_3$ in CD$_3$CN incorporating an

ERETIC signal at 9.0 ppm chemical shift (expanded in the region downfield

of 7.0 ppm chemical shift).
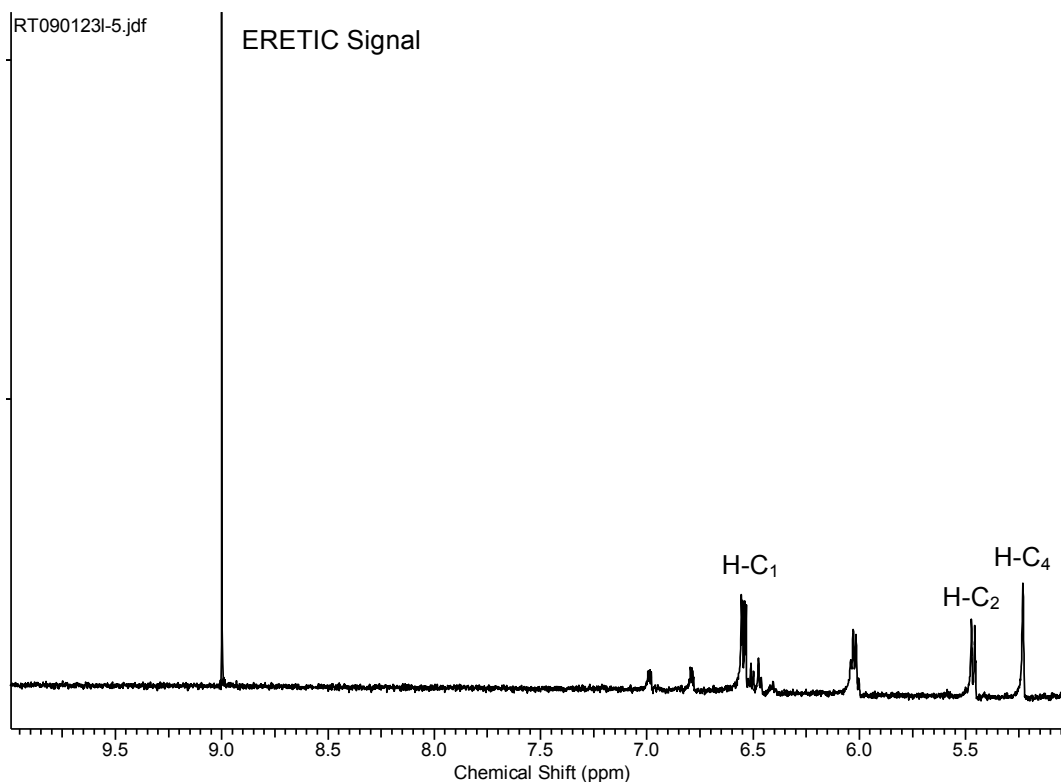
Figure 3.1.6.5 - ^{1}H NMR spectrum of saturated suspension of budesonide incorporating an ERETIC signal at 9.0 ppm chemical shift (expanded in the region downfield of 5.0 ppm chemical shift).

Calculation of the solubility of budesonide in HPFP using this experimental approach is shown (Section 2.2.7). The value of 76 µg/mL compares favourably with the value of 87 µg/mL obtained using the direct standard incorporation described and the HPLC validated data. There is however an inaccuracy of > 10% when compared to these values and there is suggestion in work by VanLockeren[142] that the ERETIC approach is less precise than classical co-axial based approaches. The operation of spectrometers unlocked without the incorporation of deuterated lock signals can lead to strange looking spectra and erroneous results (as highlighted previously).[125,138,145] The time advantages also cited are considered minimal when initial signal calibration has been carried out. It is for these reasons that

further development and investigation using ERETIC approaches was not undertaken in these studies, and the co-axial methodologies considered to this point were utilised in assessment of solubility by NMR.

3.1.7 Temperature Calibration of NMR Probe

The analysis of solubility at pressure has already been described and the benefits discussed. A further advantage offered by the newly developed NMR method is the ability to control temperature *in-situ*. Saturated suspensions can be formed within the NMR tube setup and allowed to equilibrate at a controlled temperature, both above and below ambient conditions as apparatus allows. The 600 MHz NMR used for the experimentation outlined in this study is equipped with a variable temperature probe controllable at temperatures above and below ambient with the aid of the FTS electronic temperature control unit supplying cooled dry air to the sample probe. The VT systems are however considered relatively inaccurate for absolute temperature control due to their lack of calibration.[125] It was imperative therefore to ensure accurate control of temperature to allow the determination of solubility values at accurately defined temperatures.

One widely accepted approach utilised in NMR temperature calibration is to use an NMR parameter that has temperature dependence as a form of thermometer.[125,146] The use of several reference materials have been reported,[147-150] though methanol and ethylene glycol are the two most widely used for temperatures between 175 – 310 K and 300 – 400 K respectively. For the temperatures of interest in these studies, the chemical shift difference between the CH_3 and OH protons in methanol allows the calibration

procedure to be performed as the OH protons shift relative to the static CH_3 resonance with changes in temperature.

Equation 3.1.7.1 holds true for the temperatures in the range of the experimentation performed.[125]

$$T\ (K) = 468.1 - 108.9\Delta\delta \qquad \textbf{Equation 3.1.7.1}$$

To carry out the temperature calibration, a solution of MeOH in MeOD was prepared and analysed as summarised in Section 2.2.8. The chemical shift differences between the OH and CH_3 protons used in equation 3.1.7.1 and the true temperatures of the sample were calculated. Table 3.1.7.1 shows the selected and calculated values with Figure 3.1.7.1 showing a plot of true sample temperature *vs*. selected temperature. These data were used in all subsequent varied temperature (VT) studies of solute solubilities to ensure accurate temperature control of the experiments performed.

Table 3.1.7.1 – Results of the temperature dependent chemical shift values of OH and CH_3 resonances in MeOH.

Selected T (K)	Chemical shift, δ		Δδ	T (K)	T (°C)
	OH	CH$_3$			
253	5.0819	3.32	1.7619	276.2	3.2
263	5.0349	3.32	1.7149	281.3	8.3
270	5.004	3.32	1.684	284.7	11.7
278	4.9611	3.32	1.6411	289.4	16.4
288	4.9227	3.32	1.6027	293.6	20.6
293	4.8946	3.32	1.5746	296.6	23.6
298	4.8694	3.32	1.5494	299.4	26.4
305	4.8437	3.32	1.5237	302.2	29.2
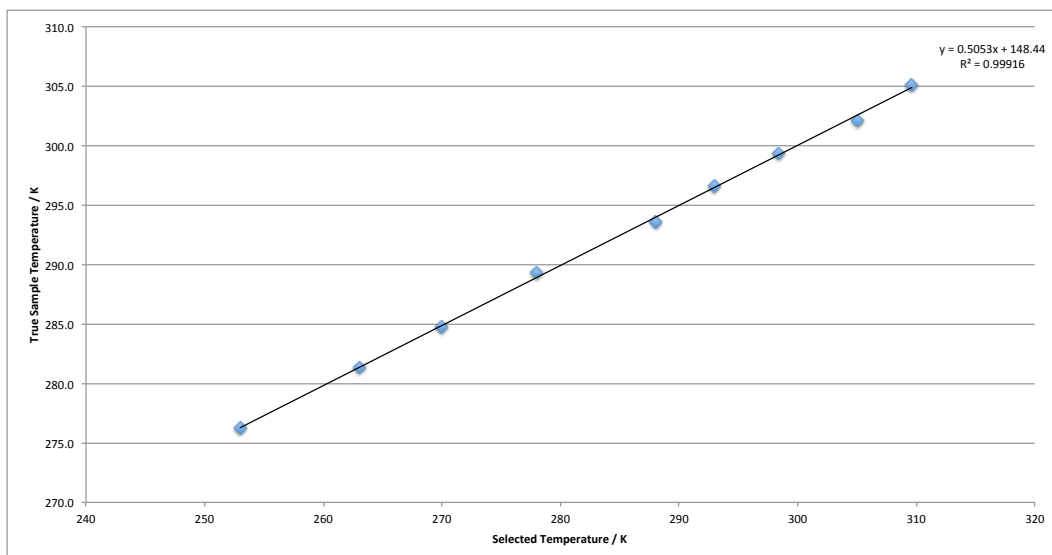
Figure 3.1.7.1 – Plot of true sample temperature *vs.* selected temperature.

3.1.8 Quantitation of Budesonide in HPFP (298, 283 & 278 K)

The developed methods were used to collect data on saturated suspensions of budesonide in the model propellant HPFP, with acquisitions made in triplicate to provide an estimation of error. Determinations were carried out at 3 discrete temperatures (i) 298 (ii) 283 and (iii) 278 K. Samples were prepared as summarised (Section 2.2.9) and equilibrated for > 24 hours at each temperature before data acquisition. Results were acquired for each temperature (Table 3.1.8.1) and are quoted with associated precision values (σ and % CV).

Table 3.1.8.1 – Budesonide solubility calculated using reversed co-axial

NMR set up at 278, 283 and 298 K.

Temp (K)	Concentration (μg/mL)				σ	% CV
	1	**2**	**3**	**Mean (n=3)**		
298	90	90	88	89	1.1	1.3
283	88	88	88	88	0.2	11.7
278	88	82	87	86	3.6	4.2

3.1.9 Cold Transfer of HFA134a / HFA227 and Associated Method Modifications

The developed NMR method using the reverse co-axial setup has been

shown to be a practical and reliable approach for the study of IPPs in volatile

fluorinated solvents. The key to the versatility and novelty of the methodology

however is the ease with which solvents can be studied in their liquid state.

The two solvents of primary interest in the formulation of APIs for inhalation

applications are HFAs 134a and 227 as discussed. Having boiling points of

246.7 and 256.5 K respectively,[151] the solvents are gaseous at room

temperature unless held under pressure for which the designed method is

particularly suitable. A specific apparatus was designed and assembled to

allow the gaseous solvents to be transferred to the pressurisable NMR tubes

at room temperature. A schematic of the apparatus is shown (Figure 3.1.9.1)

whereby liquid solvent from a pressurised cylinder (Section 2.1) was

transferred through a coil cooled by immersion in solid CO_2. The liquefied

gas passes through a valve into a pressure vessel where it can be stored.

Each time an NMR tube fill is required, the valve attached to the dip-leg of

the storage vessel is opened and allows liquefied gas to flow through into the

NMR tube where it can be maintained in its liquid state by closure of the J Young valve. The transfer process can be aided by evacuation of the NMR tube prior to opening to the liquid storage vessel as necessary. A photograph of the apparatus is provided in Experimental section 2.2.10.

Pressure vessel filling
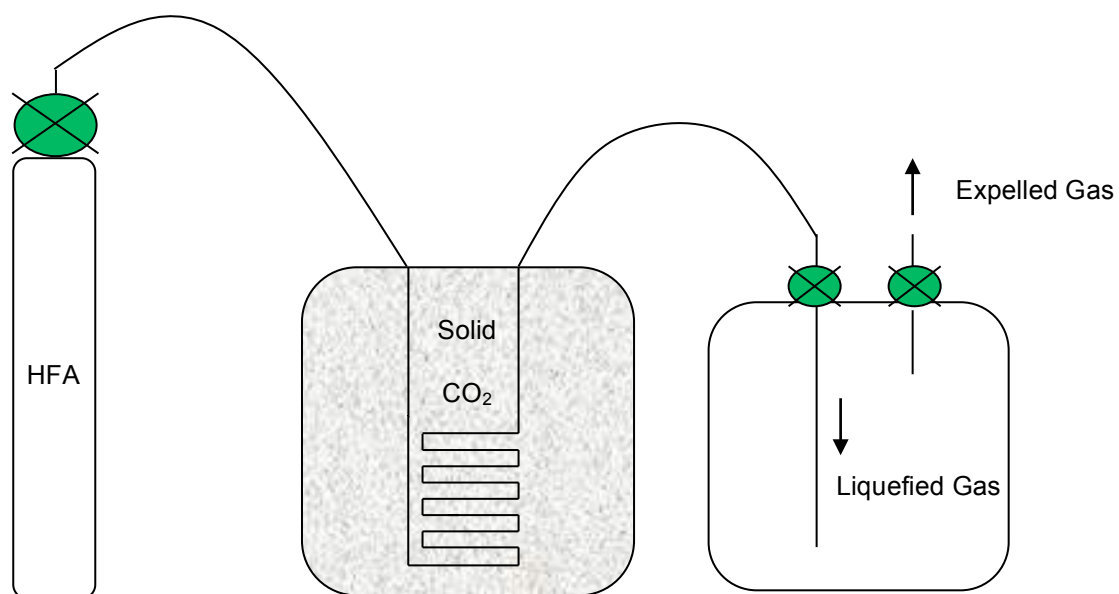
NMR tube filling
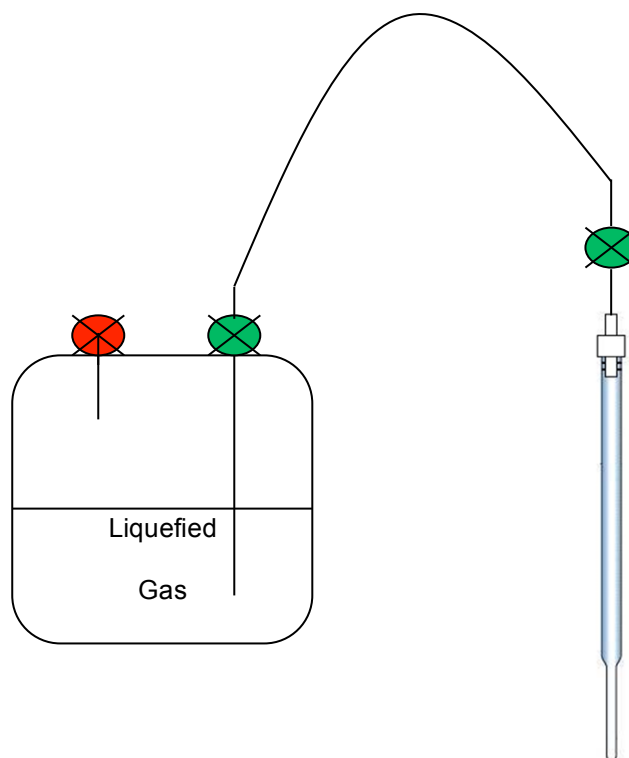
Figure 3.1.9.1 – Schematic representation of the cold transfer apparatus for filling NMR tubes with liquefied gases.

Blank solutions of HFAs 134a and 227 were examined in the reversed co-axial tube set up. The solvents used are different molecular entities and therefore have a unique NMR response that requires, as with HPFP, solvent suppression to maximise the sensitivity of the method for the analyte resonances. The ^{1}H spectra for HFAs 134a and 227 are shown (Figures 3.1.9.2 and 3.1.9.3) with coupling data given in Tables 3.1.9.1 and 3.1.9.2.[134]
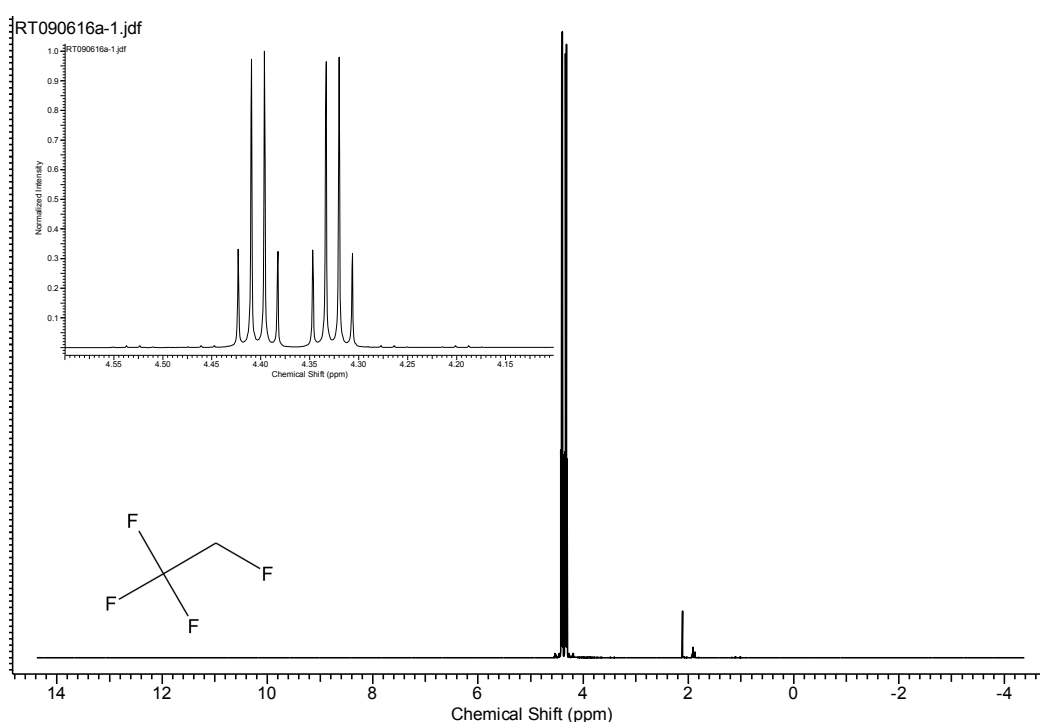
Figure 3.1.9.2 – ^{1}H NMR spectrum of HFA134a obtained using the reverse co-axial setup.

Table 3.1.9.1 – Coupling constant data for ^{1}H NMR of HFA134a.

Chemical Shift (ppm)	Spin-Spin Coupling Data
4.37	$^2J(H,F) = 45.7$ Hz, $^3J(CF_3) = 8.3$ Hz
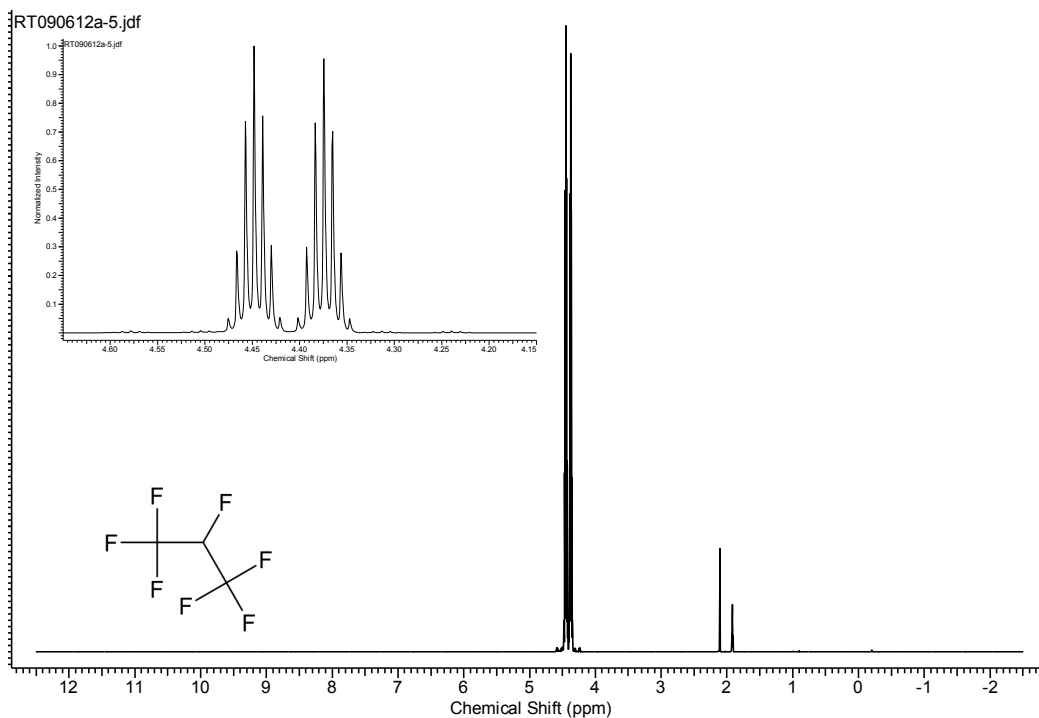
Figure 3.1.9.3 – ^{1}H NMR spectrum of HFA227 obtained using the reverse co-axial setup.

Table 3.1.9.2 – Coupling constant data for ^{1}H NMR of HFA227.

Chemical Shift (ppm)	Spin-Spin Coupling Data
5.07	$^{2}J(CHF) = 43.7$ Hz, $^{3}J(CHCF_3) = 5.4$ Hz

The solvent suppression developed for HPFP was modified to suppress the signals obtained from the two further solvents by shifting the presaturation set point to the centre point of the chemical shift values obtained for HFA134a and HFA227.

The resonances observed for the three solvent signals also displayed temperature dependence, and shifted slightly to higher field values with a reduction in temperature. Further method modification was required with respect to suppression positioning to allow for this signal shift.

For each solvent, three separate methods were developed to allow routine deployment at the three selected temperatures, giving a total of nine separate methods for deployment in quantitation of APIs in HPFP, HFA134a and HFA227 at 278, 283 and 298K.

3.1.10   NMR Assignment of Inhaled Compounds of Interest

A limited ^{1}H spectral assignment was carried out on each of the APIs analysed to allow a reliable resonance to be determined in each case for use in the quantitative assay of solubility in the three propellant systems. Full spectral assignment was unnecessary as the primary requirement was to reliably identify specific signal(s) from each API that could be assigned. It is clearly of paramount importance however that the number of protons associated with the chosen resonances is correctly determined to avoid any error in the quantitative results obtained from the experiments. ^{1}H spectra of each of the APIs analysed are shown as Figures 3.1.10.1 to 3.1.10.10 with spectral assignments.[152-163] Several factors in the selection of specific resonances to utilise in the quantitative experiments have to be considered; primarily the resonance or resonances have to occupy a chemical shift environment sufficiently free from interferences from the other signals in the spectrum *e.g.* the main solvent response (or proximity to the applied suppression), residual solvent signals from CD_3CN and any other impurity signals observed in the blank solvent systems. They should also, where possible, be intense signals associated with the maximum number of protons with the lowest multiplicities possible, thus maximising the sensitivity of the experiment for each analyte. A good example here is the tertiary butyl (t-Bu)

signal in terbutaline and salbutamol samples being an intense, sharp singlet

arising from the 9 protons of the functional group.
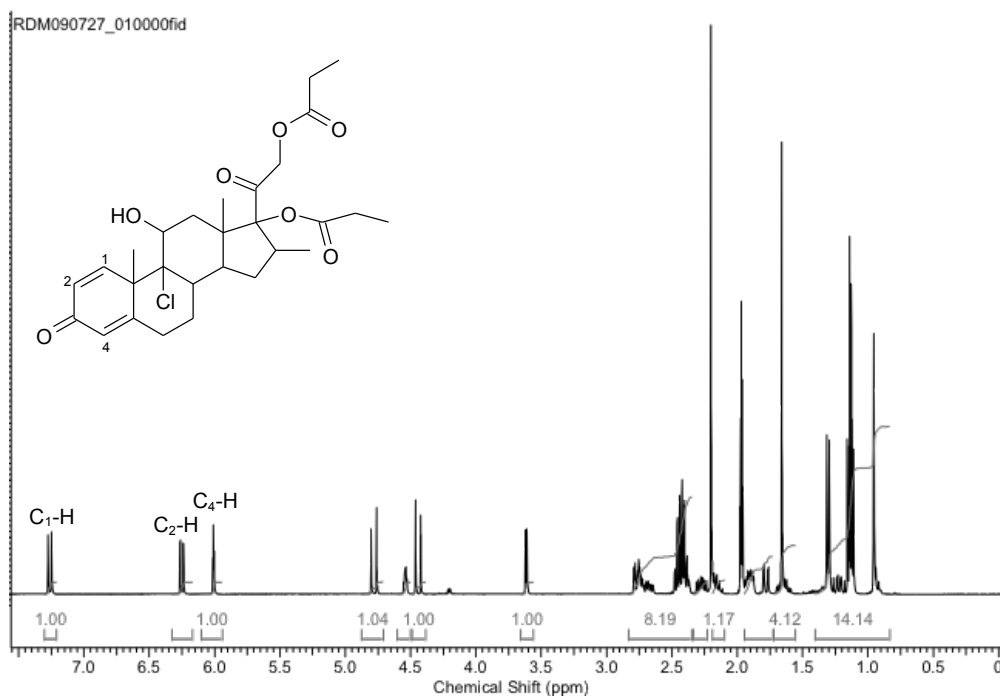
Figure 3.1.10.1 – ^{1}H NMR of beclomethasone dipropionate BP, BMD-N-004-09.
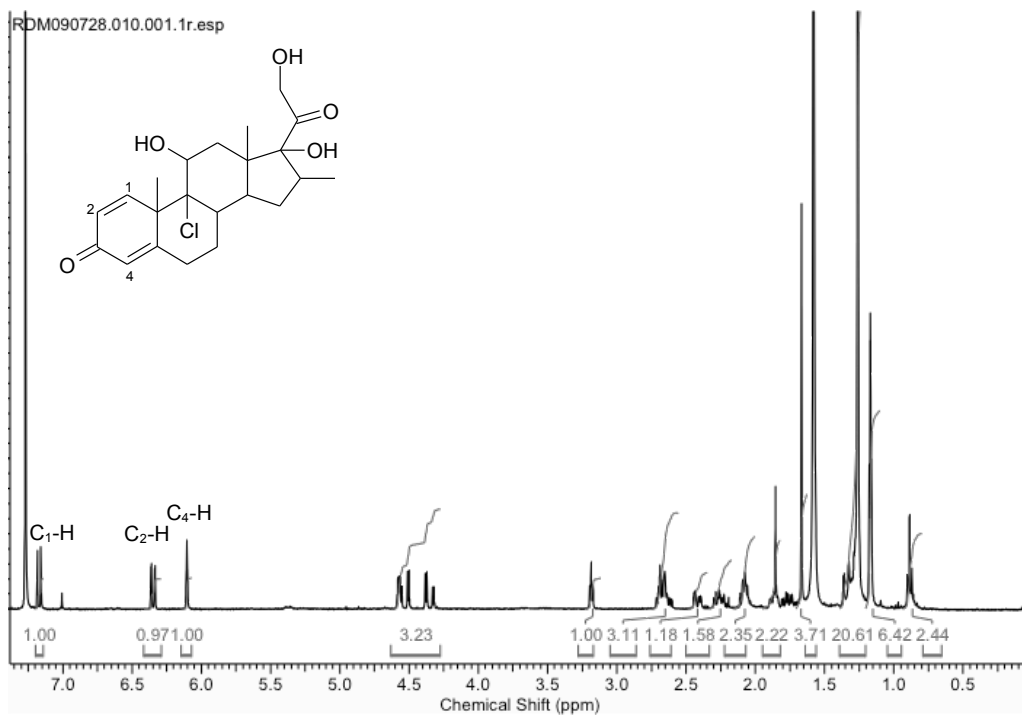
Figure 3.1.10.2 - ^{1}H NMR of beclomethasone base, BMD-N-006-09.
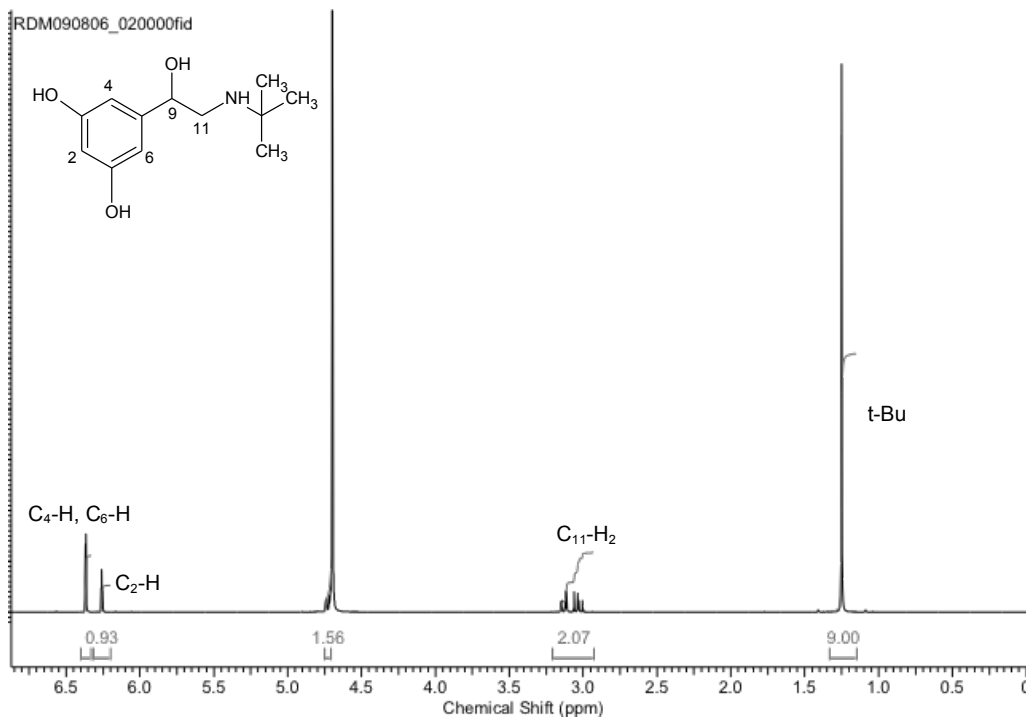
Figure 3.1.10.3 – ^{1}H NMR of terbutaline sulphate USP, TBS/105/07-08.
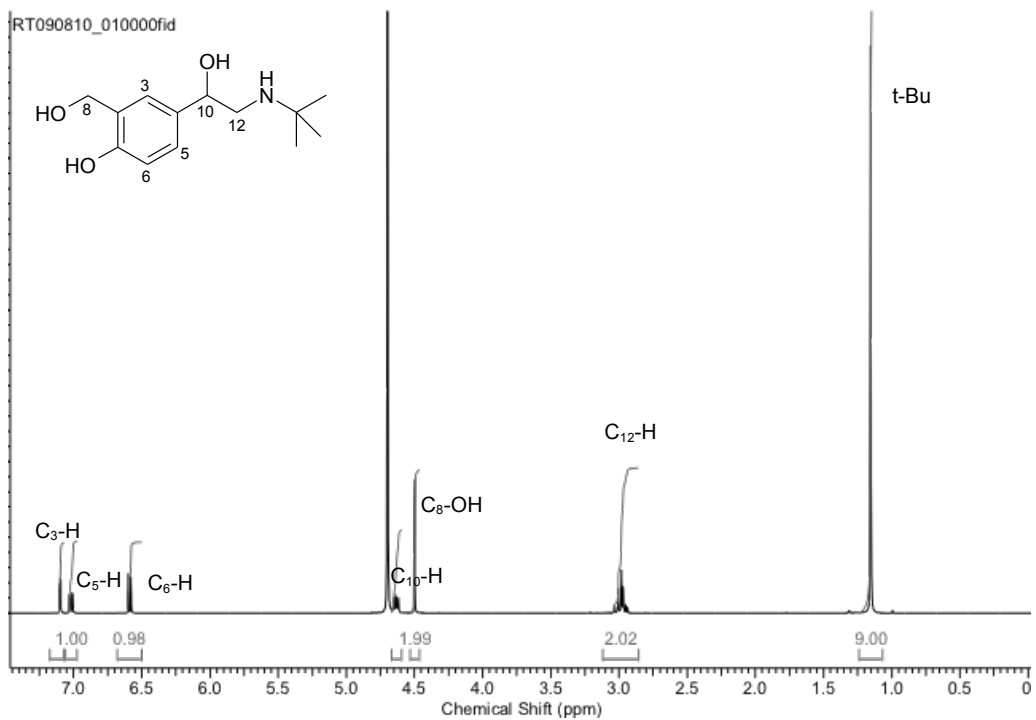
Figure 3.1.10.4 – ^{1}H NMR of salbutamol base BP, SB/101/09-10.
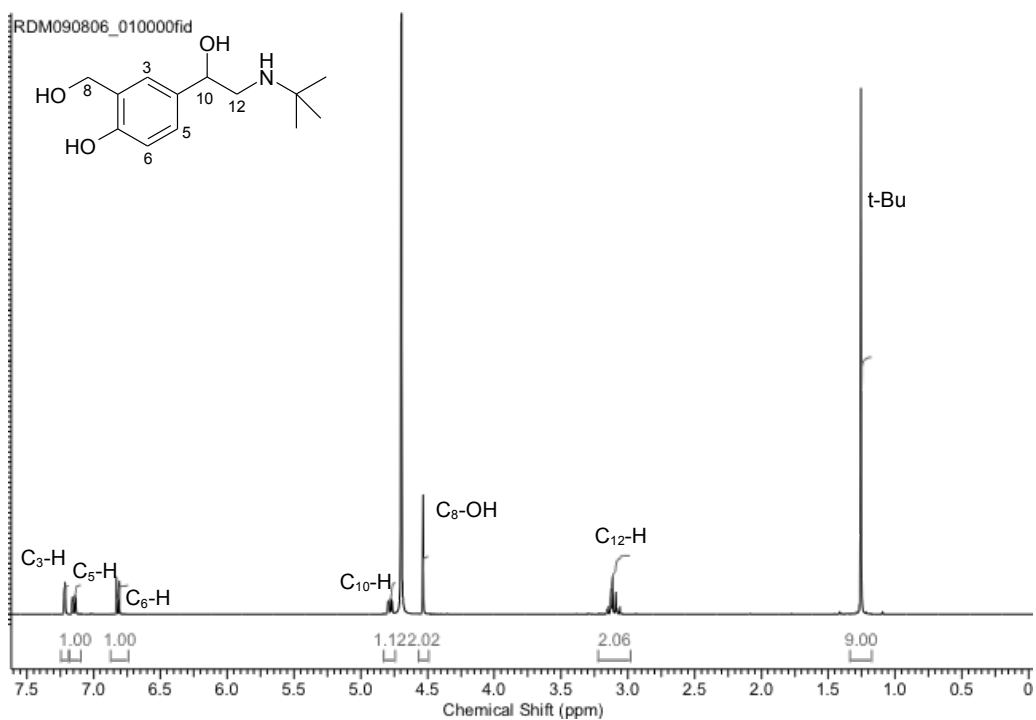
Figure 3.1.10.5 – ^{1}H NMR of salbutamol sulphate BP, SS/103/09-10.

118
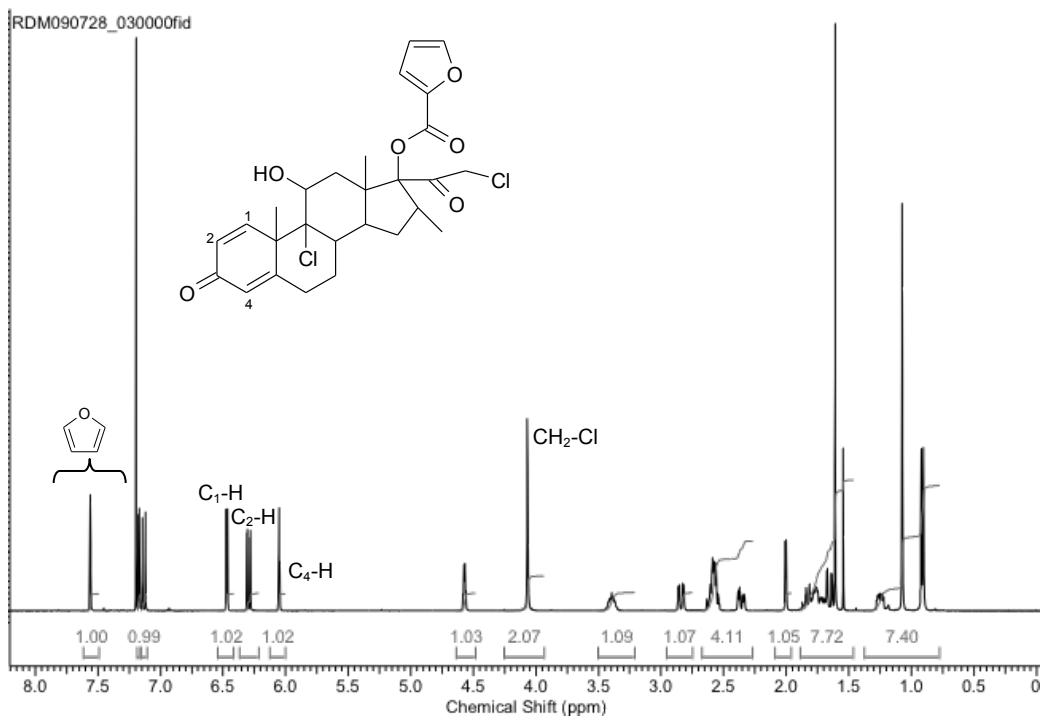
Figure 3.1.10.6 – ^{1}H NMR of mometasone fuorate USP, APL/72/C-09.
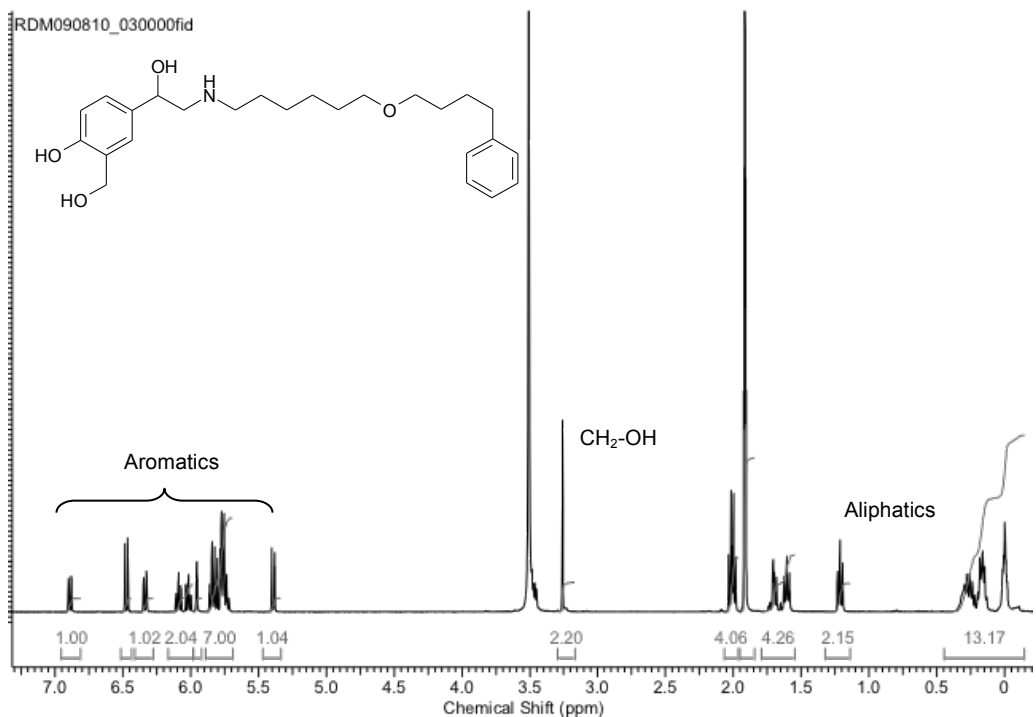
Figure 3.1.10.7 – ^{1}H NMR of salmeterol xinafoate Ph. Eur, SX-V/009/08.

119
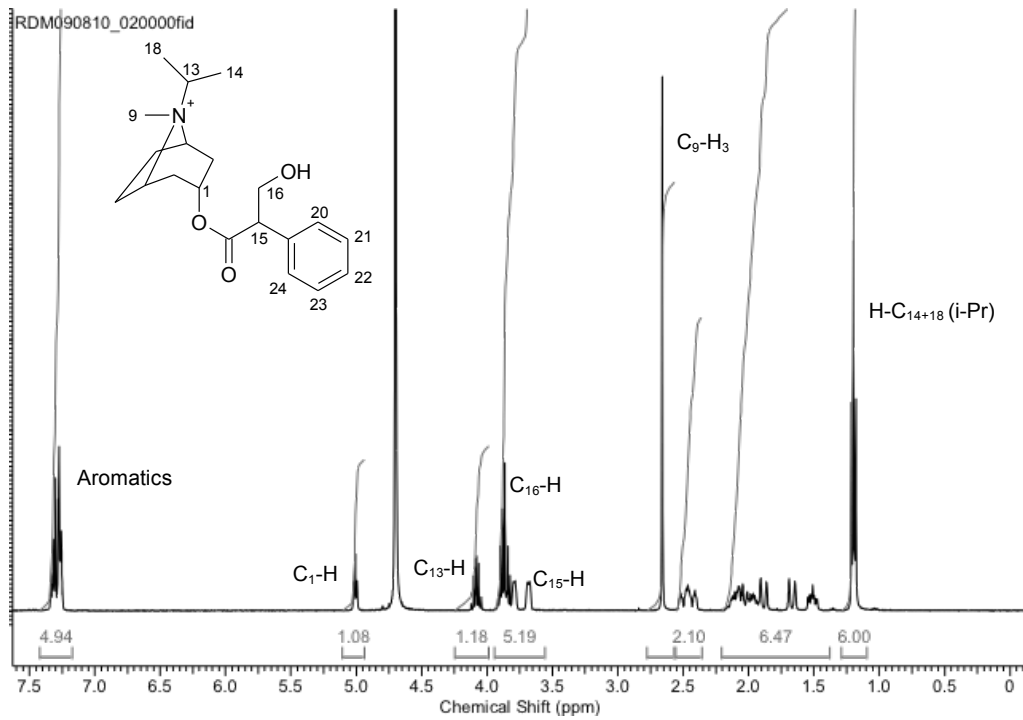
Figure 3.1.10.8 – ^{1}H NMR of ipratropium bromide BP, IPI-0109001.
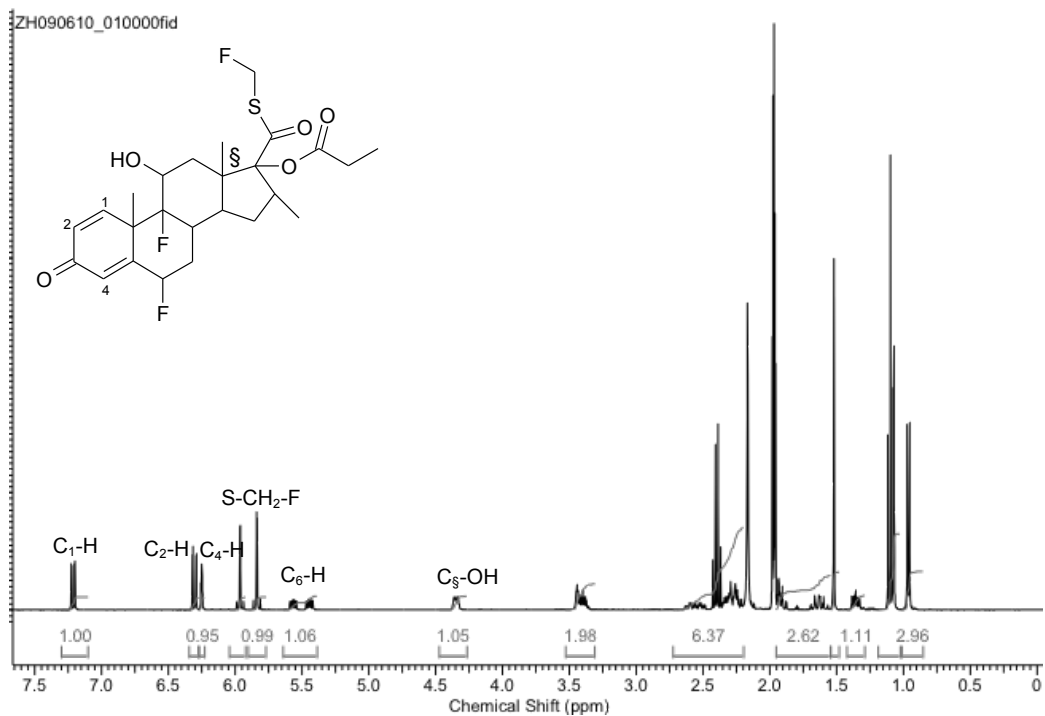
Figure 3.1.10.9 – ^{1}H NMR of fluticasone propionate USP, 408901-FP.
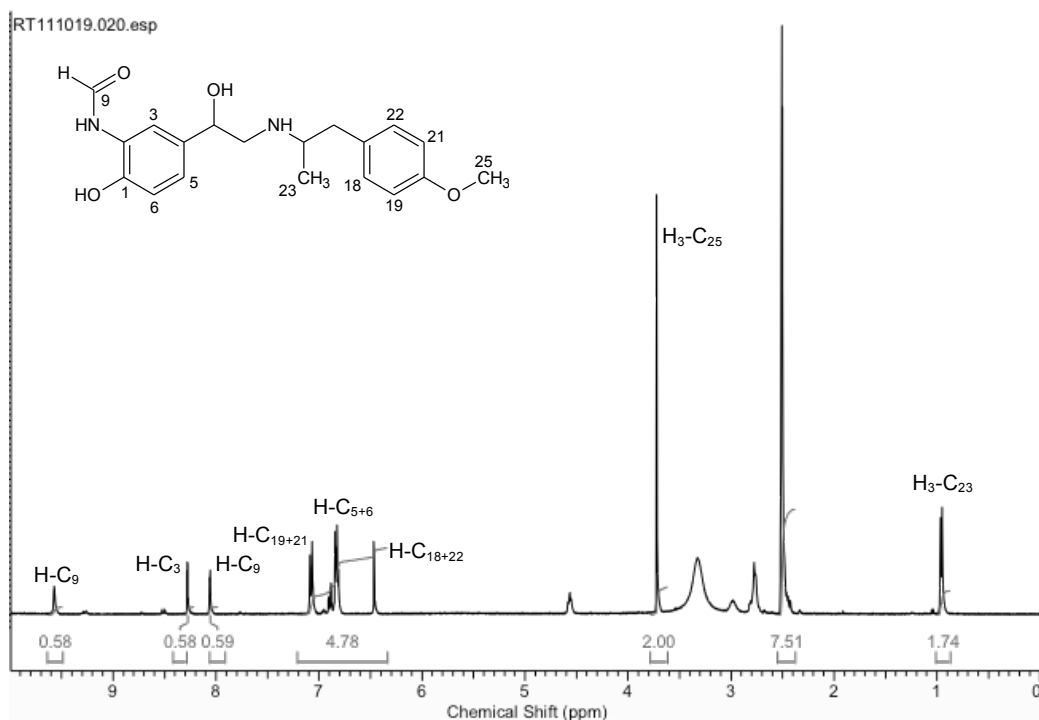
Figure 3.1.10.10 – ^{1}H NMR of formoterol fumarate, 019K4705.

3.1.11   HPLC

The developed NMR methodology has provided a rapid and sensitive means of determining the solubility of many of the IPPs under study, and these data are presented (Sections 4.1.1 and 4.1.2). The LOD / LOQ values obtained for the currently operated method are discussed (Section 3.1.3), and in the cases of certain IPPs, they do not allow quantification within these limits. In these cases, HPLC approaches have been used to complete the data set for the HPFP samples equilibrated at 298 K. These approaches are however time-consuming and only allow the study of samples easily in HPFP (liquid) without the use of significant additional apparatus; pressure filtration methods whereby prepared pMDI canisters are filtered through micro-porous membranes (typically 0.22 µm) to receiver canisters have been used to prepare propellant based formulations for solubility study by HPLC [122,123]

121

and more recently Myrdal *et al.*[124] have developed a direct injection protocol using modified Rheodyne™ injection systems to introduce filtered sample from prepared canisters directly to the HPLC system.

For each of the systems that gave a result below the LOD of the NMR approach, saturated suspensions were created in HPFP and equilibrated for > 24 hours at 298 K. Preparation of the solutions and HPLC methods deployed are summarised (Section 2.3.2). The calibration lines calculated for each analyte gave linear responses in all cases with correlation coefficients (r^2) ≥ 0.99. These data are presented (Table 3.1.11.1) and were used to calculate solubility of each IPP studied in this manner. The results are presented in Chapter 4 (Section 4.1.1).

Table 3.1.11.1 – Correlation data obtained for the calibration lines calculated from HPLC analysis of IPPs with solubility values undeterminable by NMR.

Analyte	Gradient, m	Correlation coefficient (r^2)
Beclomethasone	961.8	0.9998
Formoterol fumarate	2143.9	0.9950
Ipratropium bromide	581.2	0.9996
Salbutamol	146.8	0.9929
Salbutamol sulphate	135.3	0.9990
Salmeterol xinafoate	999.5	0.9980
Terbutaline sulphate	143.3	0.9995

3.1.12   NMR of Co-solvated Systems

To allow the study of co-solvated solvent systems including ethanol, further development of the system was required. The previously developed method utilised a solvent suppression regime to improve dynamic range issues encountered with unsuppressed methods when analysing protonated solvents. Incorporation of ethanol into a HFA system complicates the setup

as there are now two further protonated signals to consider; the CH_2 quartet and CH_3 triplet resonances of ethanol. An unsuppressed ^1H NMR spectrum of a budensonide saturated suspension in 10 % EtOH / 90 % HPFP system is shown, highlighting the additional ethanol resonances observed (Figure 3.1.12.1).
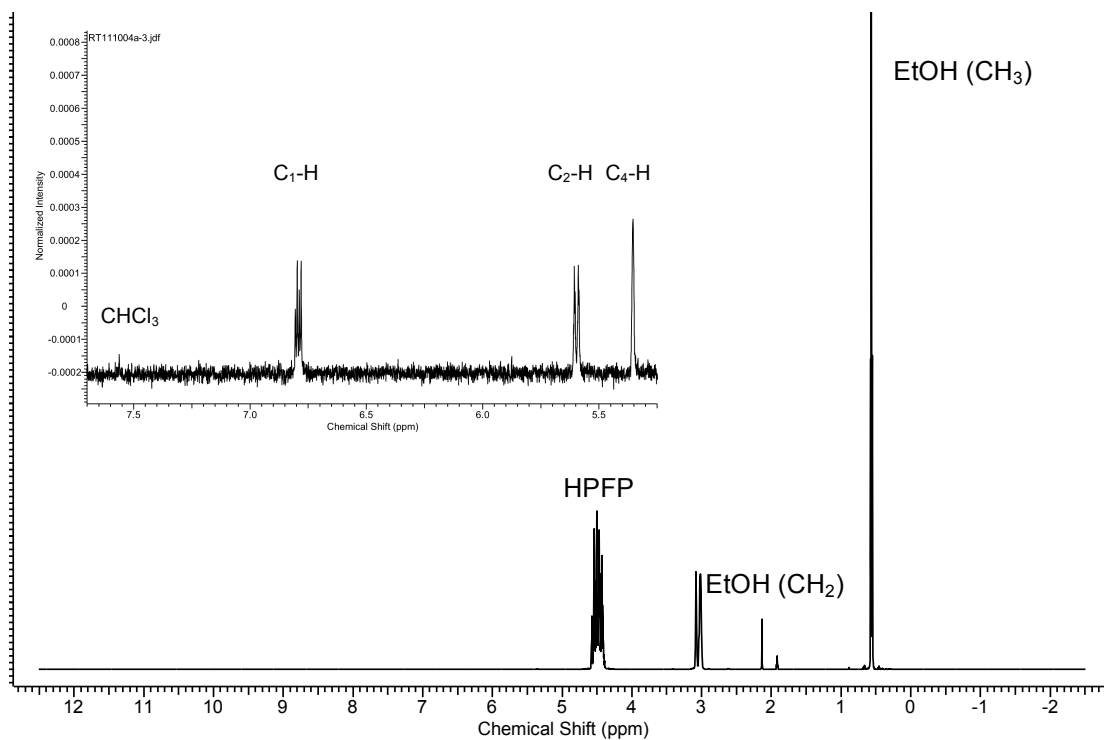
Figure 3.1.12.1 – ^1H NMR spectrum of budesonide saturated suspension in 10 % EtOH / 90 % HPFP.

Though the solubility of budesonide and other IPPs in ethanol co-solvated systems is likely to be considerably higher,[124] the resonances are still very small in comparison to those of the protonated solvent system. A revised solvent suppression protocol was developed to attempt to reduce the intensity of the fluorine coupled multiplet previously observed for HPFP, the CH_2 quartet and the CH_3 triplet from the ethanol in concert. For this, a specific experiment was written using the pre-saturation previously utilised in

suppression of the HPFP multiplet, whilst concurrently supressing the two ethanol signals using the *dante* pre-saturation channels available on the JEOL ECA 600 NMR. A representative ^{1}H NMR spectrum of a saturated suspension of budesonide in a 10 % EtOH / 90 % HPFP system with suppression applied to all solvent signals is shown (Figure 3.1.12.2) highlighting the S:N improvements observed when compared to that resulting from the method operated with suppression (Figure 3.1.12.1).
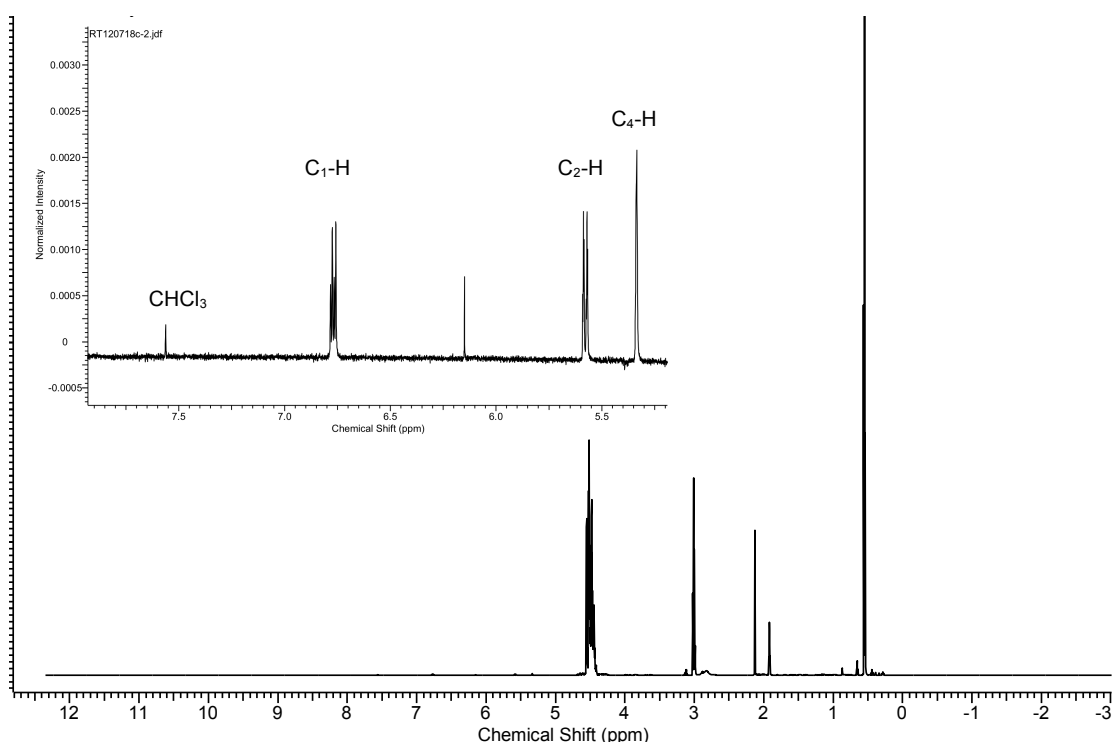
Figure 3.1.12.2 - ^{1}H NMR spectrum of a saturated suspension of budesonide in a 10 % EtOH / 90 % HPFP system with suppression applied to all signals; inset shows spectral expansion in the region of the budesonide A-ring resonances.

A further modification was necessary in the methodology to account for the chemical shift values encountered for the base solvent resonance and the shifted EtOH resonances in the HFA134a base. These chemical shift values

were used in the methods (operated otherwise unchanged). It should be noted that the experimental work involved in preparing the ethanol doped HFA134a is considerably more complicated than that of HPFP based systems. The cold transfer methodologies employed to fill the reversed co-axial NMR tube arrangement (Section 2.2.10) make addition of a liquid ethanol sample very difficult; addition before HFA134a proves unreliable to achieve an accurate volume as ethanol tends to be displaced on addition of the HFA134a, however addition of EtOH after HFA134a is made more complex as it is only the vapour pressure maintaining the liquid state, meaning removal of the J Young cap releases the contained HFA. The method ultimately employed was to fill HFA134a by cold transfer to the correct volume, freeze in liquid N_2 and add ethanol to the desired concentration whilst frozen. On warming the HFA134a and ethanol are allowed to mix as liquids and equilibrate to form the desired saturated suspension. The modified experimental approaches were used to assess solubilities of IPPs under co-solvated systems (Sections 4.2.1.1 and 4.2.1.2).

The work presented in this chapter demonstrates the successful development and validation of a qNMR approach to study solubility of solutes in HFA134a, HFA227 and HPFP propellants. Novel sample preparation methods have been developed to enable the study of volatile HFAs at elevated pressure *in-situ*, with co-axial external reference solutions. Development of the method using solvent suppression, increased field strength and extended acquisition times yielded LODs of *ca.* 1 µg/mL – a very sensitive NMR assay. Validation has been successfully undertaken with HPLC methods. NMR assignments have been carried out for 11 ICS, β_2-

agonist and antimuscarinic compounds currently prescribed in the treatment

of asthma and COPD for use in subsequent quantitative experiments

(Chapter 4). Full conclusions are presented in Chapter 7.

4 Physical Chemistry of Inhaled Pharmaceutical Products in HFAs

This chapter describes the work performed on IPPs as saturated solutions in the model propellant HPFP, and in volatile propellants HFA134a and HFA227, primarily using the NMR method developed and summarised in Chapter 3. The focus of the studies are in determining solubility for saturated suspensions of selected IPPs in the 3 propellants at ambient and sub-ambient temperatures, and access to the thermodynamic data inherent in these measurements. From this basis, strategies for solubility enhancement are also considered. These are (i) use of a co-solvent (ethanol) and (ii) pharmaceutically acceptable excipients to form inclusion complexes (cyclodextrins). The values determined provide an insight in to the physical chemistry of the formulations under study and the data derived are of potential use in directing the pre-formulation strategies for these products. Structural insight from the NMR method is also considered in more detail here, and provides data on the molecular structure of the corticosteroid / cyclodextrin inclusion complexes formed in the model propellant HPFP.

4.1 Solubility Measurements

4.1.1 Ambient (298 K)

Determination of solubility has been performed for each of the 11 IPP compounds under study in HPFP, HFA134a and HFA227 at 298 K using the NMR approaches developed and validated (Chapter 3). Resonances have been chosen for quantitation of each compound to satisfy two primary criteria (i) chemical shift of the signal is located in a region free of interferences or proximity to interfering signals and (ii) to maximise the sensitivity of the approach as highlighted in section 3.1.3, with resonances of maximum intensity being selected for *e.g.* tertiary-butyl functional group on salbutamol molecule whilst still satisfying (i). Representative ^{1}H NMR spectra are shown for the determinations completed for the compound budesonide in HPFP, HFA134a and HFA227 (Figure 4.1.1.1) highlighting the A-ring resonances and $CHCl_3$ standardisation resonance used in the calculation (Section 2.2.6). The chemical shifts of the budesonide are clearly solvent dependent, and a subtle movement is noted in the three propellant systems. Assignments are still consistent with those made in Chapter 3.
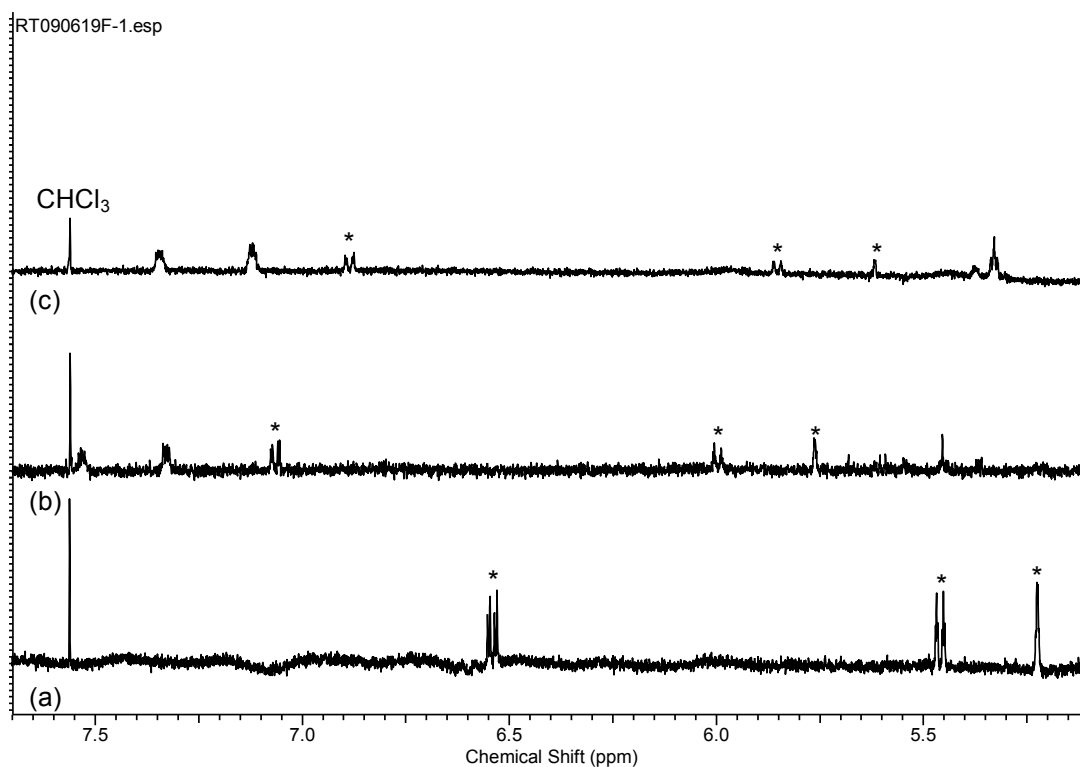
Figure 4.1.1.1 – Representative ^{1}H NMR spectra of budesonide in HPFP (a), HFA134a (b) and HFA227 (c) used in the quantitation of solute solubility at 298 K (shown in the lowfield region highlighting the A-ring resonances of the solute and the CHCl₃ reference).

The quantitative data obtained are shown (Table 4.1.1.1) for triplicate determinations in HPFP, HFA134a and HFA227 for each of the IPPs analysed. Mean values and associated precision measurements are quoted in the form of population standard deviation (σ) and coefficient of variation (% CV). % CV values are ≤ 15% for systems showing solubility values > 30 μg/mL, with increasing precision values for the samples that are approaching the LOQs of the method.

For systems dropping below LOQ for the NMR methodologies, additional testing has been performed by HPLC for the solutions in HPFP as

summarised in Section 2.3.2 and these data are also displayed with associated mean values and precision measurements (Table 4.1.1.2). Precision values are in line with the expected increase for decreasing mean values which are themselves in good agreement with the data obtained using the NMR method in that they all fall below the expected LOD values for the NMR method as operated with the exception of salbutamol base and ipratropium bromide. The lack of a result offered by NMR in these two instances when the HPLC data suggest they should be above LOD is due to interferences in the high field region of the spectrum obscuring the tertiary-butyl and iso-propyl groups.

Table 4.1.1.1 – Results of IPP solubilities at 298 K in HPFP, HFA134a and HFA227 determined by NMR

IPP	Propellant	Solubility (µg/mL)				σ	% CV
		1	2	3	Mean (n=3)		
Budesonide	HPFP	90	90	88	89	1.1	1.3
	HFA134a	52	58	50	53	4.1	7.9
	HFA227	52	66	59	59	7.1	11.9
Fluticasone propionate	HPFP	21	25	21	22	2.0	10.5
	HFA134a	23	19	25	23	3.1	13.3
	HFA227	< 15	< 15	< 15	<15	-	-
Salbutamol base	HPFP	< 1	< 1	< 1	< 1	-	-
	HFA134a	5	5	3	4	0.8	28.9
	HFA227	6	5	7	6	1.2	13.3
Formoterol fumarate	HPFP	< 15	< 15	< 15	< 15	-	-
	HFA134a	< 15	< 15	< 15	< 15	-	-
	HFA227	< 15	< 15	< 15	< 15	-	-
Salbutamol sulphate	HPFP	< 1	< 1	< 1	< 1	-	-
	HFA134a	< 1	< 1	< 1	< 1	-	-
	HFA227	2	2	2	2	0.3	16.0
Beclomethasone dipropionate	HPFP	341	327	336	334	7.2	2.1
	HFA134a	167	156	166	162	5.7	3.7
	HFA227	112	146	115	125	18.6	15.0
Beclomethasone	HPFP	< 15	< 15	< 15	< 15	-	-
	HFA134a	< 15	< 15	< 15	< 15	-	-
	HFA227	< 15	< 15	< 15	< 15	-	-
Mometasone furoate	HPFP	27	18	28	24	5.4	22.9
	HFA134a	< 15	< 15	< 15	< 15	-	-
	HFA227	< 15	< 15	< 15	< 15	-	-

Terbutaline sulphate	HPFP	< 1	< 1	< 1	< 1	-	-
	HFA134a	< 1	< 1	< 1	< 1	-	-
	HFA227	< 1	< 1	< 1	< 1	-	-
Ipratropium bromide	HPFP	< 1	< 1	< 1	< 1	-	-
	HFA134a	< 1	< 1	< 1	< 1	-	-
	HFA227	< 1	< 1	< 1	< 1	-	-
Salmeterol xinafoate	HPFP	< 15	< 15	< 15	< 15	-	-
	HFA134a	< 15	< 15	< 15	< 15	-	-
	HFA227	< 15	< 15	< 15	< 15	-	-

Table 4.1.1.2 – Solubility values for IPPs in HPFP at 298 K as determined by HPLC.

IPP	Solubility (µg/mL)				σ	% CV
	1	2	3	Mean (n=3)		
Salbutamol base	1.35	1.42	1.37	1.38	0.04	2.90
Formoterol fumarate	0.14	0.13	0.15	0.14	0.01	7.14
Salbutamol sulphate	0.19	0.17	0.18	0.18	0.01	5.56
Beclomethasone base	0.21	0.16	0.19	0.19	0.03	15.79
Terbutaline sulphate	0.05	0.05	0.04	0.05	0.01	20.00
Ipratropium bromide	2.00	2.10	2.00	2.03	0.06	2.96
Salmeterol xinafoate	0.06	0.06	0.05	0.06	0.01	16.67

A number of studies have been performed to relate solubility to solute properties in solutions of different compositions based on aqueous and non-aqueous systems. These studies have observed correlations between the solubility (log molar fraction solubility, χ) and physico-chemical properties of the solutes such as melting point and polarity. Work performed by Dickinson et al.[164] reported similar studies with HFA based propellants, and concluded that no such correlations were discernable, specifically stating that there was no absolute relationship between logP and solubility, though there was a trend towards increasing solubility with lower logP values. Hoye et al.[165] have recently observed a more fundamental relationship. Their work on solubility in HFA134a used a range of compounds chosen to have a range of physico-chemical characteristics, and relates experimentally derived solubility

values accessed *via* remote analysis of filtered samples[166,124] to theoretical solubility values (ideal and regular solution theory models) and to material properties such as molecular weight, melting point, hydrogen bonding potential and polarity, with some successful approaches proposed.

The values presented in this thesis however appear to be the first to be determined in-situ without the need for filtering and remote analytical work providing the advantages discussed previously (Section 1.3.1). They also present data that will aid in the understanding of formulation possibilities for these IPPs. A summary of physical properties of the IPPs under study is shown with the solubility measurement results (Table 4.1.1.3). These data show a broad correlation between solubility and compound type i.e. the ICS compounds (budesonide, beclomethasone dipropionate, fluticasone dipropionate and mometasone) are markedly more soluble in the three propellants than are the β_2-agonists and muscarinic bronchodilators (salbutamol, formoterol fumarate, terbutaline, ipratropium and salmeterol xinafoate) with the exception of beclomethasone, which shows an anomalously low solubility under this conclusion. The data suggest that the fluorinated propellants HPFP, HFA134a and HFA227 show a degree of oleophilicity facilitating the marginal solubility for the corticosteroids; however the true solubilising potential remains very low. Interestingly, a broad correlation with solvent relative permittivity (dielectric constant, ε_r) is observed. While the scope of the data is narrow here, permittivity is commonly correlated to solvent polarity[167] and these follow the order HPFP > HFA134a > HFA227 with values of 15.1, 9.8 and 4.1 respectively[126]

(Section 1.3.1, Table 1.3.1.2), consistent with the observed solubility order for the ICS compounds.

Table 4.1.1.3 – Solute solubility in HPFP shown alongside physical properties of the IPPs under study.

IPP	Solubility (µg/mL)			LogP	Rmm
	HPFP	HFA134a	HFA227		
Beclomethasone	0.2			2.439	409
Beclomethasone dipropionate	334	162	125	4.073	521
Budesonide	89	53	59	3.204	430
Formoterol fumarate	0.1	-	-	2.072	384
Fluticasone propionate	22	23	-	2.029	501
Ipratropium bromide	2	-	-	0.21	412
Mometasone furoate	24	-	-	3.594	521
Salbutamol base	1.4	4	6	0.692	239
Salbutamol sulphate	0.2	-	2	-	288
Salmeterol xinafoate	0.05	-	-	3.714	603
Terbutaline sulphate	0.05	-	-	0.696	274

LogP obtained from Advanced Chemistry Development (ACD/Labs) Software V11.02 (© 1994-2012 ACD/Labs) *via* SciFinder Scholar

It would be reasonable to expect a broad correlation between the solubility values of the IPP and logP values. LogP is defined as the log of the partition coefficient, P, between water and octanol[168,169] and is commonly taken as a measure of a compound's hydrophobicity / hydrophilicity (polarity). These relationships have been used successfully in studies of other solvent systems as solubility predictors.[169] A plot of log solubility (logχ) *vs.* logP (Figure 4.1.1.2) reveals a reasonable numerical correlation for the corticosteroid compounds in all three propellants HPFP, HFA134a and HFA227, though the latter two are based on limited data points, having correlation coefficients, r^2, of > 0.89 in all cases.
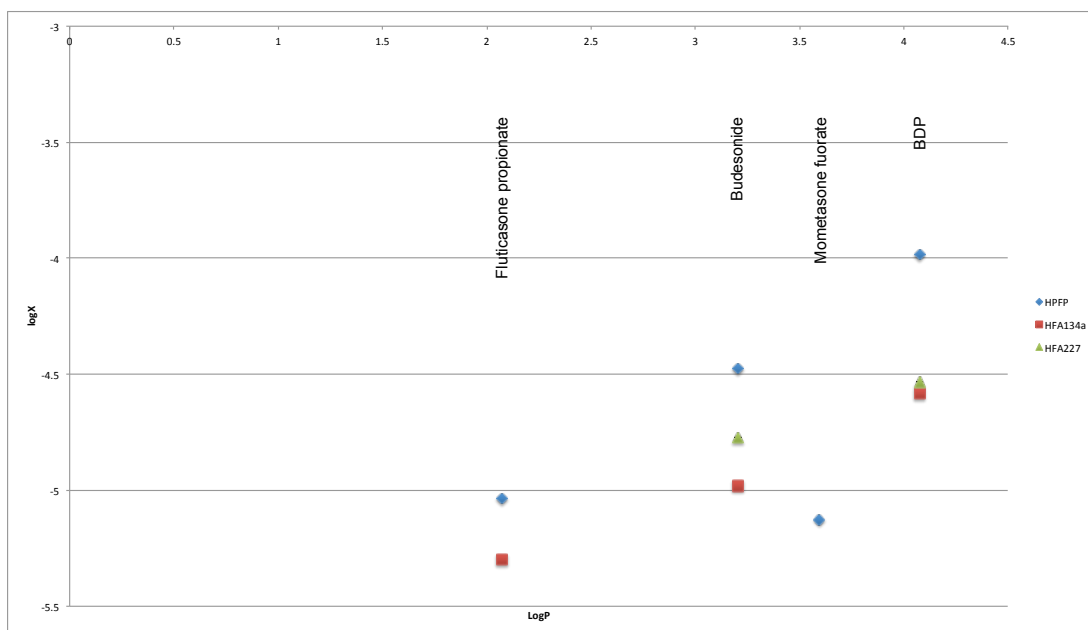
Figure 4.1.1.2 – Plot of mean log mole fraction solubility (n=3, ± σ) *vs*. logP for corticosteroid compounds budesonide, beclomethasone dipropionate, mometasone and fluticasone dipropionate.

Treatment of the data determined here in a manner based on the approaches taken by Hoye *et al.* [165] however, reveals little correlation. Ideal solubility models are used, whereby the crystal structure of a molecule is used to predict a value for mole fraction solubility. The greater the change in free energy the molecule has to overcome in dissociating from the crystal lattice, the less soluble the material will be, hence the solubility is governed by the free energy of melting. Their approach uses three assumptions (i) the van't Hoff expression assuming heat capacity change at melting (ΔCp) is equal or near to zero (ii) the Hildebrand expression assumes this to be equal to the entropy change at melting (ΔS_m) and (iii) Walden's rule stating that rigid organic compounds, ΔS_m can be assumed to be 56.5 $J.K^{-1}.mol^{-1}$. These assumptions combined simplify the ideal solubility factor to that shown in equation 4.1.1.1 at 298 K.[165]

$$log\chi^{ideal} = -0.01(T_m - 298)$$ **Equation 4.1.1.1**

Ideal solubilities calculated in this way are shown (Table 4.1.1.4), and correlated to measured solubility in the plot shown as Figure 4.1.1.3. The calculations based on melting points taken from literature values yielded a set of ideal solubility data that showed no meaningful correlation to experimental values. Melting points of these materials are prone to be accompanied by decomposition *e.g.* budesonide,[172] and clearly such correlations are therefore not appropriate with these systems.

Table 4.1.1.4 – Melting point data[170-172] and calculated ideal solubility values for each of the IPPs under study.

Compound	Melting Point, Tm (K)	Tm – 298	$log\chi^{ideal}$	Ideal solubility, χ^{ideal} (x10^{-3})
Beclomethasone	490[170]	192	-1.92	12.023
Beclomethasone dipropionate	485[171]	187	-1.87	13.490
Budesonide	493[172]	195	-1.95	11.220
Formoterol fumarate	411[172]	113	-1.13	74.131
Fluticasone propionate	545[172]	247	-2.47	3.388
Ipratropium bromide	504[172]	206	-2.06	8.710
Mometasone furoate	493[172]	195	-1.95	11.220
Salbutamol base	430[172]	132	-1.32	47.863
Salbutamol sulphate	475[172]	177	-1.77	16.982
Salmeterol xinafoate	410[172]	112	-1.12	75.858
Terbutaline sulphate	520[172]	222	-2.22	6.026
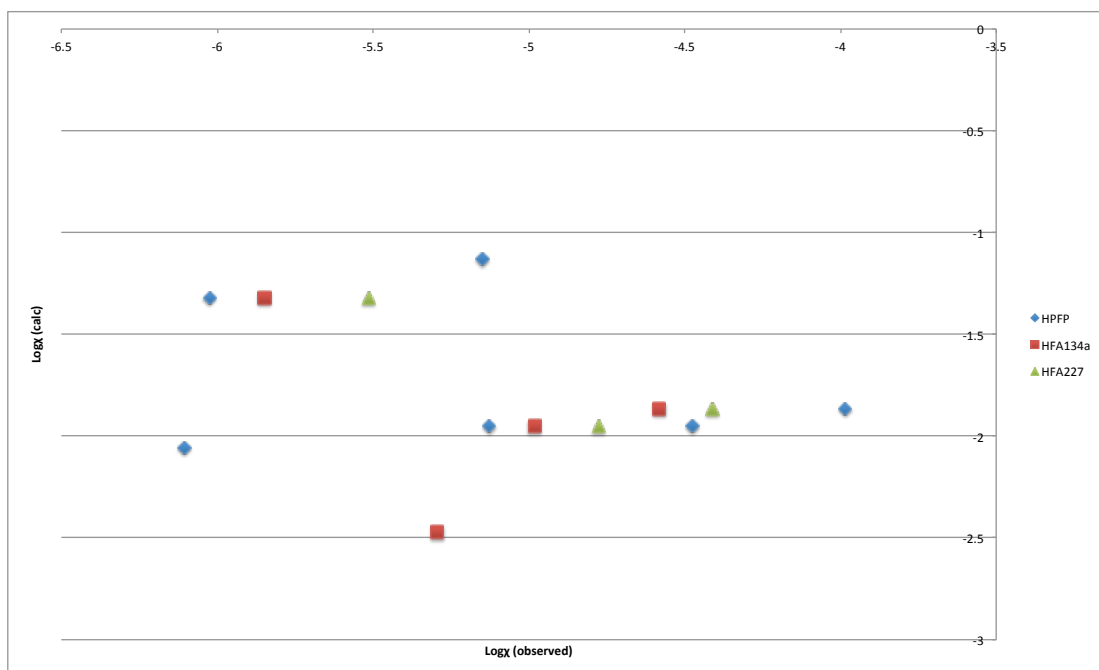
Figure 4.1.1.3 – Plot of calculated ideal solubility values (Equation 4.1.1.1) *vs.* observed solubility values experimentally determined.

4.1.2 Temperature Variation (VT NMR) and van't Hoff Plots

The solubility of any crystalline solid is dependent on the energetics associated to the process; the Gibbs free energy change, ΔG_{sol}, being the controlling factor. The less the energy change occurs during the process, the higher the value of solubility expected. ΔG_{sol} is given by Equation 4.1.2.1, where ΔH_{sol} is enthalpy change of solution, T is temperature (K) and ΔS_{sol} is the entropy change associated.

$$\Delta G_{sol} = \Delta H_{sol} - T\Delta S_{sol} \qquad\qquad \textbf{Equation 4.1.2.1}$$

One of the major advantages offered by the developed NMR approach to solubility determination is the ability to easily control the conditions at which the solubility values are assessed. The temperature at which the system is equilibrated and analysed will allow solubility values to be determined at

136

temperatures above and below ambient conditions offering (i) understanding of likely behaviours of IPPs in propellants over extended storage periods (stability) and (ii) insight into the physical chemistry of the solutions using van't Hoff approaches to access ΔH_{sol} values for the series available, hence calculation of ΔS_{sol}.

The van't Hoff equation is frequently used to calculate thermodynamic properties of solutions at equilibrium,[174-177] as is the case with the saturated suspensions of solutes in a given solvent system. If the van't Hoff equation is considered in the format of a linear plot (Equation 4.1.2.2) it can be seen that the magnitude of the gradient provides information on the energetics of the solubility process as change in heat of solution, ΔH_{sol}, in the form $y = mx + c$, where R is the universal gas constant (8.314 J.K^{-1}.mol^{-1}) and T the temperature in degrees Kelvin.

$$ln\chi = \frac{-\Delta H_{sol}}{R} \times \frac{1}{T} + c \qquad \textbf{Equation 4.1.2.2}$$

The Gibbs free energy change for the solution and the entropy change can be estimated by consideration of equations 4.1.2.3 and 4.1.2.4.

$$\Delta G_{sol} = -RTln\chi \qquad \textbf{Equation 4.1.2.3}$$

$$\Delta S_{sol} = \frac{\Delta H_{sol} - \Delta G_{sol}}{T} \qquad \textbf{Equation 4.1.2.4}$$

For the systems successfully analysed at 298 K, repeat analysis was performed at 283 and 278 K after re-equilibration, with quantitative data derived from the same resonances used in the previous work at 298 K. These data are shown (Tables 4.1.2.1 and 4.1.2.2) with estimates of precision (s) and mean values displayed in each case.

Table 4.1.2.1 – Results of solute solubilities at 283 K in HPFP, HFA134a and

HFA227.

IPP	Propellant	Solubility (µg/mL)				σ	% CV
		1	2	3	Mean (n=3)		
Budesonide	HPFP	87.7	88.1	88.2	88	0.2	0.2
	HFA134a	48.4	52.7	54.0	48	5.6	11.7
	HFA227	55.0	54.3	51.5	54	1.9	3.5
Fluticasone propionate	HPFP	15.0	14.6	18.0	16	1.9	11.9
	HFA134a	< 15 (*ca.* 12)	< 15 (*ca.*10)	< 15 (*ca.* 3)	< 15 (*ca.*12)	1.5	13.1
	HFA227	Not analysed					
Salbutamol base	HPFP	Not analysed					
	HFA134a	< 1	< 1	< 1	< 1	-	-
	HFA227	< 1	< 1	< 1	< 1	-	-
Salbutamol sulphate	HPFP	Not analysed					
	HFA134a						
	HFA227	< 1	< 1	< 1	< 1	-	
Beclomethasone dipropionate	HPFP	163.7	145.4	139.3	150	12.6	8.4
	HFA134a	45.6	46.5	38.5	44	4.4	10.0
	HFA227	66.1	54.2	51.6	57	7.7	13.5
Mometasone fuorate	HPFP	< 15 (*ca.*13)	< 15 (*ca.*12)	< 15 (*ca.*12)	< 15 (*ca.*12)	0.6	4.7
	HFA134a	Not analysed					
	HFA227						

Table 4.1.2.2 – Results of solute solubilities at 278 K in HPFP, HFA134a and HFA227.

| IPP | Propellant | Solubility (µg/mL) | | | | σ | % CV |
		1	2	3	Mean (n=3)		
Budesonide	HPFP	88.1	81.6	87.3	86	3.6	4.2
	HFA134a	27.9	26.6	25.8	27	1.0	3.7
	HFA227	43.1	50.8	48.9	48	4.0	8.3
Fluticasone propionate	HPFP	< 15 (*ca.* 13)	15.9	17.9	16	2.4	15.0
	HFA134a	< 15 (*ca.* 7)	< 15 (*ca.* 8)	< 15 (*ca.* 6)	< 15 (*ca.* 8)	1.0	14.3
	HFA227	Not analysed					
Salbutamol base	HPFP	Not analysed					
	HFA134a	< 1	< 1	< 1	< 1	-	-
	HFA227	< 1	< 1	< 1	< 1	-	-
Salbutamol sulphate	HPFP	Not analysed					
	HFA134a						
	HFA227	< 1	< 1	< 1	< 1	-	
Beclomethasone dipropionate	HPFP	119.9	111.2	122.9	118	6.1	5.2
	HFA134a	33.8	29.1	30.7	31	2.4	7.7
	HFA227	58.6	47.8	53.8	53	5.4	10.2
Mometasone fuorate	HPFP	< 15 (*ca.* 8)	< 15 (*ca.*10)	< 15 (*ca.* 6)	< 15 (*ca.* 8)	2.0	25.0
	HFA134a	Not analysed					
	HFA227						

The summarised method of producing van't Hoff plots of lnχ (mole fraction solubility) *vs.* reciprocal temperature are in accordance with recent publications by Eghrary *et al.*[174] and Manrique *et al.*[175] and show the equilibrium solubility is increased with increasing temperature. The data are shown (Tables 4.1.2.3 and 4.1.2.4) for an example corticosteroid compound, beclomethasone dipropionate, with the van't Hoff plot (Figure 4.1.2.1) highlighting the linear trends associated (correlation coefficient, $r^2 \geq 0.97$) for determinations carried out in all three propellant systems.

Table 4.1.2.3 – Summary of values extracted from the van't Hoff plots of BDP in the three propellant systems studied.

Propellant	Gradient ($\Delta H^{sol}/R \times 10^{-3}$)	Intercept, C	Correlation coefficient (r^2)	ΔH^{sol} (kJmol^{-1})
HPFP	-4.351	5.419	0.999	36.17
HFA134a	-6.953	12.720	0.997	57.81
HFA227	-3.740	2.092	0.970	31.10

Table 4.1.2.4 – Summary of thermodynamic properties calculated from the van't Hoff plots for BDP in the three propellant systems studied.

Propellant	ΔH^{sol} (kJmol^{-1})	ΔG^{sol} (kJmol^{-1})	ΔS (J K^{-1} mol^{-1})
HPFP	36.2	22.7	45.1
HFA134a	57.8	26.1	106.3
HFA227	31.1	25.9	17.6

Values for ΔG_{sol} and ΔS calculated at 298 K
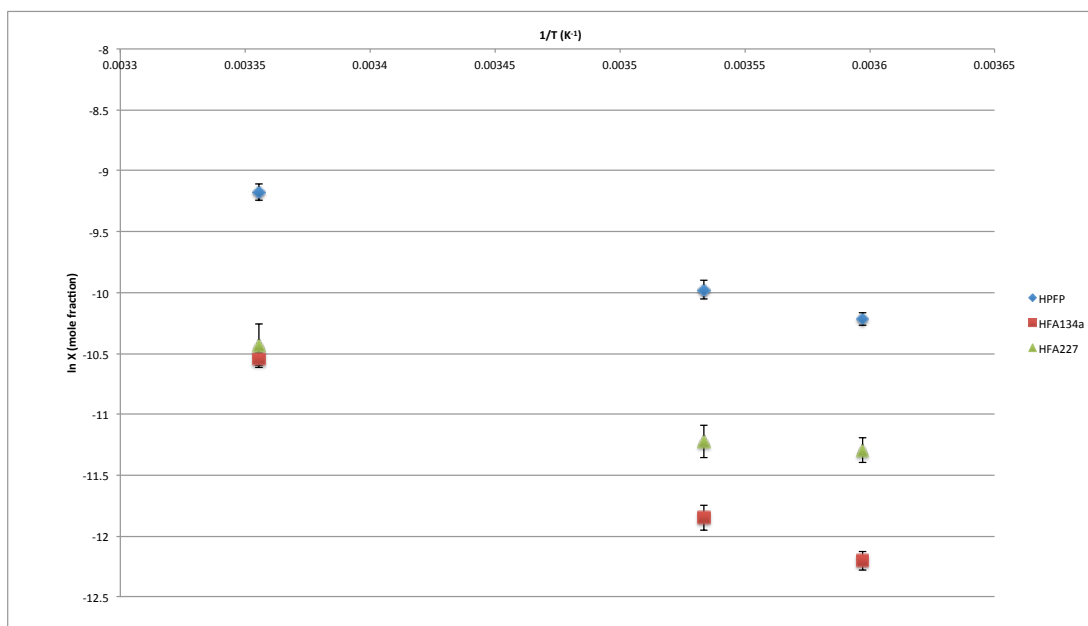
Figure 4.1.2.1 – Van't Hoff plot of mean solubility (n=3, ± σ) *vs.* temperature for the compound beclomethasone dipropionate in HPFP, HFA134a and HFA227 over the temperature range 278 to 298 K.

Van't Hoff plots have been produced for each of the IPPs showing solubility levels within the limits of determination for the NMR methodology utilised

over the three temperatures under study. The values obtained for the compounds beclomethasone dipropionate, budesonide, mometasone and fluticasone provide an insight into the thermodynamics involved in the dissolution process (Table 4.1.2.5). The observed enthalpies of solution are endothermic in all cases and the Gibbs free energy change values show an inverse correlation to the solubility values determined for the compounds, as anticipated. Values obtained for ΔS provide information about the entropic vs. enthalpic control of the solubilisation processes occurring, and it appears that the materials tested are exhibiting entropic control, with relatively large entropy change values compared to enthalpy change.[178] The numerical data derived from these approaches are comparable with those obtained by Rousseau *et al.*[176] in their studies on sodium naprxoxen and Bustamante *et al.*[177] in their studies on paracetamol, nalidixic acid and acetanilidein solutions comprising increasing ratios of dioxane in water. More compellingly, studies by Yusuff *et al.*[179] show data for spironolactone, itself a corticosteroid compound, directly comparable to those obtained here (ΔH = 26.5 kJ.mol^{-1}, ΔG=33.7 kJ.mol^{-1} and ΔS = -24.4 J.K-$^{-1}$.mol^{-1}), though it should be noted that these results were obtained in aqueous solution and comparisons should be used with caution.

Table 4.1.2.5 - Summary of thermodynamic properties calculated from the van't Hoff plots for beclamethasone dipropionate, budesonide, mometasone and fluticasone in the three propellant systems studied.

Compound	Propellant	ΔH^{sol} (kJmol^{-1})	ΔG^{sol} (kJmol^{-1})	ΔS (J K^{-1} mol^{-1})
Beclomethasone dipropionate	HPFP	36.2	22.7	45.1
	HFA134a	57.8	26.1	106.3
	HFA227	31.1	25.9	17.6
Budesonide	HPFP	1.0	25.5	-82.2
	HFA134a	19.2	28.3	-30.5
	HFA227	6.5	27.3	-70.0
Mometasone fuorate	HPFP	36.7	29.3	24.8
	HFA134a	-	-	-
	HFA227	-	-	-
Fluticasone	HPFP	13.6	29.4	-53.1
	HFA134a	35.1	30.9	14.1
	HFA227	-	-	-

This approach has also been extended to co-solvated systems and those using inclusion complexes formed with budesonide and cyclodextrin; both of which are summarised later in this Chapter (Sections 4.2.1 and 4.2.2).

4.2 Strategies for Solubility Enhancement in HFAs

The solubility work carried out here, supported by other studies using off line analytical methodologies (evaporation of volatiles and re-constitution[180] and direct injection HPLC approaches[100,122,123,124]) have shown the propellants used in pMDI systems after the Montreal Protocol in 1987 to be poor at solvating IPPs, and other chemical entities used as excipients, with typical solubility values in the low ppm (μg/mL) range. Several studies have addressed the solubility of IPPs in HFA based propellant systems, and work has been undertaken to study the application of co-solvent models for this purpose.[123,181,182] Ethanol, being miscible with HFAs, and in current use in commercial pMDI products (QVAR™; beclomethasone dipropionate and

Aerospan™; flunisolide) has been chosen for evaluation here. Hoye *et al.* have recently published a study[166] in which the solubility of various organic compounds have been assessed in HFA134a and HFA134a / ethanol systems, though these compounds do not focus on IPPs and are instead organic compounds of varied description chosen to have wide ranging physical properties. Their approach was to utilise HPLC with direct injection filtered systems.[181,183] This uses large quantities of the compounds in question and requires the preparation of pMDI canisters, which is both time consuming and expensive. The same systems can be prepared and evaluated using the developed NMR set up described, with creation of saturated suspensions of API in HFA134a doped with any chosen concentration of ethanol. The preparation and evaluation of the systems is rapid and efficient.

A second and less well-studied approach is the use of complexation agents to improve the solubility of organic compounds in HFA based formulations. A great deal of work has been undertaken surrounding the use of complexation agents in drug delivery formulations to enhance the solubility of APIs, to control their stability characteristics and to increase their bioavailabilty.[148,184-196] Of particular interest to this study are the use of cyclodextrin compounds to improve the solubility of IPPs in HFA propellants, and the use of the newly developed NMR methodology to assess their solubility enhancing characteristics and also aid in characterising any inclusion complexes formed in combination with other remotely operated analytical approaches. As discussed previously, the NMR methodology allows more detailed information to be derived from the systems under study; the chemical shift

and multiplicity of the NMR signals observed potentially offer significant information about the behaviour of the host / guest complexes formed *in-situ*.

4.2.1 Co-solvent Models

The use of co-solvents in aqueous based systems may be well understood, with the co-solvent altering the polarity of the aqueous system to shift towards the polarity of the solute in question. The incorporation of co-solvents in HFA propellant systems to modify solubility of both drug and excipients used as stabilisers[126] has been utilised in several commercially available pharmaceutical products and is beginning to be discussed further in recent literature,[97,98] though their effect and action appears to be less well understood. For example, little work has been reported in the area of solvent interactions in pure HFA solvents, and no conclusions have been drawn as to whether molecules in the solvents undergo hydrogen bonding. Recent work by Conti *et al.*[197] has studied the effect of increasing the volume fraction of ethanol in HPFP on the solubility of alkyl, ether and ester functions using chemical force microscopy (an analogue of atomic force microscopy using modified tips) to determine the adhesion force of these moieties to HPFP with and without ethanol present. This was undertaken with a view to understanding the role of ethanol co-solvents in surfactant pMDIs such as those formulated with oleic acids (alkyl), polyethylene glycols (ether) and polylactic acids (ester) excipients. They determine experimentally that the addition of ethanol to the HPFP decreases the adhesion force of the moieties in order of ester > ether > alkyl hence predicting an increase in the solubility in the same order. They postulate that the interaction is in the ethanol's alkyl chains orienting themselves to surround the alkyl containing solute, offering

the OH groupings to the HPFP solvent. Cote *et al.*[198] have undertaken

similar studies with HPFP and its fully fluorinated analogue perfluoropentane

establishing miscibility parameters (lower critical solution temperatures) for

the systems with polyethylene glycols and polyethylene oxides. It appears

that limited work has been undertaken to examine the effects of ethanol

addition to HFAs for compounds used specifically in inhaled formulations.

The studies performed here have begun to provide an insight into these

specific compounds, and used van't Hoff approaches to ascertain

thermodynamic characteristics of the budesonide system using approaches

similar to those employed in the pure HFAs (Section 4.1.2).

4.2.1.1 Solubility Measurements in HPFP / Ethanol

The NMR method developed and discussed in this thesis allows the rapid

study of HFA propellant systems co-solvated with ethanol in this way, though

further development of the system was required for the analysis of systems

incorporating ethanol (Section 2.5.1). The revised method was used to study

systems of budesonide in HPFP (and HFA134a, Section 4.2.1.2) co-solvated

with ethanol, and it is immediately apparent that the solubility increases

markedly. The developed method was used to study budesonide in HPFP

with increasing ratios of ethanol at 2.5, 5, 10, 15 and 20 % v/v. Gupta *et

al.*[181] concluded that ethanol concentrations above 20% v/v have been

shown to plateau in terms of solubility and concentrations even lower than

this can have detrimental effect on the aerosolisation properties of the

formulation. Smyth[113,116] also showed that the aerodynamic particle size

fractions were detrimentally affected by larger volume fractions of ethanol

with the reduction of vapor pressure brought about by the co-solvent

inclusion. The study performed here was therefore limited to preparations below this level (20 % v/v maximum). The tabulated data are displayed (Table 4.2.1.1.1) with a graphical representation of the budesonide solubility as a function of the ethanol co-solvent concentration shown as Figure 4.2.1.1.1, demonstrating a linear relationship (correlation coefficient, $r^2 \geq 0.99$) between the budesonide solubility and ethanol concentration at the levels analysed. The effect is thought to be a result of the changing polarity of the solution, with increasing ethanol fractions shifting the polarity of solvent towards that of the solute.

Table 4.2.1.1.1 – Solubility levels of budesonide in solutions of increasing volume ratio of ethanol in HPFP as determined by *in-situ* NMR.

EtOH (% v/v)	Budesonide solubility (µg/mL)				σ	% CV
	1	2	3	Mean (n=3)		
0.0	90	90	88	89	1.1	1.3
2.5	386	362	338	362	23.9	6.6
5.0	1209	1127	1204	1180	46.1	3.9
10.0	2106	2073	2123	2101	25.6	1.2
15.0	3756	3617	3670	3681	69.9	1.9
20.0	4559	4416	4435	4470	77.5	1.7

Figure 4.2.1.1.1 – Mean budesonide solubility (n=3, ± σ) as a function of ethanol co-solvent concentration (% v/v) in HPFP.

Further experiments were performed using VT NMR to study the temperature effects on solubility for the budesonide system in 10% v/v ethanol, accessing the associated thermodynamic data as with previous systems in pure HPFP (Section 4.1.2). Systems were analysed at five temperatures between 303 and 278 K, with the van't Hoff plot (Figure 4.2.1.1.2) showing the linear trend associated (correlation coefficient, $r^2 \geq 0.95$) with this system. These data are consistent with those observed in pure HPFP and in systems incorporating cyclodextrins as complexation agents. The thermodynamic data aid in the understanding of the interaction of budesonide in HPFP and inference may be extended to the other corticosteroid systems. Table 4.2.1.1.2 shows ΔH_{sol}, ΔG_{sol} and ΔS_{sol} values calculated using the van't Hoff approaches for budesonide in pure HPFP, with 10% v/v EtOH in HPFP and with

incorporation of TRIMEB as a complexation agent summarised later in this Chapter (Section 4.2.2). The data strongly suggest a shift in the thermodynamics of the systems; ΔG values show the previously observed and expected inverse relationship to solubility *i.e.* less free energy change associated with the dissolution process results in an elevated solubility value. However, the ΔH and ΔS values are key to understanding the solubilisation enhancement brought about by the CD inclusion and the EtOH co-solvent. Significant differences are observed in ΔH and ΔS values obtained, with both increasing. The difference between the ΔH and ΔS values decreases markedly with inclusion of CD in the formulation, and further still by addition of ethanol. This suggests that the systems are moving away from entropic control and towards enthalpic control[177,178] *i.e.* the entropy component is contributing less to the solubilising process. This suggests that the addition of TRIMEB to HPFP and to a greater extent addition of EtOH to HPFP increases the entropy of the solution meaning the solvent system is becoming less ordered, favouring solubility of budesonide in the solvent mixture.
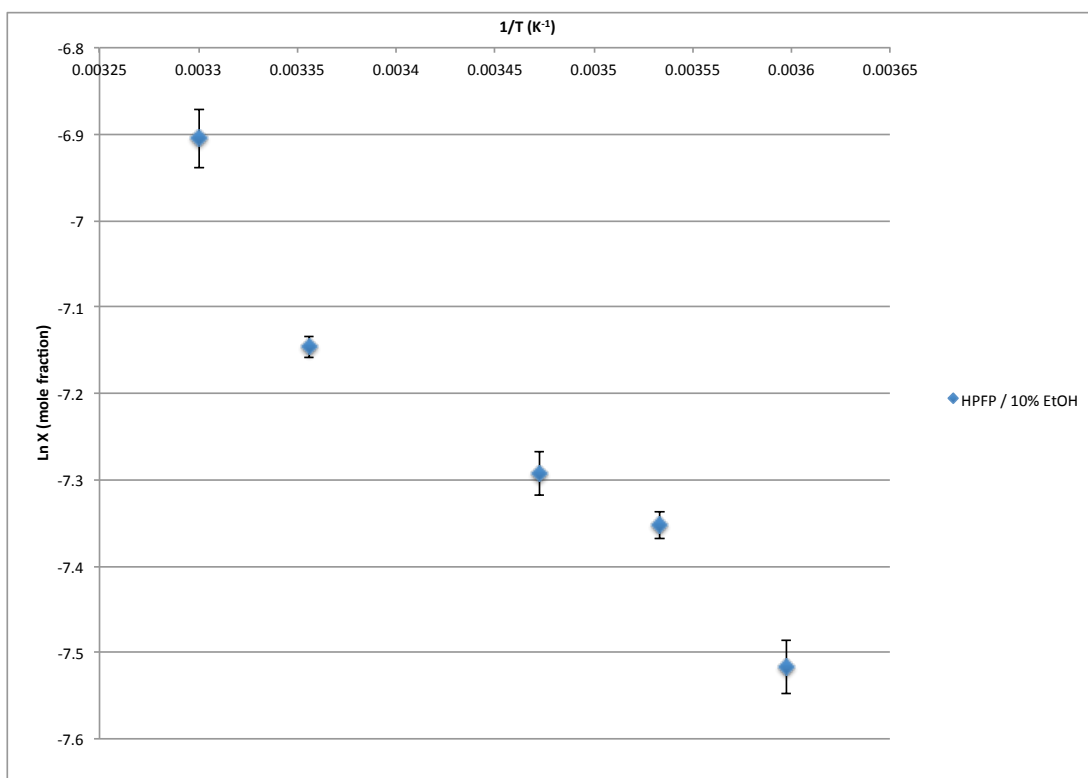
Figure 4.2.1.1.2 – Van't Hoff plot of solubility (n=3, ± σ) *vs.* temperature for budesonide in HPFP co-solvated with 10 % v/v ethanol over the temperature range 278 to 303 K.

Table 4.2.1.1.2 – Thermodynamic data derived from van't Hoff approaches for budesonide in pure HPFP, with TRIMEB inclusion and with 10 % v/v EtOH co-solvent.

	ΔH_{sol} (kJ.mol^{-1})	ΔG_{sol} (kJ.mol^{-1})	ΔS_{sol} (kJ.mol^{-1})
HPFP	1.8	26.5	-80.0
TRIMEB	8.4	21.8	-45.0
HPFP / 10 % v/v EtOH	15.2	17.4	-7.3

Values for G_{sol} and ΔS calculated at 298 K

4.2.1.2 Solubility Measurements in HFA134a / Ethanol

Measurements made in HFA134a / EtOH give data that can be used in the assessment of product formulation strategies for truly representative pMDI systems. The NMR method has been modified very slightly to supress

HFA134a proton signals in concert with ethanol resonances. A repositioning of the suppression chemical shift values to account for the difference in the HFA134a multiplet and the slight shift in the ethanol resonance positions in the different solvent are the only method parameters that need addressing, and the exercise can be repeated (though a modified sample preparation method has to be employed and is given in Chapter 3, Section 3.1.12). The results for the solubility of budesonide assessed in HFA134a co-solvated with 2.5, 5, 10, 15 and 20 % v/v EtOH are shown (Table 4.2.1.2.1) with Figure 4.2.1.2.1 displaying a plot of the solubility *vs*. EtOH concentration. As with HPFP model propellant the relationship is shown to be linear over the range of ethanol concentrations investigated (correlation coefficient, $r^2 \geq 0.99$), though the values are shown to be consistently lower than those determined in HPFP. These data and the ease and speed with which they were obtained using the developed NMR method should prove to be extremely useful for formulators looking to propose new pMDI formulations for budesonide, and show the speed and ease with which other compounds can be assessed in formulations doped with any concentration of ethanol or any other co-solvent of interest. The data are consistent with those observed by Hoye *et al*.[166] where they also observe a linear relationship between solute solubility and ethanol concentration for the compounds under investigation.

Table 4.2.1.2.1 – Solubility levels of budesonide in solutions of increasing

volume ratio of ethanol in HFA134a as determined by *in-situ* NMR.

| EtOH (% v/v) | Budesonide solubility (µg/mL) | | | | σ | % CV |
	1	2	3	Mean (n=3)		
0.0	52	58	50	53	4.1	7.9
2.5	285	271	277	278	7.4	2.7
5.0	862	822	837	841	20.2	2.4
10.0	1364	1372	1423	1386	31.8	2.3
15.0	1943	1983	1913	1946	34.8	1.8
20.0	2979	2958	2916	2951	32.0	1.1

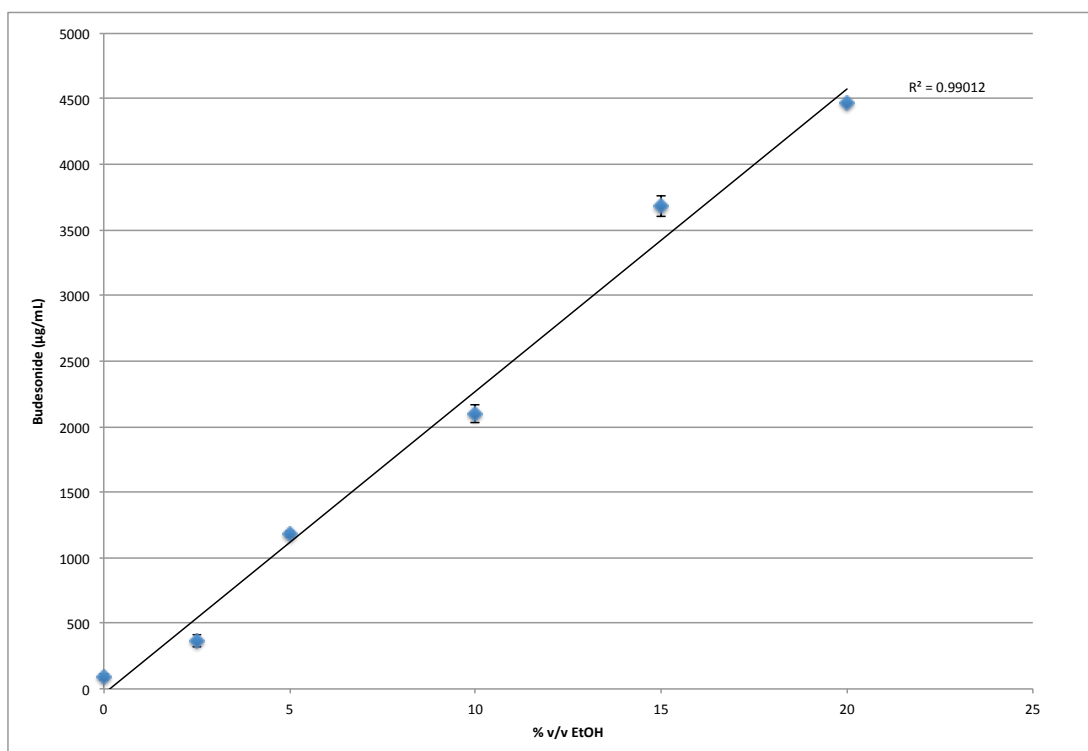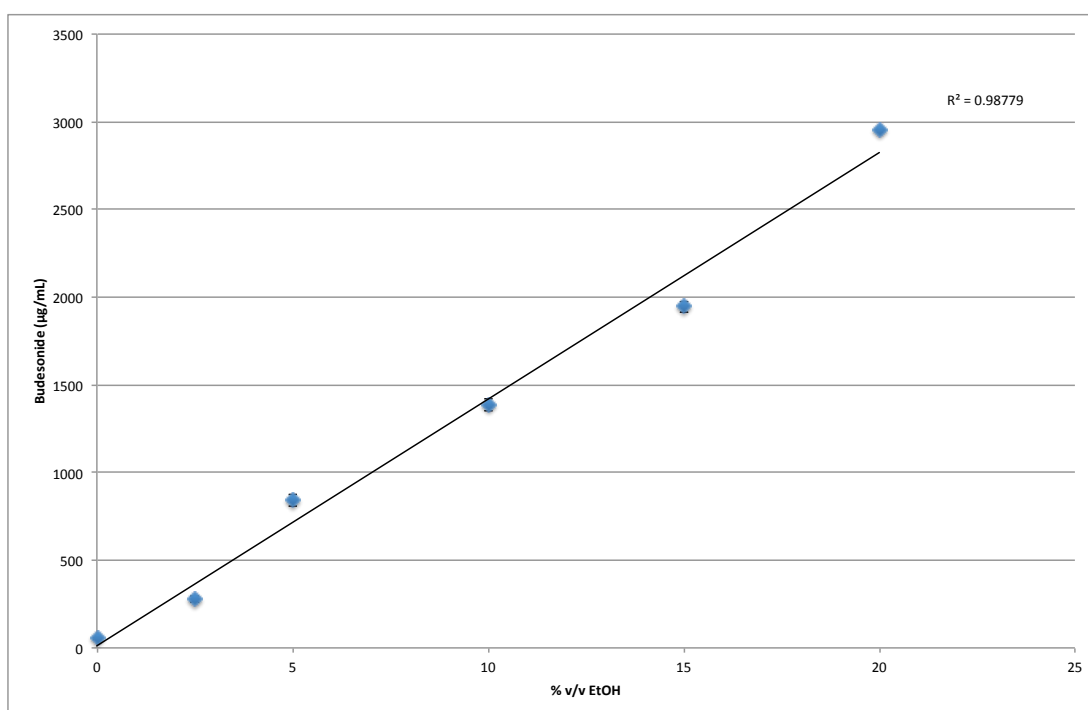**Figure 4.2.1.2.1** – Mean budesonide solubility (n=3, ± σ) as a function of

ethanol co-solvent concentration (% v/v) in HFA134a.

4.2.1.3 **Solubility Enhancement of IPPs in Ethanol Co-solvated HPFP**

Further to the study of budesonide in ethanol co-solvated HPFP and HFA134a systems, the IPPs investigated in HPFP, HFA134a and HFA227 have been re-evaluated in HPFP co-solvated with 10 % ethanol. The model system is easy to work with and gives very rapid indicative data for the behaviour of the IPPs under study in formulations containing ethanol co-solvents. The data obtained are displayed in Table 4.2.1.3.1 shown alongside solubilities in pure HPFP for comparison (Section 4.1.1). The majority of the samples examined show an increase in solubility as may be expected with the addition of a polar solvent to the systems; three compounds (salbutamol sulphate, salmeterol xinafoate and terbutaline sulphate) show values less than LOD of the method, and so conclusion cannot be drawn here. Each of the ICS compounds has shown a considerable increase, with factors of up to 1200 times the solubility values of those determined in pure HPFP. The more polar compounds have shown a less dramatic effect, with salbutamol base and ipratropium bromide being the only compounds in this category to show a large step change in solubility value. The logP values of HPFP and EtOH are 3.84 and -0.19[166] respectively; therefore the addition of ethanol to the fluorinated compound increases the polarity of the solution (lowers logP). It may be expected that the increase in polarity would have a more dramatic effect on the compounds more polar in nature themselves *i.e.* the β_2 agonists, though that is not what has been observed here. These data contradict those observed by Hoye *et al.*[166], though their studies were performed in ethanol co-solvated HFA134a,

itself more polar than HPFP with a logP value of 1.1.[166] It is suspected that

the addition of ethanol to HFA134a has a more significant effect on the

overall polarity of the matrix when compared to HPFP / ethanol mixtures, and

this may account for the disparity in the data sets. Additionally, it may be

indicative of the solubility enhancement being more complex than by

controlling polarity alone and further study of fluorinated solvents such as

those undertaken by Conti *et al.*[197] and Cote *et al.*[198] are required to better

understand the interactions taking place.

Table 4.2.1.3.1 – Solubility data for IPPs formulated in HPFP and 10 %

ethanol doped HPFP as determined by reverse co-axial NMR and HPLC at

298 K.

IPP	Concentration (µg/mL)		Factor Increase
	HPFP	10 % EtOH / HPFP	
Beclomethasone dipropionate	334	6399	19
Beclomethasone base	0.2	254	1270
Budesonide	89	2100	24
Fluticasone propionate	22	443	20
Ipratropium bromide	2.0	250	125
Mometasone fuorate	24	381	16
Salbutamol base	1.4	961	686
Salbutamol sulphate	0.2	< 15	-
Salmeterol xinafoate	0.06	< 15	-
Terbutaline sulphate	0.05	< 15	-

4.2.2   Complexation

Cyclodextrin (CD) molecules have been used for a considerable time in

pharmaceutical preparations. The ability of CDs to solubilise and stabilise

pharmaceutical compounds was first described in the 1950's.[184] Their use in

aqueous based formulations as solubility enhancers is well

documented,[185,186] with β-CD being most widely used as host because its

cavity size is most suited to the inclusion of small molecule (pharmaceutical) guests.[179] It has however, the lowest aqueous solubility of the commonly available CDs (Table 4.2.2.1). This has been attributed to an increase in the intra-molecular hydrogen bonding detracting from the available solvation sites in the molecule and hence, aqueous solubility.[179] Derivatisation of any of the hydroxyl groups with aliphatic groups (producing, for example, methoxy or ethoxy substituents) dramatically increases aqueous solubility. The aqueous solubility of methylated β-CD increases with degree of methylation and reaches a maximum when 14 of the 21 available hydroxyl groups are substituted. Further methylation reduces the solubility, though the completely substituted (permethylated) version of the molecule still has a considerably higher solubility than that of the unsubstituted β-cyclodextrin.[195]

Table 4.2.2.1 – Characteristics of the common cyclodextrin molecules.

	α	β	γ	δ
No. glucopyranose units	6	7	8	9
Molecular weight	972	1135	1297	1459
Central cavity diameter (Å)	4.7-5.3	6.0-6.5	7.5-8.3	10.3-11.2
Aqueous solubility (% w/v @ 25°C)	14.5	1.85	23.2	8.19

The molecular structures of β-CD and heptakis-(2,3,6-tri-o-methyl)-β-cyclodextrin (TRIMEB) are shown in Figure 4.2.2.1. The two β-CD compounds were chosen for further study due to the cavity size; it being extensively used in solubilisation studies with pharmaceutical molecules. As the β-CD is to be utilised in fluorinated solvent systems as opposed to aqueous based media, the unsubstittuted form was investigated alongside the permethylated version of the molecule, TRIMEB, to maximise the possibility of solubility enhancement.
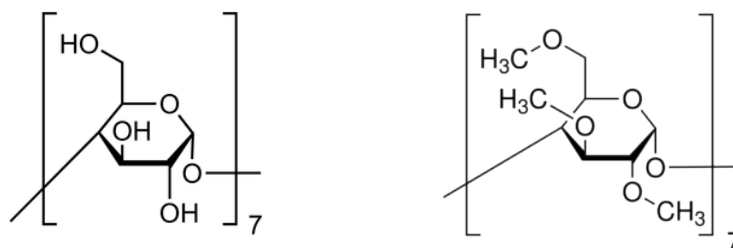
Figure 4.2.2.1 – Molecular structures of β-CD and TRIMEB showing the addition of methyl groupings on the TRIMEB molecule.

For each of the systems analysed at 298 K, solubility data for the individual CDs and the complexed budesonide / TRIMEB samples in each of the fluorinated solvent systems were calculated. Note that the budesonide / β-CD system was not analysed as a complex in light of the low β-CD solubility in pure form. The data obtained in these experiments is summarised (Tables 4.2.2.2 and 4.2.2.3) quoted with a mean value and associated precision estimate (σ and % CV).

Table 4.2.2.2 – Results of CD solubilities at 298 K in HPFP, HFA134a and HFA227.

| Compound | Propellant | Solubility (µg/mL) | | | | σ | % CV |
		1	2	3	Mean		
β-CD	HPFP	< 15	< 15	< 15	< 15	-	
	HFA134a	< 15	< 15	< 15	< 15	-	
	HFA227	< 15	< 15	< 15	< 15	-	
TRIMEB	HPFP	3700	3800	3900	3800	0.1	2.6
	HFA134a	3100	3300	3800	3400	0.4	10.6
	HFA227	4500	4000	4600	4500	0.1	1.3

Table 4.2.2.3 – Results of budesonide / TRIMEB solubilities from the mixed solutions at 298 K in HPFP, HFA134a and HFA227.

Compound	Propellant	Solubility (µg/mL)				σ	% CV
		1	2	3	Mean		
TRIMEB	HPFP	2900	2500	2600	2700	0.2	7.8
	HFA134a	1300	1000	1000	1100	0.2	15.7
	HFA227	2500	2500	2300	2400	0.1	4.7
Budesonide	HPFP	333.9	439.1	414.2	395.7	55.0	13.9
	HFA134a	130.5	130.8	126.2	129.2	2.6	2.0
	HFA227	627.8	849.9	853.9	777.2	129.4	16.6

It is clear that TRIMEB has a significant solubility in the fluorinated solvent systems employed in these studies, having values between 1 and 3 mg/mL compared to values of *ca.* 10 – 100 µg/mL for the IPP molecules. It follows that any complexation occurring with budesonide and TRIMEB in solution should have a dramatic effect on the solubility in association. Results for the β-CD suggest that the solubility of this compound is low in all three solvent systems, and the structural differences between the two sugars would account for the differing solubility. The TRIMEB has the addition of three methoxy functional groups on the ring (per monomer) which appear to be interacting with the fluorinated solvents and increasing solubility as is observed in aqueous systems[179] and highlighted earlier in this section.

The solubilities of budesonide in the systems including TRIMEB have shown significantly increased solubility in HPFP, HFA134a and HFA227, with increases of x4.5, x2.5 and x13.2 respectively showing the largest increase in HFA227. The increasing solubility seen over the replicates in HFA227 and the resultant increase in precision values observed also suggest the systems may take a significant time to reach equilibrium; itself indicative of complex

formation. It is notable that the budesonide solubility increase appears at the expense of TRIMEB solubility *i.e.* the TRIMEB solubility is retarded providing further evidence that a complex is formed between the two compounds, where the carrier compound controls the process.[179]

Further experiments were performed on the solutions of budesonide, TRIMEB and the 50:50 mix in HPFP, to allow the physical chemistry of the inclusion complex to be studied further by incorporating further data points in the van't Hoff plots (308 and 288 K) for the budesonide and generating new data series for the TRIMEB and the mix. The van't Hoff plots are shown as Figure 4.2.2.2, with the additional data points resulting in minor numerical changes to ΔH, ΔG and ΔS values calculated for budesonide (Table 4.2.2.5) by slightly altered slope values obtained over the extended data range (compared to data shown in Section 4.1.2). Data for TRIMEB and both components of the mix are also shown.
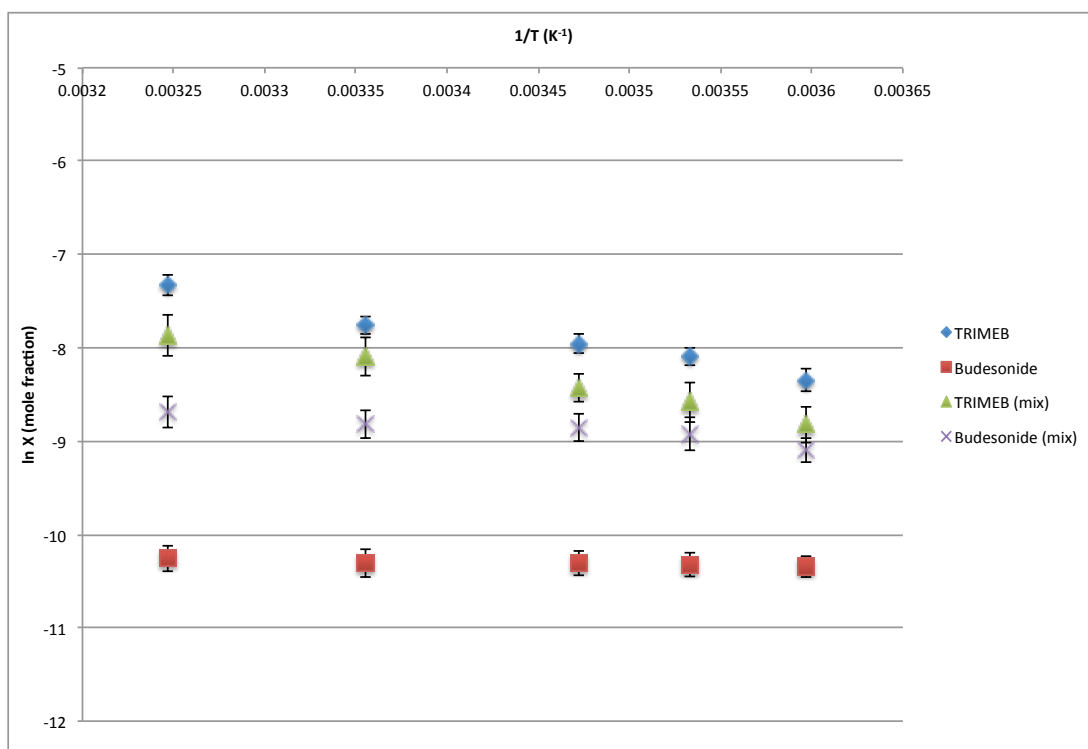
Figure 4.2.2.2 – Van't Hoff plot of mean solubility (n=3, ± σ) *vs.* temperature for the compounds budesonide, TRIMEB, and the mix (budesonide / TRIMEB) in HPFP over the temperature range 278 to 308 K.

Table 4.2.2.4 – Summary of values extracted from the van't Hoff plots of budesonide, TRIMEB and the mix.

Compound	Gradient ($\Delta H_{sol}/R \times 10^{-3}$)	Intercept, c	Correlation coefficient (r^2)	ΔH^{sol} (kJmol^{-1})
Budesonide	-0.216	-9.56	0.85	1.8
TRIMEB	-2.693	1.37	0.97	22.3
Budesonide (mix)	-1.004	-5.41	0.90	8.4
TRIMEB (mix)	-2.713	0.97	0.99	22.6

Table 4.2.2.5 – Summary of thermodynamic properties calculated from the van't Hoff plots for budesonide, TRIMEB and the mix.

Compound	ΔH_{sol} (kJmol^{-1})	ΔG_{sol} (kJmol^{-1})	ΔS_{sol} (J K^{-1} mol^{-1})
Budesonide	1.8	25.5	-79.6
TRIMEB	22.3	19.2	10.67
Budesonide (mix)	8.4	21.8	-45.2
TRIMEB (mix)	22.6	20.1	8.4

Values for G_{sol} and ΔS calculated at 298 K

These thermodynamic data aid in understanding the solubility changes observed in complexed form. Although they exclude any contribution from molecular interactions between similar molecules in solution,[179] the thermodynamic calculations aid in interpreting the solubility observations made. Budesonide exhibits a larger ΔS value and a lower ΔG value in its complexed form when compared with the values obtained for the free compound and in contrast, a decrease in ΔS for TRIMEB is observed hence an increase in the solubility of budesonide is apparent.

Further to the numerical data for solubility values derived from the NMR approach, the method allows structural data inherent in NMR data to be interrogated. If we compare NMR spectra of budesonide, TRIMEB and budesonide / TRIMEB complexes, it is apparent that there are significant differences in the chemical shift and multiplicity values showing structural changes within the systems. Stacked NMR spectra of budesonide and budesonide / TRIMEB complex are shown with a spectral expansion in the lowfield range showing the A-ring resonances (Figure 4.2.2.3). The spectra have been referenced (δ) to the CHCl$_3$ incorporated for quantitation, and it is immediately apparent that there are significant shifts in the resonance frequencies for the A-ring protons of the budesonide molecule downfield,

consistent with observations made when compounds are successfully complexed by Castiglione *et al.*[187] and Marangoci *et al.*[188] in their studies using TRIMEB and unsubstituted β-CD respectively. More minor frequency changes are observed for the chemical shift values of TRIMEB in isolation and when complexed with budesonide (Figure 4.2.2.4), where the ring protons show only subtle shifts in δ, particularly those of the C_6-H, C_5-H and C_3-H protons at 3.26, 3.17 and 2.90 ppm respectively. These observations are consistent with Marangoci *et al.*[188] who conclude that these protons are on the inner cavity of the TRIMEB, and are providing the primary interaction in the complex, leaving the outer protons and those on the methyl functionalities largely unaffected.
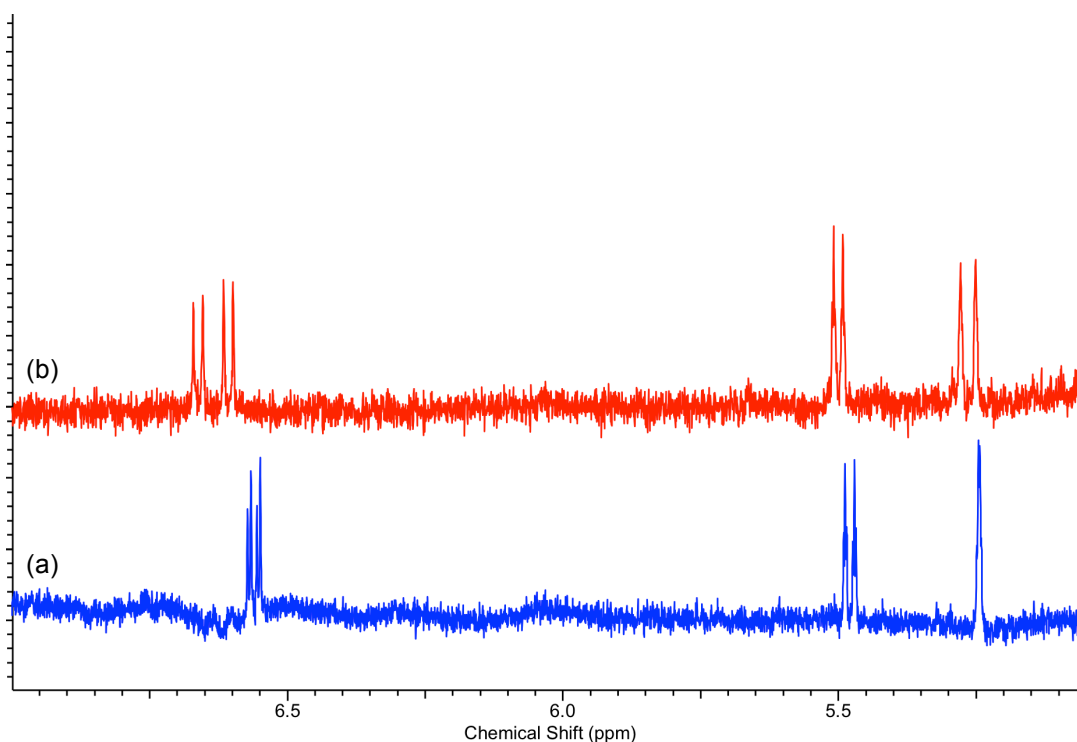
Figure 4.2.2.3 – ^{1}H NMR spectra of budesonide (a) and budesonide / TRIMEB complex (b) in HPFP expanded in the high field region showing budesonide A-ring chemical shift and multiplicity changes.
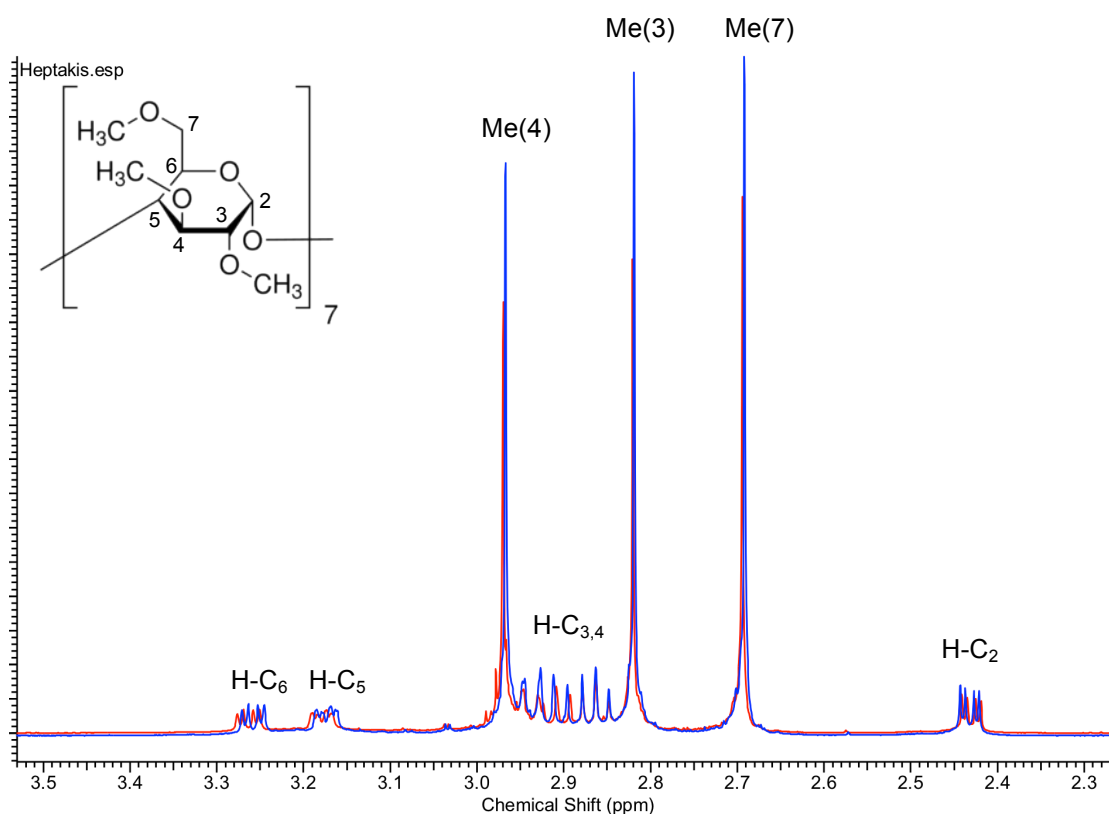
Figure 4.2.2.4 – ^{1}H NMR spectra of TRIMEB (blue) and budesonide / TRIMEB complex (red) in HPFP expanded in the region showing CD chemical shift changes.

The effect seen in HPFP is also observed in HFA134a and HFA227. Spectral overlays of budesonide and budesonide / TRIMEB expanded in the low field region show similar chemical shift and multiplicity changes in the A-ring protons of budesonide (Figures 4.2.2.5 and 4.2.2.6). The data observed in all three propellant systems would suggest that inclusion complexes are occurring; the solubility is increased by large factors, particularly in HFA227, and the movements in chemical shift values indicate there is an interaction between the budesonide and the TRIMEB molecule, particularly in the A-ring region of the steroidal backbone.
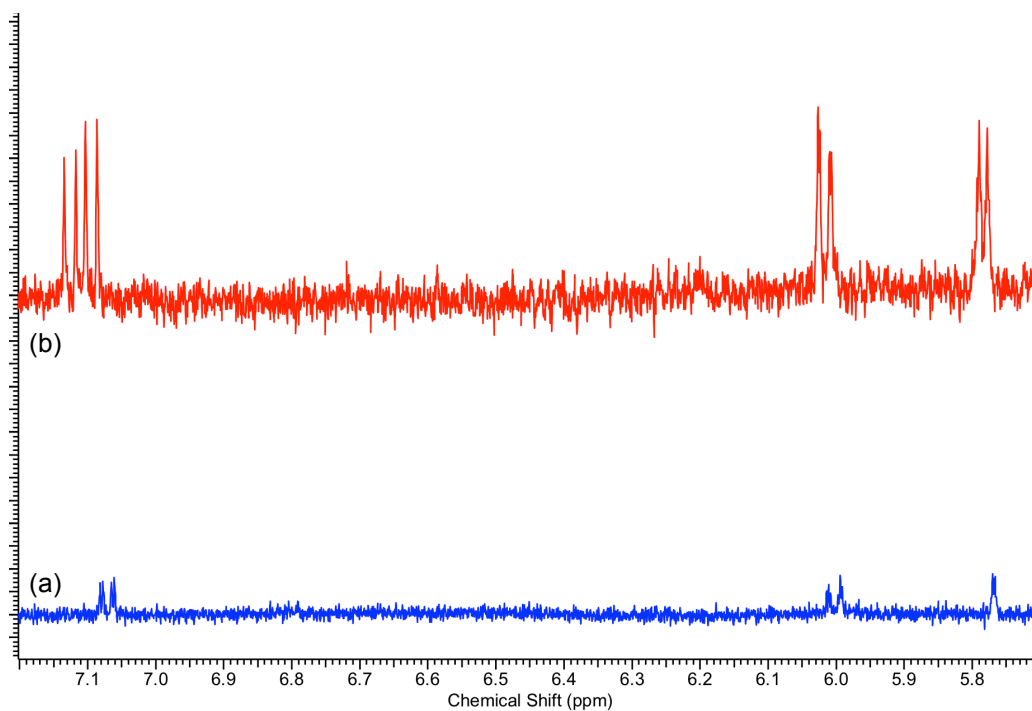
Figure 4.2.2.5 – ^{1}H NMR spectra of budesonide (a) and budesonide / TRIMEB complex (b) in HFA134a expanded in the high field region showing budesonide A-ring chemical shift and multiplicity changes.
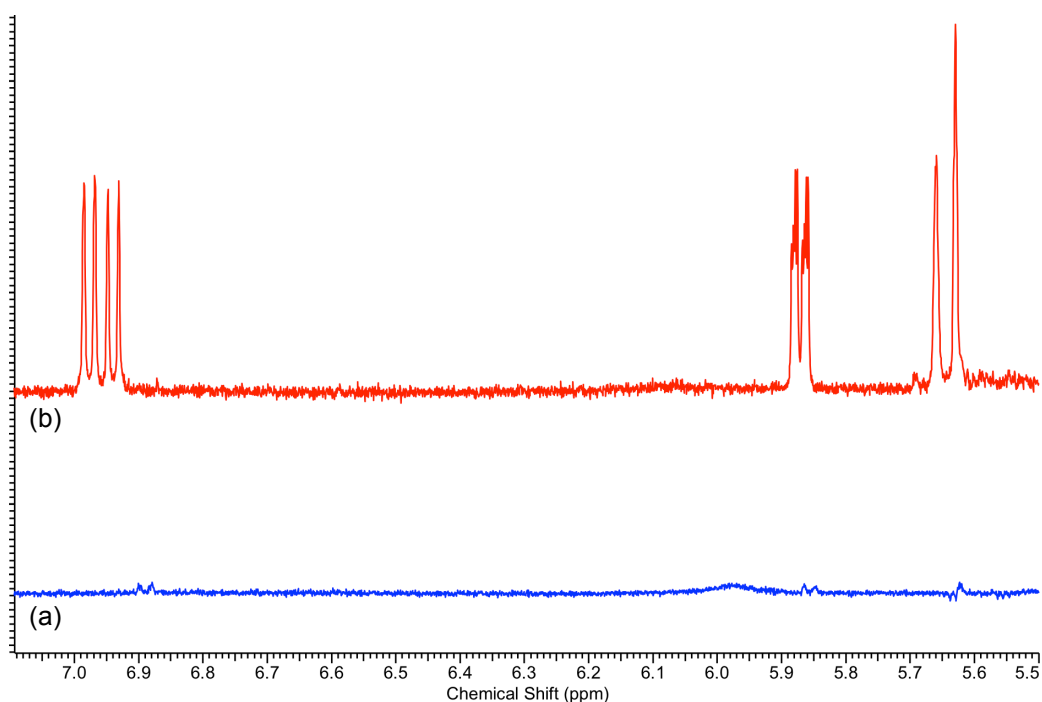
Figure 4.2.2.6 – ^{1}H NMR spectra of budesonide (a) and budesonide /
TRIMEB complex (b) in HFA227 expanded in the high field region showing
budesonide A-ring chemical shift and multiplicity changes.

Further systematic study was undertaken with controlled molar ratios of

budesonide : TRIMEB in an attempt to characterise and increase our

understanding of the dynamic inclusion systems. Preparation of physical

mixtures of the substances at 0.5:1, 1:1 and 2:1 mole ratio were dissolved in

HPFP doped with ethanol as outlined in experimental section 2.4.4. Crystals

were harvested and investigated further using FTIR and Raman

spectroscopy. Vibrational spectroscopy highlights some subtle differences

between the isolated complexes that are consistent with the data obtained in

the *in-situ* NMR measurements. Wavenumber shifts are observed in the

complexed material produced from solution, particularly around the

budesonide A-ring. Previous work by Ali *et al.*[200] has made the following

Raman assignments in the A-ring (i) 1602 cm^{-1}, v(C=C), ring (ii) 1626 cm^{-1},

v(C=C), ring (iii) 1655 cm^{-1}, v(C=C), quinone and (iv) 1712 cm^{-1}, v(C=O), quinone. These bands show significant changes in the material produced in the complexation experiments when compared to those of pure budesonide. Particularly apparent, are the shift of the intense band at 1655 cm^{-1} moving to a higher wavenumber (1661 cm^{-1}) and the significant reduction in the band at 1626 cm^{-1}. There is also a marked shift and band shape difference in the v(C=O) quinone function, thought to be a result of hydrogen bond interactions with the TRIMEB, and the bands are also all significantly broadened. These band differences are shown in the overlaid Raman spectra of budesonide and TRIMEB references shown with the 1:1 complex material produced from solution (Figures 4.2.2.7 and 4.2.2.8).
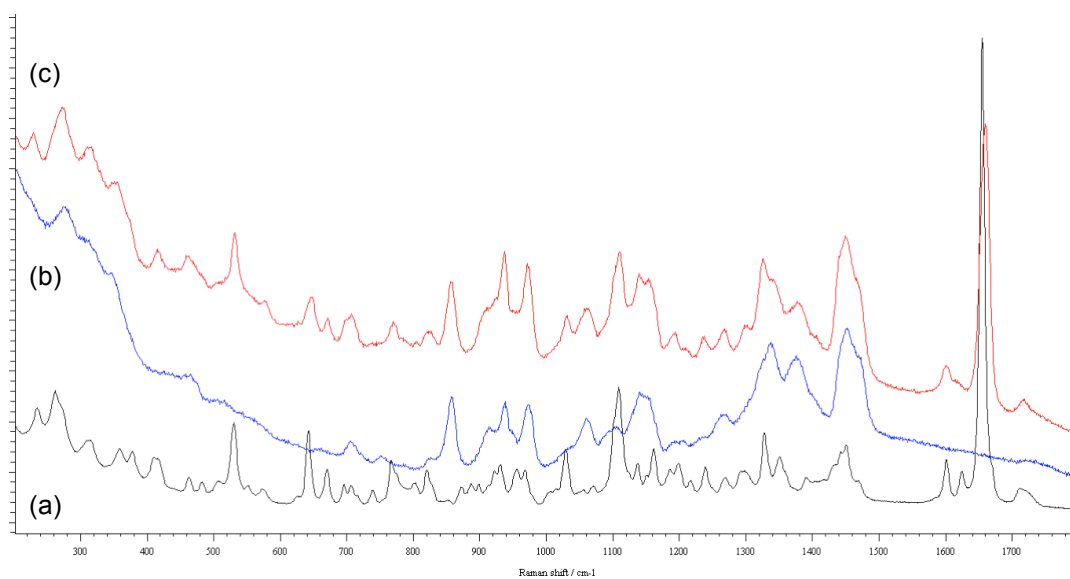
Figure 4.2.2.7 – Raman spectra of pure budesonide (a), pure TRIMEB (b) and 1:1 complex (c) material produced from solution in the region 200 – 1800 cm^{-1}.
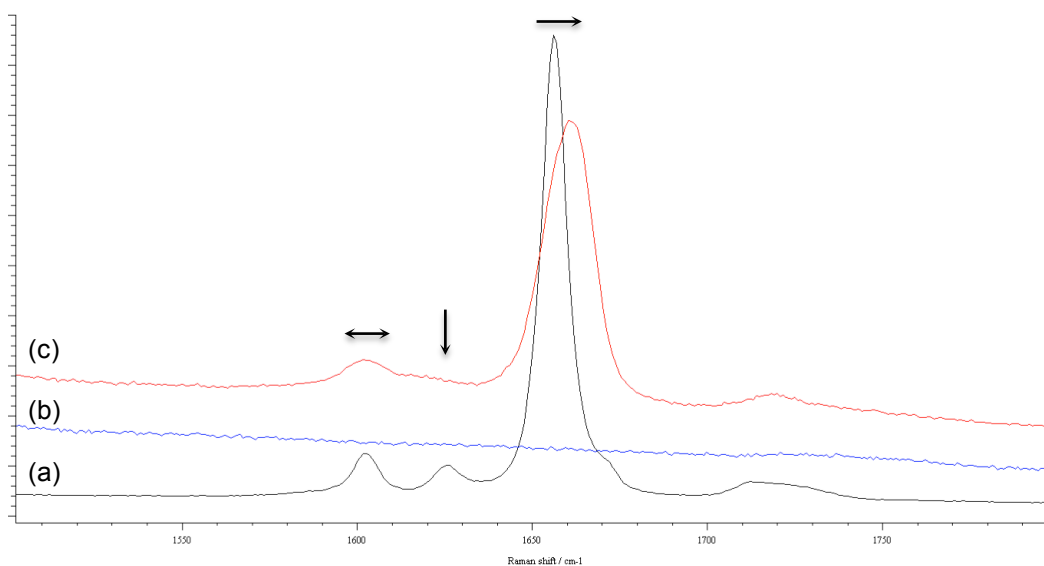
Figure 4.2.2.8 –Raman spectra of pure budesonide (a), pure TRIMEB (b) and 1:1 complex material (c) produced from solution in the spectral region 1500 – 1800 cm^{-1} showing shifts in the A-ring bands.

FTIR data obtained on the same materials shows shifts in the same bands as the Raman data (Figures 4.2.2.9 and 4.2.2.10).
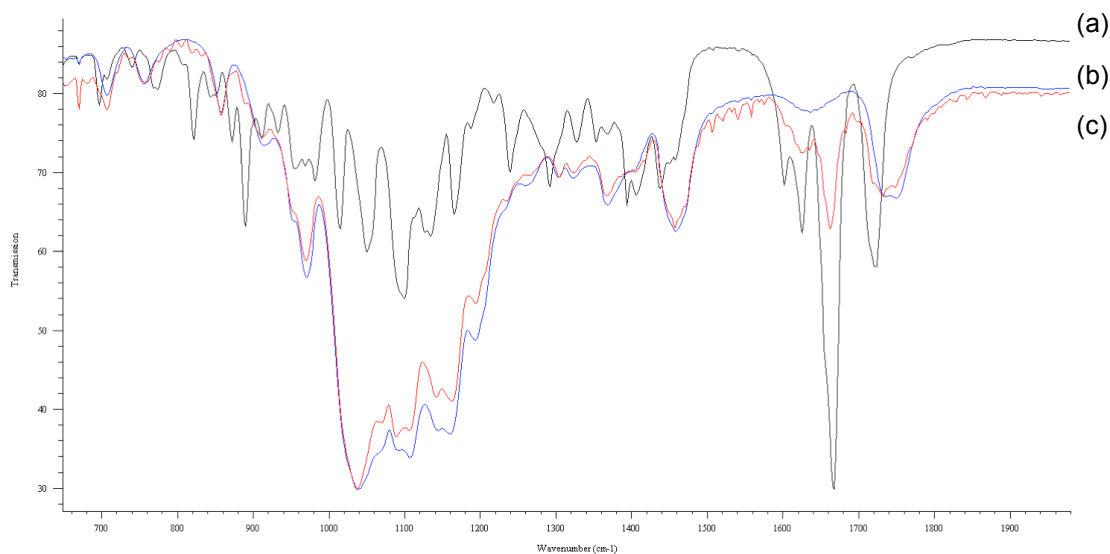
Figure 4.2.2.9 – FTIR spectra of pure budesonide (a), pure TRIMEB (b) and 1:1 complex material (c) produced from solution in the spectral region 700 – 2000 cm^{-1}.
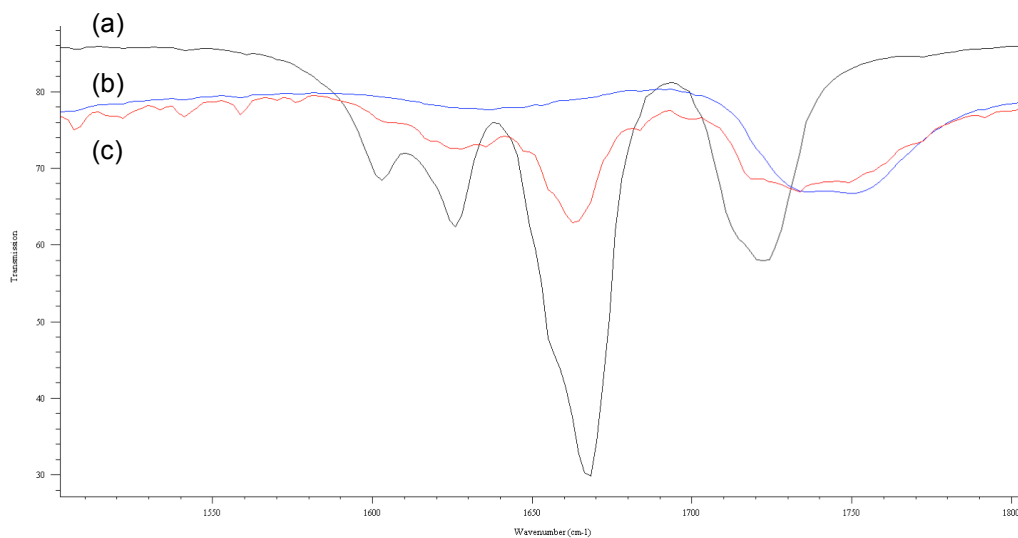
Figure 4.2.2.10 – FTIR spectra of pure budesonide (a), pure TRIMEB (b) and 1:1 complex material (c) produced from solution in the spectral region 1500 – 1800 cm^{-1}.The data observed *in-situ* using the NMR methodology and by remote spectroscopic means post crystallisation approaches are consistent

with materials forming complexes. The spectral data in all cases highlight marked differences in the A-ring region of the budesonide molecule, suggesting that complexes formed with the TRIMEB are involving this region of the molecule. These observations are consistent with those made by Glomot *et al.*[201] and Nikai *et al.*,[202] in which observations of spectroscopic carbonyl shifts are made in inclusion complexes with cyclodextrins and steroid molecules. A study by Bandi *et al.*[38] has also shown carbonyl shifts in FTIR measurements made on budesonide : hydroxypropyl-β-cyclodextrin complexes derived from supercritical fluid processing that are consistent with those observed and reported here. These data suggest that the inclusion complexes formed are consistent with the steroidal 'backbone' of the budesonide molecule interacting with the cavity of TRIMEB.

The studies presented in this chapter have utilised the qNMR method developed (Chapter 3) to establish the solubility of IPPs in HFAs for the first time. These are below 100 µg/mL, with the exception of the ICS BDP. The ICS compounds consistently show higher solubility levels than the β_2-agonist and antimuscarinic bronchodilators, though the capacity of the HFAs for solubilising these compounds remains very low in absolute terms. VT-NMR has allowed access to thermodynamic behaviours of the systems through van't Hoff approaches. The solvation processes show the anticipated reduction in Gibb's free energy change with increasing solubility, and suggest entropic over enthalpic control. Solubility enhancements brought about by inclusion of ethanol as a co-solvent show a linear relationship for the ICS budesonide in the model propellant HPFP and in HFA134a with concentration. Derivatised and underivatised β-cyclodextrin solubility in the propellants has been assessed; TRIMEB showing significant solubility and underivatised being sparingly soluble. TRIMEB has also been shown to significantly increase the solubility of budesonide in the HFAs under study and spectroscopic techniques have been successfully used to evidence the formation of host : guest inclusion complexes. Full conclusions are presented in Chapter 7.

5   Solid State Characterisation of IPPs Post Deposition

This chapter describes the development approaches for the investigation of the solid state of materials deposited from pMDI formulations. Previous chapters in these studies have primarily focussed on the development of methodologies to provide an insight into the behaviour of IPPs in solutions / suspensions in HFAs used in pMDI formulations. However, of equal importance are the properties of the materials after actuation of the pMDI device and as they deposit on the surface. Whilst the assessment of aerodynamic parameters such as mass median aerodynamic diameter (MMAD), geometric standard deviation (GSD) and fine particle dose / fraction (FPD/FPF) on pMDI products is commonplace,[203,204] few approaches are developed to probe the material properties in terms of their physical form and their particle morphology, size and distribution at deposition. In the following sections, several new approaches are developed for the study of the deposited materials and highlight the insight these give in combination with modern analytical approaches.

5.1   Methods for Aerodynamic Particle Size Distribution (APSD)

Dynamic Light Scattering (DLS) and Laser Diffraction (LD) are common methods for the assessment of particle size in suspensions and powders, and their application to aerosols has become more commonplace as attachments for study of doses emitted from nebulisers, DPIs and pMDIs have become available.[205,206] However, impaction and impingement apparatus for measurement of aerodynamic particle size (APSD) are widely accepted in the pharmaceutics arena and are necessary in the regulation of

inhaled products.[132] These broadly use the principles of inertial impaction to segregate particles of different aerodynamic particle size.[76] Most commonly, the apparatus comprise a series of stages, with jets (nozzles) of specific diameter through which air is drawn by vacuum pumping, underneath which sits a collection plate for each stage. The particles are introduced at the top of the apparatus by actuation of the inhalation device and are segregated onto the series of plates by means of whether the particle impacts on the stage or is retained in the airflow and travels further through the system (gravitational and electrical effects are assumed negligible). The aerodynamic particle size, and hence its inertia, dictate which particular stage it will be deposited on. This is an important distinction as the density is included in the measurement *i.e.* mass and velocity are important (momentum), unlike with more conventional particle sizing approaches such as DLS and LD.[84] The impaction measurement and calculation of APSD is however based on the assumptions that (i) the particles are spherical and of unit density and (ii) there is no particle bounce.[207] Figure 5.1.1 shows a schematic diagram highlighting the principles of inertial impaction under which these apparatus operate. Impactor and impinger systems offer the opportunity to interrogate particulate fraction in the context of lung deposition. They will be used as appropriate as the basis for fractionating solid deposits for subsequent microscopic and macroscopic interrogation. It will, therefore, be useful in the context of these studies to briefly describe the configuration of the apparatus; important in discussing the application and limitations of applying these for the study of deposited materials.
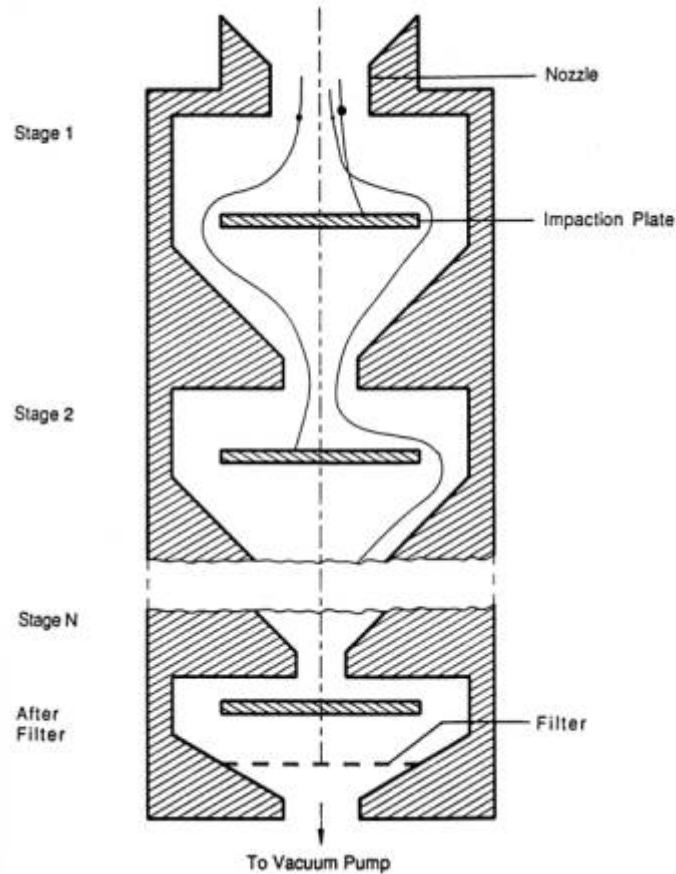
Figure 5.1.1 – Schematic representation of the mode of action of inertial impaction apparatus.[212]

These types of apparatus have been widely utilised over several decades[213] to characterise inhaled products and form the basis for the Pharmacopoeial (USP and PhEur)[132] assessment of aerodynamic particle size from pMDI and DPI devices. Additionaly, as well as the more recently developed aqueous droplet inhalers (ADIs), they also form the basis for tests on nebulisers and nasal devices with minor adaptations. The related impinger apparatus use the same physical principles of inertial impaction, though are termed differently as they collect the impacted particles on a liquid surface as opposed to solid collection plates. The measurements are of critical importance to pharmaceutical product development, forming the basis for the

in-vitro testing performed on inhaled products to ascertain the viable dose likely to reach the inner airways of the lung and have a therapeutic effect. In their simplest form, an impaction or impingement device will separate the dose into two fractions; respirable and non-respirable. Such fractions are normally defined as those which deposit in the inner airways, and those which deposit in the oropharynx and are ingested. Additionally, such classification can be further separated into sub-fractions of defined aerodynamic particle size, particularly useful in estimating the propensity for intra-thoracic deposition.[76]

Both types of apparatus are used by convention (and following Pharmacopoeial methods) in conjunction with quantitative remote analysis. This is usually based on chromatographic methods HPLC / GC, and gives the amount of API deposited on each stage. These quantitative levels of API then allow the subsequent calculation of aerodynamic properties such as fine particle dose (FDP), fine particle fraction (FPF) and mass median aerodynamic diameter (MMAD) / geometric standard deviation (GSD) after further data manipulation.[76] Whilst also considered here, of particular interest to these *in-situ* characterisations are the utilisation of impactors and impingers to fractionate inhaled materials into stages by respirable and non-respirable portions (and by more discrete portions as appropriate) for isolation and microscopic / solid form studies. This approach requires modifications to be made to the impingement apparatus to collect solid material before it is entrained in the liquid of the receiver. By contrast, impaction devices can be operated as per Pharmacopoeial methods with little modification. Five specific types of impinger / impactor are listed in the US

and European Pharmacopoeia (i) Twin Stage Glass Impinger (TSI) (ii) Multi-Stage Liquid Impinger (MSLI) (iii) Marple Miller Impactor (MMI) (iv) Anderson Cascade Impactor (ACI) and (v) Next Generation Impactor (NGI). Only three are shared between the two and are summarised in more detail in the following sections 5.1.1 to 5.1.3.

5.1.1   Twin Stage Impinger (TSI)

The TSI is the simplest form of inhalation assessment and was developed originally at Glaxo SmithKline's laboratories in Ware, UK. It has, to a large extent, been superseded by the use of ACI and NGIs as it is generally accepted that the apparatus should have a minimum of 5 stages to provide adequate size distribution results. However, it still has a useful role in initial quality assessment because of the speed and ease of use. The simple arrangement of glassware (Shown in Section 2.5.4, Figure 2.5.4.1) separates the non-respirable portion by deposition in the throat (sections B and C) and upper impingement chamber (section D), with a particle cut-off of 6.4 µm when operated at a flow of 60.0 L/min.[76] The respirable fraction of the test substance, *i.e.* that of < 6.4 µm, is passed through to the second stage of the apparatus and is collected by liquid impingement in the solution contained in the final flask (section G).

5.1.2   Anderson Cascade Impactor

The ACI has previously been considered to be the most commonly used of the impaction devices within the pharmaceutical sector, though is perhaps becoming superceeded by the NGI (5.1.3). The ACI fulfils the requirement for an impaction device to have a minimum of 5 collection stages. The fully

assembled ACI has a total of 8 stages to collect deposited material. The apparatus allows the product from pMDI or DPI devices to be separated into respirable and non-respirable fractions by the principles of inertial impaction. The respirable fraction is divided into 8 particle cut-off levels (a primary advantage over the TSI). The particle size cut-offs are given in Table 5.1.2.1. These cover the size ranges of importance in pulmonary deposition (0.1 to 10 µm)[205] when operated as stated in Ph.Eur methodology[132] at 28.3 L/min.

Table 5.1.2.1 – Particle size cut-offs of the ACI when operated at 28.3 L/min as outlined in the Ph.Eur[132]

Stage	Particle Size / µm
0	> 9.0
1	5.8
2	4.7
3	3.3
4	2.1
5	1.1
6	0.7
7	0.4

The stages are arranged in a vertical orientation in an ACI, with the stream of airbourne particles passing down the system. Particles with sufficient inertia will impact on the stage and be retained there, whilst those with insufficient inertia (*i.e.* the smaller particles) will remain in the airflow and pass through to the next stages of the system. A schematic is shown as Figure 5.1.2.1. Several drawbacks to the use of the ACI have been described. Particle bounce and re-entrainment into the airflow have been noted, particularly with the use of DPI devices, while overloading of the impaction stages and inter-stage losses have also been identified.[76,205]
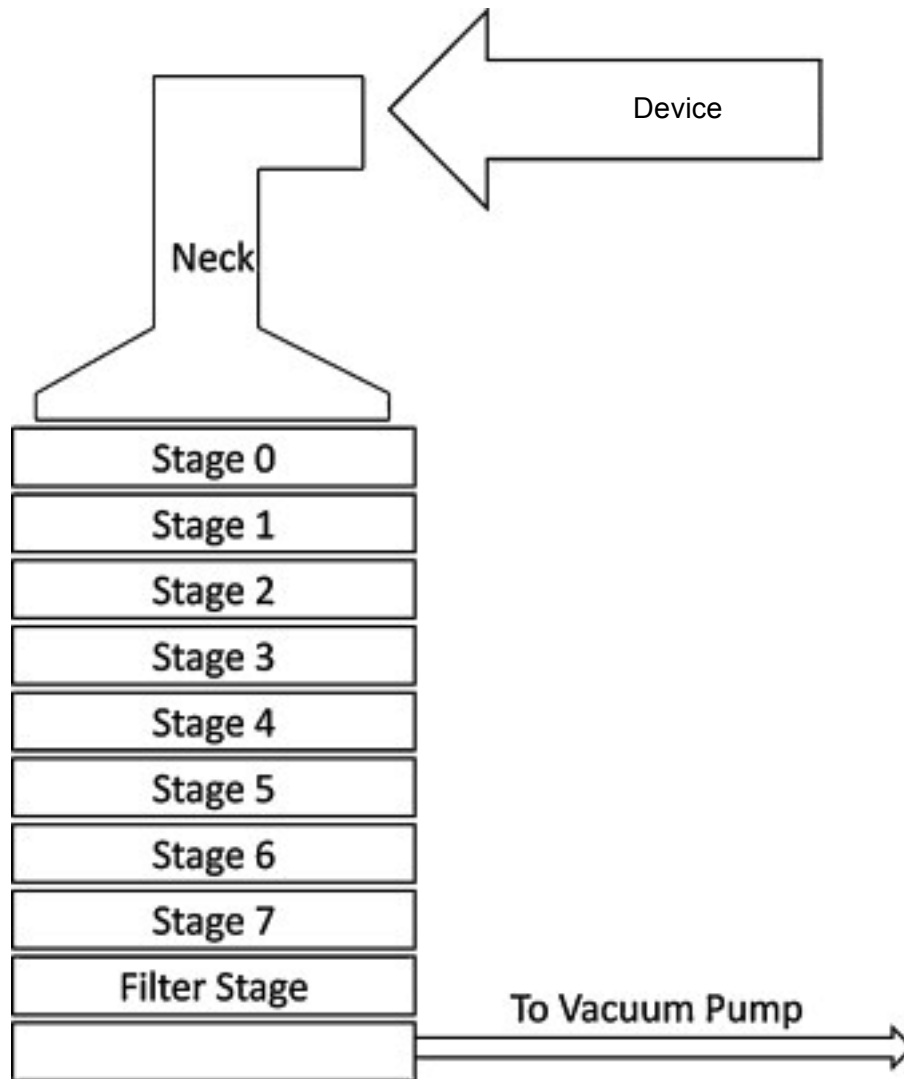
Figure 5.1.2.1 – Schematic diagram of an Anderson Cascade Impaction apparatus.[206]

5.1.3 Next Generation Impactor

The NGI device was developed from 1997 by a consortium of several large pharmaceutical companies.[76] The apparatus was launched in 2000 and was adopted by both the USP and PhEur in 2005. The apparatus works on the principles of inertial impaction as with other devices, however the horizontal orientation of the airstream flowing in a saw-tooth path is unique. The NGI comprises 7 stages and a micro-orifice collector (MOC), with 5 of the stages

having cut-off diameters between 0.5 and 5 µm. The apparatus has been developed to allow use over a larger flow range than other devices without the need for further modification, and will allow experimentation between 30 and 100 L/min with cut-off diameters between 0.24 and 11.7 µm,[132] with nebulisation experimentation at 15 L/min being possible with an additional calibration step. At a flow rate of 60 L/min when operated in accordance with Ph.Eur methodology[132] the NGI gives fractionation as presented in Table 5.1.3.1.

Table 5.1.3.1 - Particle size cut-offs of the NGI when operated at 60.0 L/min as outlined in the Ph.Eur.[132]

Stage	Particle Size / µm
1	8.06
2	4.46
3	2.82
4	1.66
5	0.94
6	0.55
7	0.34

The NGI stages are in the form of removable cups, aiding greatly in dissolution of the contents into a solvent for remote chromatographic analysis. Automated sample workup systems are now available from specific apparatus manufacturers.[76] The final stage of the NGI (the MOC) has a nominal 4032 hole (70 µm diameter) configuration, and is capable of removing in excess of 80% of 0.14 µm particles when operated at a flow rate of 60 L/min.[132] This removes the need for a filter stage for most applications. A schematic diagram of an NGI is shown (Figure 5.1.3.1).
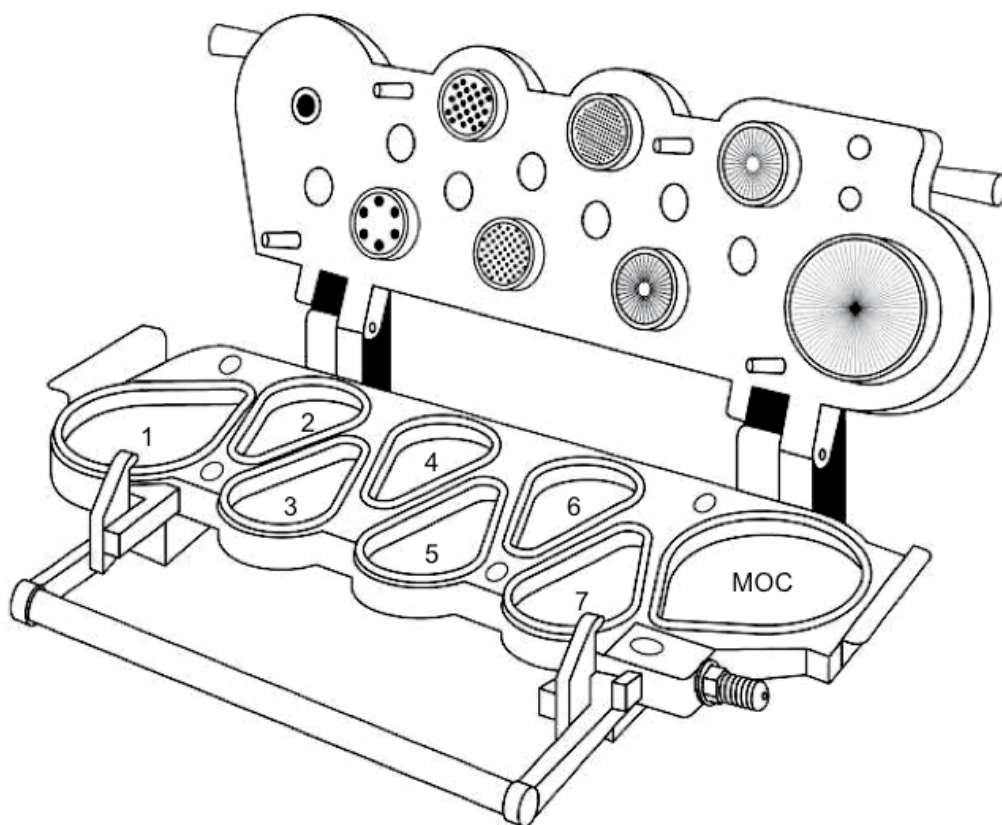
Figure 5.1.3.1 – Schematic diagram of a Next Generation Impactor apparatus.[76]

5.2   Method Development for Solid Form Investigations

5.2.1   Aerodynamic Particle Size Distribution (APSD)

Use of the summarised impaction / impingement systems (section 5.1) for the characterisation of FPF / FPD (and MMAD / GSD) has become the pharmaceutical industry standard and is incorporated in the USP and Ph.Eur. The latter states "This test [preparation for inhalation] is used to determine the fine particle characteristics of the aerosol clouds generated by preparations for inhalation. Unless otherwise justified and authorised, one of the following apparatus and test procedures is used (i) Twin Stage Impinger

(ii) Multi Stage Liquid Impinger (iii) Anderson Cascade Impactor or (iv) Next Generation Impactor."[132]

Experimental methods are outlined in each case for the assessment of aerodynamic particle size (though not MSLI in the USP) from nebulisers, pMDIs and DPIs separately, and are not transposed *verbatim* in this text. For each apparatus, a calculation method is given to calculate reliably the aerodynamic properties of the test item. The method specified for determination using an ACI type apparatus is shown below, and is transposed directly:[132]

"From the analysis of the solutions, calculate the mass of active substance deposited on each stage per discharge and the mass of active substance per discharge deposited in the induction port, mouthpiece adaptor and when used, the pre-separator.

Starting at the final collection site (filter), derive a table of cumulative mass *vs.* cut-off diameter of the respective stage (Table 5.2.1.1). Calculate by interpolation the mass of the active substance less than 5 µm. This is the Fine Particle Dose (FPD).

If necessary, and where appropriate (*e.g.* where there is a log-normal distribution), plot the cumulative fraction of active substance *vs.* cut-off diameter on log probability paper, and use this plot to determine values for the Mass Median Aerodynamic Diameter (MMAD) and Geometric Standard Deviation (GSD) as appropriate. Appropriate computational methods may be used"

Table 5.2.1.1 – Calculations for apparatus D (ACI) used at a flow rate of 28.3 L/min.

Cut-off diameter (μm)	Mass of API deposited per discharge	Cumulative mass of API deposited per discharge	Cumulative fraction of API (%)
$d_7 = 0.4$	mass from stage 8, m_8	$c_7 = m_8$	$f_7 = (c_7/c) \times 100$
$d_6 = 0.7$	mass from stage 7, m_7	$c_6 = c_7 + m_7$	$f_6 = (c_6/c) \times 100$
$d_5 = 1.1$	mass from stage 6, m_6	$c_5 = c_6 + m_6$	$f_5 = (c_5/c) \times 100$
$d_4 = 2.1$	mass from stage 5, m_5	$c_4 = c_5 + m_5$	$f_4 = (c_4/c) \times 100$
$d_3 = 3.3$	mass from stage 4, m_4	$c_3 = c_4 + m_4$	$f_3 = (c_3/c) \times 100$
$d_2 = 4.7$	mass from stage 3, m_3	$c_2 = c_3 + m_3$	$f_2 = (c_2/c) \times 100$
$d_1 = 5.8$	mass from stage 2, m_2	$c_1 = c_2 + m_2$	$f_1 = (c_1/c) \times 100$
$d_0 = 9.0$	mass from stage 1, m_1	$c_0 = c_1 + m_1$	$f_0 = (c_0/c) \times 100$
	mass from stage 0, m_0	$c = c_0 + m_0$	100

5.2.2 Method Development for Microscopic Assessment of Particle Form, Morphology and Distribution Using Raman Spectroscopy

Raman spectroscopy has proved itself to be an invaluable tool in the investigation of materials as wide ranging as specialty chemical and polymers,[212] artworks,[213,214] illicit materials such as drugs of abuse and contraband ivories[215,216] and its frequent use in the investigation of biological and archaeological materials.[217-220] The technique has also been heavily utilised in the investigation of pharmaceutical materials, including molecular and form identification.[221,222] Modern instrumentation has seen Raman spectrometers coupled to confocal light microscopes allowing acquisition of Raman spectra from highly specific points on (and sub) sample surfaces, as well as offering the user the ability to obtain multiple spectra across a sample to generate a two dimensional hyperspectral arrays. These spectral arrays can be processed to produce false colour representations over the recorded area and provide an excellent visual means by which to display distributions

of compounds, as well as distributions of differing physical forms and other subtle sample inhomogeneities only discernable through spectroscopy.

Treatment of diseases of the lung such as asthma and COPD utilise the locally acting IPPs delivered *via* pMDIs (and other devices) to control symptoms. In cases where treatment with ICS such as budesonide, BDP etc. does not fully control the symptoms, the administration of SABAs, LABAs or LAMAs in addition is recommended.[57] A more detailed review of the applicability of these combination products is given (Section 1.1), though clinical trials have shown that addition of LABAs is more beneficial than simply increasing the dose of the steroid.[130] Other studies confirm that delivery with combination therapies *i.e.* co-formulated in the same device, have a greater therapeutic effect than doses delivered sequentially with separate devices,[130] and there is evidence that their co-administration is synergistic through the effect of each one on the receptor for the other.[223-225] For this effect to be observed, it is thought that the co-administration is vital, as inhalation through sequentially administered doses reduces the likelihood of drug being delivered to the same site.[225] Recent work by Adi *et al.*[226] has extended dual therapies to investigated combination therapies containing three IPPs co-formulating an ICS, a LAMA and a LABA (budesonide, ipratropium bromide and formoterol fumarate), using only impaction methods with HPLC to investigate the depositions and aerodynamic properties. They conclude that the three entities are deposited in a fixed 1:1:1 ratio, and contrast these findings to Symbicort® (AstraZeneca) where the quantitative ratios vary by stage. They interpret these findings as indicative of deposition as separate entities. The following sections present method development

activities undertaken to establish a micro-Raman (µ-Raman) based approach to assess particles deposited *in-vitro* using impactors.

Controlled depositions can be undertaken with any of the impaction apparatus discussed previously (Section 5.1). These studies are based on the subsequent µ-Raman investigation on the deposited materials from stages chosen to represent particle size cut-offs of interest. Raman data can provide qualitative information on the deposited material in terms of particle morphology, deposition profiles, and molecular information including functional groups and solid form, distinguishing polymorph differences[227,228] and amorphous materials.[229] Most importantly in this context however, using assemblages of spectra recorded over a defined area, information relating to patterns of depositions can be derived from false colour 'maps'. These can be analysed with relevant image processing software to provide semi- or even fully-quantitative data based on the relative intensities of signals and the frequency of occurrence.

Importantly, Raman mapping analysis has been applied recently to a commercially available combination therapy, Seretide® (GSK) to investigate the deposition of particulates of the different APIs, potentially demonstrating some deposition 'cooperatively' for combination delivery to the same microscopic site.[230] These studies aim to develop similar µ-Raman methods using Symbicort® (AstraZeneca) and Seretide® (GSK) in their different formulation dose ratios to assess the applicability of the approach to assess distribution *in-vitro* and the ability to confirm sites of co-deposition.

5.2.2.1   Seretide® and Symbicort® Raw Material Analysis

The Seretide® product is based on combined formulation of fluticasone propionate and salmeterol xinafoate. These are co-formulated at three separate dosage levels; 25 µg fluticasone and either 50, 125 or 250 µg salmeterol per dose. The products are formulated in HFA134a as suspensions and are marketed as pMDIs. Symbicort® formulations are available in pMDI form whereby budesonide and formoterol fumarate dihydrate are co-formulated at two separate dosage levels; 4.5 µg formoterol and either 80 and 160 µg budesonide per dose in HFA227.

To obtain reference spectra, each of the API materials was analysed by Raman spectroscopy using 785 nm high powered diode laser for excitation. The samples were exposed to *ca.* 1 mW at the site of analysis for 10 seconds, with 5 averaged accumulations acquired in each case. Data are consistent with previously reported spectral assignments[227,231,232] and are not reproduced here. Spectra for individual components were analysed for interferences *i.e.* areas in the spectra where peaks overlap, obscuring one another. This analysis also directs the 'static' scan recorded during rapid mapping acquisitions. This scanning mode describes a reduced spectral window (*i.e.* the wavenumber spectral width recorded at each scan), essentially projecting an image from the spectrograph across the CCD detector without shifting the diffraction grating, hence a considerably reduced scan time important for rapid data acquisition. The reference spectra for the 4 components are presented (Figures 5.2.2.1.1 to 5.2.2.1.4), and spectral overlays (Figures 5.2.2.1.5 and 5.2.2.1.6) show envelopes chosen for hyper-

spectral array acquisition for the Seretide® and Symbicort® depositions containing unique spectral features for the relevant APIs.

Fluticasone propionate and salmeterol xinafoate (Seretide®) are distinguished spectrally with the intense band at 1662 cm^{-1} [v(C=C), quinone] in fluticasone and the four closely sited bands from 1340 to 1470 cm^{-1} [v(CH), v(CH$_2$), v(CH$_3$)] of salmeterol being particularly characteristic. Budesonide and formoterol fumarate (Symbicort®) having bands at 1654, 1610 and 1305 cm^{-1} [v(C=O), v(C-C-CH$_3$) and v(CH$_3$] in formoterol and 1656 cm^{-1} [v(C=C), quinone] in budesonide allowing adequate differentiation.
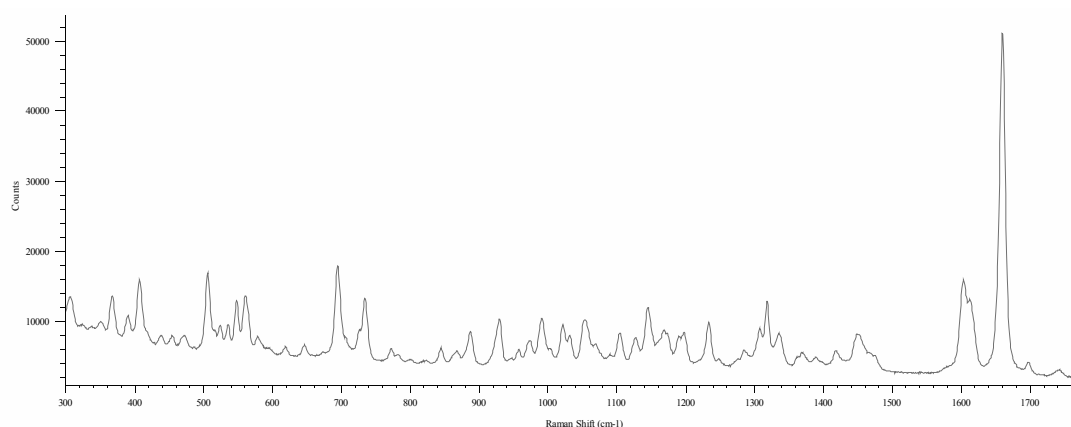
Figure 5.2.2.1.1 – Raman spectrum of fluticasone propionate acquired using 785 nm excitation with ca. 1 mW laser power at sample, 10 second exposure and 5 averaged accumulations expanded in the region 300 to 1700 cm^{-1}.
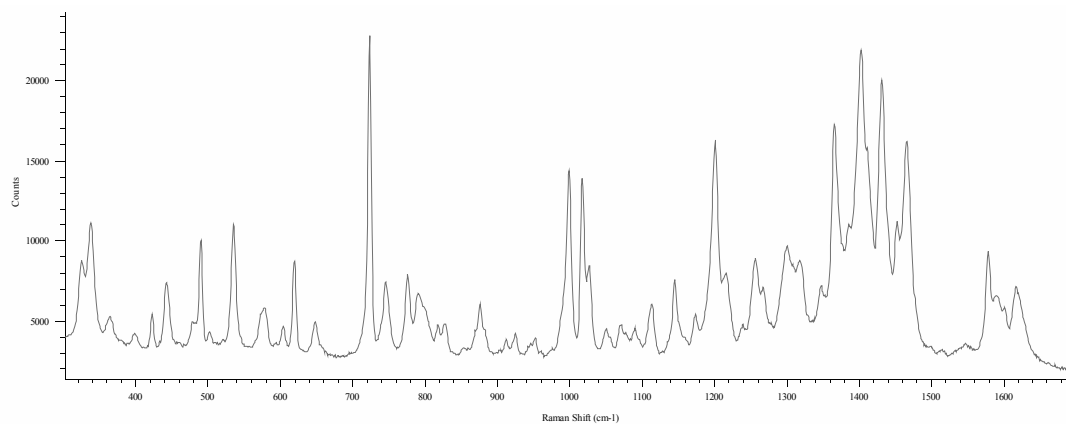
Figure 5.2.2.1.2 – Raman spectrum of salmeterol xinafoate acquired using 785 nm excitation with *ca.* 1 mW laser power at sample, 10 second exposure and 5 averaged accumulations expanded in the region 300 to 1700 cm^{-1}.
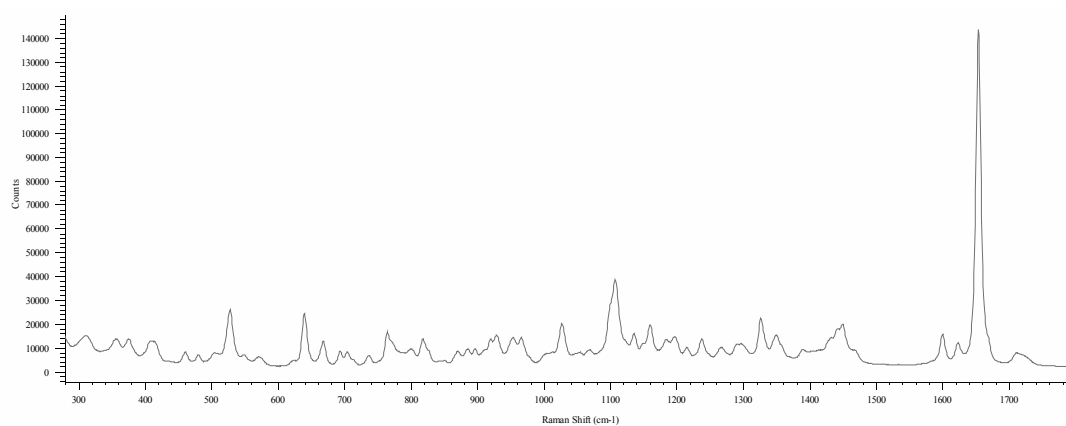
Figure 5.2.2.1.3 – Raman spectrum of budesonide acquired using 785 nm excitation with *ca.* 1 mW laser power at sample, 10 second exposure and 5 averaged accumulations expanded in the region 300 to 1800 cm^{-1}.
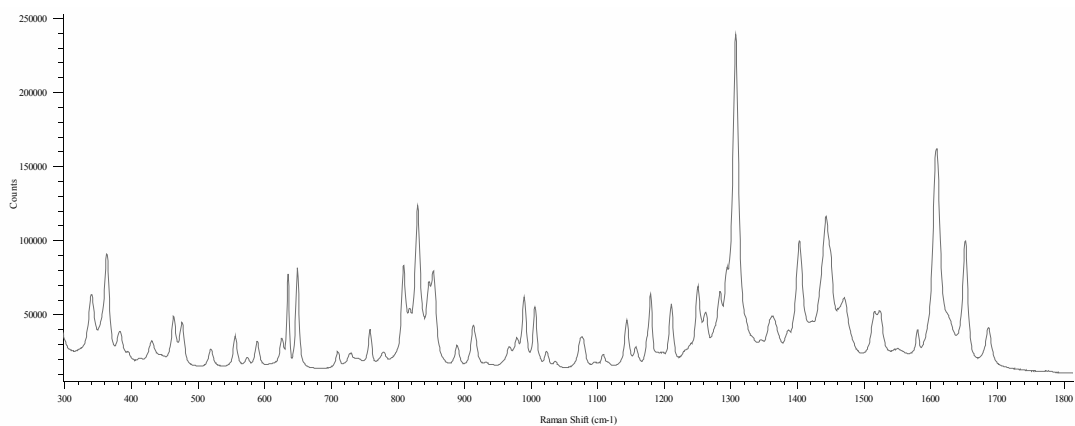
Figure 5.2.2.1.4 – Raman spectrum of formoterol fumarate acquired using 785 nm excitation with *ca.* 1 mW laser power at sample, 10 second exposure and 5 averaged accumulations expanded in the region 300 to 1800 cm^{-1}.

Fluticasone
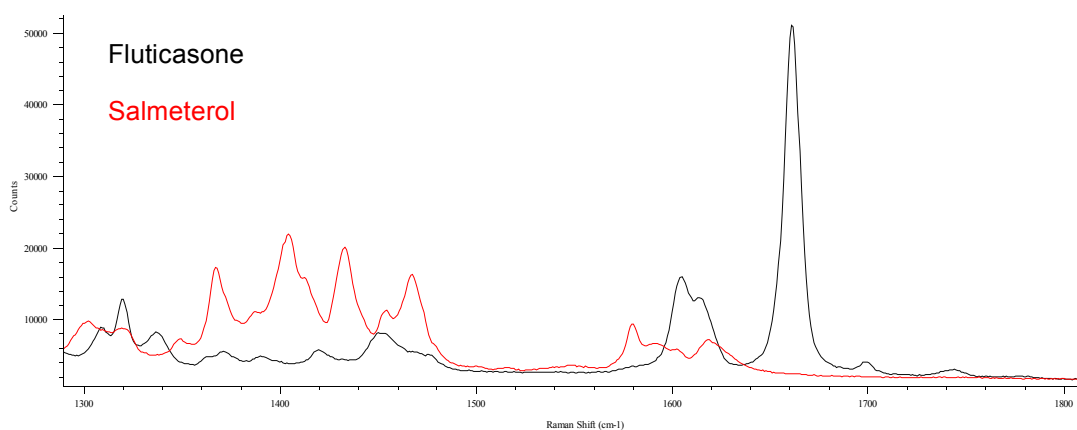
Salmeterol

Figure 5.2.2.2.5 – Raman spectra of fluticasone (black) and salmeterol (red) shown in the spectral region between 1290 and 1810 cm^{-1} showing key spectral features used for the component matching processing of the maps.
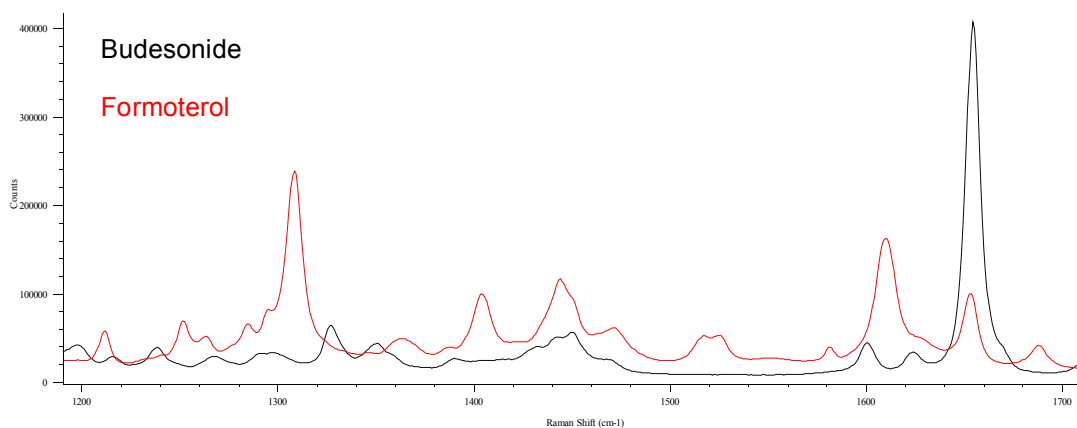
Figure 5.2.2.2.6 – Raman spectra of budesonide (black) and formoterol (red) shown in the spectral region between 1190 and 1710 cm^{-1} showing key spectral features used for the component matching processing of the maps.

5.2.2.2   Raman Analysis of Deposited Seretide® and Symbicort® Materials

Depositions were performed using an Anderson Cascade Impactor to fractionate the particulates into discrete particle size fractions as discussed in detail in Section 5.1. The ACI was setup and operated in accordance to the Pharmacopoeial method at 28.3 L/min flow giving particle cut-off values of between 2.1 and 3.3 µm on plate 4, considered to be representative of the central airways[233] where delivery of ICS and β_2 agonist compounds to sites where glucocorticoid and β_2 receptors are present is considered useful.[14] Addition of microscope cover slips to the plates of the ACI was performed to allow the depositions to be conveniently removed for analysis by µ-Raman. One single actuation was performed after eleven 'dummy' actuations. Photographs of the depositions on plate 4 from Symbicort® 80/4.5 are shown with a representative white light image taken using the µ-Raman (x 50 objective, 0.75 N$_A$) (Figure 5.2.2.2.1). Point analyses on discrete particles

over the spectral range 100 to 2500 cm^{-1} shows high background signals

(Figure 5.2.2.2.2). Analysis in regions where no particulate depositions are

visible produces similar Raman spectra and the background signal is

attributed to glass from the substrate.
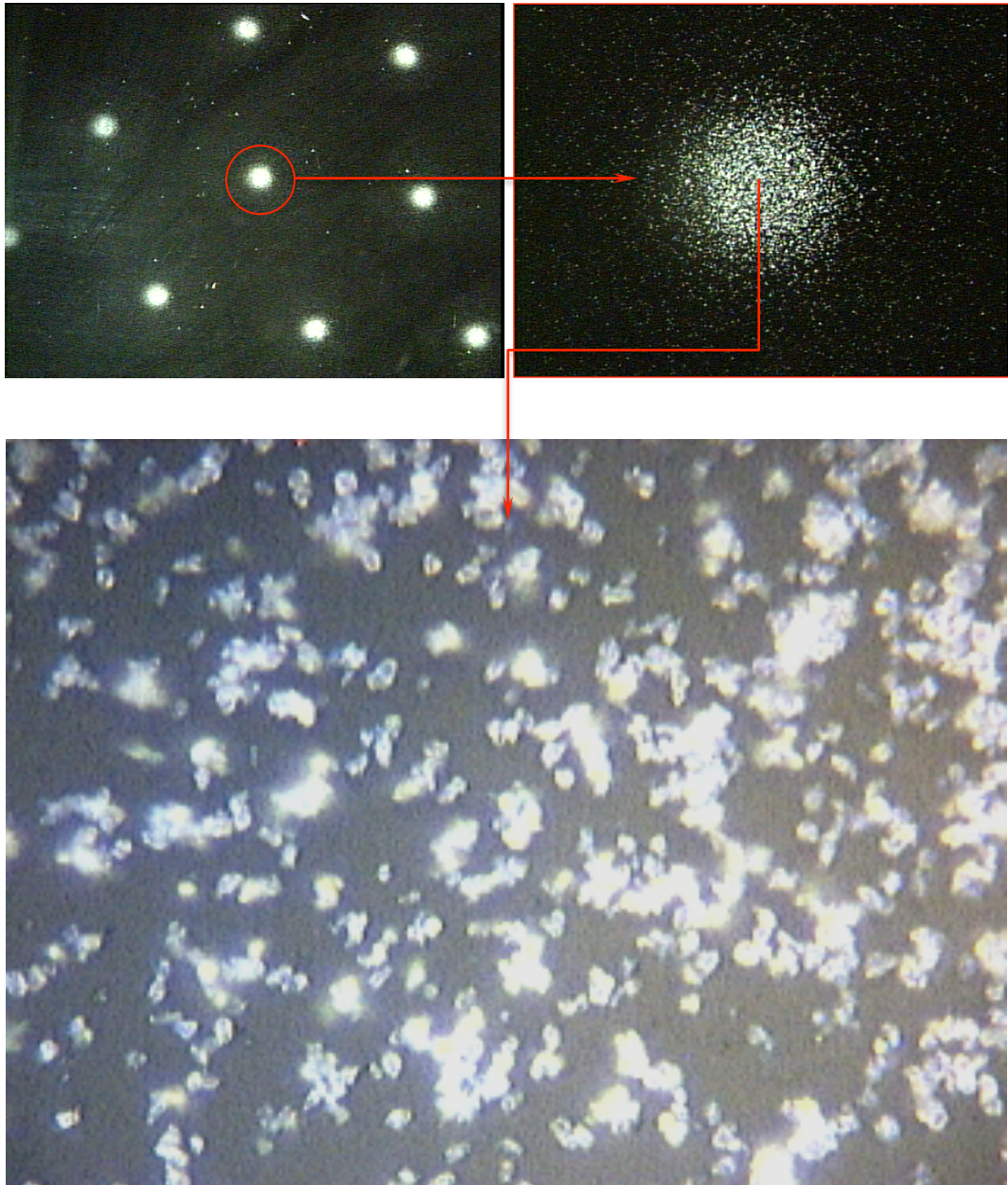
Figure 5.2.2.2.1 – Photograph of the depositions from Symbicort® 80/4.5 on

glass cover slip positioned on Plate 4 of the ACI.
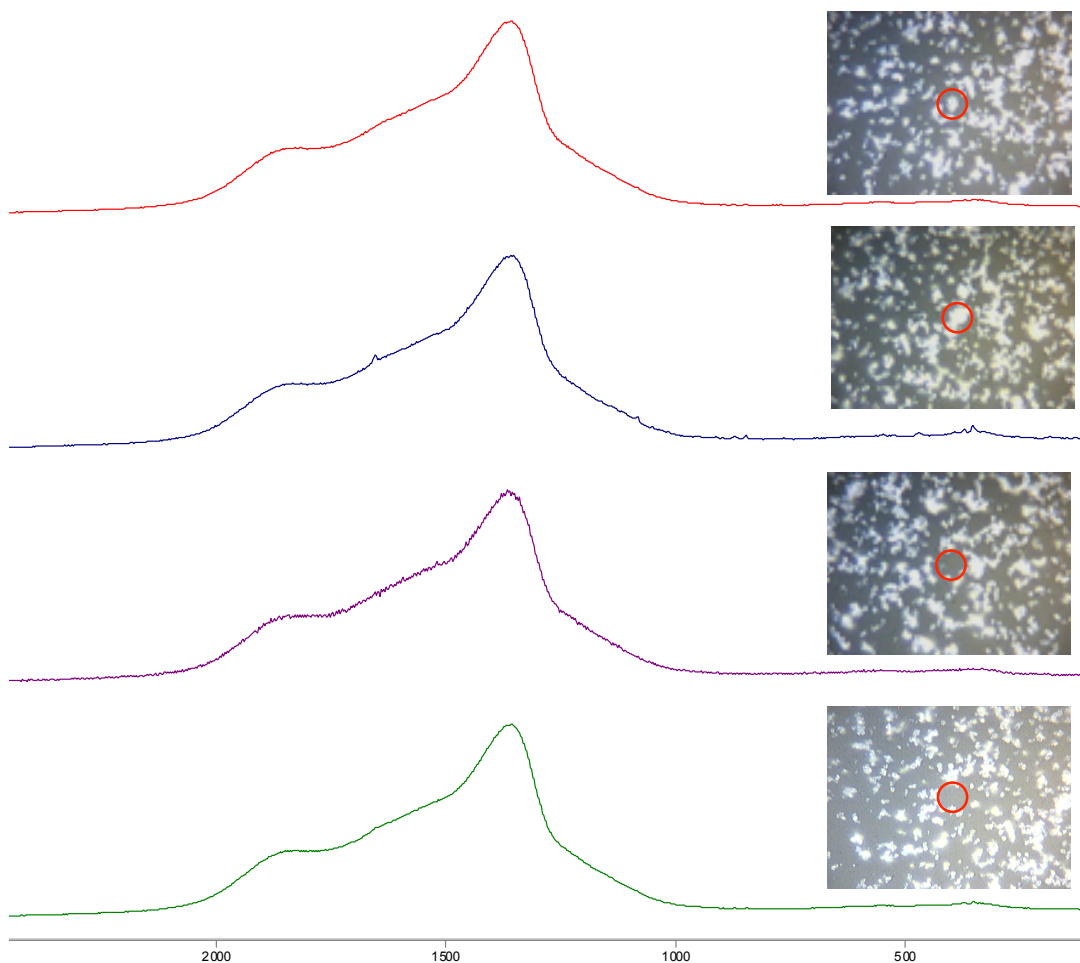
Figure 5.2.2.2.2– Raman spectra acquired on particulate depositions from Symbicort® 80/4.5 and regions of no visible deposition on glass cover slip positioned on Plate 4 of the ACI.

The glass coverslips were replaced with aluminium plates to avoid the background interferences and the depositions were repeated. Aluminium plates of less than 1 mm thickness were chosen to minimise the geometry changes in the ACI and hence changes in impaction behaviour. Point Raman analyses acquired in region of particulate deposits over the spectral range 100 to 2500 cm^{-1} shows minimum interfering background signals in the regions of interest, with only two intense broad bands below 500 cm^{-1} visible.

Figure 5.2.2.2.3 shows multiple spectra acquired on particulate deposits and in regions of aluminium background.
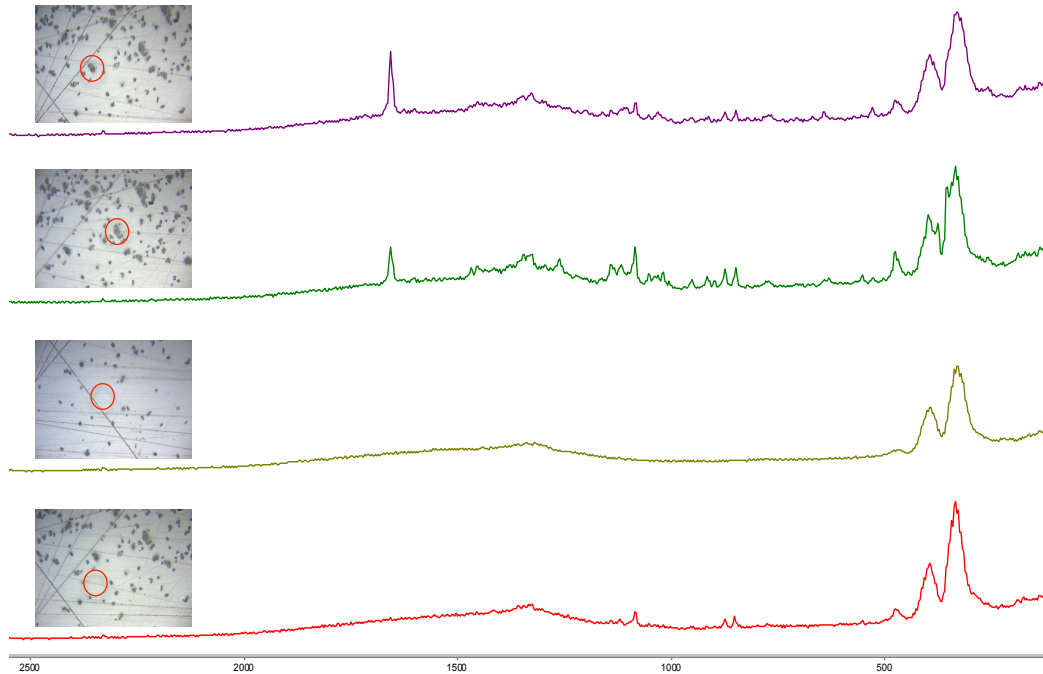
Figure 5.2.2.2.3- Raman spectra acquired on particulate depositions from Symbicort® 80/4.5 and regions of no visible deposition on aluminium plate positioned on Plate 4 of the ACI (x50 objective).

The point spectra presented to this point have been recorded using the x50 objective lens of the microscope. Sampling volume, or 'spot-size' of the laser on the sample is reduced using higher magnification objectives of higher numerical aperture, N_A. With lenses of high N_A, the spot size is reduced adhering to Equation 5.2.2.2.1.[234]

$$Laser\ spot\ size = \frac{1.22\lambda}{N_A} \qquad\qquad \textbf{Equation 5.2.2.2.1}$$

It follows that use of the largest objective available with the highest N_A value will provide data with the highest spatial resolution. A modification to equation

189

5.2.2.2.1 yields the theoretical diffraction limited spatial resolution of an optical microscope (Equation 5.2.2.2.2):[234]

$$Spatial\ resolution = \frac{0.61\lambda}{N_A}$$ **Equation 5.2.2.2.2**

Use of the equations gives spot sizes of 1.064 and 1.276 μm, with theoretical spatial resolutions of 0.532 and 0.638 μm for the x100 and x50 lenses used on the Renishaw InVia μ-Raman having N_A values of 0.90 and 0.75 respectively. Lower wavelength excitation also has a dramatic effect in reducing the spatial resolution of the system, however the 785 nm is the only laser to have a linefocused geometry allowing faster mapping to be performed and dictates the use of this setup. It follows that acquisition using the x100 objective will maximise spatial resolution available. This is an essential parameter to consider as the purpose of the experimentation is to assess the potential for co-deposition for the particulates anticipated to be between 2.1 and 3.3 μm in size. Point acquisition of particulates from the Seretide® 50 deposition on the aluminium substrate and regions of no deposited material were performed using the x100 objective lens (Figure 5.2.2.2.4).
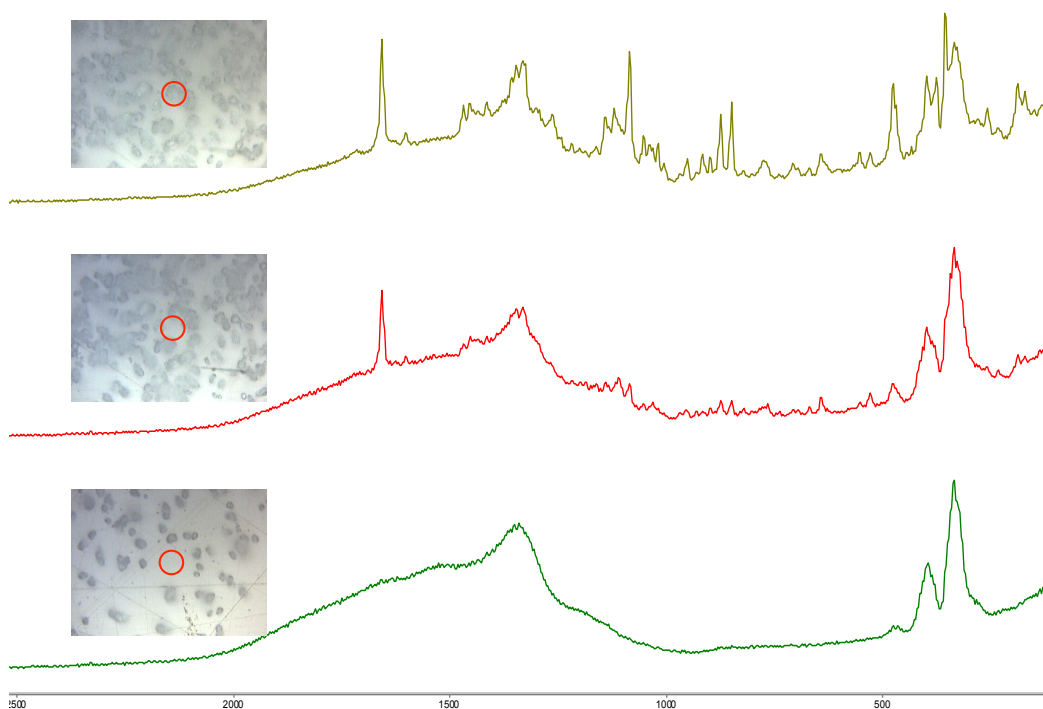
Figure 5.2.2.2.4- Raman spectra acquired on particulate depositions from Symbicort® 80/4.5 and regions of no visible deposition on aluminium plate positioned on Plate 4 of the ACI (x100 objective).

The spectra recorded show signals consistent with the components of the pMDI formulation, budesonide and formoterol fumarate, and the instrument set up is providing adequate spatial resolution, returning spectra consistent with only the background signal in regions selected away from any visible deposits.

Importantly, the μ-Raman approach needs to be assessed to establish whether it can discerne components present in the deposits and whether it can identify deposits of individual, adjacent and co-deposited materials. Deposits from the Seretide® preparation were performed using the ACI according to the Pharmacopoeial method at 28.3 L/min. One actuation was performed after 11 'dummy' actuations. The aluminium plates were removed

191

for analysis by μ-Raman using the x100 objective lens as described previously. Point analyses at specific deposit (particulate) sites show spectra consistent with both components (fluticasone propionate and salmeterol xinafoate) in the formulation, and of mixed spectra showing the presence of both components. Figure 5.2.2.2.5 shows spectra recorded on four isolated particulate depositions alongside the references, clearly showing spectra consistent with fluticasone and in one instance (red) a spectrum showing clear features of both compounds concomitantly.
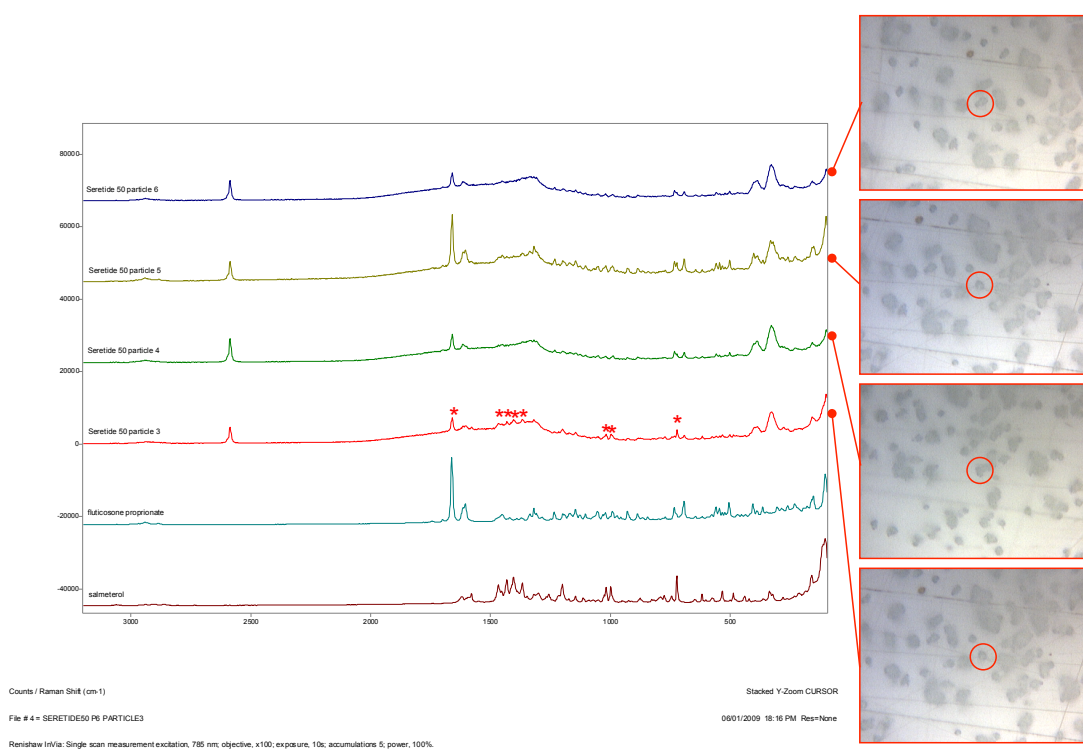
Figure 5.2.2.2.5- Raman spectra acquired on particulate depositions from Seretide® 50 on aluminium plate positioned on Plate 4 of the ACI (x100 objective) showing features (marked *) in spectrum (red) corresponding to fluticasone and salmeterol.

5.2.2.3 Hyper-spectral Arrays (Raman Maps) of Deposited Seretide® and Symbicort® Materials

The previous section has presented the development exercises undertaken to ensure the components of the Seretide® and Symbicort® formulations can be discerned spectrally from one another, and to optimise the spatial resolution obtainable using objective lenses of maximum N_A. Hyper spectral arrays were recorded over small regions of the previously deposited Seretide® 50 sample to assess the success of a final 'mapping' approach using a 785 nm high-powered diode laser to excite the sample. Processing of the arrays recorded was performed using a direct classical least squares (DCLS) component matching algorithm available in the Renishaw Windows interface for Raman Environment (WiRE v. 3.2). Previously acquired reference spectra (Section 5.2.2.1) were used in the component matching approach. Figure 5.2.2.3.1 shows a hyper-spectral array acquired over a region of *ca.* 15 x 15 µm superimposed on the white light image, processed using DCLS for fluticasone (left) and salmeterol (right) separately. Also shown are Raman spectra from positive matches for each, showing excellent correlation in each case.
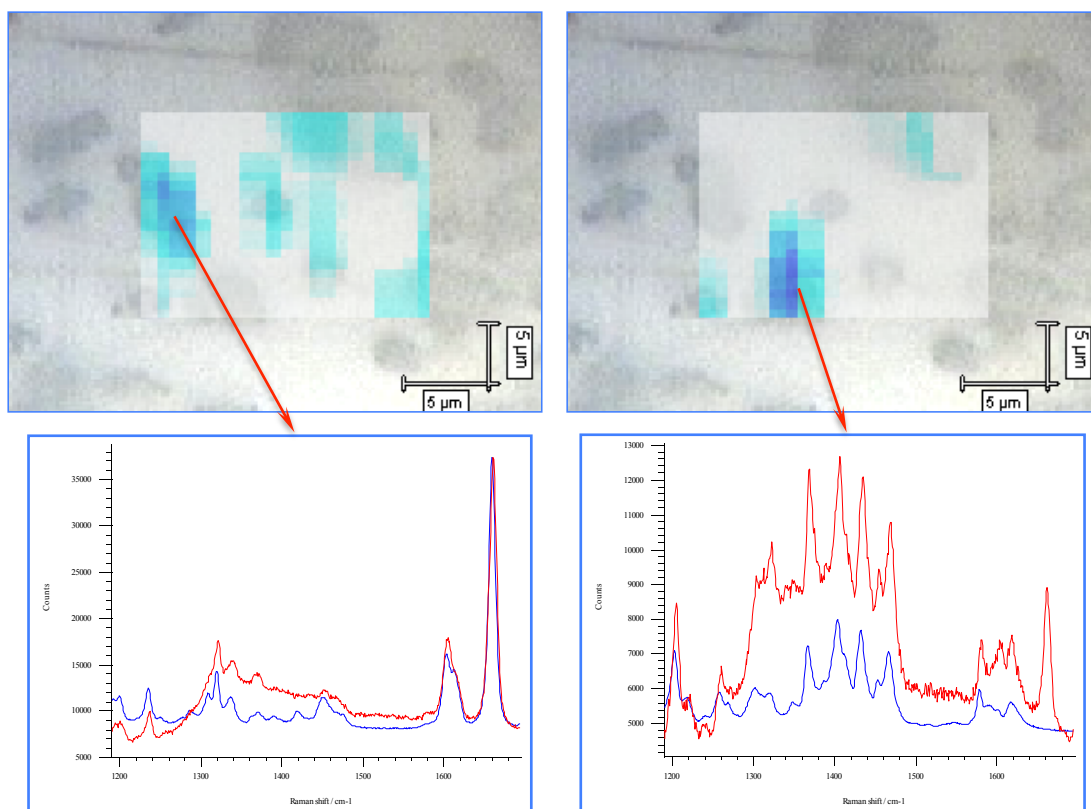
Figure 5.2.2.3.1 – Hyper-spectral arrays acquired over 15 x 15 μm region from plate 4 of a Sertide® 50 deposition, processed using direct classical least squares component matching for fluticasone (left) and salmeterol (right). Also shown are spectra obtained from regions of positive match for both compounds.

The conditions used in the acquisition of hyper-spectral arrays over the 15 x 15 μm area equate to extremely long acquisition times (> 12 hours) and their deployment on deposited samples over larger regions of statistical relevance was prohibitive. The conditions developed were deployed on an equivalent instrument (Renishaw InVia) equipped with proprietary fast mapping technologies, StreamLine™ (Renishaw, Wotton-under-Edge, UK). Traditional Raman acquisition operates in a sequential manner, in turn opening the detector shutter, collecting the scattered light, closing the shutter, reading the

data and finally moving the sample. By contrast, the StreamLine™ approach opens the shutter at the start of the experiment, and operates sample movement, light collection and data readout in parallel throughout, before closing the shutter at the end of the experiment. This results in significant time-savings, with up to 4000 individual spectra being recorded in 1 minute.[230] For Seretide® depositions hyper-spectral arrays were recorded with static scans centred at 1550 cm^{-1} recording data in the spectral region between 1290 to 1810 cm^{-1}. Similarly, Symbicort® hyper-spectral arrays were recorded with static scans centred at 1450 cm^{-1} recording data in the spectral region between 1190 to 1710 cm^{-1}. The spectral arrays recorded were processed using DCLS component matching in both instances using reference spectra of fluticasone / salmeterol (Seretide®) and budesonide / formoterol (Symbicort®) as previously. Figures 5.2.2.3.2 to 5.2.2.3.6 show the false colour representations of the arrays recorded for the products analysed, clearly showing successful differentiation of the two components present in each case (fluticasone & budesonide shown in red, salmeterol & formoterol in green).
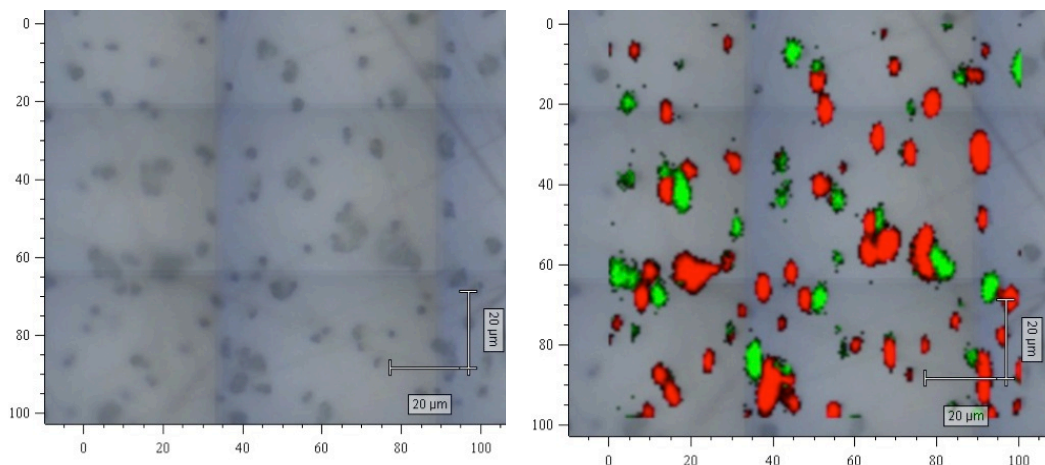
Figure 5.2.2.3.2 – White light image and Raman map of Seretide® Evohaler 50 (ACI plate 4) processed using DCLS component matching for fluticasone (red) and salmeterol (green).
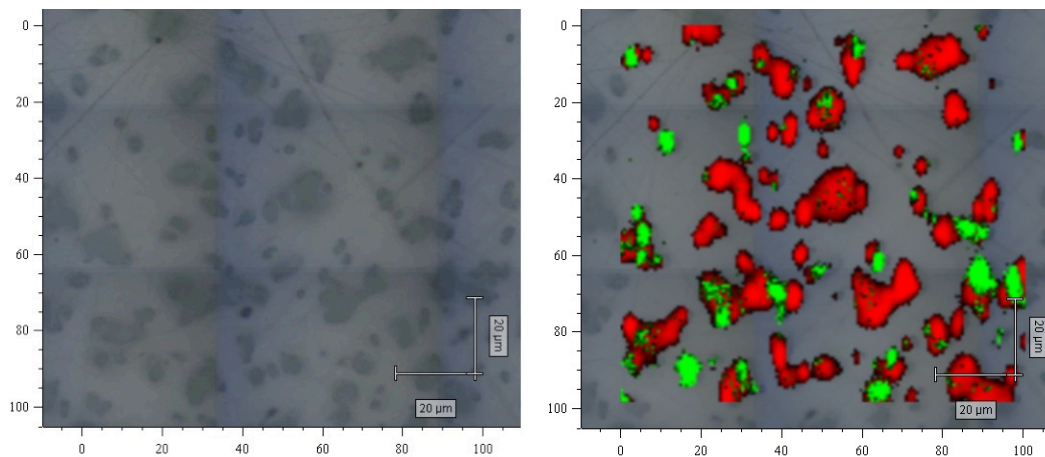
Figure 5.2.2.3.3 – Raman map of Seretide® Evohaler 125 (ACI plate 4) processed using DCLS component matching for fluticasone (red) and salmeterol (green).
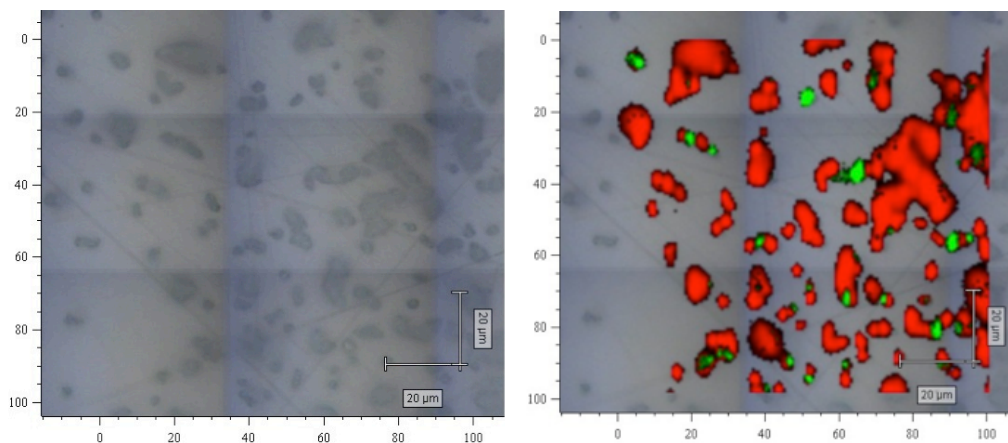
Figure 5.2.2.3.4 – White light image and Raman map of Seretide® Evohaler 250 (ACI plate 4) processed using DCLS component matching for fluticasone (red) and salmeterol (green).
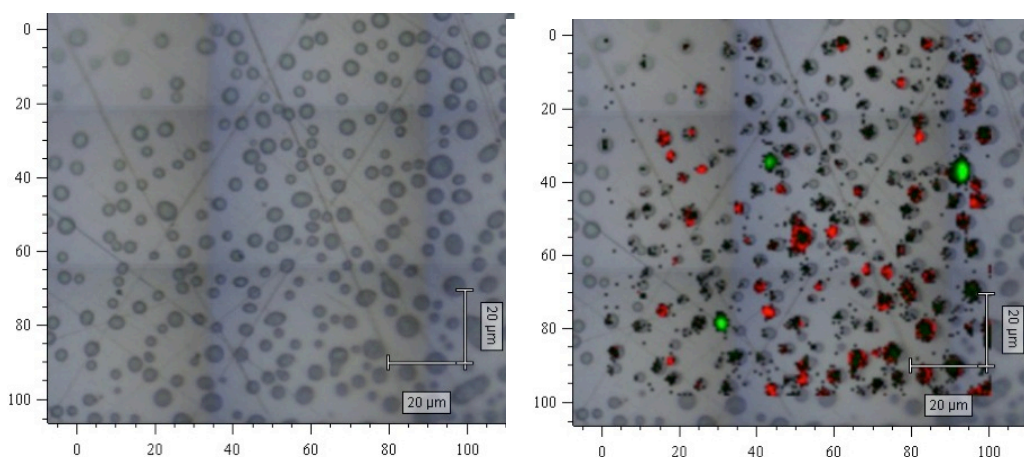
Figure 5.2.2.3.5 – White light image and Raman map of Symbicort® 80/4.5 (ACI plate 4) processed using DCLS component matching for formoterol (green) and budesonide (red).
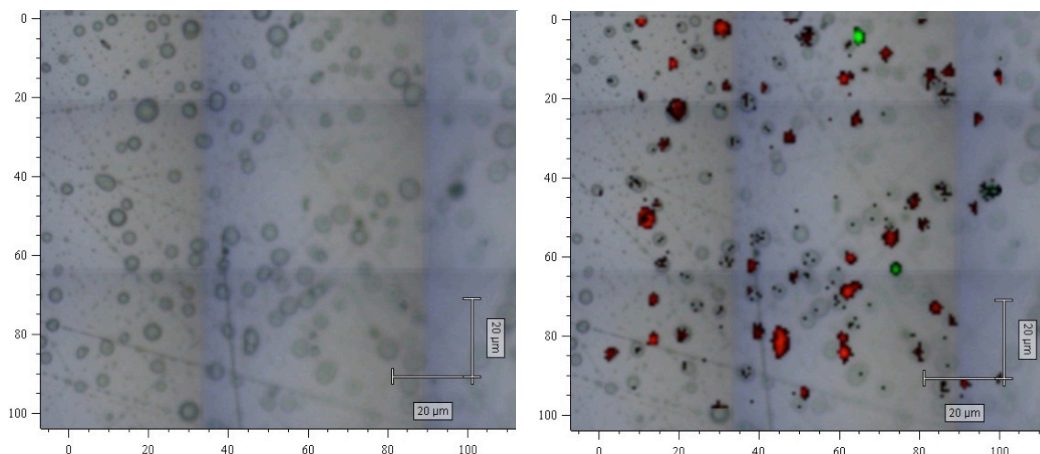
Figure 5.2.2.3.6 – White light image and Raman map of Symbicort® 160/4.5 (ACI plate 4) processed using DCLS component matching for formoterol (green) and budesonide (red).

As the concentration of the ICS fluticasone relative to the LABA compound salmeterol is increased though the 50, 125 and 250 products, there is a clear correlation to the abundance of fluticasone deposited. It appears to deposit as discrete particulates and in clusters / agglomerates. The salmeterol deposits are visible in isolated positions in the processed images, and show evidence for association to the fluticasone particulates in a number of instances, leading to the conclusion that the deposits from Seretide® pMDI devices do show instances of co-deposition *in-vitro*. These findings corroborate those from similar studies by Theophilus *et al.*[230] who observe co-depositions using similar approaches and conclude synergistic interaction between drugs from co-formulated pMDI products. The methods applied to depositions from triple therapies such as those undertaken by Adi *et al.*[226] would be very interesting and potentially substantiate their claims that the particles (budesonide, ipratropium and formoterol) are associated and deposit in exactly equal proportions in *in-vitro* testing. Data processing using

the DCLS (and other model) approaches should also be considered. The false colour images are produced using a threshold that can be adjusted to essentially switch on / off the response in a binary fashion. *i.e.* if a different threshold value is chosen, pixels representing fluticasone, for example, can be switched on or off. It is important to consider this in terms of conclusions drawn on co-deposition. If false colour representations on the processed map are contiguous for particles of fluticasone and salmeterol at a particular threshold level they may be considered co-deposited. If this threshold level is shifted (lowered) to the point whereby the particles are no longer contiguous this conclusion changes. It is important to remember that the data can be manipulated to some degree and it must be processed at fixed threshold levels to avoid any subjectivity in the interpretation of results.

The results for the Symbicort® systems provide less conclusive evidence. Although the components present in the formulation (budesonide and formoterol) give strong Raman spectra that show clear spectral differences, the data recorded on the deposited materials are considerably less intense. Examination of the white light images of the deposits shows differences when compared to those of the Seretide® depositions. Symbicort® deposits appear circular as opposed to displaying crystalline like morphologies as in the Seretide® depositions. The images are suggestive of an amorphous form, though without further evidence from other analytical approaches this is a difficult conclusion to substantiate.

5.2.3 Methods for Bulk Assessment

The previous section in this chapter has discussed microscopic approaches for the assessment of deposited materials from aerosolisation devices and Chapters 3 and 4 summarise the work performed to develop an NMR method suitable of assessing the bulk properties of solutions *in-situ* (solubility and complex characterisation). A further consideration are the bulk properties of the deposited materials and are part of the method developments associated with these studies. In collaboration with colleagues at King's College London (KCL), the following sections describe novel approaches for the capture of these materials and their study to interrogate the solid state properties.

Twin Stage Impingers (TSIs) (summarised in Section 5.1.1) are one of the simplest apparatus for *in-vitro* deposition of inhaler devices including pMDIs. Their design is such that material of respirable particle size finds its way through to the lower (second) stage of the apparatus, with material larger than respirable size depositing out in the upper (first) stages. This separation mechanism allows the quantitation of respirable portions of pMDI deposits to be calculated by remote analysis of the individual stages by chromatographic approaches such as HPLC. The work undertaken here has implemented a modification to the apparatus to allow collection of the respirable fraction from the second stage of the apparatus onto a solid substrate mounted underneath the stage 2 exit nozzle. This allows analysis on the solid materials deposited, and has formed the basis for a study of the solid form of the inhaled corticosteroid beclomethasone dipropionate (BDP) pMDI products QVAR® and Synasthmax® (Chiesi, Italy). This has incorporated

thermal, microscopy and epithelial cell diffusion studies[133] and a detailed description of the PXRD study is described here.

QVAR® and Synasthmax® differ in the amount of ethanol co-solvent contained in the formulation (8 and 10% respectively) and the inclusion of glycerol as an excipient (0 and 1.3% respectively). Both are solution formulations, *i.e.* those whereby the BDP is fully dissolved rather than existing as a suspension as with many pMDI preparations.[133] This is of great importance as the solid particles formed after actuation of the device do so very quickly as the volatile propellant evaporates. This means (i) the particles cannot be studied *in-situ* and (ii) the material formed on actuation could differ greatly in its physical form from the crystalline material used in their preparation.

5.2.3.1   PXRD

As part of the platform of method development studies for analysis of solid deposits after actuation, PXRD was used to demonstrate bulk analysis from materials deposited using a modified twin stage impinger. PXRD has long been utilised in the study of crystalline form, and to demonstrate crystalinity *vs.* amorphous form. To trial its applicability to materials directly delivered from pMDIs, a study was undertaken with two commercial BDP pMDIs; QVAR® and Synasthmax® (Chiesi, Italy). The TSI exit nozzle was modified to allow the capture of material onto solid substrates as summarised in experimental section (2.5.4). Deposition onto Mylar sheets was performed (160 actuations over 10 – 12 minutes) and the samples prepared as summarised on PXRD holders and sealed underneath additional Mylar.

Blank Mylar preparations and reference BDP were also prepared in the same way to eliminate interferences and obtain reference diffraction patterns. The Mylar substrate appears to be suitable for collection of the BDP formulations, showing no interfering peaks in the collected pattern. The patterns generated on the reference show the material to be crystalline in nature, with characteristic peaks at 10, 12, 15, 19 and 23° (2θ). Three distinct forms of BDP have been structurally characterised (i) an anhydrate form[236] (CCDC : WOYPAB) (ii) a monohydrate form[237] (CCDC : BCLMSN) and (iii) three clathrate forms based on the same isomorphic channel structure [BDP: EtOH[238] (CCDC : INECOT), BDP:EtOAc[239] (CCDC : VORSEB) and BDP:EtOH:CH_2F_4[240] (CCDC : VATMOT)] These structures were used to simulate PXRD patterns . In the case of the clathrates, the isostructural nature of the channel solvate gives essentially identical PXRDs. For assignment purposes, the ethanol solvate (INECOT) was used, alongside the anhydrate (WOYPAB) and hydrate (BCLMSN) forms. The reference material shows a PXRD pattern consistent with that generated from WOYPAB and suggests it is the anhydrate form of BDP. Figure 5.2.3.1.1 shows the diffraction patterns obtained for the blank and reference preparations, with the simulated PXRD pattern shown for BDP anhydrate (WOYPAB).
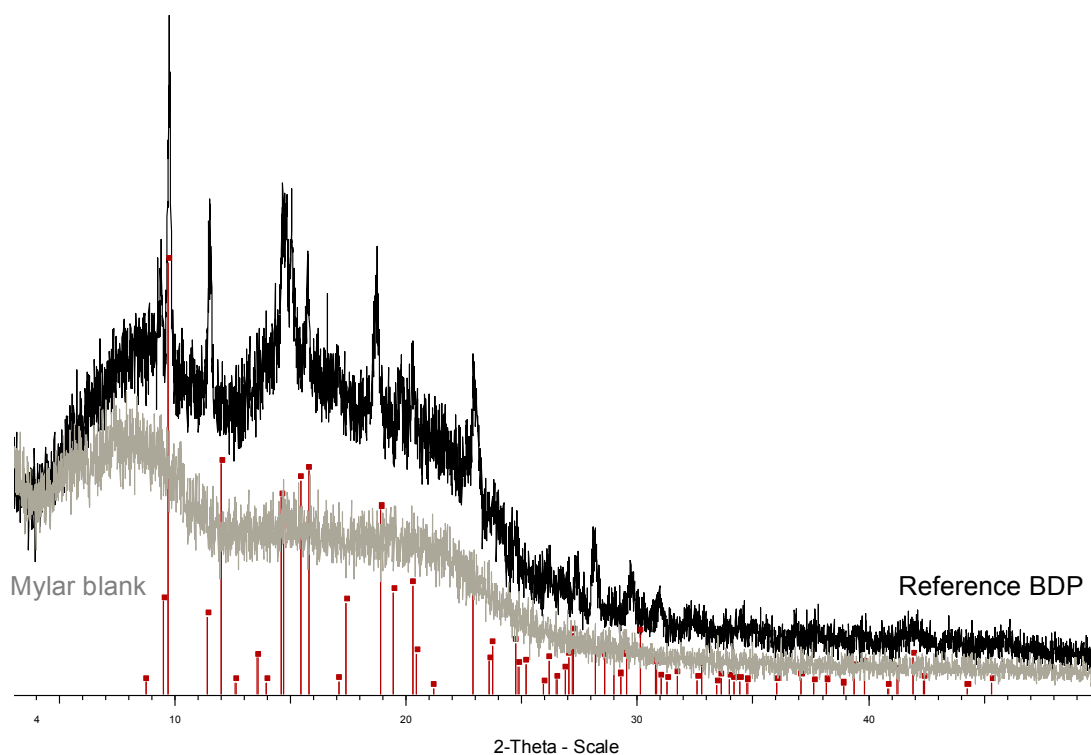
Figure 5.2.3.1.1 – Diffraction patterns obtained for blank Mylar (grey) and reference preparation (black) shown with reference pattern positions for the simulated PXRD pattern for BDP anhydrate (WOYPAB).[236]

The PXRD patterns generated on the deposited QVAR® product show material that appears to have a degree of crystallinity on initial deposition, though the peaks in the diffraction pattern recorded are very low intensity. The peak positions of the recorded data differ from those observed in the reference pattern, with the most intense occurrences at 8, 11 and 13° (2θ), suggesting that the crystal form of the material differs. Comparison to the previously summarised simulated PXRD patterns show an excellent correlation to the hydrated form (BCLMSN).[237] The peak intensity continues to increase in the patterns recorded over a 250 minute period, and it appears that the BDP is recrystallising to the hydrate over time. Figure 5.2.3.1.2

shows the initially recorded pattern and time-lapse patterns alongside the crystalline reference material and simulated PXRD pattern for the hydrate form of BDP.
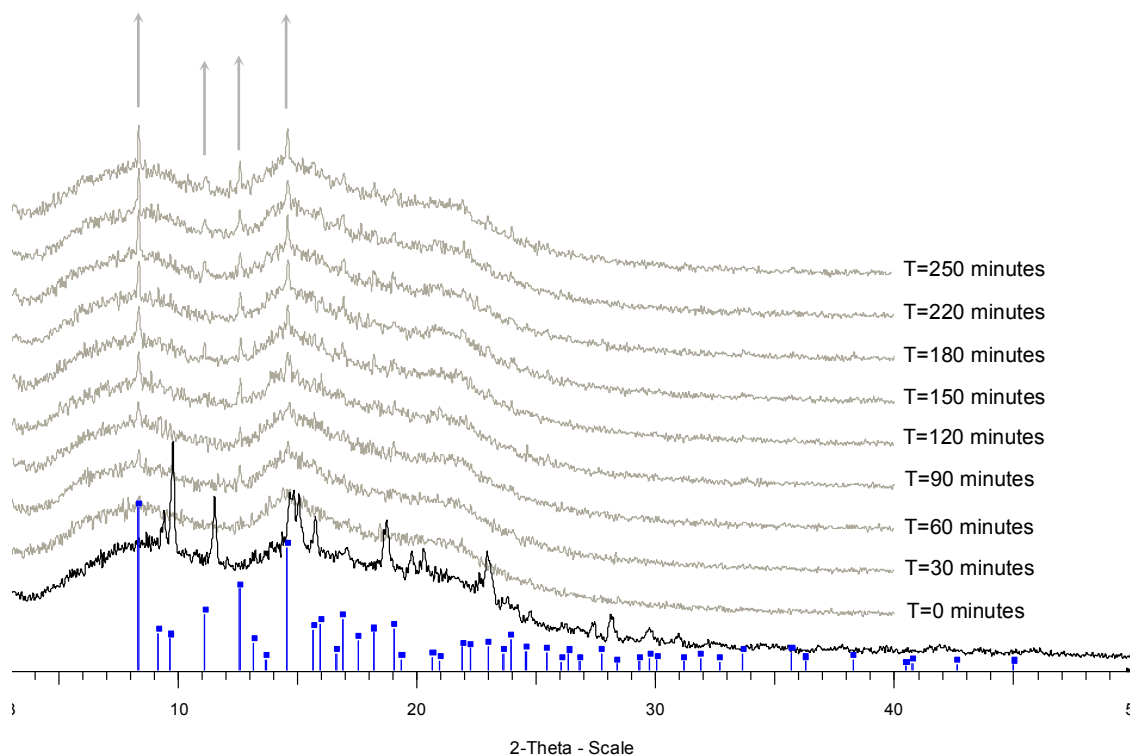
Figure 5.2.3.1.2 – PXRD patterns over a 250 minute period (grey) of the emitted dose of QVAR® 100 pMDI device (160 actuations) collected in the modified second stage of the Copley TSI apparatus shown with reference BDP (black) and simulated pattern positions for BDP hydrate [blue (BCLMSN)].[237]

Data recorded on the Synasthmax® preparation showed no peaks on collection of the initial pattern, suggesting the material collected was largely amorphous in nature. However, as with the QVAR® preparation, peaks in the patterns recorded over an extended period on the collected sample started to increase in intensity, and were consistent with those observed in the QVAR®

material at 8, 11 and 13° (2θ) suggesting recrystallisation to BDP hydrate in the same manner. Figure 5.2.3.1.3 shows the initially recorded pattern and those recorded at 30 minute intervals. The simulated PXRD pattern of BDP hydrate (BCLMSN) is also shown.
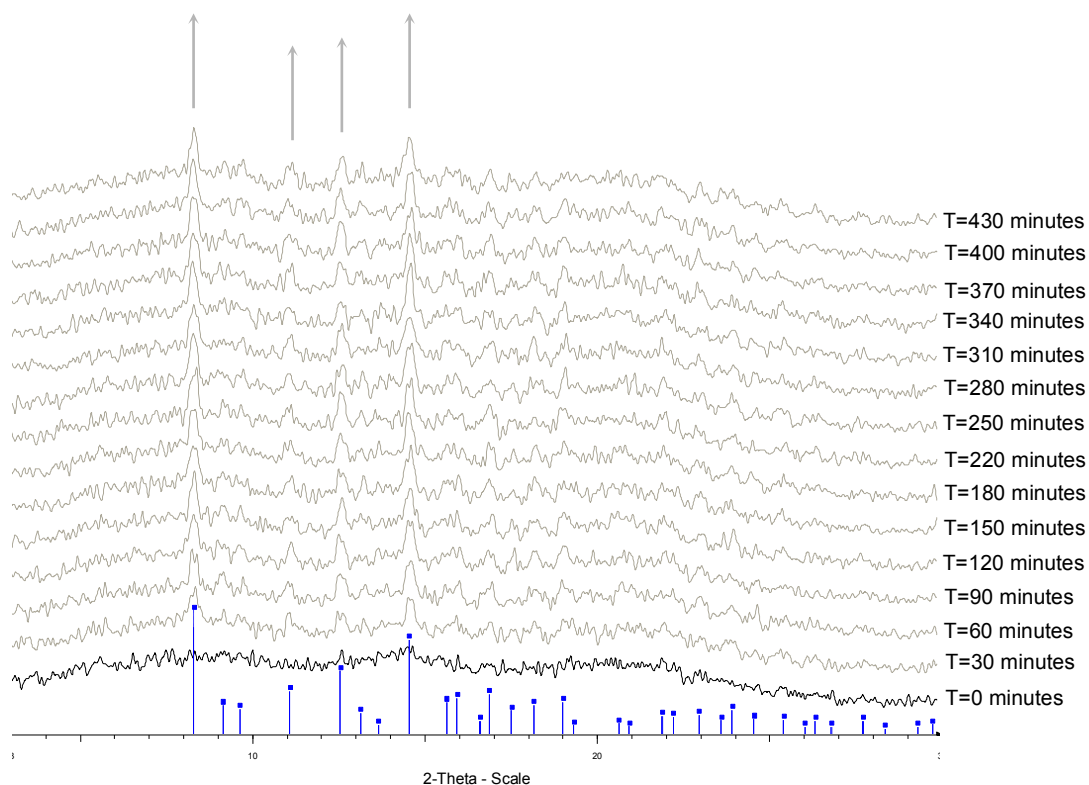
Figure 5.2.3.1.4 – PXRD patterns over a 430 minute period (grey) of the emitted dose of Synasthmax® 100 pMDI device (160 actuations) collected in the modified second stage of the Copley TSI apparatus shown with reference BDP (black) and simulated pattern positions for BDP hydrate [blue (BCLMSN)].[237]

5.2.3.2   Thermal Analysis

Thermal data were recorded for the two deposited formulations, and for the BDP reference compound at KCL, and these provide useful comparison to the PXRD data. The deposition method developed shows itself to be

successful in depositing sufficient material for study by thermal techniques, and allows significant differences between the two formulations to be observed. Data have been recorded for QVAR® and Synathsmax®, along with a crystalline BDP reference and blank foil substrate used in the collection of material (available in the published data).[133] The reference material, displays two primary endotherms corresponding to volatile loss (water) at *ca.* 100°C, confirmed by TGA, and the melting transition at 212.7°C. No recrystalisation exotherm or glass transition were noted, suggesting the material was crystalline in nature, consistent with the data observed in the *X*-ray studies (Section 5.2.3.1).

The thermograms recorded for the deposited formulations show clear differences between the materials, and compared to the reference compound. QVAR® shows a behaviour similar to the reference material, having an endotherm at *ca.* 100°C and a second at 207.5°C. The latter is thought to be a melt transition, however differs significantly from that observed in the reference material. No evidence of recrystallisation / glass transition were apparent; it is therefore proposed that the material has deposited with a different crystal form than that of the reference. These proposals are further evidenced by the data observed in the PXRD studies (Section 5.2.3.1), with peaks observed on material deposited initially confirming crystalinity, and their different positions (2θ) suggesting the hydrated form by matching to patterns generated from published structures.[237] The Synasthmax® formulation showed no evidence of crystalline BDP, with no melt endotherm observable in the data. A small transition at 175.8°C corresponded with a significant (80%) weight loss in the

TGA suggesting the material is decomposing at this temperature. PXRD data shows no peaks on initial deposition suggesting an amorphous form, consistent with the recorded thermal data.

It should be noted that the thermal analysis was conducted at KCL and is reproduced here with reference to the joint publication.[133] Other analysis on the deposited materials was carried out at KCL including aerodynamic particle sizing by ACI, electron microscopy to provide a visual analysis of the deposited particle's morphology and surface properties (porosity, smoothness) and absorptive drug transfer quantitation using diffusion through epithelial cell layers.

Importantly, the deposition technique developed has been shown to be suitable for the capture of materials for remote analysis by PXRD, SEM, thermal analysis (DSC, TGA and TGA–MS for solvate identity) and potentially extended to spectroscopic techniques such as Raman and FTIR. The modified capture method outlined operated in conjunction with the analytical techniques presented aids greatly in the characterisation of the solid forms emitted, and provides a powerful means by which to study emitted particles from both solution and suspension pMDIs, as well as those emitted from other inhalation devices such as DPI, nebuliser and nasal sprays.

The work presented in this chapter has established analytical approaches to assess the solid form of material deposited on actuation of pMDI devices. Raman methods have been developed and operated to assess the deposition profiles of commercially available ICS / β_2-agonist pMDI

formulations, and provides clear evidence of co-deposition of both types of drug in Seretide® and Symbicort® formulations. Similarly, analysis of formulations of BDP in HFA134a / ethanol using modified TSI depositions has provided an insight into solids deposited in terms of their morphology and form, with clear evidence differentiating amorphous materials (Synasthmax®) from crystalline forms (QVAR®). Full conclusions are presented in Chapter 7.

6   Investigation of Solution and Solid State Properties of Novel Budesonide pMDI Prototypes

This chapter describes the preparation and assessment of several concept pMDI prototypes of budesonide, a corticosteroid compound used in commercially available inhaled preparations, and used extensively throughout the studies described in this thesis.

The formulation of budesonide in these prototypes uses approaches to increase its solubility through (i) the addition of ethanol (as a co-solvent) to HFA134a and (ii) the use of TRIMEB, a derivatised cyclodextrin compound (Sections 4.2.1 and 4.2.2 respectively). pMDI canisters were prepared using micronized budesonide, and selected molar ratio preparations of budesonide and TRIMEB in both HFA134a and HFA134a / EtOH (10 % v/v).

6.1   Preparation of pMDI Canisters

API formulations in HFAs are generally formulated as suspensions of respirably sized particles[84] and are based on micronised preparations of the drug of the correct particle size for delivery to the lung. These can be prepared with or without excipients. Actuation of the pMDI device delivers a pre-determined dose of the suspended solids ready for the user to inhale. However, the stability of these preparations can be seriously affected by several physical processes described in Section 1.2.4. With the exception of the corticosteroid beclomethasone dipropionate, compounds used in these studies have been shown to have solubility values in the low µg/mL range in HFA134a and are therefore vulnerable to mechanisms of destabilisation of suspension (Section 4.1.1).

Therefore, there are several potential benefits for formulating the IPP as a solution. These include homogeneity and the respective control of administered dose, as well as increased stability by avoiding sedimentation, agglomeration and creaming effects observed on the suspended particulates or changing particle size through Ostwald ripening.[84] The behaviour of a solution based formulation is likely to be different from a suspension on actuation. The rapid evaporation of propellant, forming solid particles *in-situ,* potentially affects the solid form of material produced and the aerodynamic behaviour (particle size distribution) of the particulates. It has been noted (Section 1.2.3), that the smaller particle sizes resulting from solution based pMDIs is potentially of most benefit to ICS compounds, where delivery to the lower airways for the topical treatment of inflammation is required. Smaller particle size for SABA, LABA, SAMA and LAMA compounds is potentially less desirable, where delivery to the upper respiratory tract is required to ensure interaction with β-receptors and smooth muscle. However, the potential for solution pMDIs of budesonide, an ICS, is clear and trial preparations have been formulated into pMDI prototype canisters as described; (i) budesonide in HFA134a as a control; (ii) budesonide in HFA134a / ethanol (10% v/v), (iii) budesonide / TRIMEB (1:1 mole ratio) in HFA134a and; (iv) budesonide / TRIMEB (1:1 mole ratio) in HFA134a / ethanol (10 % v/v).

For the study, a batch of budesonide was micronised with a laboratory scale jetmill (Section 2.6.1) and the resulting particulates were assessed using SEM and laser diffraction PSD analysis. This confirmed the material had a particle size distribution in the respirable range, and based on these

measurements and observations, the material was deemed acceptable for use in the production of the test pMDI devices. The PSD (Figure 6.1.1) has the mean undersize cumulative dimension, X_{90}, value of 2.93 μm (± 0.04, n=3). SEM photomicrographs (Figure 6.1.2) confirm the particulates as either discrete or agglomerates with edge length dimensions of less than 5 μm. It is notable that the particulates are faceted, consistent with retention of largely crystalline characteristics.
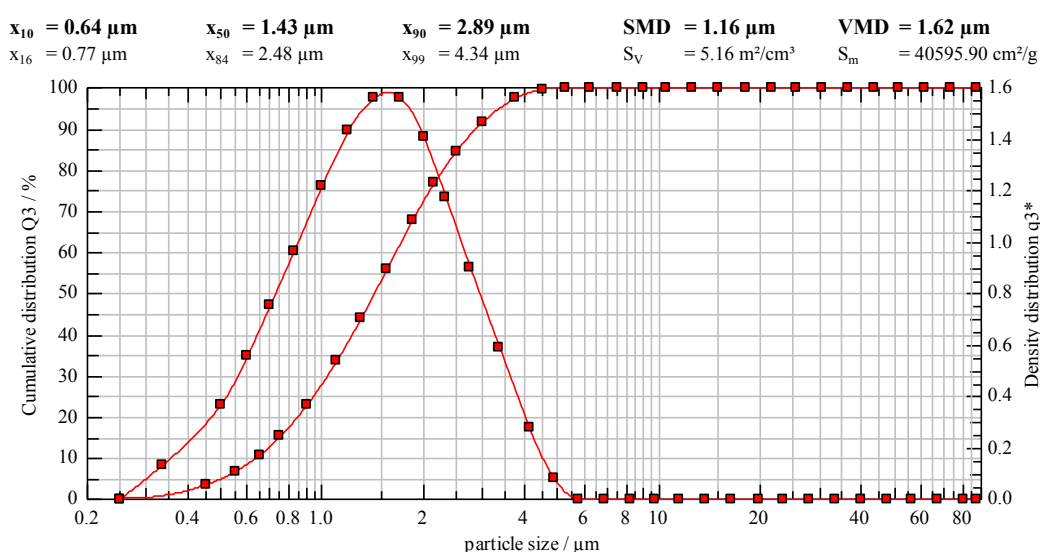
x_{10} = 0.64 μm	x_{50} = 1.43 μm	x_{90} = 2.89 μm	SMD = 1.16 μm	VMD = 1.62 μm
x_{16} = 0.77 μm	x_{84} = 2.48 μm	x_{99} = 4.34 μm	S_V = 5.16 m²/cm³	S_m = 40595.90 cm²/g

Figure 6.1.1 – Representative Laser Diffraction PSD and X_{90}, X_{50} and X_{10} values for the micronised budesonide used in the preparation of the pMDI devices.

The material was formulated into pMDI canisters at the University of Bath as the four preparations described above and formed the basis of the subsequent analytical study.
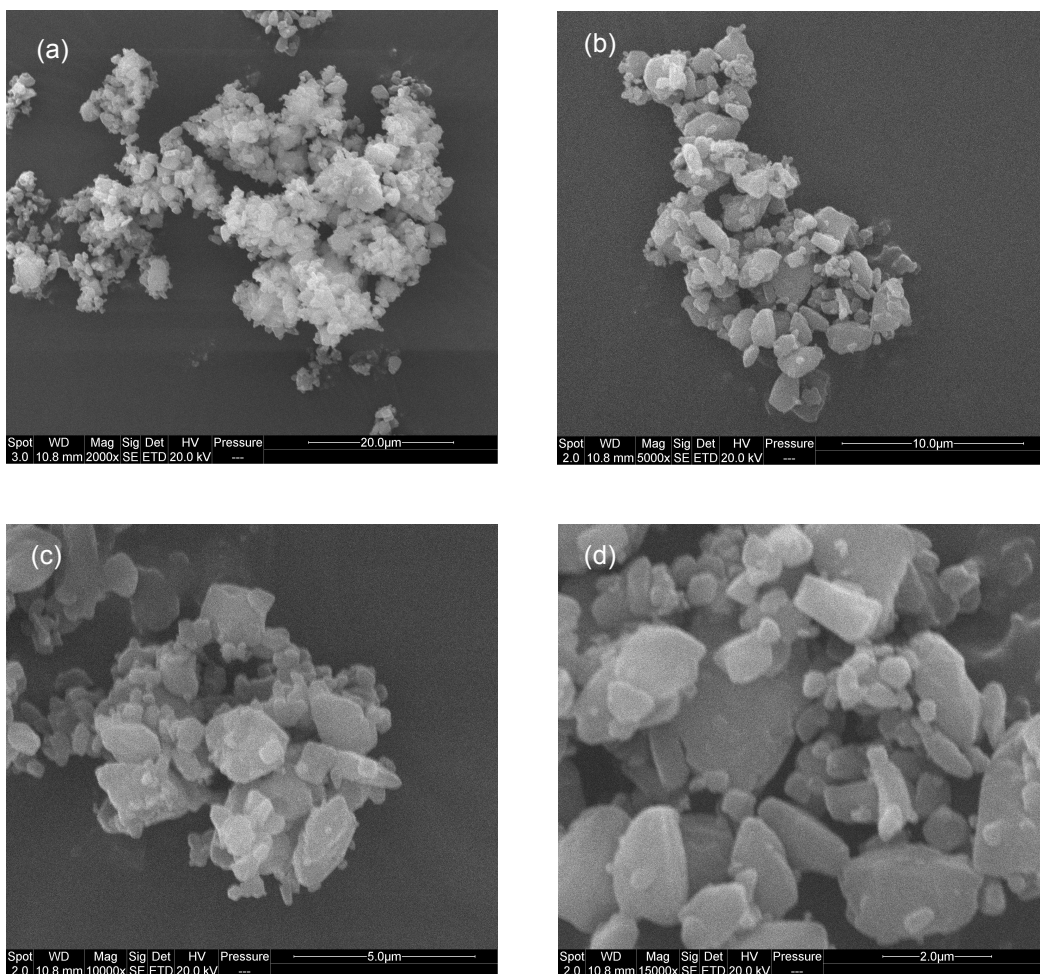
211

Figure 6.1.2 – SEM photomicrographs at x2 k (a), x5 k (b), x10 k (c) and x 15 k (d) of the micronised budesonide used in the preparation of the pMDI devices showing the micronised particulates of less than 5 μm dimensions and therefore suitable for formulation as suspended solids in HFA for pMDI delivery.

6.2   Studies of Products in Solution by ^{1}H NMR

The NMR methods developed in these studies have been deployed on the prepared budesonide formulations. The studies were undertaken to confirm the formulation concentrations in the canisters and provide comparison with theoretical models described in Chapter 4. Actuation of the canisters and transfer into the reversed co-axial NMR tubes provided an initial visual

examination of the contents of the pMDI canister. It was immediately apparent that the budesonide in pure HFA134a formulation was a suspension, with white material observed in suspension in the transferred liquid. Budesonide in HFA134a / ethanol (10 % v/v) also showed signs of suspended solids in the liquid propellant, though these were significantly fewer than in pure HFA134a, in line with increased solubility determined in this medium (Sections 4.1.1 and 4.2.1.2). Budesonide / TRIMEB in pure HFA134a also showed some solid components within the transferred liquid, and signs of deposited solids were identified on the wall of the NMR tube, again consistent with the previously determined solubility for this system. In contrast, budesonide / TRIMEB in HFA134a / ethanol (10% v/v) showed no evidence of suspended material present in the liquid transferred, indicating this system is a solution, whilst each of the others was a suspension. With these samples, quantitative solubility data were obtained from the NMR spectra acquired (Table 6.2.1). The data show the increased solubility of budesonide and TRIMEB when ethanol is added to the systems as a co-solvent. The solubility values determined for (i) budesonide in HFA134a (ii) budesonide in HFA134a/EtOH and (iii) budesonide / TRIMEB in HFA134a are consistent with those previously evaluated as part of the solubility studies in the model systems (Chapter 4, Sections 4.1.1, 4.2.1.2 and 4.2.2 respectively), and show no significant changes to the systems on pMDI preparation. Importantly, the solubility of budesonide / TRIMEB in HFA134a/EtOH has not been evaluated previously and this system shows a major increase in the solubilisation of budesonide hence this is the only solution at the concentrations prepared in the pMDIs.

Table 6.2.1 – Results of solubility measurements calculated from triplicate NMR experiments carried out on the prepared formulations.

Formulation	Solubility (µg/mL)				σ	% CV
	1	2	3	Mean		
HFA134a	56	61	52	56	3.7	6.5
HFA134a/EtOH	1401	1489	1523	1471	51.4	3.5
HFA134a + TRIMEB	143	132	139	138	4.5	3.3
HFA134a/EtOH + TRIMEB	3012	2856	2946	2938	63.9	2.2

6.3 Evaluation of Solid Depositions from Anderson Cascade Impactor Studies

6.3.1 Aerodynamic Particle Size Distribution

Impaction experiments were performed on the pMDI formulations prepared using an ACI operated as highlighted in the Ph.Eur[132] (Section 2.6.2) for bulk assessment by HPLC from washes of each impactor plate (Section 2.6.2.1). These measurements indicate the particle size distribution through aerodynamic properties of the pMDI formulation produced. These can, therefore, provide critical information about potential sites of deposition of these products in the lung. The quantities of budesonide deposited at each stage of the ACI were obtained for each preparation (Figure 6.3.1.1). Importantly, the profiles obtained are significantly different and are worthy of detailed consideration. Broadly, two profiles are apparent, that appear to be primarily dependent on the composition of the solvent in the preparation (i) budesonide and budesonide / TRIMEB in HFA13a show maximum deposition on stage 4 of the ACI, corresponding to maximum deposition in the central airways[228] (ii) budesonide and budesonide / TRIMEB in HFA / ethanol show maximum deposition at stage 7 and stage 6 respectively. The aerodynamic

properties of the products, MMAD, GSD and FPF (material < 5 µm) are given in Table 6.3.1.1. The results show that the MMAD reduces significantly when ethanol is incorporated as a co-solvent. This is consistent with increased solubility in the co-solvated system. The mechanism for particle formation in these largely solubilised systems is likely to involve rapid evaporation of propellant containing the API. The aerodynamic behaviour of these solubilised systems is likely to be complex, possibly initially dependent on the dimensions of the solution droplet, reducing as the solvent evaporates before, ultimately, relating to the dimensions of the solid particulate.

No analysis of this type has been undertaken with solubilised budesonide, but these observations are somewhat similar to those described by Williams III *et al.*[182] observing that the MMAD of betamethasone valerate was lower in an ethanol co-solvated HFA134a system than those of triamcinolone acetonide formulated as suspensions in HFA134a alone. In contrast, Gupta *et al.*[181] noted increased deposition of beclomethasone dipropionate with increasing ethanol co-solvent concentration in the nine pMDI formulations they studied at differing ethanol concentrations, but found the MMAD was largely unaltered with changing ethanol concentrations. The solubility of BDP is considerably higher than that of budesonide in HFA134a, and it is therefore conceivable that ethanol has less influence on the solubility in these systems than for the budesonide systems under consideration here.

The formulation containing budesonide in HFA134a / ethanol with TRIMEB incorporated appears to have the lowest MMAD of all the preparations, with significantly increased FPF values suggesting an increased propensity for lung deposition and reduced losses in the throat of the ACI setup. This is

consistent with the observations made with the SEM / Raman (Section 6.3.2 and 6.3.3) where it might be concluded that the formulation forms host / guest complexes and exists as a solution; the rapid evaporation of solvent yields relatively homogenous solid spheroids giving reduced aerodynamic particle size distributions.
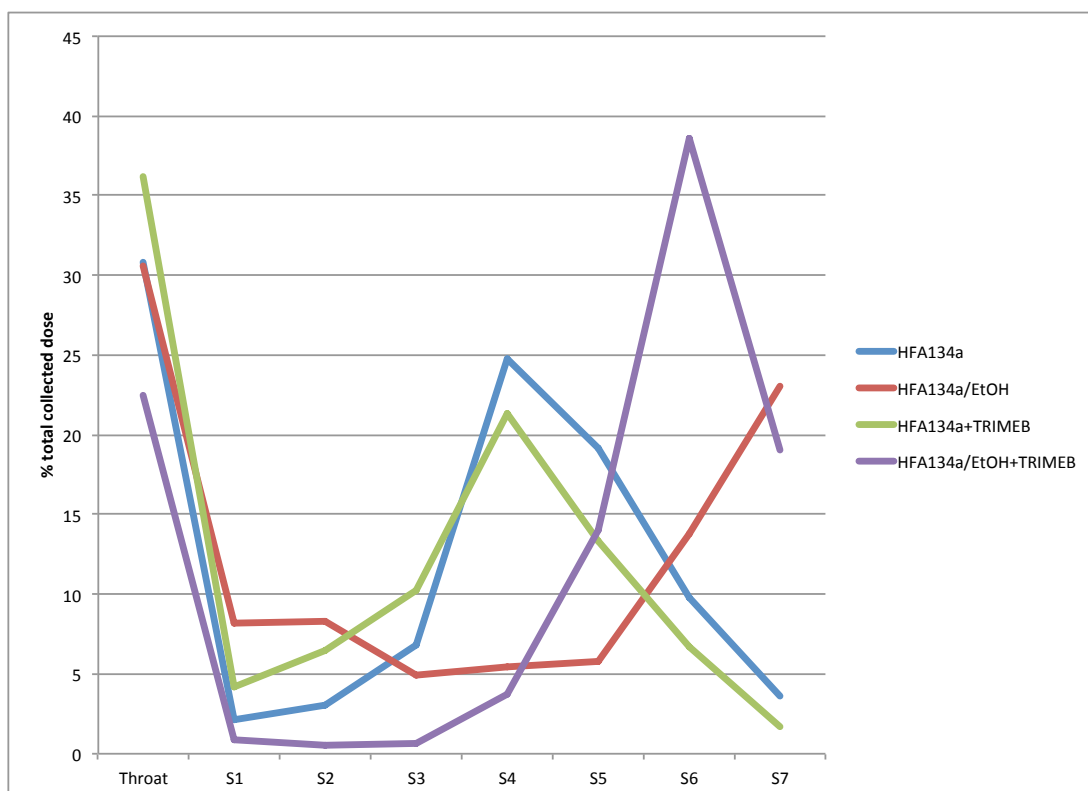
Figure 6.3.1.1 – Aerodynamic particle parameters for budesonide formulations prepared with (i) HFA134a (ii) HFA134a/EtOH (iii) HFA134a+TRIMEB and (iv) HFA134a/EtOH+TRIMEB.

Table 6.3.1.1 – MMAD and GSD values calculated for the four formulations prepared in (i) HFA134a (ii) HFA134a/EtOH (iii) HFA134a+TRIMEB and (iv) HFA134a/EtOH+TRIMEB.

Formulation	MMAD (µm)	GSD (µm)	FPF (%)
HFA134a	2.1	1.5	67
HFA134a/EtOH	1.0	2.4	61
HFA134a + TRIMEB	2.6	1.7	60
HFA134a/EtOH + TRIMEB	0.9	1.4	77

6.3.2 Particle Morphology and Size Distribution by SEM

Impaction experiments were performed on the pMDI formulations prepared using an ACI operated as highlighted in the Ph.Eur[132] (Section 2.6.2) for microscopic study. The plates of the ACI were removed and analysed by SEM and Raman microscopy to establish the form of material deposited, particularly to assess the distribution of the budesonide and TRIMEB in the particulates deposited. Plates 1 to 7 were evaluated, with plate 4 presented here as representative of the types of particulate observed and considered to be representative of the central airways.[233] Plate 7 is also presented for the preparations of budesonide / TRIMEB in HFA134a and budesonide / TRIMEB in HFA134a/EtOH as these show significant deposition on this stage. SEM has provided valuable visual information on the materials deposited. Photomicrographs of material deposited on stage 4 of the ACI show a marked difference in the materials deposited from the separate formulations prepared. It is noticeable that two types of particle appear to be present as (i) crystallites (either isolated or agglomerated) with clear facets and sharp edges and faces or (ii) spheroids with relatively smooth surfaces (Figure 6.3.2.1). Crystallites were observed in the images of budesonide in

HFA134a, budesonide in HFA134a / ethanol and budesonide / TRIMEB in HFA134a deposits. Spheroids were observed in budesonide / TRIMEB in HFA134a and budesonide / TRIMEB in HFA134a / ethanol. The presence of crystallites is consistent with observations of solid suspensions and in concentrations determined in NMR studies. Particle sizes are comparable with one another (≤ 3 µm) in all the photomicrographs studied – this is clearly a function of the fractionation of the ACI deposition.

Both samples prepared with TRIMEB show the spheroid particulates (*ca.* 2 µm diameter). This morphology is likely to correspond with amorphous solids formed by rapid evaporation of propellant during flight.[121]

These spheroids are present alongside crystalline material in deposits from pure HFA134a, but, significantly, are the only particulate morphology obtained form HFA134a / ethanol. The increased solubility in this co-solvated system produces a solution and this appears to be the origin of this homogeneity of form. Interestingly, the spheroids may be host-guest complexes as observed in previous work (Section 4.2.2). In order to characterise the particulates, a µ-Raman study was undertaken (Section 6.3.3).

(a)
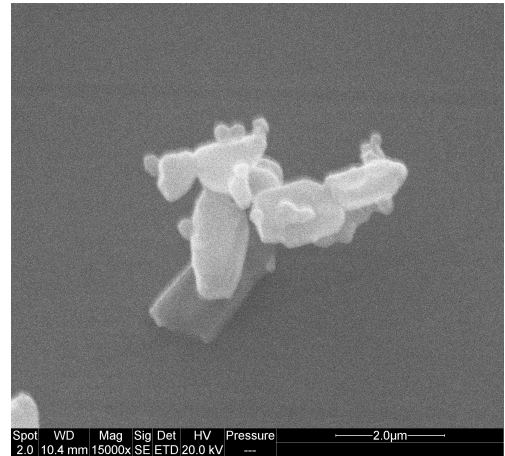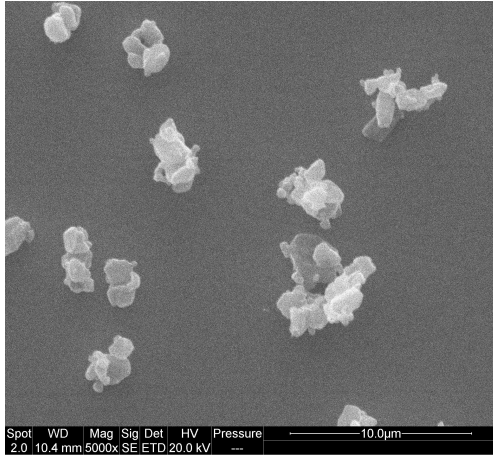
(b)
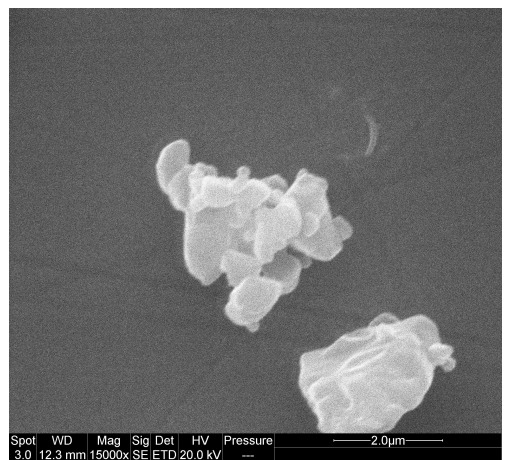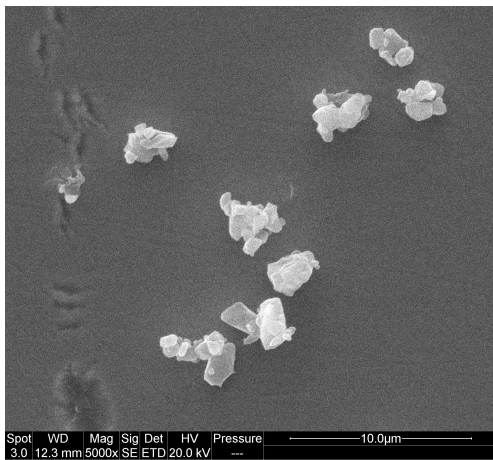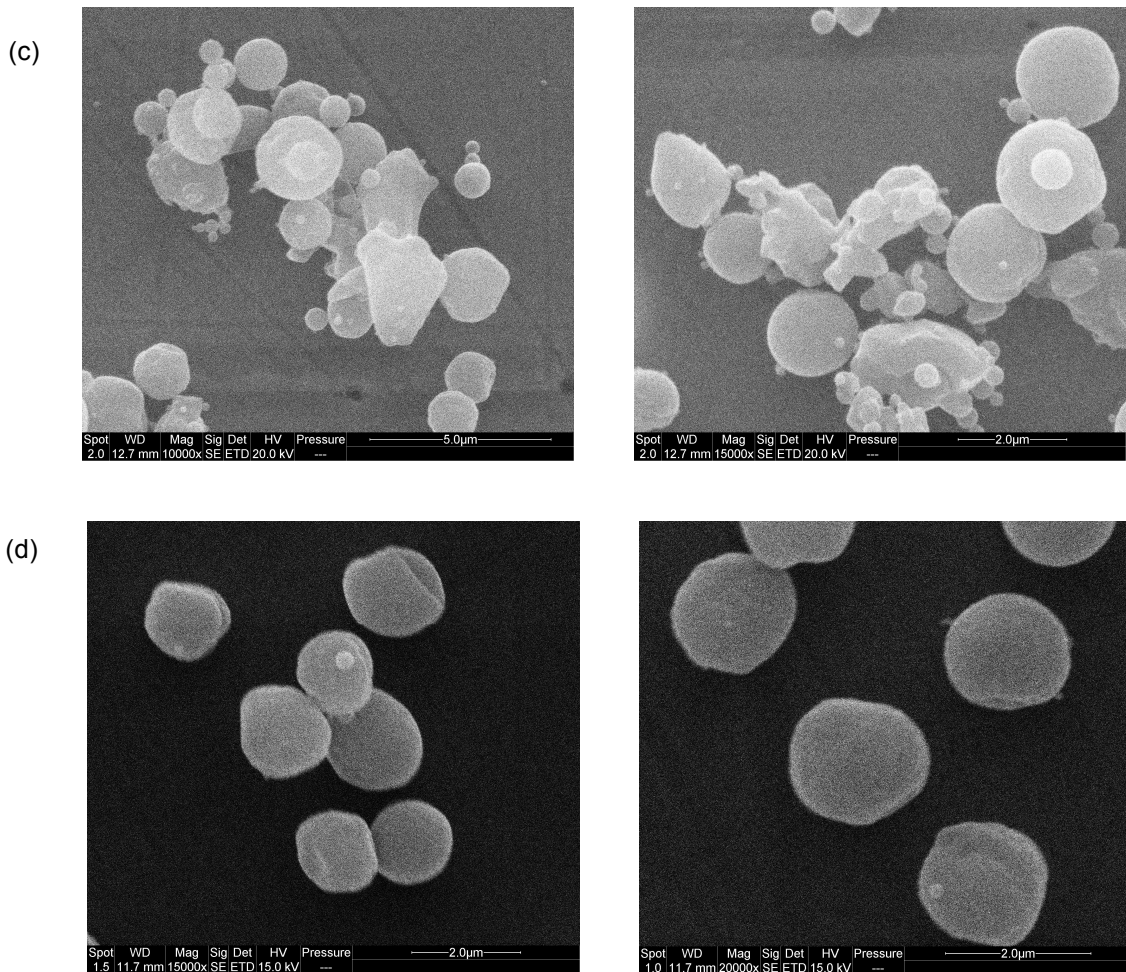
(c)

(d)

Spot WD Mag Sig Det HV Pressure —5.0µm—
2.0 12.7 mm 10000x SE ETD 20.0 kV ---

Spot WD Mag Sig Det HV Pressure —2.0µm—
2.0 12.7 mm 15000x SE ETD 20.0 kV ---

Spot WD Mag Sig Det HV Pressure —2.0µm—
1.5 11.7 mm 15000x SE ETD 15.0 kV ---

Spot WD Mag Sig Det HV Pressure —2.0µm—
1.0 11.7 mm 20000x SE ETD 15.0 kV ---

Figure 6.3.2.1 – SEM photomicrographs of material deposited (ACI plate 4) from (a) budesonide in HFA134a, (b) budesonide in HFA134a / ethanol (10% v/v), (c) budesonide / TRIMEB in HFA134a and (d) budesonide / TRIMEB in HFA134a / ethanol (10% v/v) at magnifications between x5 and x20 k (specified in the data bar).

Photomicrographs recorded on deposits from stage 7 of the ACI are shown for the preparations of budesonide / TRIMEB in HFA134a and budesonide / TRIMEB in HFA134a/EtOH (Figure 6.3.2.2). These clearly show the increased particle numbers in line with aerodynamic profiles and in each case the deposition is exclusively spheroid particulates. Interestingly, the

preparation of budesonide / TRIMEB in HFA134a now shows no evidence of crystallites as with the observations made on stage 4 of the same deposition experiment. This is attributed to the crystallite size and their removal in the earlier stages of the ACI. The budesonide reaching stage 7 must be associated to the spheroids and is likely to be present as host / guest complex.
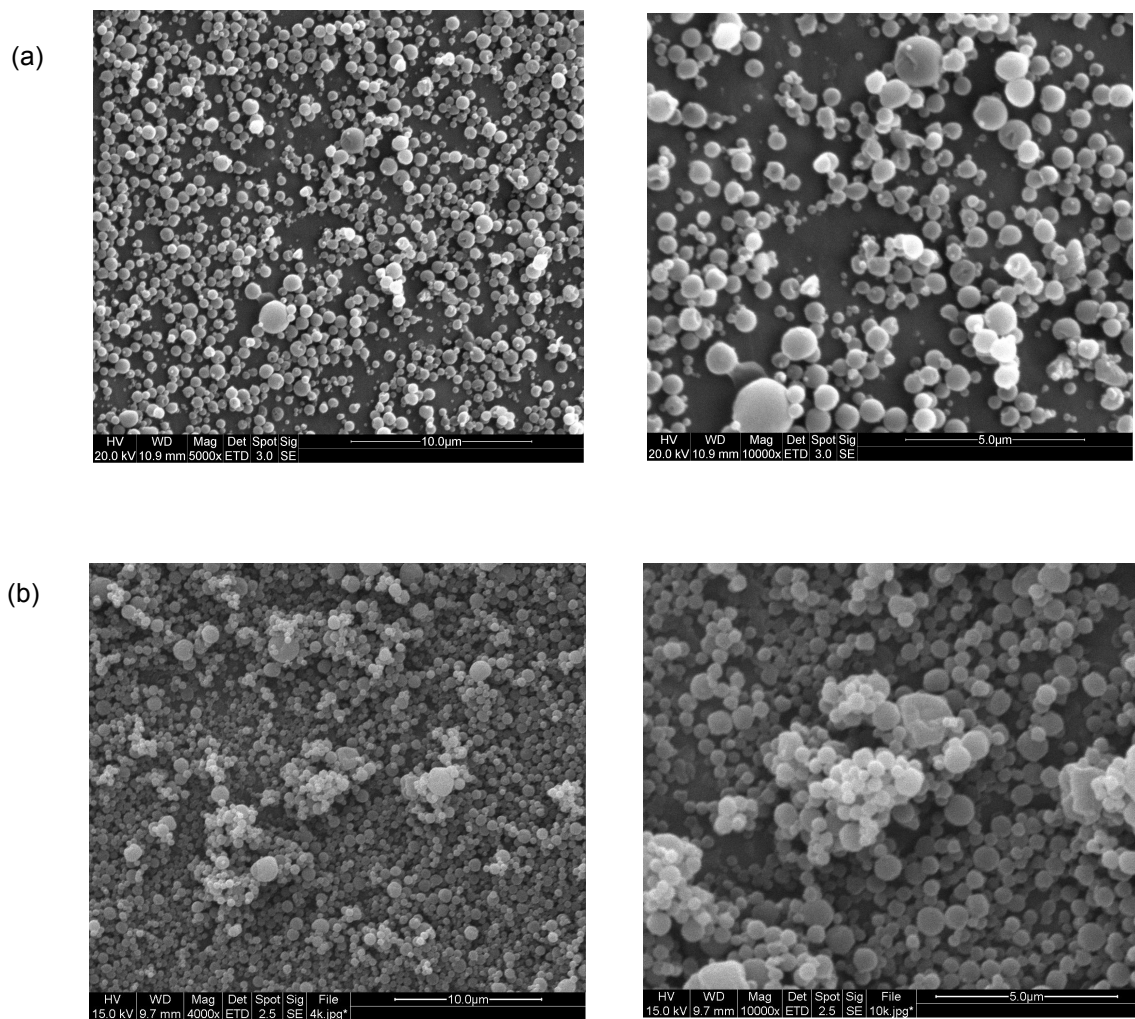
Fig 6.3.2.2 - SEM photomicrographs of material deposited (ACI plate 7) from (a) budesonide / TRIMEB in HFA134a and (b) budesonide / TRIMEB in HFA134a / ethanol (10% v/v) at magnifications between x4 and x10 k (specified in the data bar).

6.3.3 Raman Microscopy

For each of the formulations prepared, Raman spectra were obtained at several sample sites on stages 4 to 7 of the ACI depositions. Comparison of the spectra collected against the reference spectra of budesonide and TRIMEB show some interesting features. The materials deposited from HFA134a and HFA134a / ethanol (*i.e.* without inclusion of TRIMEB) show spectra that correspond well with budesonide (Figure 6.3.3.1). The spectra show relatively sharp bands indicating that the particulates deposited are crystalline budesonide consistent with the inferences made from SEM analysis.
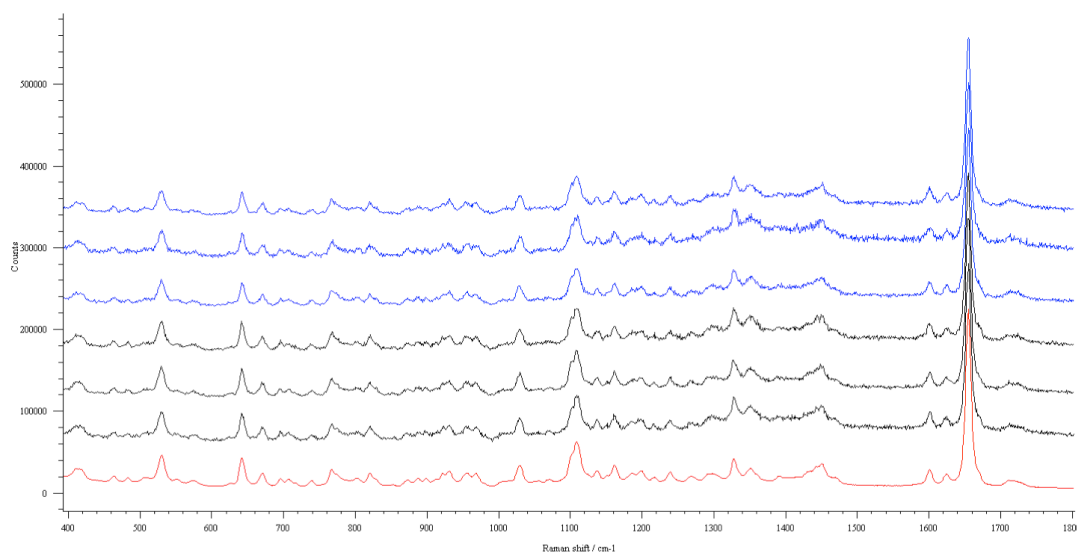
Figure 6.3.3.1 – Representative Raman spectra in the region 1800 and 500 cm^{-1} for six budesonide particles deposited on ACI stage 4 from (i) budesonide in HFA134a (blue spectra, left image) and (ii) budesonide in HFA134a / ethanol (10 % v/v) (black spectra, right image) formulation compared to pure budesonide (red).

The spectra acquired for spheroid particulates in the TRIMEB based formulations show Raman features that are consistent with depositions of the host / guest complexes. The spectra of the spheroid forms are consistent with those obtained in the investigation of host / guest complexes of budesonide / TRIMEB (Section 4.2.2). All the spectra recorded (> 30 in total) show (i) bands consistent with both TRIMEB and budesonide in each spectrum recorded and (ii) shifts of key signals consistent with those of the host / guest complex *e.g.* ν(C=C) quninone band shifted to 1661 cm^{-1} in the complex from 1656 cm^{-1} in pure budesonide. The relatively broad bands of the spheroid deposits may indicate largely amorphous deposits. A summary of peak widths at half height are presented in Table 6.3.3.1 for the ν(C=C) quinone band in the crystalline budesonide and when observed in the host / guest complex demonstrating the peak broadening effect. This is consistent with the spheroid morphology, devoid of the facets expected in crystalline systems. The features are shown in Figures 6.3.3.2 and 6.3.3.3. These data strongly indicate that the spheroid particulates formed from the formulations including TRIMEB in HFA134a / ethanol are indeed host / guest solid complexes deposited as amorphous spheroids.
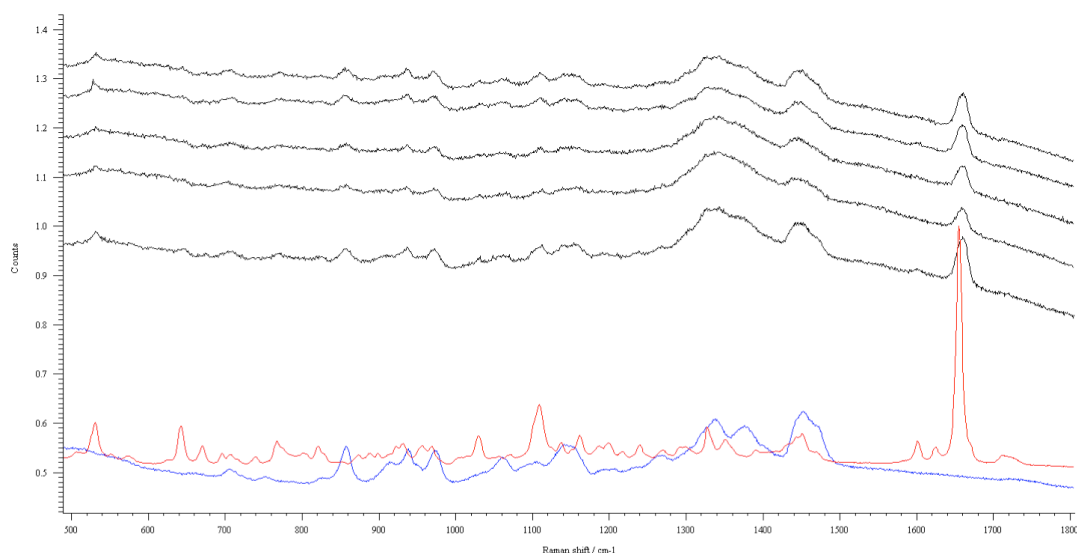
Figure 6.3.3.2 – Representative Raman spectra in the region 1800 and 800 cm^{-1} for five spheroid particles deposited on ACI stage 6 from budesonide / TRIMEB in HFA134a / 10% v/v formulation compared to (i) pure budesonide (red) and (ii) TRIMEB (blue) spectra.
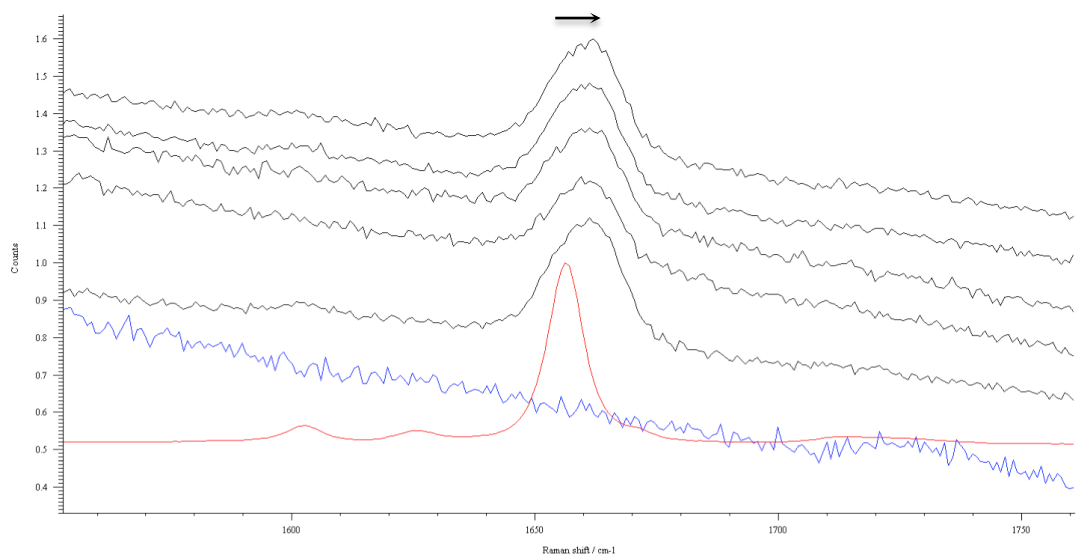
Figure 6.3.3.3 – Representative Raman spectra in the region 1800 and 1500 cm^{-1} for five spheroid particles deposited on ACI stage 6 from budesonide / TRIMEB in HFA134a / 10% v/v formulation compared to (i) pure budesonide (red) and (ii) TRIMEB (blue) spectra.

**Table 6.3.3.1** – Mean peak width ($PW_{1/2}$) of $v(C=C)$ band of budesonide calculated from crystalline material and observed in replicate spectra of host / guest complex (n=5) shown in Figure 6.3.3.3.

	Peak Centre (cm^{-1})	$PW_{1/2}$ (cm^{-1})
Crystalline Reference	1656	10
Host/Guest Complex	1661	19

The formulation prepared using TRIMEB in pure HFA134a shows both crystallite and spheroid particles. The µ-Raman study of these materials was consistent with the three products (i) crystallites of budesonide (ii) spheroids of budesonide / TRIMEB complex and (iii) spheroids of pure TRIMEB. The broadening of the Raman spectra and the spheroid morphology are again consistent with deposition of products in amorphous form through evaporation of solvent. The presence of TRIMEB from solution and budesonide from suspension is not surprising, as not all the budesonide has been dissolved in this solvent system leaving 'unreacted' TRIMEB from the 1:1 preparation. Representative Raman spectra acquired on stage 6 of the ACI, corresponding to host / guest, pure budesonide and pure TRIMEB are given in Figure 6.3.3.3.
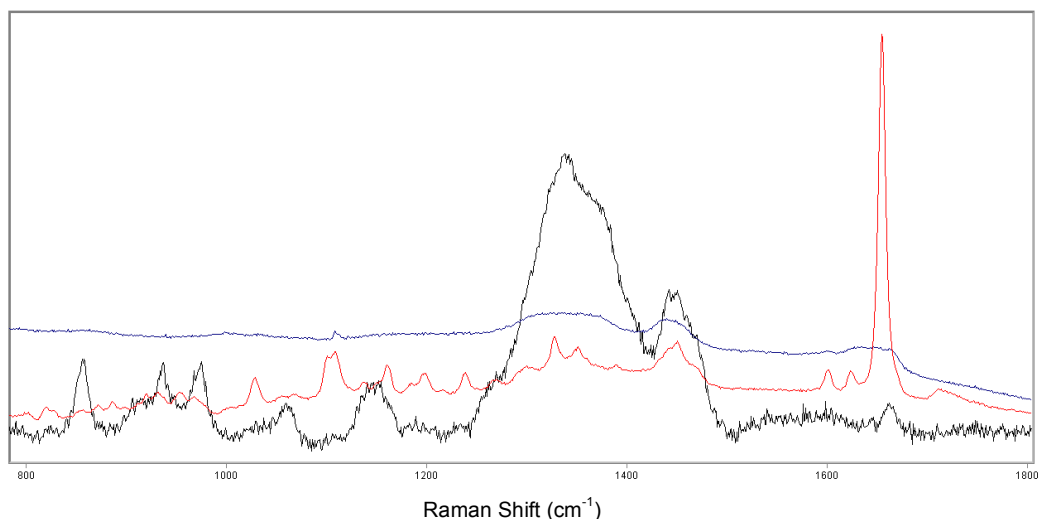
Figure 6.3.3.4 – Representative Raman spectra in the region 1800 to 800 cm^{-1} acquired on ACI stage 6 from pure HFA134a formulation showing instances of pure (i) budesonide (red) (ii) pure TRIMEB (blue) and (iii) host / guest complex (black).

6.4 Discussion

Consideration of the NMR, SEM, Raman and APSD data collected for the four formulations in concert leads to a number of discussion points that can be considered in terms of the solid form of the materials deposited and their aerodynamic properties.

The addition of solubilising agents to the preparations of budesonide has a significant effect on the behaviour in solution and hence their solid form on deposition. A summary is presented for each of the preparations (i) budesonide in pure HFA134a shows very low solubility, with SEM photomicrographs and Raman showing crystalline budesonide (ii) incorporation of ethanol to the system markedly increases solubility. SEM and Raman studies are again consistent with budesonide crystallites (iii) Addition of TRIMEB to the formulation in HFA134a (and in absence of an

ethanol co-solvent) increases budesonide solubility. SEM shows both spheroid and crystallite deposits. Raman shows budesonide crystallites and spheroid particles as budesonide / TRIMEB complex and residual TRIMEB; (iv) the final preparation incorporating both TRIMEB and ethanol co-solvent shows complete dissolution of API. SEM data indicates the deposited spheroids may be amorphous in nature, while Raman data shows these to be host / guest complexes. The spectral broadening is consistent with amorphous deposits.

Consideration of the aerodynamic characteristics of the prototype formulations reveals some interesting data and suggests that the enhanced solubilisation resulting from the addition of ethanol and / or TRIMEB to the formulations is having a significant effect on the aerodynamic characteristics. Trends in MMAD, GSD and FPF are summarised in Section 6.4.1 to 6.4.3.

6.4.1　　　　　Mass Median Aerodynamic Diameter

HFA134a preparations show an increase from 2.1 to 2.6 µm on addition of TRIMEB to the formulation, associated to the increased deposition on the early stages (1 and 2) of the ACI for the formulations of budesonide and TRIMEB compared to budesonide alone.

The preparations including ethanol have significantly reduced MMAD values of 1.0 and 0.9 for the formulations of budesonide and budesonide / TRIMEB respectively. The reduction in MMAD values when compared with those of the preparation in pure HFA134a are attributed to the increased solubility of budesonide. Particles formed from solution as the volatile propellant evaporates rapidly after actuation of the pMDI being controlled by the droplet

size of the aerosol and not restricted by the pre-formed crystallites as with the suspensions in pure HFA134a. It is notable that the maximum deposition from the preparation of budesonide and TRIMEB is earlier (stage 6) than that of budesonide (stage 7) showing a greater number of larger particles. This is the opposite observation than might be drawn from direct comparison of MMAD values.

6.4.2 Geometric Standard Deviation

GSD values are only strictly meaningful for log-normal distributions of data, with a values of 1.0 showing ideal, < 1.22 homogeneous and > 1.22 heterogeneous distributions.[241] Budesonide prepared in HFA134a / ethanol (10 % v/v) has a GSD value (2.4) significantly higher than the three other preparations under study, which are broadly similar (1.4, 1.5 and 1.7). This value corresponds to the unusual bimodal distribution observed with increased deposition on stages 1 and 2.

6.4.3 Fine Particle Fraction

The fine particle fractions calculated as the total material less than 5 µm (ACI stages 2 to 7) show values in two groups (i) *ca.* 60 % for preparations of budesonide in HFA134a / ethanol (10 % v/v) and budesonide / TRIMEB in HA134a and (ii) *ca.* 70 % for preparations of budesonide in HFA134a and budesonide / TRIMEB in HFA134a / ethanol (10 % v/v). These data are consistent with the observation that larger material is present in the preparation in (i) with significant depositions on stages 2 and 3 of the ACI. Those in (ii) show smaller population on stages 2 and 3.

In summary, the behaviour of these systems can be described in terms of facilitated Ostwald ripening (shown schematically in Figure 6.4.3.1), increasing the rate of transfer from smaller to larger particles.[242] Suspensions in media with enhanced solubility will more quickly move to a larger particle size. The solution concentration of API in these systems will clearly be higher, leading to solid (amorphous spheroids) depositing from actuated droplets giving an overall mixed particulate system. The fully solubilised system leads to spheroid deposition exclusively.
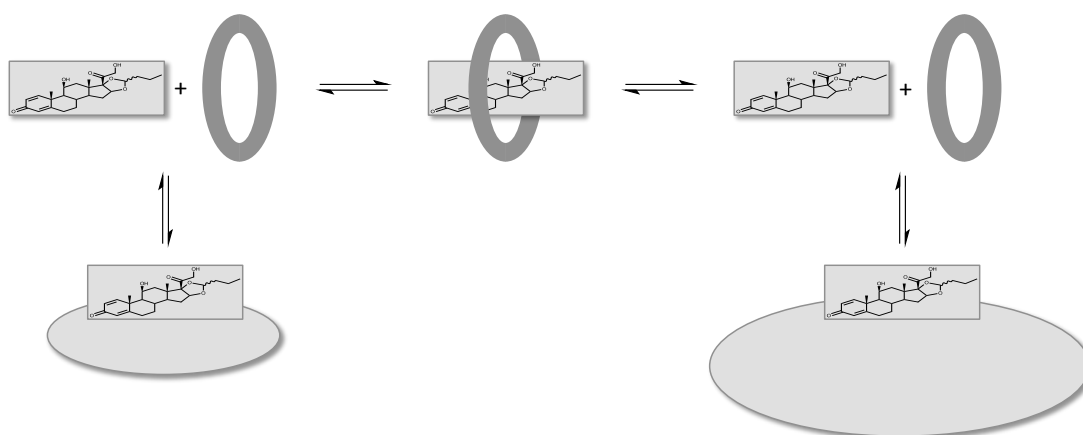
Figure 6.4.3.1 – Schematic illustration of the facilitation of Ostwald ripening processes by the inclusion of solubilising agents TRIMEB / ethanol (represented by an ellipse) in the pMDI preparations of budesonide.

In summary, prototype pMDI formulations of the ICS budesonide in HFA134a have been produced with ethanol as a co-solvent and the derivatised cyclodextrin TRIMEB. *In-situ* measurements with in-house NMR methods at pressure have shown the formulations to differ in solubility as anticipated. The formulation with ethanol and TRIMEB gave complete solubilisation of the API *i.e.* a solution based preparation. Impactor experiments have revealed some interesting behaviour, with suspension preparations showing crystalline deposits of budesonide. Amorphous deposits of TRIMEB, or amorphous deposits of budesonide : TRIMEB as host : guest complexes were established with consistent spheroid particle morphologies identified in SEM and spectroscopic evidence of complexation by μ-Raman. APSD measurements have shown markedly different MMAD and GSD profiles for the pMDI formulations. Particle size distributions are consistent with increased particle sizes for formulations where the API is in suspension (*i.e.* not fully dissolved) in a more solubilizing medium *i.e.* with addition of ethanol or TRIMEB. Such observations are consistent with facilitated Ostwald ripening, accelerating the growth of crystalline particulates in the suspension. Detailed conclusions are presented in Chapter 7.

7　　　　Conclusions and Further work

7.1　　　　Solution Approaches

The work presented in this thesis has provided a novel means by which to study IPPs in HFAs *in-situ* and at pressure using a quantitative NMR based methodology – a system representative of pMDI systems used extensively worldwide for the delivery of therapeutics to the lung. The method has been developed and validated, and has been shown to be accurate and precise with a limit of determination of *ca.* 1 µg/mL (ppm). These approaches have allowed the study of solubility in HPFP, HFA134a and HFA227 along with those co-solvated with ethanol and including cyclodextrin complexation agents. The method has also allowed access to thermodynamic data using VT methods and van't Hoff based approaches.

The studies have shown that the HFAs under study have poor absolute solubilising properties for selected β_2-agonist, antimuscarinic bronchodilators and corticosteroid compounds used in inhaled therapies, though the latter show higher solubilities than β_2-agonist and antimuscarinic bronchodilators. All compounds show equilibrium solubility values < 100 µg/mL (ppm), with the exception of the widely used corticosteroid molecule beclomethasone dipropionate which has previously been shown to have a significantly higher solubility than that of other corticosteroid molecules used in the same type of treatments.[84] The solubility data derived using the NMR approach show a strong correlation to the compound's polarity (logP) in the case of the corticosteroids, though the relationship appears less applicable to the β_2 agonists. The data do not however show a strong correlation to the material's

other physico-chemical characteristics such as melting point (hence ideal solubility) in contradiction of the data presented by Hoye et al.[165] who highlight a relationship between experimentally determined solubility and ideal solubility for the compounds in their studies (not specifically IPPs).

HPFP, a compound shown to be useful as a model propellant for studies of this type[126] is shown to be a better solvent in terms of solubilising IPPs, having greater solubility values for all the compounds under study compared to HFAs 134a and 227. This is a factor consistent with observations made by Hoye et al.[165] and one that should be considered if using HPFP to predict properties of formulations in HFAs 134a and 227. The solubility trend of HPFP > HFA134a > HFA227 also shows correlation to the solvent's dielectric constant values for the ICS compounds; potentially useful for formulators looking to investigate solubility of IPPs in these solutes.

VT studies and van't Hoff approaches have accessed thermodynamic data for the solutions formed in HFAs. The solubilisation process has been shown to be endothermic in nature, with positive enthalpy changes noted for all IPPs studied in HPFP, HFA134a and HFA227. As anticipated, the systems show an inverse correlation of solubility to Gibbs free energy change i.e. less energy is required to go from a solid to a solution, meaning increased solubility. The systems studied also tend to show a large difference in the entropy change associated to the process compared to the enthalpy change i.e. ΔS_{sol} values differ significantly from ΔH_{sol}, suggesting that the solubilisation process in HFAs is largely under entropic control.[177,178] Interestingly, the VT studies performed with cyclodextrin incorporated as a complexation agent and those with ethanol co-solvated systems show a

significant increase in entropy change values compared to the change in enthalpy increase observed. It appears that the addition of these entities has modified the solvent properties of the HFA, and the processes are shifting further towards enthalpic control.

The studies performed in HPFP co-solvated with ethanol show an increase in solubility for the IPPs under study, with a general trend towards larger increase factors being observed for the corticosteroid compounds compared to β_2-agonists and antimuscarinic bronchodilators. Further studies of the corticosteroid compound budesonide in HPFP and HFA134a co-solvated with ethanol at multiple concentrations between 0 and 20% v/v have shown a linear relationship between ethanol concentration and solubility. These observations are in line with those made by Hoye et al.[166] using similar solvent systems (not IPP compounds), though are different to those made by Yalkowsky et al.[173] who noted log-linear relationships in co-solvated ethanol / water systems.

The methylated cyclodextrin compound TRIMEB (heptakis-(2,3,6-tri-o-methyl)-β-cyclodextrin) has been shown to have a significant solubility in HPFP, HFA134a and HFA227 ranging from 3.4 to 4.5 mg/mL, with HFA227 showing the greatest solubilising properties for this compound. Notably, non-methylated β-cyclodextrin showed very low solubility in all three HFAs, being < 15 µg/mL in each case. Evidence of complexation was observed for the corticosteroid compound budesonide when formulated with TRIMEB in HPFP, HFA134a and HFA227, with solubility values being increased by x4.5, x2.5 and x13.2 respectively for budesonide. A concomitant retardation of the TRIMEB solubility was observed suggesting that a host / guest complex is

formed, where the host compound controls the process.[175] Structural information from the NMR measurements has provided evidence of complexation in the form of shifts in δ (chemical shift) values of the budesonide and TRIMEB resonances. These data are an inherent advantage of the NMR approach to the studies and are further corroborated by observations made using vibrational spectroscopy to analyse materials crystallised from HPFP. Wavenumber shifts are noted in the Raman and FTIR spectra of materials crystallised from HPFP in the presence of TRIMEB compared to those of pure reference materials, particularly in the bands associated to the quinone function (A-ring) of budesonide, suggesting an interaction is taking place with the TRIMEB in this area of the molecule.

VT NMR studies on budesonide / TRIMEB in HPFP shows data consistent with that observed in ethanol co-solvated systems. The entropy change values increase and become closer in magnitude to those of the enthalpy change, which also increase. This suggests that the system is moving towards enthalpic control in the same way as the ethanol / HPFP systems.

7.2 Solid State Approaches

The solid state work presented in this thesis has established methods to access information on solid state materials deposited after actuation of pMDI devices using analytical approaches used in combination with modified impaction and impingement devices. Raman approaches have been used to interrogate budesonide / formoterol fumarate and fluticasone propionate / salmeterol xinafoate combination therapies in the form of Symbicort® and Seretide® pMDIs from AstraZeneca and GlaxoSmithKline respectively. The

technique has been shown to spectroscopically distinguish the two IPPs used from one another in each preparation, and has been successfully deployed to capture two-dimensional hyper-spectral arrays on material deposited on the plates of an Anderson Cascade Impactor. The data clearly demonstrate that the material shows instances of co-deposition, where particles of both compounds are deposited adjacent to or on top of one another. These data are particularly useful as it is claimed that there is a significant therapeutic benefit over therapies administered separately.[223-225] The technique has the potential for further development to investigate more than two components, such as IPPs in formulations containing triple therapies of inhaled corticosteroids, β_2-agonists and antimuscarinic bronchodilators such as those recently formulated by Adi *et al.*[226]

A novel adaptation to the Twin Stage Impinger (TSI) apparatus used in deposition experiments has been used successfully in the investigation of material properties after actuation and deposition of pMDI devices. Two commercially available formulations of the corticosteroid beclomethasone dipropionate have been investigated using this modified apparatus in combination with powder *X*-ray diffraction (PXRD), thermal techniques including Differential Scanning Calorimetry (DSC) and Thermo Gravimetric Analysis (TGA) and Scanning Electron Microscopy. The PXRD data recorded as part of these studies was performed after capture of respirably sized material (on stage 2 of the TSI) on Mylar® using a modified TSI apparatus. The results highlight a clear difference between the two formulations; QVAR® material deposits with a degree of crystalinity, with evidence of low intensity peaks in the diffraction patterns recorded. Furthermore, the pattern

suggests a different crystal form compared to that of the reference beclomethasone dipropionate material, with peaks at different 2θ values. Simulated PXRD patterns generated from previously published crystal structures of BDP and its solvates, confirm this is the monohydrate form,[237] with the reference material used being an anhydrate.[236] The Synasthmax® formulation however was shown to be largely amorphous in nature on initial deposition with no observable peaks in the diffraction pattern recorded. Time-lapse experiments showed the material from this preparation began to recrystallise over time, with peaks in the diffraction pattern growing over a period of *ca.* 6 hours. The 2θ values of the peaks appearing after recrystallisation were consistent with those observed in the QVAR material after deposition and the simulated PXRD pattern, showing both products recrystallise to the monohydrate form of BDP. These observations are consistent with those from the thermal analyses and the SEM imaging carried out at King's College London on the same preparations.

7.3　　　Novel Budesonide pMDI Prototypes

Production of prototype pMDI formulations of the inhaled corticosteroid compound budesonide have been successfully performed using crystalline material micronised to a mean cumulative undersize dimension, X_{90}, of 2.9 µm to produce formulations of (i) budesonide in HFA134a (ii) budesonide in HFA134a / EtOH (10 % v/v) (iii) budesonide / TRIMEB in HFA134a and (iv) budesonide / TRIMEB in HFA134a / EtOH (10 % v/v). The developed NMR method has been used to ascertain the solubility of budesonide in these media, and show increases consistent with those determined in previous studies on model systems (Sections 4.11, 4.2.1.2 and 4.2.2) for (i), (ii) and

(iii). Importantly, the solubility of the preparation including EtOH and TRIMEB shows a major increase in solubility, and is the only formulation to achieve total solubility at the concentrations prepared. Anderson Cascade Impaction (ACI) experiments have been performed on the pMDI preparations to deposit solid material and have allowed assessment of aerodynamic particle size distribution (APSD) and solid form characterisation using SEM and μ-Raman spectroscopy.

The particles deposited from budesonide in HFA134a and budesonide in HFA134a / EtOH (10 % v/v) appear crystalline, with SEM clearly showing facets and edges to the deposits. μ-Raman produces spectra consistent with those of crystalline budesonide references. Deposits from the preparations of (i) budesonide / TRIMEB in HFA134a and (ii) budesonide / TRIMEB in HFA134a / EtOH (10 % v/v) show different form and morphology. Deposits from (ii) appear exclusively as spheroids and have Raman spectra consistent with amorphous host / guest complexes of budesonide / TRIMEB, displaying broadened bands and indicative peak shifts observed previously in the characterisation of these complexes. The homogeneity of the deposits is attributed to the increased (total) solubility of the materials in this preparation. Deposits from (i) show a mix of spheroids and crystallites consistent with the partial solubility of this formulation.

APSD measurements have revealed some interesting data, with two broad profiles apparent; (i) budesonide and budesonide / TRIMEB in HFA134a show maximum deposition on stage 4 of the ACI, whilst (ii) budesonide and budesonide / TRIMEB in HFA134a / EtOH (10 % v/v) show maximum deposition on the later stages (7 and 6 respectively), with a significantly

237

reduced mass median aerodynamic diameter (MMAD) on addition of EtOH. These observations are consistent with those made by Williams III *et al.*[182] who also noted decreased MMAD with EtOH addition to pMDI formulations of betamethasone valerate. The decrease is attributed to increased solubility and rapid evaporation of the propellant. The lowest MMAD observed in these studies is from the solution formulation of budesonide / TRIMEB in HFA134a / EtOH (10 % v/v), consistent with this hypothesis. It is also noteworthy that the preparation of budesonide / TRIMEB in HFA134a has the highest MMAD, and that it is greater than that of budesonide in HFA134a alone. This is potentially explained by the increase in solubility observed on addition of TRIMEB, facilitating the Ostwald ripening phenomenon and increasing the rate of production of larger particles at the expense of smaller ones. This is consistent with the MMAD increase and the 'fronting' observed in the APSD profile, showing increased deposition on the early stages (1, 2 and 3) and causing a bimodal distribution.

7.4　　　　Further Work

The work completed to date warrants extension in a number of different directions.

The methods developed form a sound basis by which to study pMDI formulations *in-situ* and after actuation / deposition. To provide further insight into materials showing solubility levels below those of the currently operated NMR method, means by which to increase the sensitivity further should be investigated. Use of higher field instruments offer obvious sensitivity gains as discussed in the main text (Chapter 3, Section 3.1.3) and accessing higher field instruments of up to 1 GHz now available at certain laboratories would be beneficial. Perhaps more readily available and cost effective would be to investigate the benefits of alternative probe technologies that exist for the sole purpose of maximising sensitivity in the NMR experiment. Cryoprobes are of particular interest in that they exhibit vastly reduced noise levels in the data recorded due to the cryogenic cooling of the radio frequency electronics in the probe assemblies, hence increased signal : noise. They are, however, cost prohibitive for many laboratories. Other, less expensive, probe designs can also offer significant sensitivity enhancements for specific experiments. It is commonplace for a general use probe to be optimised for sensitivity of the X-nuclei, *i.e.* have the inner coil of the probe utilised for low-sensitivity ^{13}C, ^{15}N experiments and the outer coil tuned for ^{1}H work where the sensitivity is inherently higher.[125] For specific experiments however, it is possible to use probes designed to optimise, for example, ^{1}H sensitivity by reversal of this setup, or having dedicated probes optimised for 1 nucleus only. These

probes tend to be less common as systems are generally purchased to allow a broad series of experiments to take place with maximum efficiency.

The *in-situ* nature of the developed NMR method lends itself extremely well to the study of material behaviour in solution, as shown in the studies of host / guest complexes (Section 4.2.2). NMR has been used previously in the study of complexation to good effect and the setup summarised in this thesis would allow similar studies to be carried out in HFAs. More extensive host / guest characterisation could be completed using approaches similar to those summarised by Pîrnāu *et al.*[195] and Zouvelekis *et al.*[243], where host / guest stoichiometry was calculated by NMR monitoring of chemical shift values during titrations to sequentially increase the host (cyclodextrin) concentrations. Furthermore, other cyclodextrins could easily be screened for solubility in HFA propellants by the NMR approaches summarised. Solubility of differently derivatised CDs could be assessed as has often been performed in aqueous and other solvent systems.[244,245]

Further consideration should be given to the excipients used in the solubility enhancement of budesonide in the final chapter of this thesis. The co-solvent ethanol and the derivatised cyclodextrin TRIMEB have been shown to enhance solubility of the corticosteroid compound budesonide and control the deposited solids after actuation. Facilitated Ostwald ripening has been shown to occur in preparations with solubility increases of suspension preparations, but a true solution pMDI of budesonide has been prepared using ethanol / TRIMEB in combination, producing small particulate amorphous host / guest solids on deposition. The investigation of other compounds, particularly poorly soluble entities, would warrant investigation in pMDI formulations

prepared using these approaches. The lung has long been of interest in the systemic delivery of small molecules and peptides[1,4] and the use of the NMR method and deposition monitoring approaches reported would allow the solubility and formulation characteristics of multiple APIs to be screened.

References

1- B.A.S. Brown, *Drug Dev. Delivery*, **2**(7), 2002: p. 1

2- H. Smyth, *Excipient Development for Pharmaceutical, Biotechnology, and Drug Delivery Systems*, CRC Press, 2006: p. 225.

3- B.L.Laube, *Respir. Care*, 2005, **50**(9): p. 1161.

4- R. U. Agu, M. I. Ugwoke, M. Armand, R. Kinget, N. Verbeke, *Respir. Res.*, 2001, **2**: p. 198.

5- J. S. Patton, J. Bukar, S. Nagarajan, *Adv. Drug Delivery Rev.*, 1999, **35**: p. 235.

6- P. A. Hollander, *Med. Gen. Med*, 2007, **9**(1): p. 45.

7- S. J. Farr, A. McElduff, L. E. Mather, J. Okikawa, E. Ward, I. Gonda, V. Licko, R. M. Rubsamen, *Diabetes Technol. Ther.*, 2000, **2**(2): p. 185.

8- N. R. Labiris, M. B. Dolovich, *J. Clin. Pharm*, 2003, **56**(6): p. 588.

9- T. J. Ritchie, C. N. Luscombe, S. J. F. MacDonald, *J. Chem. Inf. Model.*, 2009, **49**: p. 1025.

10-K. G. Tantisira, S. Lake, E. S. Silverman, L. J. Palmer, R. Lazarus, E. K. Silverman, S. B. Liggett, E. W. Gelfand, L. J. Rosenwasser, B. Richter, E. Israel, M. Wechsler, S. Gabriel, D. Altshuler, E. Lander, J. Drazen, S. T. Weiss, *Hum. Mol. Genet.*, 2004, **13**(13): p. 1353.

11-Global Strategy for the Diagnosis, Management and Prevention of Chronic Obstructive Pulmonary Disease, Global Initiative for Chronic Obstructive Lung Disease (GOLD), 2013, www.goldcopd.org.

12-P. J. Barnes, *Nature Reviews*, 2002, **1**: p. 437.

13-K. R. Chapman, D. P. Tashkin, D. J. Pye, *Chest*, 2001, **119**(6): p. 1691.

14-P. J. Barnes, J. M. Drazen, S. I. Rennard, N. C. Thopson, *Asthma and COPD,* 2nd Ed, Elsevier Academic Press, USA, 2009.

15-Global Strategy for Asthma Management and Prevention, Global Initiative for Asthma (GINA), 2012, www.ginasthma.org.

16-P. J. Barnes, *J. Allergy Clin. Immunol.*, **129**(1): p. 48-59.

17-K. Fujimoto, M. Yasuo, K. Urushibata, M. Hanaoka, T. Koizumi, K. Kubo, *Eur. Respir. J.*, 2005, **25**: p. 640.

18-V. M. Keatings, P. D. Collins, D. M. Scott, P. J. Barnes, *Am. J. Respir. Crit. Care. Med.*, 1996, **153**: p. 530.

19-P. J. Barnes, *Thorax*, **61**(9): p. 742.

20-D. G. Tinkelman, C. E. Reed, H. S. Nelson, K. P. Offord, *Paediatrics,* **92**(1), 1993: p. 64-77.

21-D. J. Evans, D. A. Taylor, O. Zetterstrom, K. F. Chung, B. J. Connor, P. J. Barnes, *New Engl. J. Med.*, 1997, **337**(20): p. 1413.

22-P. J. Barnes, *Nature Reviews*, 2002, **1**: p. 437.

23-P. J. Barnes, *Thorax*, 2003, **58**: p. 803.

24-P. H. Rothbarth, B. M. Kepen, M. J. W. Sprenger, *Am. J. Respir. Crit. Care. Med.*, 1995, **151**(5): p.1641.

25-L. J. Tata, J. West, T. Harrison, P. Farrington, C. Smith, R. Hubbard, *Thorax*, 2003, **58**: p. 835.

26-K. R. Murphy, A. Eivindson, K. Pausens, W. J. Stein, G. Tellier, R. Watts, P. Leophonte, S. J. Sharp, E. Loeschel, *Clin. Drug Invest.*, 2000, **20**(5): p. 337.

27-N. Ferrari, R. Seguin, P. Renzi, *Future Med. Chem.*, 2011, **3**(13): p. 1647.

28-S. O. Shaheen, J. A. C. Sterne, R. L. Thompson, C. E. Songhurst, B. M. Margetts, P. G. Burney, *Am. J. Respir. Crit. Care. Med.*, 2006, **164**(10): p. 1823.

29-I. Rahman, *Int. J. Chronic Obstruct. Pulmon. Dis.*, 2006, **1**(1): p. 15.

30-R. J. Shiner, A. J. Nunn, K. F. Chung, D. M. Geddes, *Lancet*, 1990, **336**(8708): p. 137.

31-M. F. Mullarkey, J. K. Lammert, B. A. Blumenstein, *Ann. Intern. Med.*, 1990, **112**(8): p. 577.

32-M. G. Matera, L. Calzetta, M. Cazzola, *Pulm. Pharmacol. Ther.*, 2010, **23**(2): p. 121.

33-W. I. DeBoer, 2005, *Drug Discovery Today*, **10**(2): p. 93.

34-R. G. Townley, F. Suliaman, *Ann. Allergy, Asthma, Immunol.*, 1987, **58**(1): p. 1.

35-P.J. Barnes, *Br. J. Pharmacol.*, 2006, **148**: p. 245.

36-B. H. Rowe, C. Spooner, F. Ducharne, J. Bretzlaff, G. Bota, *Cochrane Database Syst. Rev.*, 2001, **1**: p. CD002178.

37-P. T. Daley-Yates, R. L. Kunka, Y. Yin, S. M. Andrews, S. Callejas. C. Ng, *Eur. J. Clin. Pharmacol.*, 2004, **60**: p. 265.

38-N. Bandi, W. Wei, C. B. Roberts, L. P. Kotra, U. B. Kompella, *Eur. J. Pharm. Sci*, 2004, **23**: p. 159.

39-P. T. Daley-Yates, *Br. J. Clin. Pharmacol.*, **52**(4): p. 459.

40-J. P. Kemp, D. P. Skoner, S. J. Szefler, K. Walton-Bowen, M. Cruz-Rivera, J. A. Smith, *Ann. Allergy, Asthma, Immunol.*, 1999, **83**(3): p. 231.

41-J. W. Baker, M. Mellon, J. Wald, M. Welch, M. Cruz-Rivera, K. Walton-Bowen, *Paediatrics*, 1999, **103**(2): p. 414.

42-C. Micheletto, M. Guerriero, S. Tognella, R. W. Dal Negro, *Ann. Respir. Med.*, 2005, **99**: p. 850.

43-J. Waugh, K. L. Goa, *Am. J. Respir. Med.*, 2002, **1**(5): p. 369.

44-D. Lynes, *The Management of COPD in Primary and Secondary Care*, M&K Publishing, UK, 2007.

45-I. A. Campbell, W. G. Middleton, G. J. R. McHardy, M. V. Shotter, R. McKenzie, A. B. Kay, *Thorax*, 1977, **32**, 424-428.

46-M. Cazzola, M. G. Matera, *Br. J. Pharmacol.*, 2008, **155**: p. 191.

47-B. G. Bender, *J. Allergy Clin. Immunol.*, 2002, **109**(6): p. S554.

48-G. P. Anderson, A. Lindén, K. F. Rabe, *Eur. Respir. J.*, 1994, **7**: p. 569.

49-H. Magnussen, B. Bugnas, P. Schmidt, F. Gerken, S. Kesten, *Ann. Respir. Med.*, **102**(1): p. 50.

50-T. Fardon, K. Haggart, D. K. Lee, B. J. Lipworth, *Ann. Respir. Med.*, **101**(6): p. 1218.

51-T. T. Hansel, H. Neighbour, E. M. Erin, A. J. Tan, R. C. Tennent, J. G. Maus., P. J. Barnes, *Chest*, 2005, **128**(4): p. 1974.

52-S. A. Antoniu, *Expert Opin. Invest. Drugs*, 2011, **20**(6): p. 871.

53-R. Fuhr, H. Magnussen, K. Sarem, A. R. Llovera, A. Kirsten, M. Falqués, C. F. Caracta, E. G. Gill, *Chest*, 2012, **141**(3): p. 745.

54-B. C. Moulton, A. D Fryer, *Br. J. Pharmacol.*, 2011, **163**(1): p. 44.

55-A. Miller-Larsson, O. Selroos, *Curr. Pharm Des.*, 2006, **12**: p. 3261.

56-A. P. Greening, P. W. Ind, M. Northfield, G. Shaw, *Lancet*, 1994, **344**: p. 219.

57-A. Papi, P. Paggiaro, G. Nicolini, A. M. Vignola, L. M. Fabbri, *Allergy*, 2007, **62**: p. 1182.

58-S. Shrewsbury, S. Pyke, M. Britton, *Br. Med. J.*, 2000, **320**: p. 1368.

59-N. R. Labiris, M. B. Dolovich, *J. Clin. Pharmacol.*, 2003, **56**(6): p. 600.

60-X. M. Zeng, G. P. Martin, C. Marriott, *Int. J. Pharm.*, 1995, **124**(2): p. 149.

61-B. Praveen, R. Kulkarni, *Medscape Drugs, Diseases and Procedures*, 2011, www.emedicine.medscape.com/article/1413366-overview.

62-S. P. Newman, *Chest*, 1985, **88**(S2): p. S152.

63-M. L. Everard, *J. Aerosol Med.*, 2001, **14**(S1): p. S59.

64-J. Hauhney, D. Price, N. C. Barnes, J. C. Virchow, N. Roche, H. Crystyn, *Ann. Respir. Med.*, 2010, **104**(9): p. 1237.

65-O. S. Usmani, M. F. Biddiscombe, P. J. Barnes, *Am. J. Respir. Crit. Care. Med.*, 2005, **172**(12): p.1497.

66-Q. Hamid, Y. Song, T. C Kotsimbos, *J. Allergy Clin. Immunol.*, 1997, **100**(1): p. 44.

67-C. Leach, G. L. Colice, A Luskin, *J. Allergy Clin. Immunol.,* 2009, **124**(S6): p. S88.

68-I. Gonda, *Int. J. Pharm.*, 1985, **27**: p. 99.

69-C. L. Leach, P. J. Davidson, R. J. Boudreau, *Eur. Respir. J.*, 1998, **12**: p.1346.

70-D. R. Hess, *Resp. Care*, 2000, **45**(6): p. 609.

71-M. Sanders, *Prim. Care Respir. J.*, 2007, **16**(2): p. 71.

72-J. F. Dessanges, *J. Aerosol Med.*, 2001, **14**(1): p. 65.

73-M. E. Placke, W. C. J. Zimlich, *Drug Delivery Technol.*, 2002, **2**(2): p. 1.

74-W. C. J. Zimlich, J. Y. Ding, D. R. Busick, R. R. Moutvic, M. E. Placke, *Respir. Drug Delivery*, 2000, **7**: p. 241.

75-S. P. Newman, J. Brown, K. P. Steed, S. J. Reader, H. Kladders, *J. Allergy Clin. Immunol.*, 2001, **108**(1): p. S26.

76-Copley Scientific, *Quality Solutions for Inhaler Testing*, 2010.

77-J. Winkler, H. Guenther, H. Derendorf, *Proc. Am. Thorac. Soc.*, 2004, **1**(4): p. 356.

78-D. R. Hess, *Resp. Care,* 2008, **53**(6): p. 699.

79-M. Taki, F. Esmaeili, G. P. Martin, *J. Drug Delivery Sci. Technol.*, 2011, **21**(4): 293.

80-M. Imgartinger, V. Carnuglia, M. Damm, J. Goede, H. W. Frijlink, *Eur. J. Pharm. Biopharm.*, 2004, **58**(1): p. 7.

81-G. Crompton, *Prim. Care Respir.,* **15**(6): p. 326.

82-A. S. Melani, L. S. Bracci, M. Rossi, *Clin. Drug Invest.*, 2005, **25**(8): p. 543.

83-*Handbook for the Montreal Protocol on Substances that Deplete the Ozone Layer*, 9th Ed., Ozone Secretariat, UNEP, 2012.

84-M. Gibson, *Pharmaceutical Preformulation and Formulation*, Informa Healthcare, 2nd Ed, 2009.

85-J. S. Stefely, *Drug Dev. Delivery*, 2002, **2**(6): p. 64.

86-Y. S. Cheng, C. S. Fu, D. Yazzie, Y. Zhou, *J. Aerosol Med.*, 2001, **14**(2): p. 255.

87-A. A. Chuffart, F. H. Sennhauser, J. H. Wildhaber, *Swiss Med. Wkly.*, 2001, **131**: p. 14.

88-R. Kempsford, M. Handel, R. Mehta, M. DeSilva, P. Daley-Yates, *Ann. Respir. Med.*, 2005, **99**(SA): p. S11.

89-A. Nolting, S. Sista, W. Abramowitz, *Biopharm. Drug Dispos.*, **22**(9): p. 373.

90-J. Goldberg, W. Böhning, P. Schmidt, E. Freund, *Ann. Respir. Med.*, 2000, **94**(10): p. 948.

91-W. W. Busse, S. Brazinky, K. Jacobson, W. Stricker, K. Scmidtt, J. Vanden Burkdt, D, Donnell, S. Hannon, G. L. Colice, *J. Allergy Clin. Immunol.*, 1999, **104**(6): p. 1215.

92-C. M. Houghton, S. J. Langely, S. D. Singh, J. Holden, A. P. Monici-Preti, D. Acerbi, G. Poli, A. Woodcock, *Br. J. Clin. Pharmacol.*, **58**(4): 359.

93-S. P. Newman, *Resp. Care*, 2005, **50**(9): p. 1177.

94-D. Ganderton, D. Lewis, R. Davier, B. Meakin, G. Brambilla, T. Church, *Ann. Respir. Med.*, 2002, **96**: p. 3.

95-G. Brambilla, D. Ganderton, R. Garzia, D. Lewis, B. Meakin, P. Ventura, *Int. J. Pharm.,* 1999, **186**(1): p. 53.

96-P. Atkins, J. DePaula, *Physical Chemistry*, 8th Ed., W. H. Freeman & Co., 2006.

97-T. M. Crowder, M. D. Louey, V. V. Sethuraman, H. D. C. Smyth, A. J. Hickey, *Pharm. Technol.*, 2001, **25**(7): p. 99.

98-A.R. Clark, *Aerosol Sci. and Technol.*, 1995, **22**: p. 374.

99-F. Podczeck, J. M. Newton, M. B. James, *J. Adhes. Sci. Technol.,* 1995, **9**:p. 1547.

100-D. Traini, P. M. Young, R. Price, P. Rogueda, *Drug Dev. Ind. Pharm.*, 2006, **32**(10): p. 1159.

101-P. C. Seville, C. Simons, G. Taylor, and P. A. Dickinson, *Int. J. Pharm.*, 2000, **195**(1-2): p. 13.

102-P. R. Byron, *J. Aerosol Med.*, 1997, **10**(S1): p. S3.

103-3M Drug Delivery Systems, 10 Ways to Protect Your pMDI Product, 2008, White Paper.

104-P. H. Hirst, G. R. Pitcairn, J. G. Weers, T. E. Tarara, A. R. Clark, L. A. Dellamary, G. Hall, J. Shorr, S. P. Newman, *Pharm. Res.,* 2002, **19**(3): p. 258.

105-E. Berg, *J. Aerosol Med.*, 1995, **8**(S3): p. S3.

106-V. Plaza, J. Sanchis, *Respiration*, 1998, **65**(3): p. 195.

107-N. A. Hannania, R. Wittman, *Chest*, 1994, **105**(1): p. 111.

108-C Vervaet, P. R. Byron, *Int. J. Pharm.*, 1999, **186**(1): p. 13.

109-W. Ostwald, *Lehrbuch der Allgemeinen Chemie*, Vol. 2, 1896.

110-D. Murnane, G. P. Martin, C. Marriott, *Pharm. Res.*, 2008, **25**(10): p. 2283.

111-Y. Liu, K. Kathan, W. Saad, R. K. Prud'Homme, *Phys. Rev. Lett.*, 2007, **98**: 036182.

112-W. L. Noorduin, E. Vlieg, R. M. Kellogg, B. Kaptein*, Angew. Chem. International Edition*, 2009, **48**: p. 9600.

113-H. D. Smyth, A. J. Hickey, *Controlled Pulmonary Drug Delivery*, Springer, 1st Ed, 2011.

114-C. Vervaet, P. R. Byron, *Int. J. Pharm.*, 1999, **186**(1): p. 13.

115-W. H. Soine, F. E. Blondino, P. R. Byron, *J. Pharm. Biomed. Sci.*, 1992, **3**: p. 41.

116-H. D. Smyth, *Adv. Drug Delivery Rev.*, 2003, **55**: p. 807.

117-P. R. Byron, *J. Aerosol Med.*, 1997, **10**(S1): p. S3.

118-J. S. Stefely, D. C. Duan, P. B. Myrdal, D. L. Ross, D. W. Schultz, C. Leach, *Respir. Drug Delivery*, 2000: p.83.

119-R. O. Williams III, J. Liu, *Eur. J. Pharm. Biopharm.*, 1999, **47**(2): p. 755.

120-H. Steckel, S. Wehle, *Int. J. Pharm.*, 2004, **284**(1-2): p. 75.

121-S. W. Stein, P. Sheth, P. B. Myrdal, *Int. J. Pharm.*, 2012, **422**: p. 101.

122-R. N. Dalby, E. M. Philips, P. R. Byron, *Pharm. Res.*, 1991, **8**(9): p. 1206.

123-R. O. Williams III, T. L. Rogers, J. Liu, *Drug Dev. Ind. Pharm.*, 1999 **25**(12): p. 1227.

124-P. B. Myrdal, K. L. Karlage, S. W. Stein, B. A. Brown, A. Haynes, *J. Pharm. Sci*, 2004, **93**(4): p. 1054.

125-T.D.W. Claridge, *High Resolution NMR Techniques in Organic Chemistry*, Elsevier, 2nd Ed, 2009.

126-P. G. Rogueda, *Drug Dev. Ind. Pharm.*, 2003, **29**(1): p. 39.

127-D. A. Skoog, F. J. Holler, T. A. Niemen, *Principles of Instrumental Analysis*, Brooks Cole, 5th Ed, 1998.

128-G. S. Remaud, V. Silvestre, S. Akoka, *Accredit. Qual. Assur.*, 2005, **10**: p. 415.

129-S. Akoka, L. Barantin, M. Trierweiler, *Anal. Chem.,* 1999, **71**: p. 2554.

130-E. D. Bateman, T. A. Bantje, M. JoaoGomes, M. G. Toumbis, R. M. Huber, I. Naya, *Am. J. Respir. Med.*, 2003, **2**: p. 275.

131-L. Nannini, C. J. Cates, T. J. Lasserson, P. Poole, *Cochrane Database Syst. Rev.*, 2007, **17**(4): p. CD003794.

132-E. HealthCare, *European Pharmacopoeia / European Directorate for the Quality of Medicines and Healthcare*, Council of Europe, 7th Ed, 2012.

133-C. I. Granger, M. Saunders, F. Buttini, R. Telford, L. L. Merolla, G. P. Martin, S. A. Jones, B. Forbes, *Mol. Pharmaceutics*, 2012, **9**(3): p. 563.

134-A. Foris, *Magn. Reson. Chem.*, 2004, **42**: p. 534.

135-X. Yang, *J. Instrum. Anal.*, 2004, **23**(5): p. 29.

136-A. Thalen, A. B. Draco, *Acta Pharm. Suec.,* 1987, **24**(3): p. 97.

137-NMR Consumables, Small Volume and External Referencing, www.wilmad-labglass.com.

138-R. Freeman, A Handbook of NMR, Wiley, 2nd Ed, 1997.

139-J. K. M. Sanders, B. K. Hunter, *Modern NMR Spectroscopy; A Guide for Chemists*, Oxford University Press, 2nd Ed, 1993.

140-J. Jonas, A. Jonas, *Annu. Rev. Biophys. Biomol. Struct.*, 1994, **23**: p. 287.

141-N. A. Foley, *Synthesis and Comparative Studies of Ruthenium Complexes for Metal Mediated Carbon-Hydrogen Activation and Olefin Hydroarylation Catalysis*, ProQuest Publishing, 2009.

142-L. VanLokeren, R. Kerssebaum, R. Willem, P. Denkova, *Magn. Reson. Chem.*, 2008, **46**(1): 63.

143-M. Lumsden, Quantitative NMR Without Internal Standards, 2007, www.nmr3-chemistry.dal.ca/bulletins/eretic.

144-V. Molinier, B. Fenet, J. Fitremann, A. Bouchu, Y. Queneau, *Carbohydr. Res.*, 2006, **341**: p. 1890.

145-R. S. Macomber, *A Complete Introduction to Modern NMR Spectroscopy*, Wiley, 1998.

146-L.D. Field, S. Sternhell, *Analytical NMR*, Wiley, 1989.

147-A. Amman, P. Meier, A. E. Merbach, *J. Mag. Reson.*, 1982, **46**: p. 319.

148-M. L. Kaplan, F. A. Bovey, H. N. Cheng, *Anal. Chem.*, 1975, **47**: p. 1703.

149-J. J. Led, S. B. Peterson, *J. Mag. Reson.*, 1978, **32**: p. 1.

150-W. H Sikorski, A. W. A. W. Sanders, H. J. Reich, *Magn. Reson. Chem.*, 1998, **36**: p. S118.

151-B. A. S. Brown, M. L. Thatcher, K. L. Smith, P. R. Johnson, J. J. Podgorski, *Respir. Drug Delivery,* 2002, **8**, (2): p. 311.

152-R. K. Harris, P. Hodgkinson, V. Zorin, J. N. Dumez, E. B. Hermann, L. Emsley, E. Salager, R. S. Stein, *Magn. Reson. Chem.*, 2010, **48**: p. S103.

153-E. Estrada, I. P. López, J. J. Tores-Labandeira, *J. Org. Chem.*, 2000, **65**(25): p. 8510.

154-T. Srichana, R. Suedee, *Drug Dev. Ind. Pharm.*, 2001, **27**(5): p. 457.

155-H. G. Brittain, *Profiles of Drug Substances, Excipients and Related Methodology*, 2003, Academic Press Ltd, London.

156-F. Foe, H. T. Cheung, B. N. Tattam, K. F. Brown, J. P. Seale, *Drug Metab. Dispos.*, 1998, **26**(2): p. 132.

157-A. Othman, B. K. Harri, P. Hodgkinson, E. A. Christopher, R. W. Lancaster, *New J. Chem.*, 2008, **32**: p. 1796.

158-S. Sahasranaman, M. Issar, G. Tóth, G. Horváth, G. Hochhaus, *Pharmazie*, 2004, **59**(5): p. 367.

159-B. Bardsley, M. S. Smith, B. H. Gibson, *Org. Biomol. Chem.*, 2010, **8**: p. 1876.

160-N. Mistry, I. M. Ismail, M. S. Smith, J. K. Nicholson, J. C. Lindon, *J. Pharm. Biomed. Anal.*, 1997, **16**(4): p. 697.

161-E. Heftmann, *Chromatography*, 6th Ed, 2004, Elsevier Science and Technology.

162-D. C. Apperley, A. F Markwell, R. K. Harris, P. Hodgkinson, *Magn. Reson. Chem.*, 2012, **50**(10): p. 680.

163-B. Venkatasubbaiah, L. R. Prakash, R. V. Dev. V. Varaprasad, K. S. Reddy, *Sci. Pharm*, 2009, **77**: p. 579.

164-P. A. Dickinson, P. C. Seville, H. McHale, N. C. Perkins, G. Taylor, *J. Aerosol Med.*, 2000, **13**(3): p. 179.

165-J. A. Hoye, A. Gupta, P. B. Myrdal, *J. Pharm. Sci.*, 2008, **97**(1): p. 198.

166-J. A. Hoye, P. B. Myrdal, *Int. J. Pharm.*, 2008, **362**: p. 184.

167-C. Reichardt, T. Welton, Solvent and Solvent Effects in Organic Chemistry, Wiley, 4th Ed., 2010.

168-A. Leo, C. Hansch, D. Elkins, *Chem. Rev.*, 1971, **71**(6): p. 525.

169-J. Sangster, *Octanol-Water Partition Coefficients: Fundamentals and Physical Chemistry*, Wiley, 1997.

170-C. H. Robinson, *J. Org. Chem.*, 1961, **26**: p. 2863.

171-A. Bouhroum, J. C. Burley, N. R. Champness, R. C. Toon, P. A. Jinks, P. M. Williams, C. J. Roberts, *Int. J. Pharm.*, 2010, **391**(1-2): p. 98.

172-G. W. A. Milne, Drugs; Synonyms and Properties, Wiley, 2nd Ed., 2000.

173-Y. Ran, S. H. Yalkowsky, *J. Chem. Inf. Model.*, 2001, **41**(2): p. 354.

174-S. H. Eghrary, R. Zarghami, F. Martinez, A. Jouyban, *J. Chem. Eng.*, 2012, **57**: p. 1544.

175-J. Manrique, F. Martinez, *Lat. Am. J. Pharm.*, 2007, **26**(3): p. 344.

176-R. W. Rousseau, Y. S. Kim, J. R. Méndez del Rio, *J. Pharm. Sci.*, 2005, **94**(9): p. 1941.

177-P. Bustamante, S. Romero, A. Pena, B. Escalera, A. Reillo, *J. Pharm. Sci.*, 1998, **87**(12): 1590.

178-P. Bustamante, B. Escalera, *J. Pharm. Pharmacol.*, **47**(7): p. 550.

179-N. Yusuff, P. York, *Int. J. Pharm.*, 1991, **73**(1): p. 9.

180-F. E. Blondino, P. R. Byron, *J. Pharm. Biomed. Anal.*, 1995, **13**(2): p. 111.

181-A. Gupta, S. W. Stein, P. B. Myrdal, *J. Aerosol Med*, 2003, **16**(2); p. 167.

182-R. O. Williams III, A. M. Patel, M. K. Barron, T. L. Rogers, *Drug Dev. Ind. Pharm.*, 2001, **27**(5): p. 401.

183-E. Mogalian, P. J. Kuehl, P. B. Myrdal, *Int. J. Pharm.*, 2007, **340**: p. 223.

184-T. Loftsson, D. Duchêne, *Int. J. Pharm.*, 2007, **329**(1-2): p. 1.

185-S. Rawat, S. K. Jain, *Eur. J. Pharm. Biopharm.*, 2004, **57**(2); p. 263.

186-T.Loftsson, M. E. Brewster, *J. Pharml Sci.*, 1996, **85**(10): p. 1017.

187-F. Castiglione, M. Valero, C. A. Dreiss, A. Mele, *J. Phys. Chem. B*, 2011, **115**: p. 9005.

188-N. Marangoci, M. Mares, M. Silion, A. Fifere, C. Varganici, A. Nicolescu, C. Deleanu, M. Pinteala, B. C. Simionescu, *Results Pharma Sci.*, 2011, **1**: p. 27.

189-J. Shi, Y. Zhou, *Spectrochim. Acta, Part A*, 2011, **83**: p. 570.

190-L. Ding, J. He, L. Huang, R. Lu, *J. Mol. Struct.*, 2010, **979**: p. 122.

191-B. Plainchont, A. Martinez, S. Tisse, J. P. Bouillon, F. Pilard, J. M. Wieruszeski, G. Lippens, D. Jeannerat, J. M. Nuzillard, *Magn. Reson. Chem.*, 2011, **49**: p. 780.

192-M. Rewster, *J. Pharm. Sci.*, 1996, **85**(10): p. 1017.

193-R. W. Rousseau, Y. S. Kim, J. R. Méndez del Rio, *J. Pharm. Sci.*, 2005, **94**(9): p. 1941.

194-P. Bustamante, S. Romero, A. Pena, B. Escalera, A. Reillo, *J. Pharm. Sci.*, 1998, **87**(12): p. 1590.

195-A. Pîrnāu, M. Bogdan, C. Floare, *J. Phys. : Conf. Ser.*, 2009, **182**: p. 012013.

196-T. Toropainen, S. Velaga, T. Heikkila, L. Matilainen, P. Jarho, J. Carlfos, V. Lehto, T. Järvinen, . Järvinen, *J. Pharm. Sci.*, 2006, **95**(10): p. 2235.

197-D. S. Conti, J. Grashik, L. Yang, S. R. P. DaRocha, *J. Pharm. Pharmacol.*, 2012, **64**(9): p. 1236.

198-M. Cote, P. G. A. Rogueda, P. C. Griffiths, *J. Pharm. Pharmacol.*, 2008, **60**(5): p. 593.

199-J. Szejtli, *Cyclodextrin Technology*, Kluwer Academic Publishers, 1st Ed, 1988.

200-H. R. Ali, H. G. M. Edwards, J. Kendrick, I. J. Scowen, *Drug Test. Anal,* 2010, **2**(9): p. 447

201-F. Glomot, L. Benkerrour, D. Duchêne, M. Poelman, *Int. J. Pharm.*, 1988, **46**(1-2): p. 49.

202-Y. Nikai, K. Yamamoto, K. Terada, D. Watanabe, *Chem. Pharm. Bull.*, 1987, **35**(11): p. 4609.

203-L. Agertoft, S. Pederson, K. Nikander, *J. Aerosol Med.*, 1999, **12**(3): p. 161.

204-S. Velaga, S. Bergh, J. Carlfors, *Eur. J. Pharm. Sci*, 2004, **21**(4): p. 501.

205-V. Mykhaylova, K. Dresely, F. Klar, N. A. Urbanetz, *Pharm. Ind.*, 2011, **73**(7): p. 1324.

206-Laser Diffraction, Particle Size Analysis, www.sympatec.com/EN/LaserDiffraction/LaserDiffraction.

207- M. S. Hassan, R. W. M. Lau, *AAPS Pharm. Sci. Tech.,* 2009, **10**(4): p.1252.

208- Particle Size Analysis, Red-Grey, www.red-grey.co.uk/general/cascade-impactor.

209- K. R. May, *J. Aerosol Sci.,* 1982, **13**(1): p. 37.

210- X. M. Zeng, G. P. Martin, C. Marriott, *Particulate Interactions in Dry Powder Formulations for Inhalation*, Taylor and Francis, London, 2001.

211- A. G. Carr, R. Mammucari, N. R. Foster, *Int. J. Pharm.,* 2011, **405**(1-2): p. 169.

212- H. G. M. Edwards, A. F. Johnson, I. R. Lewis, *J. Raman Spectrosc*, 1993, **24**(8): p. 475.

213- H. G. M. Edwards, E. R. Gwyer, J. W. F. Tait, *J. Raman Spectrosc*, 1997, **28**(9): p. 677.

214- P. Vandenabeele, B. Wehling, L. Moens, H. G. M. Edwards, M. DeReu, G. Van Hooydonk, *Anal. Chim. Acta*, 2000, **407**: p. 261.

215- K. Buckley, P. Matousek, *Non-Invasive Detection of Illicit Drugs Using Spatially Offset Raman Spectroscopy, in Infrared and Raman Spectroscopy in Forensic Science*, 1st Ed, Wiley, 2012.

216- H. G. M. Edwards, D. W. Farwell, J. M. Holder, E. E. Lawson, *Spectrochim. Acta, Part A*, 1997, **53**(13): p. 2403.

217- P. J. Caspers, G. W. Lucassen, G. J. Puppels, *Biophys J.,* 2003, **85**(1): p. 572.

218- B. W. Barry, H. G. M. Edwards, A. C. Williams, *J. Raman Spectrosc*, 1992, **23**(11): p. 641.

219-H. G. M. Edwards, J. M. Chalmers, *Anal. Bioanal. Chem.*, 2006, **385**(6): p. 1037.

220-H. G. M. Edwards, A. R. David, R. H. Brody, *J. Raman Spectrosc*, 2008, **39**(8): p. 966.

221-C. J. Strachen, T. Rades, K. C. Gordon, J. Rantanen, *J. Pharm Pharmacol.*, 2007, **59**(2): p. 179.

222-J. Saunier, V. Mazel, C. Paris, N. Yagoubi, *Eur. J. Pharm. Biopharm.*, 2010, **75**(3): p. 443.

223-P. J. Barnes, *Eur. Respir. J.*, 2002, **19**(1): p. 182.

224-B. J. Lipworth, T. C. Fardon, *J. Allergy Clin. Immunol.*, 2004, **113**(1): p. 178.

225-H. S. Nelson, K. R. Chapman, S. D. Pyke, M. Johnson, J. N. Pritchard, *J. Allergy Clin. Immunol.*, 2003, **112**(1): p. 29.

226-H. Adi, P. M. Young, D. Traini, *J. Pharm. Pharmacol.*, 2011, **64**: p. 1245.

227-H. R. Ali, H. G. M. E. Edwards, M. D. Hargreaves, T. Munshi, I. J. Scowen, R. J. Telford, *Anal. Chim. Acta*, 2008, **620**(1-2): p.103.

228-A. P. Ayala, *Vib. Spectrosc.*, 2007, **45**(2): p. 112.

229-J. Jenhelička, H. G. M. Edwards, S. E. J. Villar, J. Pokorny, *Spectrochim. Acta, Part A*, 2005, **61**(10): p. 2390.

230-Theophilus, A. Moore, D. Prime, S. Rossomanno, B. Whitcher, H. Chrystyn, *Int. J. Pharm. Sci.*, 2006, **313**: p. 14.

231-H. R. Ali, H. G. M. E. Edwards, J. Kendrick, I. J. Scowen, *Spectrochim. Acta, Part A*, 2008, **72**: p. 244.

232-H. R. Ali, H. G. M. E. Edwards, J. Kendrick, T. Munshi, I. J. Scowen, *J. Raman Spectrosc.*, 2007, **38**(7): p. 903.

233-S. W. Stein, *Int. J. Pharm.*, 1999, **186**: p. 43.

234-N. Everall, J. Lapham, F. Adar, A. Whitely, E. Lee, S. Mamedov, *Appl. Spectrosc.,* 2007, **61**: p. 251.

235-StreamLine™ Plus: Raman Chemical Imaging Just Got Faster, 2008, Renishaw Spectroscopy Products Division: www.renishaw.com/en/streamline-plus-raman-imaging--9449.

236-J. W. Millard, P. B. Myrdal, *Acta Crystallogr., Section E: Struct. Rep. Online*, 2002, **58**: p. 712.

237-W. L. Duax, V. Cody, P. D. Strong, *Acta Crystallogr. Sect. B: Struct. Crystallogr. Cryst. Chem.*, 1981, **37**: p. 383.

238-P. J. Kuehl, M. D. Carducci, P. B. Myrdal, *Acta Crystallogr., Section E: Struct. Rep. Online*, 2003, **59**: p. 1888.

239-A. Othman, R. K. Harris, P. Hodgkinson, E. A. Christopher, R. W. Lancaster, *New. J. Chem.* 2008, **32**: p. 1796.

240-J. A. Harris, M. D. Carducci, P. B. Myrdal, *Acta Crystallogr., Section E: Struct. Rep. Online,* 2003, **59**: p. 1631.

241-M. Lee, *Gibaldi's Drug Delivery System in Pharmaceutical Care*, AHSP, 2007.

242-G. S. Banker, C. T. Rhodes, *Modern Pharmaceutics*, Marcel Dekker, New York, 4th Ed., 2002.

243-D. Zouvelkis, K. Yannakopolou, I. M. Mavridis, E. Anotoniadou-Vyza, *Carbohdr. Res.,* 2002, **337**: p. 1387.

244-K. G. Flood, E. R. Reynolds, N. H. Snow, *J. Chromatogr., A*, 2000, **903**: p. 49

245-J. Frank, J. F. Holzwarth, W. Saenger, *Langmuir*, 2002, **18**: p. 5974.